A

PhD thesis

entitled

Effect of functionalization of $(Ba,Sr)TiO_3$ on dielectric and energy storage behavior of PVDF-$(Ba,Sr)TiO_3$ nanocomposites

submitted in the partial fulfillment of the requirement
for the award of degree of

Doctor of Philosophy (Ph.D.)

under the guidance of

Dr. Dwijendra P. Singh
(Professor)

by

Sachin Jaidka
(Reg. no.: 901812006)

Department of Physics and Material Science
Thapar Institute of Engineering and Technology,
Patiala (Punjab), INDIA – 147004

(February 2024)

हर हर महादेव!!

Dedicated to my grandfather, Dr. Tek Chand Jaidka, thank you for the dream and unwavering the belief in myself…

DECLARATION

I hereby certify that the present work in my thesis ***'Effect of functionalization of $(Ba,Sr)TiO_3$ on dielectric and energy storage behavior of PVDF-$(Ba,Sr)TiO_3$ nanocomposites"*** in the partial fulfillment of the requirement for the award of the degree of **DOCTOR OF PHILOSOPHY (Ph.D.)** in the Department of Physics and Material Science, Thapar Institute of Engineering and Technology, Patiala is an authentic record of my own work carried out under the supervision of **Dr. Dwijendra P. Singh**. The matter embodied in this thesis has not been submitted in part or full to any other institute/university for the award of any degree.

Sachin Jaidka

This is to certify that the above statement made by the candidate is true to the best of my knowledge.

Dr. Dwijendra P. Singh
(Professor)
Department of Physics and Material Science
Thapar Institute of Engineering and Technology
Patiala (Punjab)- 147004

CONTENT

ACKNOWLEDGMENT

This thesis owes its successful completion to the unwavering support and encouragement of numerous individuals who played pivotal roles in my academic journey. I extend my heartfelt gratitude to my supervisor, **Dr. Dwijendra P. Singh**, for his exceptional guidance, constant motivation, valuable suggestions, and the conducive academic and personal environment he provided. His faith in me during challenging times was instrumental, and I am deeply thankful.

I am fortunate to acknowledge **Prof. Padmakumar Nair (Director)** of Thapar Institute of Engineering and Technology, Patiala, for generously providing resources and assistance throughout various stages of my work. Special thanks are also due to the current and previous Heads of DPMS for their consistent support and encouragement.

I express whole-hearted thanks to the members of my doctoral committee for their unwavering support, insightful comments, and constructive criticisms. Gratitude extends to my teachers at DPMS, including **Dr. Kulvir Singh**, **Dr. Poonam Uniyal**, **Dr. Bhupendra N. Chudasama**, **Dr. Bhaskar C. Mohanty** and **Dr. Loveleen K. Brar**, for their continuous support. I would also like to thank **Dr. Hitesh K. Mehtani** for his timely guidance and assistance. Timely assistance from individuals such as **Mr. Surinder Kumar**, **Mrs. Amandeep, Ms. Jaskiran, Mr. Paramjeet, Mr. Gurvinder, Mr. Purshottam Singh** and **Mr. Lal Ji** deserves acknowledgment.

My journey was enriched by the companionship of **Daksh Shelly**, **Nishtha**, **Anushka Garg**, **Ajeet Singh**, **Vikash Ranjan**, **Aayush Gupta**, **Varun Singhal**, **Mohd. Abuzar Saeed**, **Ghanshyam Mourya**, **Rahul Gupta**, **Sneha Jha**, **Arun Bishnoi** and **Nidhee Nagpal**. I express gratitude to my seniors and lab mates at Energy Materials Lab, including **Dr. Shobhneek Kaur** and **Dr. Nisha**. Their presence and the positive atmosphere in the lab made my journey both exciting and fulfilling.

I extend my appreciation to all my friends for infusing joy and positivity into my life. My deepest love, regard, and thanks go to my family, especially **Jeeyansh**, **Lavanya**, **Nakshita**, **Pranjal** and **Ekanksh**, for standing by me throughout this lengthy journey. I am grateful to **Parul**, **Sandeep Beri, Kunal Sarna** and **Gourav Behal** for keeping me grounded and focused on essential aspects of life. I am profoundly grateful for the unwavering support of my parents, **Mr. Surender Pal** and **Mrs. Usha Jaidka**, whose love, encouragement, and sacrifices were the bedrock of my journey, providing the strength and inspiration needed to navigate the challenges and reach this significant milestone. Their constant belief in me has been a guiding light, shaping both my personal and academic growth.

Lastly, I acknowledge the Mahadev for the blessings and positive energy that sustained me throughout this endeavor, and I am thankful for the gift of the special people surrounding me.

Sachin Jaidka

LIST OF PUBLICATIONS

From PhD work:

1. **S. Jaidka**, A. Aggarwal, S. Chopra, D.P. Singh, Significantly enhanced dielectric behavior of polyvinylidene fluoride-barium strontium titanate flexible nanocomposite thick films: Role of electric field-induced effects, *Journal of Electronic Materials,* **51**, 5429-5439 **(2022)** https://doi.org/10.1007/s11664-022-09784-4
2. **S. Jaidka**, S. Chopra, A. Aggarwal, D.P. Singh, Effect of interfacial layers on the temperature-dependent dielectric and impedance behavior of flexible PVDF-BST nanocomposite thick films, *Journal of Physics and Chemistry of Solids*, **184**, 111667 **(2024)** https://doi.org/10.1016/j.jpcs.2023.111667
3. **S. Jaidka** and D.P. Singh, Ultrahigh efficiency and enhanced discharge energy density at low loading of nanofiller in trilayered polyvinylidene fluoride-$Ba_{0.8}Sr_{0.2}TiO_3$ nanocomposites, *Polymer Composites* **45**, 4561 **(2024)** https://doi.org/10.1002/pc.28081
4. **S. Jaidka** and D.P. Singh, Tailored multilayered films of the PVDF/Ba0.8Sr0.2TiO3 nanocomposites with surface-modified nanoparticles for superior dielectric and energy storage performance, *(Journal of Alloys and Compounds – under review)*

Other publications:

5. P. Kundu, **S. Jaidka**, D.P. Singh, Enhanced dielectric properties of thick PVDF composite films with small loading of barium titanate, *AIP Conference Proceedings*, **2995**, 020107/1- 020107/5 https://doi.org/10.1063/5.0178051
6. P. Gupta, **S. Jaidka**, D.P. Singh, Quenching induced modified nanoarchitectonics in the dielectric and energy storage behavior of poly (vinylidene fluoride)/$Ba_{0.7}Sr_{0.3}TiO_3$ composites thick films, *Applied Physics A,* **130**, 279 **(2024)** https://doi.org/10.1007/s00339-024-07420-y

LIST OF CONFERENCES & SEMINARS

1. Oral presentation on *"Dielectric study of BT-PVDF nanocomposite films prepared using tape casting technique"* in National E-Conference on Advanced Research in Materials Science-2021.

2. Participated in ACS seminar on *"Advances in Polymer Nanocomposites"*, Oct 2021.

3. Participated in ACS seminar on *"Advances in Multifunctional Nanomaterials"*, 5-6 May 2022.

LIST OF FIGURES

Chapter 3

Chapter 4

Chapter 5

Chapter 6

LIST OF TABLES

PREFACE

High-energy density capacitors are essential components in modern electronics due to their application in pulsed power systems such as military, aerospace and hybrid electric vehicles. The high energy density capacitors store large amounts of electrostatic energy per unit volume, which is readily available for delivering to a load in a very short span of time. There are certain ceramic materials which are found to exhibit extremely high energy density in the form of thin films, but they cannot be processed over larger areas in the capacitors constituting energy banks. The dielectric polymer-ceramic nanocomposites have the ease of processability in the form of flexible thin films, which could serve the purpose of high energy density as well as miniaturization of modern electronic devices. These electronic devices, e.g., avionics in aerospace cover 70% of its volume by capacitors. Despite of having high mechanical and breakdown strength, the dielectric polymers have a drawback of low dielectric constant. On the other hand, the ceramics have high dielectric constant but relatively very low breakdown strength. Therefore, dielectric polymer ceramic nanocomposites having a moderate dielectric constant, high breakdown strength and low tangent loss could serve the purpose of high energy density capacitor materials.

A large number of polymers are used as a matrix, such as polyvinyl chloride (PVC), polyethylene terephthalate (PET), polyvinylidene fluoride (PVDF), etc., with particular interest surrounding PVDF due to its favorable functional attributes, high breakdown strength, flexibility, and ease of processing. On the other hand, some examples of ceramics fillers are $PbZrTiO_3$ (PZT), $PbTiO_3$ (PTO), $BaTiO_3$ (BTO), $BaSrTiO_3$ (BST), HfO_2, etc., which are highly appealing for their applications in various fields as they have high dielectric constant. Among these ceramic fillers, barium strontium titanate (BST) exhibits an exceptionally high dielectric constant (e.g., 2500-3000) at room temperature and maintains a nearly constant dielectric constant over a wide temperature range (-173°C to 120°C) and frequency range (100 Hz to 1 MHz).

Extensive literature has documented thorough examinations of the energy storage characteristics of polymer-ceramic nanocomposites, emphasizing on the pivotal role of breakdown strength and dielectric performance. The investigations carried out have adopted several approaches based on the engineered processing, such as the use of nanowires, nanotubes etc., functionalization, poling, incorporation of wide band gap nanofillers and engineered multilayer structure in the dielectric polymer ceramic

nanocomposites. Moreover, the use of polymer-ceramic nanocomposite thick films in harsh conditions (room temperature to 100 °C) is very important to operating it for strategic purposes. Therefore, understanding the cause that deteriorates its energy storage performance at high temperatures requires deeper understanding since the understanding will lead towards the solution.

The existing literature survey necessitates and demands a thorough investigation of polyvinylidene fluoride (PVDF)-(Ba,Sr)TiO_3 (BST) nanocomposites towards improvement in dielectric properties, breakdown strength, discharge energy density and energy efficiency. Consequently, the present thesis is divided into seven chapters consisting of aforesaid physical parameters, which are as follows:

Chapter 1 provides a concise synopsis of polyvinylidene fluoride (PVDF) polymers, ceramics, and polymer-based ceramic nanocomposites. PVDF polymers exhibit a high breakdown strength but a low dielectric constant, whereas ceramics have a high dielectric constant but a low breakdown strength. The combination of these materials presents an opportunity to create a nanocomposite with a moderate dielectric constant and high breakdown strength. Such nanocomposite materials, leveraging polymers and ceramics, are recognized as promising materials for high-energy density capacitors. The chapter emphasizes the potential dielectric ceramic fillers to be included in the polymeric matrix, including barium strontium titanate ((Ba,Sr)TiO_3), BST), as they stand out for their impressive dielectric constant (~3000) across a broad frequency range (100Hz - 1MHz) and temperature range (-173 °C-120 °C). The chapter concludes with the methods and approaches adapted in the existing literature leading towards the motivation and objectives of the thesis entitled "*Effect of functionalization of (Ba,Sr)TiO_3 on dielectric and energy storage behavior of PVDF-(Ba,Sr)TiO_3 nanocomposites*".

Chapter 2 is focused on the synthesis procedures and experimental methodologies utilized for the analysis of synthesized materials, namely $Ba_{0.8}Sr_{0.2}TiO_3$ (BST) nanopowder and polyvinylidene fluoride-$Ba_{0.8}Sr_{0.2}TiO_3$ (PVDF-BST) nanocomposite thick films. The BST nanopowder is synthesized employing the hydrothermal method, whereas the fabrication of PVDF-BST nanocomposite thick films is accomplished through the tape-casting technique.

Chapter 3 is related to studies of the effect of an applied electric field on the dielectric and structural properties of polyvinylidene fluoride-$Ba_{0.8}Sr_{0.2}TiO_3$ (PVDF-BST) nanocomposite thick films synthesized using a tape-casting technique. These films were

exposed to an electric field for varying durations. The study reveals that the electric field induces changes in the crystalline phases of PVDF, specifically enhancing the β phase. The dielectric behavior of the nanocomposite films is significantly improved under the electric field, with the film exposed for 60 minutes showing the highest dielectric constant (~25) and low tangent loss (~0.02) at 1 kHz. The enhancement is attributed to increased dipolar density resulting from modifications in structural and interfacial behavior, as well as molecular motion of the dipoles in the PVDF chain. The findings suggest that electric field-induced modifications could serve as an effective strategy for developing flexible nanocomposite films with low ceramic filler loading for various electronic applications.

Chapter 4 is associated with one of the important requirements for utilizing polyvinylidene fluoride-$Ba_{0.8}Sr_{0.2}TiO_3$ (PVDF-BST) nanocomposites for high energy density capacitors operating in harsh conditions, i.e., in high-temperature electronics and electrical power systems (RT-100ºC). This requirement necessitates the investigation of the temperature-dependent dielectric behavior, AC conductivity, and impedance of flexible PVDF-$Ba_{0.8}Sr_{0.2}TiO_3$ nanocomposite thick films. Tape-casting is used to synthesize flexible PVDF-$Ba_{0.8}Sr_{0.2}TiO_3$ nanocomposite thick films with varying BST concentrations (0.75%, 1.5%, 2.25%, and 3% by volume). An increase in the dielectric constant and a decrease in the tangent loss is found with an increase in the loading of BST nanoparticles in the nanocomposite thick films. The highest dielectric constant (~25) and the lowest tangent loss (~0.03) are observed for 3 vol% BST-loaded PVDF-BST nanocomposite at 1 kHz; the dielectric constant and the tangent loss increase to ~93 and ~1.64, respectively, at 150 °C. The dielectric constant and the tangent loss of all the PVDF-BST nanocomposites are thermally stable up to 70 °C and then increase with further increases in temperature. A phenomenological model is proposed to explain the experimentally observed behavior, which might be attributed to the thermally induced translational motion in the polymeric chains of PVDF, the motion of ions, and the migration of space charge in the interfacial layer of the PVDF matrix and BST nanoparticles.

Chapter 5 focuses on the processing of polyvinylidene fluoride-$Ba_{0.8}Sr_{0.2}TiO_3$ (PVDF-BST) nanocomposite films to achieve high discharge energy density, higher breakdown strength, and high efficiency. The articulated synthesis process of fabrication of PVDF-BST trilayered nanocomposites has been adopted with varying BST nanoparticle concentrations (0.75%, 1.50%, 2.25%, and 3.00% by volume). By using the tape casting technique, the upper and lower layers of the nanocomposites are cast in the same direction,

while the middle layer is cast in the opposite direction. The 3.00 vol% BST-loaded nanocomposite demonstrates notable dielectric properties, including high dielectric permittivity (~25), low tangent loss (~0.03), and moderately high breakdown strength (~282 MV/m). Additionally, it exhibits a high discharge energy density (~7.8 J/cc at 1400 kV/cm) and efficiency (~93%). A mechanism is proposed that involves the interfacial dipoles and the distribution of the local electric field, contributing to the enhanced energy storage behavior. The results suggest the potential application of these trilayered nanocomposites in high-energy density capacitors for pulsed power systems.

Chapter 6 is dedicated to exploring the role of surface functionalization on dielectric and energy storage behavior. For this purpose, the surface of BST nanoparticles is functionalized with -OH and PO_4^{3-} using H_2O_2 and H_3PO_4 surface modifiers. The surface modification of BST nanoparticles is confirmed through Fourier transform infrared (FTIR) spectra and energy dispersive spectroscopy (EDS) mapping. The resulting polyvinylidene fluoride-$Ba_{0.8}Sr_{0.2}TiO_3$ (PVDF-BST) nanocomposites, particularly H_3PO_4 modified, exhibit improved dielectric constants, with the highest value of ~30 at 1 kHz. The addition of BST nanoparticles enhances energy storage capabilities, as indicated by increased discharge energy density and efficiency. The H_3PO_4-modified nanocomposite film demonstrates superior performance with higher saturation polarization, lower remanent polarization, increased discharge energy density, and efficiency. The breakdown strength of nanocomposites, however, decreases compared to pure PVDF. It is reported that surface modification using H_3PO_4 leads to an increase in the mechanical strength of the nanocomposites. This enhancement in the mechanical strength further leads to an increment in the dielectric constant and electrical breakdown strength of the H_3PO_4-modified PVDF-BST nanocomposite as compared to H_2O_2-modified and unfunctionalized PVDF-BST nanocomposite thick films.

Chapter 7 presents the summary of the findings and conclusions derived from the conducted investigations. Additionally, potential directions for future research are proposed to expand on the current insights and contribute to the ongoing scientific investigations in this field.

Chapter 1

Introduction

1.1 Introduction

The polymer-based dielectric nanocomposites have become the integral contributory in the list of modern advanced materials due to their prospects of application in sensors, piezoelectric actuators, capacitors, etc. [10,11]. These materials have the capability to store high electrostatic energy in small volumes, i.e., high energy density; this energy can be released in the form of high current in a very short duration (0.1~μs) [12,13]. The high energy density capacitors are too much in demand in high voltage capacitors, pulsed power systems, and energy storage banks. The essential electrical properties that make them suitable are moderately high dielectric constant, low tangent loss and high dielectric breakdown strength [14–19]. The dielectric properties of ceramic dielectric has been widely investigated [20–23] and they have been found to have a very high dielectric constant but low breakdown strength, which is not favorable for high energy density capacitors. Since electrostatic stored energy density varies directly with the dielectric constant and quadratically with breakdown strength [24]. Some examples of dielectric ceramics are $PbZrTiO_3$ (PZT), $PbTiO_3$ (PTO), $BaTiO_3$ (BTO), $(Ba,Sr)TiO_3$ (BST), HfO_2, etc., which are otherwise useful for several other applications [20–23,25,26]. A comparative table showing the dielectric constant, tangent loss at 1 kHz and the breakdown strength is presented in Table 1.1. The investigation and development of dielectric polymers have also been carried out in order to miniaturize and cost-effective application in the modern electronics such as sensors [27,28], actuators [29,30], transistors and resistors [31,32] and capacitors [11,33,34]. The polymers falling under the

Table 1.1 Comparative table of dielectric constant, tangent loss at 1 kHz and breakdown strength for different ceramics

Sample	Dielectric constant (ε') at 1 kHz	Tangent loss (tanδ) at 1 kHz	Breakdown strength (BDS)	Ref.
$BaTiO_3$	1000	0.9	15 kV/mm	[1,2]
$BaSrTiO_3$	3000	0.02	43 kV/mm	[3,4]
$PbTiO_3$	1100	0.02	1.1 MV/cm	[5,6]
$PbZrTiO_3$	1300	0.01	8 MV/m	[7,8]
$CaCu_3Ti_4O_{12}$	14892	0.03	8.7 kV/cm	[9]

category of dielectric polymers include polyimide (PI), polyvinyl chloride (PVC), polyethylene terephthalate (PET), polyvinylidene fluoride (PVDF) and its copolymers, polypropylene (PP), etc. [14–19,35].

Table 1.2 Comparative table of dielectric constant, tangent loss at 1 kHz and breakdown strength for different polymers

Sample	Dielectric constant (ε') at 1 kHz	Tangent loss (tanδ) at 1 kHz	Breakdown strength (BDS)	Ref.
PVDF	10-11	0.02-0.05	314 MV/m	[36,37]
PVDF-TrFE	15	0.05	280 kV/mm	[38,39]
BOPP	2.25	0.005	681 V/μm	[40,41]
PVA	14.7	2.7	100 kV/mm	[42,43]
PVC	4.25	0.08	518 MV/m	[44,45]

A comparative table showing the dielectric constant, tangent loss and breakdown strength for different polymers is given in Table 1.2. The polymers are found to have a very low dielectric constant (~2-12), low tangent loss (~0.001-0.003) and high breakdown strength [46,47]. Therefore, the dielectric polymer-ceramic nanocomposites are expected to have moderate dielectric constant, low tangent loss and high breakdown strength, which makes them suitable for the high energy density capacitor application [48–53]. These nanocomposites can be processed in the form of large-area thin films, which is very useful for developing the miniaturized energy storage banks since, in various high-power electronic applications, capacitor banks cover 70 percent of the space of the electronic system [54–56]. Among the available polymers, PVDF (polyvinylidene fluoride) is on edge due to its relatively high dielectric constant (~12), low tangent loss (~0.03) and high breakdown strength (~MV/m). These electrical behavior of PVDF are tunable due to its various crystalline phases, i.e., α, β, γ, δ and ε [57–59]. Among the ceramic fillers, barium strontium titanate (BST) exhibits a high dielectric constant and low tangent loss over a wide frequency range (100 Hz-1 MHz), which is helpful for its application in various electronic devices [60–62], which makes BST as suitable ceramic filler in polymeric matrix for developing polymer ceramic nanocomposites.

This chapter briefly discusses about the dielectric properties, energy storage behavior and breakdown strength of the nanocomposites, as well as their modification by different processing conditions. The discussion is centered around PVDF-based dielectric polymer nanocomposites. The aim of the thesis is outlined in the final section of this chapter.

1.2 High-energy density capacitors: Properties and applications

The electrostatic energy density of a capacitor is given as (U_E) = $\frac{1}{2}\varepsilon_r\varepsilon_0 E_b^2$, where ε_0, ε_r are the vacuum permittivity (8.854 x 10^{-12} F/m) & dielectric constant and E_b is the dielectric breakdown strength [24]. Also, the charging and discharging energy density for a given dielectric material can be calculated from unipolar displacement vs. electric field data, as shown in Fig. 1.1. The charging energy density (U_C) is calculated using $\int_0^{Pmax} E.dP$, whereas discharge energy density (U_D) is calculated using $\int_{Pr}^{Pmax} E.dP$ and the final energy efficiency (η) is calculated by using the following formula [63]:

$$\% \eta = \frac{Discharge\ energy\ density\ (U_D)}{Charge\ energy\ density\ (U_C)} \times 100\% \quad (1.1)$$

Fig.:1.1 Schematic representation for the calculation of charging and discharging energy density using unipolar D-E loop

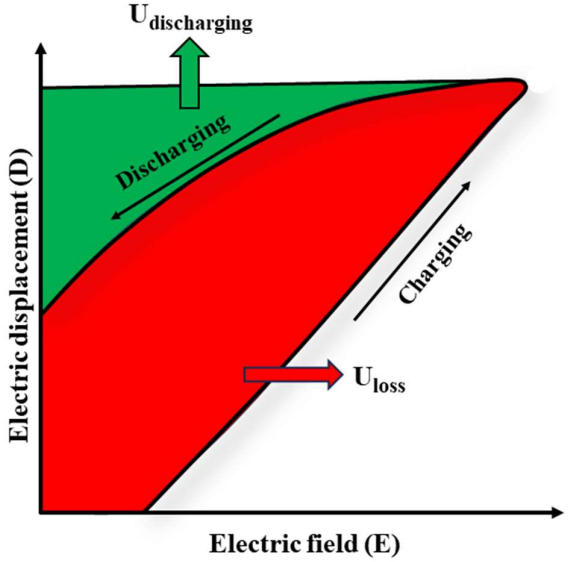

High-energy density capacitors are essential components in modern electronics, serving as energy storage devices that can rapidly discharge stored energy when needed [64–66]. The polypropylene (PP) has been employed as a commercial high-energy density capacitor material (~2J/cc) [67]. The low dielectric constant of PP limits its discharge energy density. However, in comparison to polypropylene, the PVDF polymer stands

out as a superior material for capacitors as PVDF has a higher dielectric constant than PP, whereas their dielectric breakdown strength is almost comparable. The nanocomposite of PVDF with high-permittivity ceramic nanofiller can lead to a material characterized by high permittivity, high dielectric breakdown strength, and ease of processing [68,69]. These materials may be suitable choices for the design and development of high-energy-density capacitors. Properties such as high voltage handling capability, fast charge/discharge rates, and long cycle life are crucial characteristics of high energy density capacitors, making them crucial in various applications, including electric vehicles, renewable energy systems, and pulse power applications, as shown in Fig. 1.2 [46,70–72].

Fig.:1.2 Applications of polymer based energy storage capacitors

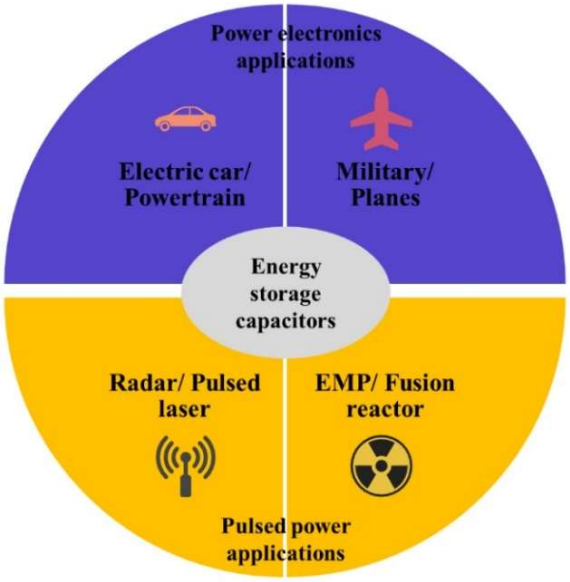

A detailed discussion about the PVDF, ceramic dielectric BST ($(Ba,Sr)TiO_3$) and the PVDF-based composites, including their structural, dielectric, energy storage and breakdown properties, is given in the following sections.

1.3 Polyvinylidene fluoride (PVDF): Properties and applications

Polyvinylidene fluoride (PVDF, $-(C_2H_2F_2)_n-$) is a polymer composed of a long carbon chain with fluorine and hydrogen atoms attached to the carbon atoms. Its melting point is 180 °C, and it is stable at room temperature. PVDF has five crystalline forms, designated as α, β, γ, δ and ε, which depend on the processing conditions. The α-phase is non-polar, while the β and γ-phases are polar. PVDF is semi-crystalline and exhibits piezoelectric, pyroelectric, and ferroelectric properties [57,58]. Among the five phases, the β-phase possesses exceptional

Fig.: 1.3 XRD pattern of (a) pure PVDF film [73]

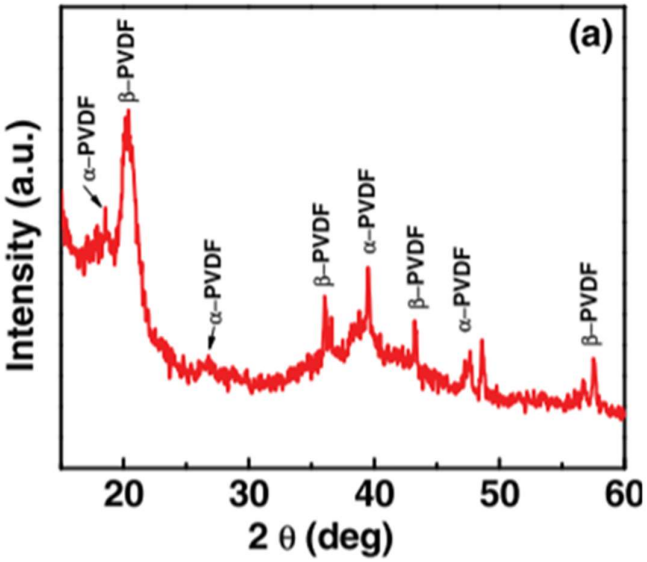

ferroelectric and piezoelectric properties and has an all-trans-trans (TTTT) configuration (making it polar). On the other hand, the α-phase has a trans-gauche (TGTG) configuration and is non-polar. The γ-phase is also polar due to its TTTG configuration, while the δ-phase exhibits a TGTG configuration with all dipoles aligned parallel to each other [73]. The formation of these phases in PVDF is influenced by various processing conditions such as temperature, poling, quenching and the method of synthesis [62,74–79]. The crystalline phases of PVDF can be determined by analyzing the X-ray diffraction (XRD) and Fourier transform infrared (FTIR) spectroscopy. The presence of different phases (i.e. α, β, γ and δ) in the PVDF polymer is confirmed by Fig. 1.3 [73] and Fig. 1.4 [57] by using X-ray diffraction (XRD) and Fourier transform infrared (FTIR) spectroscopy as shown above. Dielectric studies, i.e., dielectric constant and tangent loss of PVDF has also been studied [35,36,62,63,68,80,81].

Fig.: 1.4 FTIR spectra of PVDF with different crystalline phases [57]

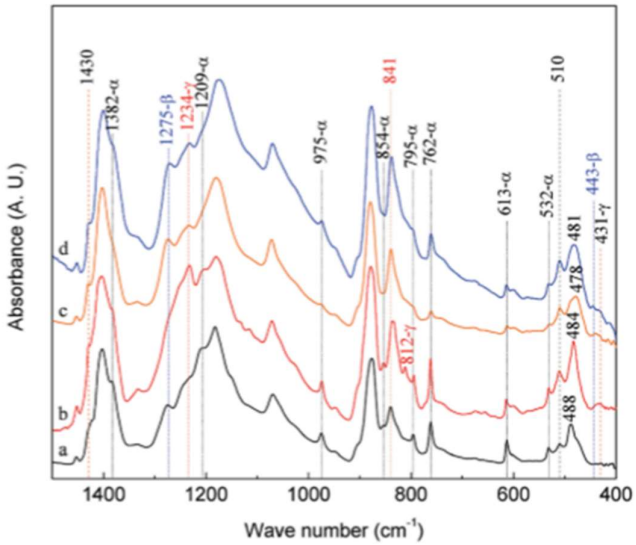

The occurrence of the dielectric constant in a material is attributed to its polarizability. The overall polarizability can be categorized into electronic, ionic, and dipolar polarization [82,83]. Electronic polarization occurs when the electron shell displacement relative to the nucleus is known, while ionic polarization happens when the displacement of a charged ion with respect to other ions is observed [82]. Dipolar polarization arises from the orientation changes of molecules with a permanent electric dipole moment in response to an applied electric field [82,83]. Heterogeneous materials accumulate charge at structural interfaces, resulting in interfacial polarization. As a result, most heterogeneous materials possess insulating properties. Interface or space polarization typically occurs at the grain boundaries or any other interface, such as the electrode-material interface [83]. The dielectric behavior of PVDF is explained on the behalf of existing physics and apparent phenomena taking place due to variations in the processing.

Fig.: 1.5 Thermal treatment dependence of dielectric contant and tangent loss of (a) α- and (b) γ-PVDF [81]

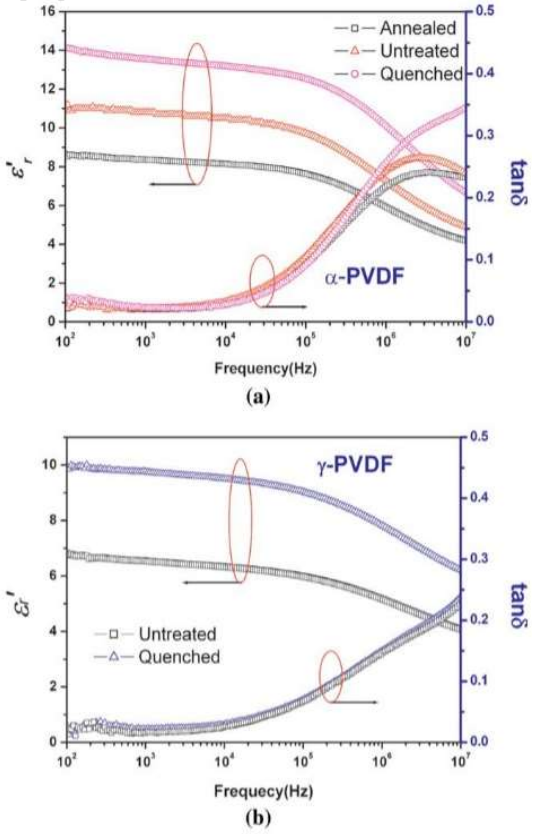

The dielectric behavior of PVDF is primarily influenced by interfacial and orientational polarizability. Interfacial polarization governs the dielectric behavior at lower frequencies, while orientation polarizability dominates at frequencies less than 10 MHz [82,83]. Typically, the dielectric constant of PVDF is higher in the lower frequency range, i.e., less than 1kHz and decreases in the high-frequency region, i.e., greater than 100 kHz. This high dielectric constant in the lower frequency range is due to the Maxwell-Wagner-Sillar (MWS), interfacial, and

space polarization [83,84]. The dielectric constant of the α and β phases is significantly higher compared to that of the γ phase, as shown in Fig. 1.5. The higher dielectric constant at a lower frequency is attributed to the interfaces among PVDF. The decrease in dielectric constant at higher frequencies is due to the dipole's lack of response in the nanocomposite film to the applied electric field frequency [36]. Losses are lower at low frequencies and increase at high frequencies, i.e. greater than 100 kHz. The tangent loss of the γ phase is lower than that of the α and β phases. The tangent loss arises due to the combined effect of electron conduction, interfacial polarization, and dipolar relaxation, with electron conduction and interfacial polarization dominating the frequency range of 1 kHz to 100 kHz [36]. The β-phase has the highest saturation polarization, affirming its ferroelectric nature, but is not ideal for capacitor-based energy storage due to a large ferroelectric loop causing energy loss, as shown in Fig. 1.6 [85,86]. In contrast, the γ-phase exhibits better energy storage characteristics, including higher discharge energy density and efficiency [87]. Hence, the PVDF polymer stands out as the most suitable matrix for making polymer-ceramic nanocomposites, given its stability, versatility, and ease of processability [80,88,89]

Fig.: 1.6 Unipolar and dipolar D–E hysteresis loops of (a) α-, (b) β- and (c) γ-PVDF films [81]

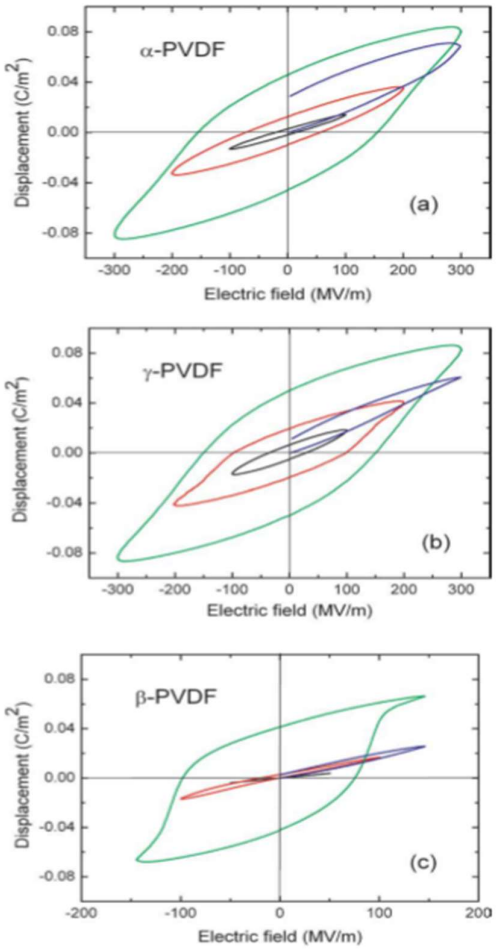

(Ba,Sr)TiO_3 (BST) has emerged as an excellent nanofiller for polymer-ceramic nanocomposites because of its peculiar characteristics, such as high dielectric constant, low

tangent loss and moderate breakdown strength, which enhance the overall performance of the composite material. BST nanoparticles contribute to increased capacitance, improved electrical insulation and high dielectric breakdown strength in the nanocomposites. The subsequent section briefly discusses the structural and dielectric properties of barium strontium titanate (BST).

1.4 Barium strontium titanate ($(Ba,Sr)TiO_3$): Properties and applications

The present section gives insights into barium strontium titanate's structural and dielectric properties.

Barium strontium titanate (BST), a ceramic compound, has received considerable attention in the field of materials science and electronics due to its unique structure and remarkable properties. BST is essentially a solid solution, blending two distinct perovskite oxides, barium titanate ($BaTiO_3$) and strontium titanate ($SrTiO_3$), with the general formula (Ba, Sr)TiO_3 [90,91]. Its structure and properties are highly tunable, making it a versatile material with a wide range of applications. The crystal structure of BST is perovskite, where a central titanium (Ti) atom is surrounded by oxygen (O) atoms, forming a cubic lattice. The key feature of perovskite materials is the arrangement of cations (in this case, barium and strontium) at the corners of the unit cell. This arrangement allows for manipulating the properties of barium strontium titanate by altering the ratio of barium to strontium [90,92]. One of the most important characteristics of BST is its stable dielectric constant over a wide range of

Fig.: 1.7 Variation of dielectric constant and tangent loss with frequency for $Ba_{0.8}Sr_{0.2}TiO_3$ ceramic

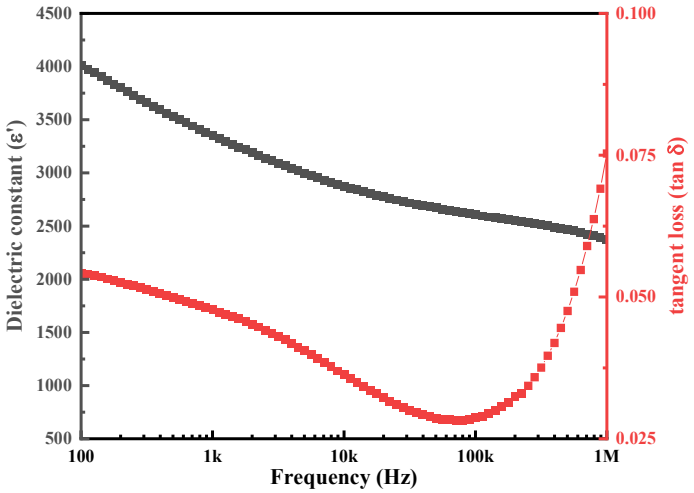

Fig.: 1.8 Room temperature polarization-electric loops of the unpoled bst ceramics at 10 hz. The inset graphic was the P-E loops under the excitation of small electric field [96]

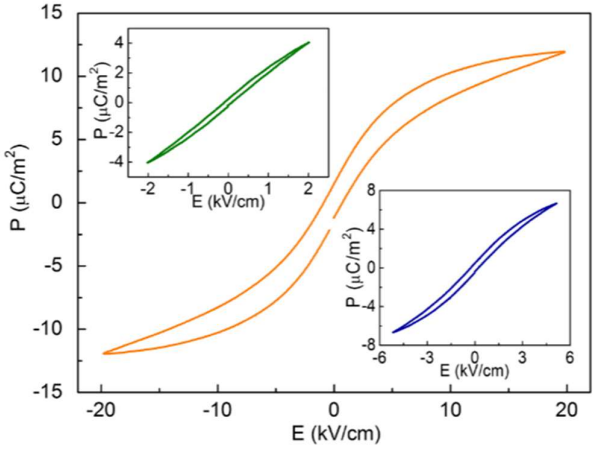

frequencies as well as low tangent loss, as shown in Fig. 1.7. The dielectric constant represents a material's ability to store electrical energy when subjected to an electric field. The BST also provides dielectric tunability, which is valuable in developing tunable capacitors [93,94]. These capacitors find applications in various electronic devices, such as tunable radio frequency filters and phase shifters, allowing precise control of signal processing in communication systems. Furthermore, BST exhibits ferroelectric behavior, i.e., it possesses a spontaneous electric polarization that can be switched by applying an external electric field, as shown in Fig. 1.8. The switching polarization characteristics of BST are used in non-volatile ferroelectric random-access memory (FeRAM) devices [95,96]. The main challenges and opportunities in developing the PVDF based nanocomposites for high energy density capacitors lie with:

i. Improvement in dielectric properties.

ii. Improvement in the breakdown strength of the material.

Combining PVDF with ceramic materials can produce nanocomposites with a moderate dielectric constant and exceptional dielectric breakdown strength. Furthermore, these nanocomposites can maintain polarization even under high electric fields, leading to the development of capacitor materials with a high energy density [12,97]. Extensive research has been conducted on polymer-ceramic nanocomposites, including PVDF, revealing their remarkable performance in terms of dielectric and energy storage characteristics. Ceramic nanoparticles, including $PbZrTiO_3$ (PZT), $PbTiO_3$ (PTO), $BaTiO_3$ (BTO), $(Ba,Sr)TiO_3$ (BST),

have been incorporated into the PVDF polymer matrix to investigate their electrical properties and to check their suitability in high-energy-density capacitor applications [63,88,98]. Table 1.3 provides the results for the dielectric constant (ε'), tangent loss (tan δ), discharging energy density (U_D) and breakdown strength (BDS) of PVDF polymer-based nanocomposites.

Table 1.3 Comparative table for PVDF-based nanocomposites

Sample	Loading	ε' at 1 kHz	tanδ at 1 kHz	U_D (J/cc)	BDS	Ref.
PVDF/PZT	20wt%	28	0.02	14	1.8 MV/cm	[73]
PVDF/CCTO	4vol%	12	0.03	0.2	-	[63]
PVDF/BT	10wt%	19.4	0.07	4.12	389 MV/m	[99]
PVDF/BST	7.5vol%	22	0.05	6.95	311 MV/m	[100]
PVDF/BF	5wt%	15	0.04	1.15	1000 kV/cm	[101]

1.5 Polyvinylidene fluoride (PVDF)-based nanocomposites

A composite material is created by blending two or more components in such a way that it exhibits a unified set of properties derived from the diverse characteristics of these components.

Fig.: 1.9 (a, b) Surface field emission scanning electron microscope (FESEM) image and (c) cross-sectional FESEM image of PVDF-BST trilayered nanocomposite with 3 vol% loading [102]

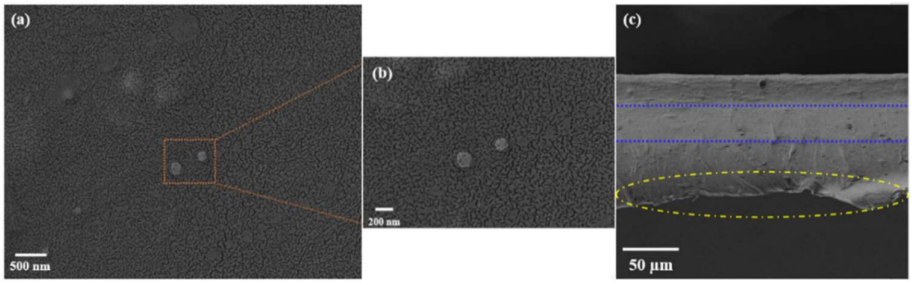

In this context, low dielectric constant polymers (such as PVDF) and high dielectric constant ceramics (such as BST) have been combined. This blending process results in the formation of films that possess a high dielectric constant, low tangent loss and high dielectric breakdown strength [68,69]. During the synthesis of nanocomposites, one important factor is the careful adjustment and measurement of the nanoparticle-to-polymer ratio. An excessive amount of polymer can lead to a situation where the benefits of enhanced dielectric properties

are diminished. One way of checking the dispersion quality can be by using scanning electron microscopy, as shown in Fig. 1.9, which shows a multilayered PVDF-BST nanocomposite thick film with no trace of agglomeration of the BST nanoparticles that are embedded in the PVDF polymer matrix. It can also be observed here that there is a diffusion of layers due to the hot-pressing process, and the bending of the film (marked in yellow) around the edge is observed due to the high power of the electron beam of the FESEM apparatus. The three-layer structure can be distinguished by the difference in the color contrast presented in the cross-sectional FESEM image of the PVDF-BST nanocomposite. This is because the top and bottom layers are cast in the same direction (dark in color) as compared to the middle layer, which is cast in the opposite direction (lighter in color) [102]. On the other hand, low polymer content can result in the incomplete suspension of the particles within the polymer matrix, leading to the formation of inconsistent and non-uniform films. Kim *et al.* [103] discovered that the highest dielectric constant in PVDF-$BaTiO_3$ thin films is achieved when using a ratio of 60% nanoparticles and 40% polymer, as shown in Fig. 1.10. However, it's worth noting that this combination also exhibits relatively high tangent loss, which is accompanied by a significant decrease in the dielectric constant as the frequency increased. Conversely, when the ratio is adjusted to 80% nanoparticles and 20% polymer, the overall dielectric constant is reduced compared to the 60% nanoparticle sample. However, this composition exhibited

Fig.: 1.10 Dielectric spectroscopy of PFBPA-BT:P(VDF-HFP) nanocomposites (a) dielectric constant and (b) loss tangent [103]

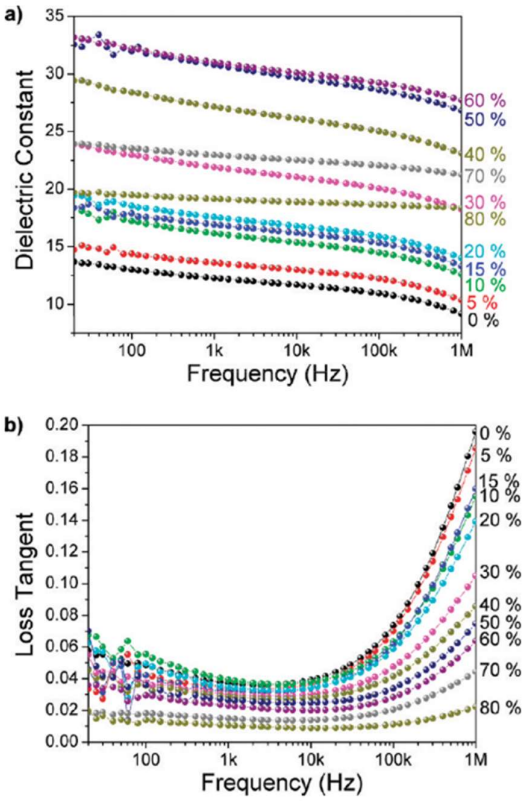

much greater stability up to 1 MHz and significantly lower tangent loss. It's important to emphasize that the ideal ratio may need to be adapted based on the size of the nanoparticles. This is because changes in particle size can affect the exposed surface area and overall density of the dipoles in the nanocomposite [104,105]. In Fig 1.10, the increase of tangent loss for frequencies >10 kHz is related to the segmental relaxation of polymeric chains i.e., α-relaxation and dipolar relaxation among the interfacial layers due to the developed local electric field [106]. The tangent loss of all the nanocomposites is higher at 100 Hz, which decreases with an increase in frequency (100 Hz-10 kHz). The high value of the tangent loss at 100 Hz is caused by the molecular motion of polymeric chains and the internal rotation of the crystal. A similar kind of observation is reported elsewhere [107,108].

Fig.: 1.11 The breakdown strengths at each volume fraction as determined from the Weibull analysis [103]

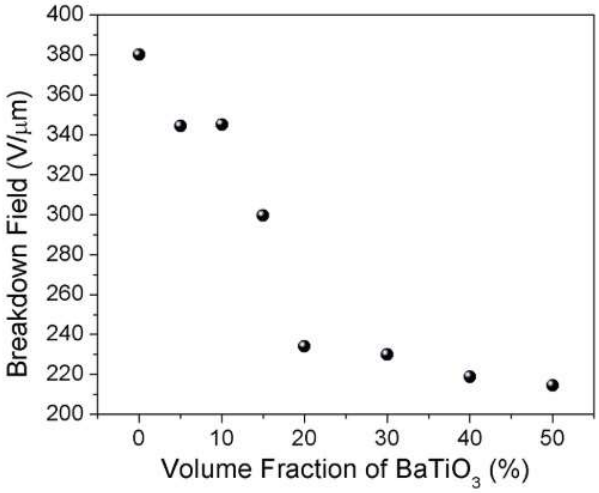

Moreover, the percolation threshold of ceramic nanoparticles in a polymer matrix is critical for understanding and enhancing the electric breakdown strength of polymer nanocomposites. When the nanoparticle concentration is below the percolation threshold, the electrical conductivity of the composite is negligible. However, as the concentration of nanoparticles surpasses the percolation threshold, the composite becomes electrically conductive due to the formation of a conductive pathway, as observed in Fig. 1.11. This is crucial in applications with high breakdown strength, such as high-voltage insulation materials or high-energy density capacitors. By carefully controlling the nanoparticle concentration and distribution in the polymer matrix, it is possible to optimize the electric breakdown strength of

the composite, making it a key factor in the development of advanced dielectric materials for various electrical and electronic applications.

Furthermore, the high-temperature use of polymer-ceramic nanocomposite thick films holds immense importance in addressing the growing demand for materials capable of withstanding extreme thermal conditions. As industries such as aerospace, automotive, energy, and electronics continue to push the boundaries of performance, the need for advanced materials that can work at elevated temperatures becomes increasingly critical [15,109,110]. Previous investigations have confirmed the significance of thermal stability concerning the dielectric behavior, specifically focusing on parameters such as dielectric constant and loss tangent. This emphasis on thermal stability is pivotal in the synthesis and design of polymer-ceramic nanocomposites tailored for high-energy density capacitors intended for utilization in elevated temperature environments and under harsh operating conditions [111,112]. Research groups around the world have studied polymer-ceramic nanocomposite films to fulfill this need by combining the unique attributes of polymers and ceramics, offering a versatile and robust solution. The electronics industry uses the high-temperature resistance of these films in the development of electronic components that operate

Fig.: 1.12 (i) Unipolar D-E loop (ii) Discharge energy density (iii) Energy efficiency under applied electric field of (a) PVDF-4CCTO, (b) PVDF-8CCTO, (c) PVDF-12CCTO and, (d) PVDF-15CCTO nanocomposite films [63]

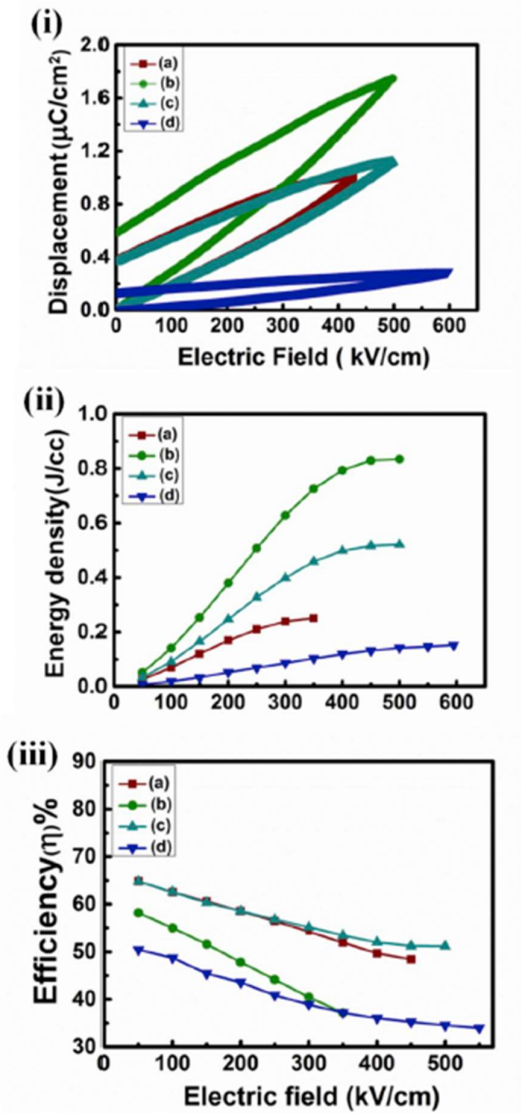

in demanding thermal environments. Their dielectric properties and thermal conductivity make them essential for high-temperature electronic circuitry, ensuring reliability and longevity [112–114].

On the other hand, polymer-ceramic nanocomposites have also emerged as an excellent choice for high-energy density capacitors, attributed to their moderate dielectric constant and impressive breakdown strength [68,69]. Several research groups have been working on the synthesis of polymer-ceramic nanocomposites with increased discharge energy density (U_D) and high breakdown strength (BDS) [99,115,116]. However, it is very important for polymer-ceramic nanocomposites to have both high efficiency (η) and discharge energy density for optimal performance in pulsed power as well as high-energy density capacitor applications. Generally, high discharge energy densities have been obtained in these nanocomposites by increasing the volume/weight percentage loading of ceramic nanoparticles. Yet, this approach often compromises the breakdown strength, which is detrimental to the overall energy storage behavior [60,117]. So, the main challenge lies in obtaining high discharge energy density with low hysteretic loss and good breakdown strength at a low loading of the ceramic nanofillers. The variation in energy storage properties of a PVDF polymer-based nanocomposite is shown in Fig. 1.12.

Though the dielectric properties, breakdown strength and energy storage properties of the dielectric polymer and ceramic nanocomposite are modified, but the extent of modification is influenced by various alterations in processing conditions and engineering of the nanocomposites, such as stretching/processing, functionalization, hierarchical engineering or multilayered structures. A brief discussion about these modifications is done in the subsequent section.

1.6 Strategies to improve the dielectric performance of polymer-ceramic nanocomposites

Apart from the choice of dielectric polymer matrix and ceramic nanofiller for making nanocomposites, the compatibility of ceramic nanoparticles with the PVDF matrix plays an important role. The modification in crystalline structure, morphological structure, dielectric behavior and energy storage behavior have been reported by several research groups. Some aspects of improving the compatibility between ceramic nanoparticles and polymer matrix have been summarized below. A comparative table showing the dielectric constant, tangent loss, breakdown strength (BDS) and discharge energy density with respect to the method type is given in Table 1.4.

Table 1.4 Comparative table for method-based nanocomposites

Method	Sample	Loading	ε' at 1 kHz	tanδ at 1 kHz	U_D (J/cc)	BDS	Ref.
Stretching/ processing	PVDF/GO	0.5 wt%	27	0.02	-	-	[118]
Functionalization	PVDF/BT	7.5 vol%	24	0.02	5.6	3300 kV/m	[119]
Hierarchical structure	PVDF/TiO_2-BT-TiO_2	10 vol%	12.6	0.03	4.4	3128 kV/cm	[55]
Multilayer structure	PVDF/BT	5 vol%	11	0.03	6.2	4474 kV/cm	[120]

a.) Stretching or processing: Stretching, or mechanical deformation, is employed to align and orient the polymer chains and nanoparticles within the composite structure. This process leads to improved crystallinity and alignment of the ferroelectric domains, resulting in enhanced dielectric properties such as permittivity and breakdown strength. The stretching-induced molecular orientation promotes better charge mobility and polarization behavior, thereby influencing the overall electrical response of the nanocomposite. This tailored approach to manipulating the material's structure through stretching not only contributes to the efficient utilization of the ferroelectric properties of ceramic nanoparticles but also enhances the overall dielectric performance of the polymer-ceramic nanocomposites [118,121,122].

Mishra *et al.* [118] observed that the mechanical stretching of PVDF-GO composites led to the development of polar β-phase structures due to the heightened stress concentration in the interfacial region. This further led to the improvement in dielectric constant (28.5 for PVDF-GO and 27.5 for PVDF-rGO) and reduced tangent loss (0.025 for PVDF-GO and 0.015 for PVDF-rGO) of such stretched PVDF polymer-based composites.

b.) Functionalization: Functionalization involves the introduction of specific functional groups onto the surface of ceramic nanoparticles or within the polymer matrix, as shown in Fig. 1.13. This modification enhances the compatibility between the polymer matrix and the ceramic filler, promoting a more uniform dispersion of nanoparticles and reducing aggregation. The improved dispersion leads to increased interfacial polarization, resulting in enhanced dielectric constant and reduced tangent loss in the nanocomposites. Additionally, functionalization can facilitate better interfacial interactions, allowing for the formation of a well-defined interface that mitigates charge carrier's scattering and leakage [123–125]. Liu *et al.* [119] reported that 3-aminopropyltriethoxysilane (APS) modified $BaTiO_3$ nanofibers could facilitate in the better dispersion of the $BaTiO_3$ nanofibers in the PVDF polymer matrix and strongly couple with the polymer matrix by chemical bonds in the interfacial layer. An energy density of 5.6 J/cc at 3000 kV/cm is observed for 2.5 vol% BT-NF-APS loading with an efficiency of 63.3%, along with a breakdown strength of 3300 kV/cm.

Fig.: 1.13 Schematic diagram illustrating hydroxylation of the BST–NPs and formation of a bond between the F atoms on the PVDF chains and the –OH groups on surface of the BST–NPs–OH [119]

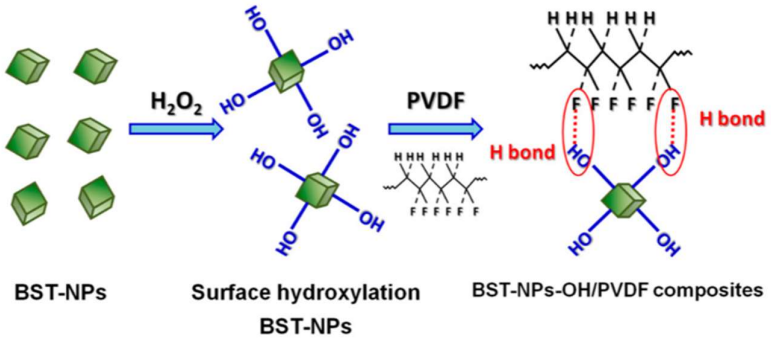

c.) Hierarchical structure: The hierarchical structural arrangement involves the incorporation of multi-level components, creating a synergistic effect that significantly improves the overall dielectric performance. At the microscale, the hierarchical arrangement ensures uniform dispersion of ceramic nanoparticles within the polymer matrix, promoting increased interfacial polarization and charge storage capabilities, as shown in Fig. 1.14. Furthermore, at the nanoscale, the specific orientation and alignment of the ceramic nanoparticles within the polymer chains contribute to the enhanced dielectric constant and reduced loss tangent. This hierarchical structure facilitates improved charge transport and storage, resulting in increased dielectric strength and enhanced energy storage capabilities in polymer-ceramic nanocomposites [55,126–128]. Prateek *et a*l. [55] constructed a hierarchical architecture of core multishell TiO_2−BT−TiO_2@dopa NPs as nanofillers to study the effect of interface modulation on the dielectric properties of the PVDF-polymer nanocomposite-based capacitors. The maximum energy density of 4.4 J/cm^3 is obtained, which is ascribed to the fact that each TiO_2−BT−TiO_2@dopa NP works as an individual capacitor with an improved interface surrounding the polymer matrix, resulting in improved dielectric performance as compared to that of PVDF. The breakdown strength of the nanocomposites improved to 3128 kV/cm, which is due to the formation of enclosed interfacial zones (TiO_2−BT and BT−TiO_2) and reduced leakage current, which helped in charge entrapment in both NPs and polymer matrix.

Fig.: 1.14 Schematic diagrams of hierarchical optimization and its contribution to energy storage properties [128]

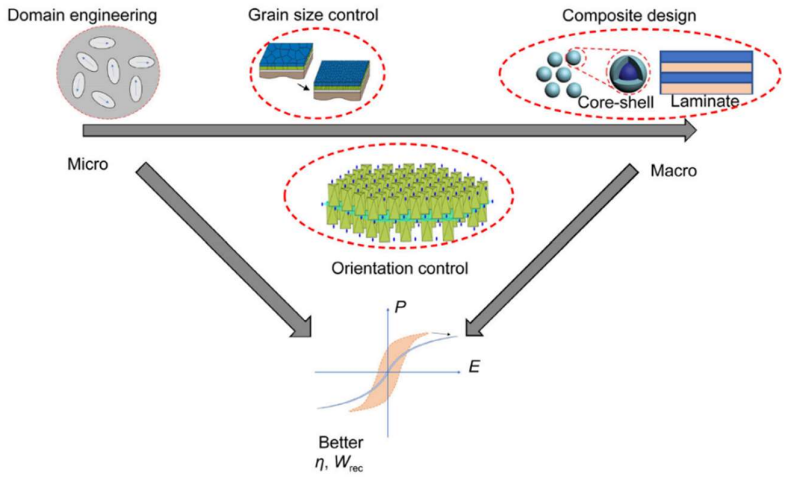

d.) Multilayered structure: The integration of a multilayered architecture in these nanocomposites offers several advantages that contribute to improved dielectric performance, as depicted by Fig. 1.15. Firstly, the multilayered structure provides a larger interfacial area between the polymer matrix and ceramic nanoparticles, promoting a more efficient interaction and distribution of the filler within the polymer matrix. This enhanced dispersion helps in reducing agglomeration, ensuring a more uniform distribution of the nanoparticles and preventing the formation of large clusters that could negatively impact dielectric properties. Additionally, the multilayered configuration may create interfaces with varying dielectric constants, leading to improved polarization and charge storage capabilities. This results in enhanced overall dielectric constant and reduced tangent loss, making multilayered nanocomposites promising materials for advanced electronic applications such as capacitors and energy storage devices [115,120,129,130]. Prateek *et al.* [120] studied the use of a polyvinylpyrrolidone (PVP) linker layer as an adhesive in multilayered $BaTiO_3$ nanofiber/PVDF nanocomposites and found that it improved the dielectric behavior and energy storage properties, which is caused by homogeneous surfaces due to the presence of the multilayer PVDF. A discharge energy density of 6.2 J/cc with a breakdown strength of 4474 kV/cm is observed for the multilayered nanocomposite structure. The integration of PVDF and $(Ba,Sr)TiO_3$ creates a synergistic approach and the exploration of the unique strengths of each material. PVDF, known for its high dielectric breakdown strength, contributes remarkable

Fig.: 1.15 Schematics of the interaction of PVP with the top and bottom layers of PVDF leading to an enhancement in the energy storage properties [120]

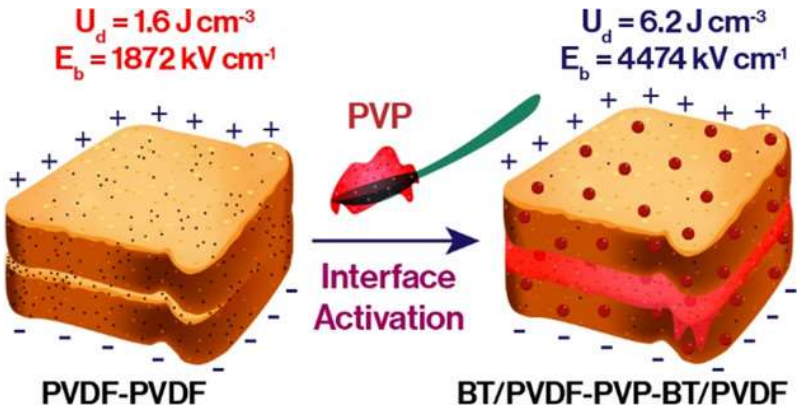

flexibility and processability, while (Ba,Sr)TiO_3 brings tunable dielectric properties to the composite. This combination not only increases the dielectric performance but also opens the doors for tailored applications, as this type of composite holds the promise of achieving high energy density in capacitors, addressing the escalating need for efficient energy storage solutions in contemporary electronic devices. The inherent thermal stability of PVDF, further improved by (Ba,Sr)TiO_3, ensures reliable performance even under harsh environmental conditions. These observations lead to the motivation of the thesis, which is given in the following section.

1.7 Motivation of thesis

The attainment of high dielectric constant, high breakdown strength and low tangent loss in the dielectric polymer ceramic nanocomposites at low volume percentage loading of the ceramic nanofiller is still challenging. The interfacial modification of the polymer/ceramic interface in the polymer ceramic nanocomposites by the various processes such as surface functionalization and by developing specially architectured structures has been found to lead towards improved direlectric and energy storage behavior. Apart from interfacial processing, the choice of ceramic nanofillers is also important for achieving the good dielectric properties.

The inherent nature of (Ba,Sr)TiO_3 materials, characterized by a notably high dielectric constant over a wider frequency range, contributes to reduced energy loss in the polyvinylidene fluoride-(Ba,Sr)TiO_3 nanocomposites, which may enhance the energy efficiency. Additionally, the ceramic filler's size and concentration in the polymer matrix should be minimized to as low as possible for maintaining breakdown and mechanical strength in the nanocomposites. A comprehensive and analytical investigation of the dielectric and energy storage characteristics of this nanocomposite holds significant importance for academic, scientific, and technological communities. Therefore, the incorporation of (Ba,Sr)TiO_3 (BST) nanoparticles in the

polyvinylidene fluoride (PVDF) matrix could lead towards promising nanocomposites for developing the high-energy density capacitors and pulsed power applications.

Taking the existing aspect of the physical parameters, the thesis aims to achieve the following objectives:

1) To synthesize and characterize the $(Ba,Sr)TiO_3$ (BST) nanoparticles.
2) To investigate the energy storage behavior of PVDF-BST nanocomposites.
3) To investigate the effect of surface functionalization of BST on the dielectric behavior of PVDF-BST nanocomposites.

References

[1] L. Singh, U.S. Rai, K.D. Mandal, B.C. Sin, H. Il Lee, H. Chung, Y. Lee, Comparative dielectric studies of nanostructured BaTiO3, CaCu3Ti4O12 and 0.5BaTiO3· 0.5CaCu3Ti4O12 nano-composites synthesized by modified sol-gel and solid state methods, Mater Charact 96 (2014) 54–62. https://doi.org/10.1016/j.matchar.2014.07.019.

[2] H.Y. Lee, K.H. Cho, H.D. Nam, Grain size and temperature dependence of electrical breakdown in BaTiO3 ceramic, in: Ferroelectrics, 2006: pp. 165–169. https://doi.org/10.1080/00150190600694415.

[3] X. Wei, X. Yao, Nonlinear dielectric properties of barium strontium titanate ceramics, Materials Science and Engineering B 99 (2003) 74–78. https://doi.org/10.1016/S0921-5107(02)00423-3.

[4] Q. Hu, T. Wang, L. Jin, X. Wei, Dielectric and energy storage properties of barium strontium titanate based glass-ceramics prepared by sol-gel method, J Solgel Sci Technol 71 (2014) 522–529. https://doi.org/10.1007/s10971-014-3403-8.

[5] R. Wongmaneerung, S. Choopan, R. Yimnirun, S. Ananta, Dielectric properties of PbTiO3/ZnO ceramic nanocomposites obtained by solid-state reaction method, J Alloys Compd 509 (2011) 3547–3552. https://doi.org/10.1016/j.jallcom.2010.12.024.

[6] K.R. Udayakumar, P.J. Schuele, J. Chen, S.B. Krupanidhi, L.E. Cross, Thickness-dependent electrical characteristics of lead zirconate titanate thin films, J Appl Phys 77 (1995) 3981–3986. https://doi.org/10.1063/1.359508.

[7] X. Dong, B. Lee, A. Ghulam, J. Akedo, H.K. Yu, J.Y. Choi, J.H. Park, Dielectric properties of lead zirconate titanate/Au composite film prepared by aerosol deposition, Mater Chem Phys 284 (2022). https://doi.org/10.1016/j.matchemphys.2022.126078.

[8] R. Moazzami, C. Hu, W.H. Shepherd, Electrical Characteristics of Ferroelectric PZT Thin Films for DRAM Applications, 1992.

[9] J. Zhang, W. Lu, R. Hao, S. Guo, Z. Lei, Y. Li, M. Tian, Microstructure and dielectric properties of CaCu3Ti4O12 ceramics with high breakdown field strength prepared via polymer pyrolysis, Mater Res Bull 155 (2022) 111946.

[10] H.P. Palani Velayuda Shanmugasundram, E. Jayamani, K.H. Soon, A comprehensive review on dielectric composites: Classification of dielectric composites, Renewable and Sustainable Energy Reviews 157 (2022). https://doi.org/10.1016/j.rser.2022.112075.

[11] S. Huang, K. Liu, W. Zhang, B. Xie, Z. Dou, Z. Yan, H. Tan, C. Samart, S. Kongparakul, N. Takesue, H. Zhang, All-Organic Polymer Dielectric Materials for Advanced Dielectric Capacitors: Theory, Property, Modified Design and Future Prospects, Polymer Reviews (2022) 1–59. https://doi.org/10.1080/15583724.2022.2129680.

[12] F. Liu, Q. Li, J. Cui, Z. Li, G. Yang, Y. Liu, L. Dong, C. Xiong, H. Wang, Q. Wang, High-Energy-Density Dielectric Polymer Nanocomposites with Trilayered Architecture, Adv Funct Mater 27 (2017). https://doi.org/10.1002/adfm.201606292.

[13] Q. Li, K. Han, M.R. Gadinski, G. Zhang, Q. Wang, High Energy and Power Density Capacitors from Solution-Processed Ternary Ferroelectric Polymer Nanocomposites, Advanced Materials 26 (2014) 6244–6249. https://doi.org/10.1002/adma.201402106.

[14] M.I.A. Abdel Maksoud, M. Bekhit, A.L. Waly, A.S. Awed, Optical and dielectric properties of polymer nanocomposite based on PVC matrix and Cu/Cu2O nanorods synthesized by gamma irradiation for energy storage applications, Physica E Low Dimens Syst Nanostruct 148 (2023) 115661. https://doi.org/10.1016/j.physe.2023.115661.

[15] Faiza, A. Khattak, A.A. Alahmadi, H. Ishida, N. Ullah, Improved PVC/ZnO Nanocomposite Insulation for High Voltage and High Temperature Applications, Sci Rep 13 (2023). https://doi.org/10.1038/s41598-023-31473-3.

[16] M. Kubin, P. Makreski, M. Zanoni, L. Gasperini, G. Selleri, D. Fabiani, C. Gualandi, A. Bužarovska, Effects of nano-sized BaTiO3 on microstructural, thermal, mechanical and piezoelectric behavior of electrospun PVDF/BaTiO3 nanocomposite mats, Polym Test 126 (2023) 108158. https://doi.org/10.1016/j.polymertesting.2023.108158.

[17] I. Vanskevičė, M.A. Kazakova, J. Macutkevic, N. V. Semikolenova, J. Banys, Dielectric Properties of Hybrid Polyethylene Composites Containing Cobalt Nanoparticles and Carbon Nanotubes, Materials 15 (2022) 1876. https://doi.org/10.3390/ma15051876.

[18] J. Hu, L. Zhang, Z.M. Dang, D. Wang, Improved dielectric properties of polypropylene-based nanocomposites via co-filling with zinc oxide and barium titanate, Compos Sci Technol 148 (2017) 20–26. https://doi.org/10.1016/j.compscitech.2017.05.009.

[19] N. Yadav, N. Yadav, S.A. Hashmi, High-Energy-Density Carbon Supercapacitors Incorporating a Plastic-Crystal-Based Nonaqueous Redox-Active Gel Polymer Electrolyte, ACS Appl Energy Mater 4 (2021) 6635–6649. https://doi.org/10.1021/acsaem.1c00703.

[20] M. Peddigari, B. Wang, R. Wang, W. Yoon, J. Jang, H. Lee, K. Song, G. Hwang, K. Wang, Y. Hou, H. Palneedi, Y. Yan, H.S. Choi, J. Wang, A. Talluri, L. Chen, S. Priya, D. Jeong, J. Ryu, Giant Energy Density via Mechanically Tailored Relaxor Ferroelectric Behavior of Pzt Thick Film, Advanced Materials (2023). https://doi.org/10.1002/adma.202302554.

[21] L. Chen, F. Li, B. Gao, C. Zhou, J. Wu, S. Deng, H. Liu, H. Qi, J. Chen, Excellent energy storage and mechanical performance in hetero-structure BaTiO3-based relaxors, Chemical Engineering Journal 452 (2023). https://doi.org/10.1016/j.cej.2022.139222.

[22] W. Huang, Y. Chen, X. Li, G. Wang, N. Liu, S. Li, M. Zhou, X. Dong, Ultrahigh recoverable energy storage density and efficiency in barium strontium titanate-based lead-free relaxor ferroelectric ceramics, Appl Phys Lett 113 (2018). https://doi.org/10.1063/1.5054000.

[23] F. Ali, D. Zhou, M. Ali, H.W. Ali, M. Daaim, S. Khan, M.M. Hussain, N. Sun, Recent Progress on Energy-Related Applications of HfO2-Based Ferroelectric and Antiferroelectric Materials, ACS Appl Electron Mater 2 (2020) 2301–2317. https://doi.org/10.1021/acsaelm.0c00304.

[24] S. Kaur, A. Kumar, A.L. Sharma, D.P. Singh, Dielectric and energy storage behavior of CaCu 3 Ti 4 O 12 nanoparticles for capacitor application, Ceram Int 45 (2019) 7743–7747. https://doi.org/10.1016/j.ceramint.2019.01.077.

[25] J. Jyoti, A. Kumar, S.R. Dhakate, B.P. Singh, Dielectric and impedance properties of three dimension graphene oxide-carbon nanotube acrylonitrile butadiene styrene hybrid composites, Polym Test 68 (2018) 456–466. https://doi.org/10.1016/j.polymertesting.2018.04.003.

[26] P. Chutia, A. Kumar, Dielectric and conductivity relaxation in poly(3,4-ethylenedioxythiophene) nanotubes, Polym Eng Sci 56 (2016) 448–457. https://doi.org/10.1002/pen.24271.

[27] A.H. M., S.C. Karumuthil, L. Rajan, Optimization of PVDF nanocomposite based flexible piezoelectric tactile sensors: A comparative investigation, Sens Actuators A Phys 353 (2023). https://doi.org/10.1016/j.sna.2023.114215.

[28] B. Stadlober, M. Zirkl, M. Irimia-Vladu, Route towards sustainable smart sensors: ferroelectric polyvinylidene fluoride-based materials and their integration in flexible electronics, Chem Soc Rev 48 (2019) 1787–1825. https://doi.org/10.1039/C8CS00928G.

[29] X. Ma, J. Liu, S. Zhang, J. Deng, Y. Liu, Recent trends in bionic stepping piezoelectric actuators for precision positioning: A review, Sens Actuators A Phys 364 (2023) 114830. https://doi.org/10.1016/j.sna.2023.114830.

[30] J. Nunes-Pereira, V. Sencadas, V. Correia, J.G. Rocha, S. Lanceros-Méndez, Energy harvesting performance of piezoelectric electrospun polymer fibers and polymer/ceramic composites, Sens Actuators A Phys 196 (2013) 55–62. https://doi.org/10.1016/j.sna.2013.03.023.

[31] S. Nair, A. Hamrah, R.B. Raj, M. Kathiresan, T. Mukundan, Fabrication of organic thin film transistors for application in flexible sensors, in: AIP Conf Proc, 2019: p. 070008. https://doi.org/10.1063/1.5093883.

[32] Q.-J. Sun, T. Li, W. Wu, S. Venkatesh, X.-H. Zhao, Z.-X. Xu, V.A.L. Roy, Printed High- k Dielectric for Flexible Low-Power Extended Gate Field-Effect Transistor in Sensing Pressure, ACS Appl Electron Mater (2019) acsaelm.9b00081. https://doi.org/10.1021/acsaelm.9b00081.

[33] Prateek, V.K. Thakur, R.K. Gupta, Recent Progress on Ferroelectric Polymer-Based Nanocomposites for High Energy Density Capacitors: Synthesis, Dielectric Properties, and Future Aspects, Chem Rev 116 (2016) 4260–4317. https://doi.org/10.1021/acs.chemrev.5b00495.

[34] S. Peng, X. Du, Z. Liang, M. Ma, Y. Guo, L. Xiong, Multilayer polymer nanocomposites based on interface engineering for high-performance capacitors, J Energy Storage 60 (2023). https://doi.org/10.1016/j.est.2023.106636.

[35] C. V. Chanmal, J.P. Jog, Study of dielectric behavior in PVDF/clay nanocomposites, E-Polymers (2009) 1–8. https://doi.org/10.1515/epoly.2009.9.1.1333.

[36] W. Xia, Z. Zhang, PVDF-based dielectric polymers and their applications in electronic materials, IET Nanodielectrics 1 (2018) 17–31. https://doi.org/10.1049/iet-nde.2018.0001.

[37] S.S. Chen, J. Hu, L. Gao, Y. Zhou, S.M. Peng, J.L. He, Z.M. Dang, Enhanced breakdown strength and energy density in PVDF nanocomposites with functionalized MgO nanoparticles, RSC Adv 6 (2016) 33599–33605. https://doi.org/10.1039/c6ra01869f.

[38] N. Meng, X. Zhu, R. Mao, M.J. Reece, E. Bilotti, Nanoscale interfacial electroactivity in PVDF/PVDF-TrFE blended films with enhanced dielectric and ferroelectric properties, J Mater Chem C Mater 5 (2017) 3296–3305. https://doi.org/10.1039/c7tc00162b.

[39] X. Jiang, R. Guo, H. Wang, Z. Gao, H. Luo, L. Liu, D. Zhang, Significantly Improved Dielectric Breakdown Strength and Energy Density in P (VDF-TrFE-CTFE) Polymer via a Facile Uniaxial Drawing Process, ACS Appl Polym Mater 4 (2022) 4741–4750.

[40] Z. Xie, D. Liu, X. Tang, Z. Fu, K. Wang, Q. Zhang, J. Wang, Q. Fu, Largely improved dielectric energy performances and safety of BOPP film via surface engineering, Compos Sci Technol (2022) 109856. https://doi.org/10.1016/j.compscitech.2022.109856.

[41] J. Lu, B. Zhu, X. Zhang, X. Wang, Dielectric Strength Structure-Activity Relationship of BOPP Film for High Energy Density Pulse Capacitor, IEEE Transactions on Plasma Science 47 (2019) 4342–4349. https://doi.org/10.1109/TPS.2019.2934762.

[42] V. Sanjay, K.M. Rajashekara, J. Johns, V. Pattar, The dielectric and impedance spectroscopy of poly vinyl alcohol doped with carbon (PVA-C), Physica B Condens Matter 650 (2023) 414561. https://doi.org/10.1016/j.physb.2022.414561.

[43] E. Tuncer, I. Sauers, D.R. James, A.R. Ellis, Dielectric properties of polyvinyl alcohol, poly(methyl methacrylate), polyvinyl butyral resin and polyimide at low temperatures, in: AIP Conf Proc, 2008: pp. 190–195. https://doi.org/10.1063/1.2900345.

[44] M.E. Ibrahim, M.A. Taman, M.A. Izzularab, A.M. Abd-Elhady, Effect of external electric field during sample preparation on dielectric properties of PVC nanocomposites, Electrical Engineering (2022). https://doi.org/10.1007/s00202-022-01708-z.

[45] Y. Feng, L. Liu, H. Qiu, M. Bo, W. Duan, Q. Deng, Obtaining high dielectric constant and breakdown strength in composites with asymmetric MXene filler and highly insulative PVC matrix, Surfaces and Interfaces 32 (2022). https://doi.org/10.1016/j.surfin.2022.102133.

[46] C.L. Cramer, E. Ionescu, M. Graczyk-Zajac, A.T. Nelson, Y. Katoh, J.J. Haslam, L. Wondraczek, T.G. Aguirre, S. LeBlanc, H. Wang, M. Masoudi, E. Tegeler, R. Riedel, P. Colombo, M. Minary-Jolandan, Additive manufacturing of ceramic materials for energy applications: Road map and opportunities, J Eur Ceram Soc 42 (2022) 3049–3088. https://doi.org/10.1016/j.jeurceramsoc.2022.01.058.

[47] L. Chen, H. Liu, H. Qi, J. Chen, High-electromechanical performance for high-power piezoelectric applications: Fundamental, progress, and perspective, Prog Mater Sci 127 (2022). https://doi.org/10.1016/j.pmatsci.2022.100944.

[48] Z. Yi, Z. Wang, Y. Li, D. Wu, Y. Xue, Tunable BaxSr1-xTiO3 nanoparticles induced high energy storage density in layer-structured asymmetric polymer-based nanocomposites, Ceram Int 48 (2022) 36620–36628. https://doi.org/10.1016/j.ceramint.2022.08.221.

[49] H. Chen, Z. Pan, W. Wang, Y. Chen, S. Xing, Y. Cheng, X. Ding, J. Liu, J. Zhai, J. Yu, Ultrahigh discharge efficiency and improved energy density in polymer-based nanocomposite for high-temperature capacitors application, Compos Part A Appl Sci Manuf 142 (2021). https://doi.org/10.1016/j.compositesa.2020.106266.

[50] H. Liu, J. Chen, J. Wang, Y. Sun, C. Wang, P. Zhang, Z. Shen, X. Zhang, B.W. Li, C.W. Nan, S. Zhang, Greatly enhanced energy density in polymer nanocomposites coated with high-k perovskite nanosheets, Mater Today Energy 31 (2023). https://doi.org/10.1016/j.mtener.2022.101213.

[51] M. Yang, W. Ren, M. Guo, Y. Shen, High-Energy-Density and High Efficiency Polymer Dielectrics for High Temperature Electrostatic Energy Storage: A Review, Small 18 (2022). https://doi.org/10.1002/smll.202205247.

[52] Z. Pan, L. Yao, J. Zhai, D. Fu, B. Shen, H. Wang, High-energy-density polymer nanocomposites composed of newly structured one-dimensional BaTiO3@Al2O3 nanofibers, ACS Appl Mater Interfaces 9 (2017) 4024–4033. https://doi.org/10.1021/acsami.6b13663.

[53] R. Qiao, C. Wang, S. Chen, G. He, Z. Liu, H. Luo, D. Zhang, High-temperature dielectric polymers with high breakdown strength and energy density via constructing the electron traps in blends, Compos Part A Appl Sci Manuf 152 (2022). https://doi.org/10.1016/j.compositesa.2021.106679.

[54] P. Saxena, P. Shukla, M.S. Gaur, Dielectric behavior and structural characterization of polymeric double layer thin films, J Appl Polym Sci 47724 (2019) 47724. https://doi.org/10.1002/app.47724.

[55] Prateek, R. Bhunia, S. Siddiqui, A. Garg, R.K. Gupta, Significantly Enhanced Energy Density by Tailoring the Interface in Hierarchically Structured TiO2-BaTiO3-TiO2 Nanofillers in PVDF-Based Thin-Film Polymer Nanocomposites, ACS Appl Mater Interfaces 11 (2019) 14329–14339. https://doi.org/10.1021/acsami.9b01359.

[56] J. Zou, H. Wang, Z. Shi, X. Hao, D. Yan, Z. Cui, Development of High- k Polymer Materials for Use as Dielectric Layer in the Organic Thin Film Transistors, The Journal of Physical Chemistry C (2019) acs.jpcc.9b00682. https://doi.org/10.1021/acs.jpcc.9b00682.

[57] X. Cai, T. Lei, D. Sun, L. Lin, A critical analysis of the α, β and γ phases in poly(vinylidene fluoride) using FTIR, RSC Adv 7 (2017) 15382–15389. https://doi.org/10.1039/c7ra01267e.

[58] Y. Li, C. Liao, S.C. Tjong, Electrospun polyvinylidene fluoride-based fibrous scaffolds with piezoelectric characteristics for bone and neural tissue engineering, Nanomaterials 9 (2019). https://doi.org/10.3390/nano9070952.

[59] A. Veved, G.W. Ejuh, N. Djongyang, Review of emerging materials for PVDF-based energy harvesting, Energy Reports 8 (2022) 12853–12870. https://doi.org/10.1016/j.egyr.2022.09.076.

[60] X. Lu, L. Zhang, Y. Tong, Z.Y. Cheng, BST-P(VDF-CTFE) nanocomposite films with high dielectric constant, low dielectric loss, and high energy-storage density, Compos B Eng 168 (2019) 34–43. https://doi.org/10.1016/j.compositesb.2018.12.059.

[61] Z. Song, H. Liu, M.T. Lanagan, S. Zhang, H. Hao, M. Cao, Z. Yao, Z. Fu, K. Huang, Thermal annealing effects on the energy storage properties of BST ceramics, Journal of the American Ceramic Society 100 (2017) 3550–3557. https://doi.org/10.1111/jace.14903.

[62] S. Jaidka, S. Chopra, A. Aggarwal, D.P. Singh, Effect of interfacial layers on the temperature-dependent dielectric and impedance behavior of flexible PVDF-BST nanocomposite thick films, Journal of Physics and Chemistry of Solids 184 (2024) 111667. https://doi.org/10.1016/j.jpcs.2023.111667.

[63] S. Kaur, D.P. Singh, On the structural, dielectric and energy storage behaviour of PVDF- CaCu3Ti4O12 nanocomposite films, Mater Chem Phys 239 (2020) 122301. https://doi.org/10.1016/j.matchemphys.2019.122301.

[64] Q.K. Feng, J.B. Ping, J. Zhu, J.Y. Pei, L. Huang, D.L. Zhang, Y. Zhao, S.L. Zhong, Z.M. Dang, All-Organic Dielectrics with High Breakdown Strength and Energy Storage Density for High-Power Capacitors, Macromol Rapid Commun 42 (2021). https://doi.org/10.1002/marc.202100116.

[65] L. Chen, S. Deng, H. Liu, J. Wu, H. Qi, J. Chen, Giant energy-storage density with ultrahigh efficiency in lead-free relaxors via high-entropy design, Nat Commun 13 (2022). https://doi.org/10.1038/s41467-022-30821-7.

[66] G. Wang, Z. Lu, Y. Li, L. Li, H. Ji, A. Feteira, D. Zhou, D. Wang, S. Zhang, I.M. Reaney, Electroceramics for High-Energy Density Capacitors: Current Status and Future Perspectives, Chem Rev 121 (2021) 6124–6172. https://doi.org/10.1021/acs.chemrev.0c01264.

[67] B. Liu, M. Yang, W.Y. Zhou, H.W. Cai, S.L. Zhong, M.S. Zheng, Z.M. Dang, High energy density and discharge efficiency polypropylene nanocomposites for potential high-power capacitor, Energy Storage Mater 27 (2020) 443–452. https://doi.org/10.1016/j.ensm.2019.12.006.

[68] X. Hu, Y. Zhou, J. Liu, B. Chu, Improved flexoelectricity in PVDF/barium strontium titanate (BST) nanocomposites, J Appl Phys 123 (2018) 154101. https://doi.org/10.1063/1.5022650.

[69] Y. Xie, W. Jiang, T. Fu, J. Liu, Z. Zhang, S. Wang, Achieving High Energy Density and Low Loss in PVDF/BST Nanodielectrics with Enhanced Structural Homogeneity, ACS Appl Mater Interfaces 10 (2018) 29038–29047. https://doi.org/10.1021/acsami.8b10354.

[70] H. Zhang, Z. Zhu, Z. Yao, H. Hao, L. Wang, M. Cao, H. Liu, On the Enhancement of Energy Storage Performance in Modified Relaxor Ferroelectric Ceramics for Pulsed Power Applications, Crystals (Basel) 13 (2023) 84. https://doi.org/10.3390/cryst13010084.

[71] Z. Li, D.X. Li, Z.Y. Shen, X. Zeng, F. Song, W. Luo, X. Wang, Z. Wang, Y. Li, Remarkably enhanced dielectric stability and energy storage properties in BNT—BST relaxor ceramics by A-site defect engineering for pulsed power applications, Journal of Advanced Ceramics 11 (2022) 283–294. https://doi.org/10.1007/s40145-021-0532-8.

[72] M. Feng, Y. Feng, T. Zhang, J. Li, Q. Chen, Q. Chi, Q. Lei, Recent Advances in Multilayer-Structure Dielectrics for Energy Storage Application, Advanced Science 2102221 (2021) 2102221. https://doi.org/10.1002/advs.202102221.

[73] P. Singh, H. Borkar, B.P. Singh, V.N. Singh, A. Kumar, Ferroelectric polymer-ceramic composite thick films for energy storage applications, AIP Adv 4 (2014). https://doi.org/10.1063/1.4892961.

[74] B. Mahale, D. Bodas, S.A. Gangal, Study of β-phase development in spin-coated PVDF thick films, Bulletin of Materials Science 40 (2017) 569–575. https://doi.org/10.1007/s12034-017-1390-4.

[75] I.O. Pariy, A.A. Ivanova, V.V. Shvartsman, D.C. Lupascu, G.B. Sukhorukov, M.A. Surmeneva, R.A. Surmenev, Poling and annealing of piezoelectric Poly(Vinylidene fluoride) micropillar arrays, Mater Chem Phys 239 (2020) 122035. https://doi.org/10.1016/j.matchemphys.2019.122035.

[76] A. Abdelaziem, A.M. Mohamed, Y.M. Yousry, R. Borayek, A.S. Razeen, N. Zhang, S. Chen, L. Zhang, K. Lin, Z. Liu, Effect of poling on the dielectric properties of synthesized β-poly (vinylidene fluoride) foam, J Appl Phys 133 (2023). https://doi.org/10.1063/5.0132002.

[77] S. Jaidka, A. Aggarwal, S. Chopra, D.P. Singh, Significantly Enhanced Dielectric Behavior of Polyvinylidene Fluoride-Barium Strontium Titanate Flexible Nanocomposite Thick Films: Role of Electric Field-Induced Effects, J Electron Mater 51 (2022) 5429–5439. https://doi.org/10.1007/s11664-022-09784-4.

[78] S. Kaur, A.L. Sharma, A. Kumar, D.P. Singh, Enhanced dielectric properties of the poly(vinylidene fluoride)-CaCu3Ti4O12 nanocomposite thick films by quenching in ice water, Mater Chem Phys 254 (2020). https://doi.org/10.1016/j.matchemphys.2020.123530.

[79] D. Thuau, K. Kallitsis, S. Ha, F. Bargain, T. Soulestin, G. Pecastaings, S. Tencé-Girault, F. Domingues Dos Santos, G. Hadziioannou, High and Temperature-Independent Dielectric Constant Dielectrics from PVDF-Based Terpolymer and Copolymer Blends, Adv Electron Mater 6 (2020). https://doi.org/10.1002/aelm.201901250.

[80] N.D. Kulkarni, P. Kumari, Development of highly flexible PVDF-TiO2 nanocomposites for piezoelectric nanogenerator applications, Mater Res Bull 157 (2023). https://doi.org/10.1016/j.materresbull.2022.112039.

[81] J. Li, Q. Meng, W. Li, Z. Zhang, Influence of crystalline properties on the dielectric and energy storage properties of poly(vinylidene fluoride), J Appl Polym Sci 122 (2011) 1659–1668. https://doi.org/10.1002/app.34020.

[82] T. Tanaka, Dielectric nanocomposites with insulating properties, in: IEEE Transactions on Dielectrics and Electrical Insulation, 2005: pp. 914–928. https://doi.org/10.1109/TDEI.2005.1522186.

[83] T. Tanaka, M. Kozako, N. Fuse, Y. Ohki, Proposal of a multi-core model for polymer nanocomposite dielectrics, IEEE Transactions on Dielectrics and Electrical Insulation 12 (2005) 669–681. https://doi.org/10.1109/TDEI.2005.1511092.

[84] M. Desmond, N. Mavrogiannis, Z. Gagnon, Maxwell-Wagner polarization and frequency-dependent injection at aqueous electrical interfaces, Phys Rev Lett 109 (2012). https://doi.org/10.1103/PhysRevLett.109.187602.

[85] S. Satapathy, S. Pawar, P.K. Gupta, B.R. Varma, Effect of annealing on phase transition in poly(vinylidene fluoride) films prepared using polar solvent, 2011.

[86] H. Tang, H.A. Sodano, Ultra high energy density nanocomposite capacitors with fast discharge using Ba0.2Sr0.8TiO3 nanowires, Nano Lett 13 (2013) 1373–1379. https://doi.org/10.1021/nl3037273.

[87] T. Garg, N. Dabra, J.S. Hundal, Dielectric Switching and Ferroelectric Studies of α, γ PVDF Phases for Energy Storage Properties, Integrated Ferroelectrics 231 (2023) 142–152. https://doi.org/10.1080/10584587.2022.2143190.

[88] E. O.Taha, H.A. Alyousef, A.M. Dorgham, O.M. Hemeda, H.M.H. Zakaly, P. Noga, M.M. Abdelhamied, M.M. Atta, Electron beam irradiation and carbon nanotubes influence on PVDF-PZT composites for energy harvesting and storage applications: changes in dynamic-mechanical and dielectric properties, Inorg Chem Commun (2023) 110624. https://doi.org/10.1016/j.inoche.2023.110624.

[89] M. Arjun Hari, K. Rakesh, R.S. Divya, L. Rajan, C.K. Subash, S. Varghese, Influence of Nanosilica in PVDF Thin Films for Sensing Applications, in: 2021 IEEE International Symposium on Smart Electronic Systems (ISES) (Formerly INiS), IEEE, 2021: pp. 70–73. https://doi.org/10.1109/iSES52644.2021.00027.

[90] N.D. Patel, M.H. Mangrola, K.G. Soni, V.G. Joshi, Structural and Electrical Properties of Nanocrystalline Barium Strontium Titanate, Mater Today Proc 4 (2017) 3842–3851. https://doi.org/10.1016/j.matpr.2017.02.282.

[91] D. Gao, D. Xiao, J. Bi, P. Yu, G. Yu, W. Zhang, J. Zhu, Hydrothermal Syntheses of Barium Strontium Titanate Thin Films, Mater Trans 44 (2003) 1320–1323. https://doi.org/10.2320/matertrans.44.1320.

[92] A.M. Henaish, M. Mostafa, I. Weinstein, O. Hemeda, B. Salem, Ferroelectric and Dielectric Properties of Strontium Titanate Doped with Barium, Magnetism 1 (2021) 22–36. https://doi.org/10.3390/magnetism1010003.

[93] Z.-X. Chen, J.-L. Sun, Q. Zhang, C.-X. Qian, M.-Z. Wang, H.-J. Feng, Ferroelectric Ba0.75Sr0.25TiO3 tunable charge transfer in perovskite devices, Chinese Physics B (2021). https://doi.org/10.1088/1674-1056/ac46c3.

[94] W. Du, H. Zeng, W. Yang, K. Zhao, F. Zhang, G. Li, Y. Li, Z. Liu, Unusual local electric field concentration in multilayer ceramic capacitors, Journal of Materiomics (2022). https://doi.org/10.1016/j.jmat.2022.09.010.

[95] P. Zhao, Z. Cai, L. Wu, C. Zhu, L. Li, X. Wang, Perspectives and challenges for lead-free energy-storage multilayer ceramic capacitors, Journal of Advanced Ceramics 10 (2021) 1153–1193. https://doi.org/10.1007/s40145-021-0516-8.

[96] L. Shu, T. Wang, X. Jiang, W. Huang, Verification of the flexoelectricity in barium strontium titanate through d33 meter, AIP Adv 6 (2016). https://doi.org/10.1063/1.4968524.

[97] L. Yao, Z. Pan, J. Zhai, G. Zhang, Z. Liu, Y. Liu, High-energy-density with polymer nanocomposites containing of SrTiO3 nanofibers for capacitor application, Compos Part A Appl Sci Manuf 109 (2018) 48–54. https://doi.org/10.1016/j.compositesa.2018.02.040.

[98] Z.M. Dang, H.Y. Wang, Y.H. Zhang, J.Q. Qi, Morphology and dielectric property of homogenous BaTiO3/PVDF nanocomposites prepared via the natural adsorption action of nanosized BaTiO3, Macromol Rapid Commun 26 (2005) 1185–1189. https://doi.org/10.1002/marc.200500137.

[99] Y. sheng Zhang, M. Wang, C. Yang, Y. wen Shao, X. dong Qi, J. hui Yang, Y. Wang, Heterogeneous BaTiO3@Ag core-shell fibers as fillers for polymer dielectric composites with simultaneously improved dielectric constant and breakdown strength, Composites Communications 27 (2021). https://doi.org/10.1016/j.coco.2021.100874.

[100] Z.B. Pan, L.M. Yao, J.W. Zhai, S.H. Liu, K. Yang, H.T. Wang, J.H. Liu, Fast discharge and high energy density of nanocomposite capacitors using Ba0.6Sr0.4TiO3 nanofibers, Ceram Int 42 (2016) 14667–14674. https://doi.org/10.1016/j.ceramint.2016.06.090.

[101] A. Sasmal, P. Maiti, S. Maity, S. Sen, A. Arockiarajan, Air-plasma discharged PVDF based binary magnetoelectric composite for simultaneously enhanced energy storage and conversion efficiency, Appl Phys Lett 122 (2023). https://doi.org/10.1063/5.0137968.

[102] S. Jaidka, D.P. Singh, Ultrahigh efficiency and enhanced discharge energy density at low loading of nanofiller in trilayered polyvinylidene fluoride-Ba0.8Sr0.2TiO3 nanocomposites, Polym Compos (2023). https://doi.org/10.1002/pc.28081.

[103] P. Kim, N.M. Doss, J.P. Tillotson, P.J. Hotchkiss, M.J. Pan, S.R. Marder, J. Li, J.P. Calame, J.W. Perry, High energy density nanocomposites based on surface-modified BaTiO3 and a ferroelectric polymer, ACS Nano 3 (2009) 2581–2592. https://doi.org/10.1021/nn9006412.

[104] M. Bi, Y. Hao, J. Zhang, M. Lei, K. Bi, Particle size effect of BaTiO3b nanofillers on the energy storage performance of polymer nanocomposites, Nanoscale 9 (2017) 16386–16395. https://doi.org/10.1039/C7NR05212J.

[105] L. Wu, Z. Cai, L. Li, X. Wang, Breakdown strength and energy density enhancement in polymer-ceramic nanocomposites: Role of particle size distribution, Compos Sci Technol 212 (2021). https://doi.org/10.1016/j.compscitech.2021.108868.

[106] C. V. Chanmal, J.P. Jog, Dielectric relaxations in PVDF/BaTiO3 nanocomposites, Express Polym Lett 2 (2008) 294–301. https://doi.org/10.3144/expresspolymlett.2008.35.

[107] K. Nakagawa, Y. Ishida, Dielectric Relaxations and Molecular Motions in Poly(vinylidene Fluoride) with Crystal Form II, Journal of Polymer Science 11 (1973) 1503–1533.

[108] Y. Miyamoto, H. Miyaji, K. Asai, Anisotropy of Dielectric Relaxation in Crystal Form II of Poly(viny1idene Fluoride), Journal of Polymer Science 18 (1980) 597–606.

[109] N. Venkat, T.D. Dang, Z. Bai, V.K. McNier, J.N. DeCerbo, B.H. Tsao, J.T. Stricker, High temperature polymer film dielectrics for aerospace power conditioning capacitor applications, Mater Sci Eng B Solid State Mater Adv Technol 168 (2010) 16–21. https://doi.org/10.1016/j.mseb.2009.12.038.

[110] F. Zhuo, U. Eckstein, N.H. Khansur, C. Dietz, D. Urushihara, T. Asaka, K. Kakimoto, K.G. Webber, X. Fang, J. Rödel, Temperature-induced changes of the electrical and mechanical properties of aerosol deposited BaTiO3 thick films for energy storage applications, Journal of the American Ceramic Society (2022). https://doi.org/10.1111/jace.18377.

[111] Z. Tang, J. Xia, H. Yin, G. Fu, X. Ai, H. Tang, C. Yang, L. Qu, Ys. Li, High-temperature-resistant barium strontium titanate @Ag/poly(arylene ether nitrile) composites with enhanced dielectric performance and high mechanical strength, Adv Compos Hybrid Mater (2021). https://doi.org/10.1007/s42114-021-00366-2.

[112] Q. Li, F.-Z. Yao, Y. Liu, G. Zhang, H. Wang, Q. Wang, High-Temperature Dielectric Materials for Electrical Energy Storage, Annu. Rev. Mater. Res 483 (2018) 1–325. https://doi.org/10.1146/annurev-matsci-070317.

[113] J.W. Zha, Y. Tian, M.S. Zheng, B. Wan, X. Yang, G. Chen, High-temperature energy storage polyimide dielectric materials: polymer multiple-structure design, Mater Today Energy 31 (2023). https://doi.org/10.1016/j.mtener.2022.101217.

[114] J.B. Ping, Q.K. Feng, Y.X. Zhang, X.J. Wang, L. Huang, S.L. Zhong, Z.M. Dang, A Bilayer High-Temperature Dielectric Film with Superior Breakdown Strength and Energy Storage Density, Nanomicro Lett 15 (2023). https://doi.org/10.1007/s40820-023-01121-6.

[115] J. Zhong, H. Ju, C. Fu, X. Ran, W. Nie, Tuning ferroelectric response of electroactive materials by controlling multilayered structures to achieve excellent energy storage performance, Adv Eng Mater (2022). https://doi.org/10.1002/adem.202101770.

[116] L. Gao, J. Zhang, Z. Chen, X. Wang, Enhancing energy storage property of polymer nanocomposites by rationally regulating shell thickness of core–shell structured nanoparticles, Polym Compos 44 (2023) 3567–3579. https://doi.org/10.1002/pc.27345.

[117] S. Peng, X. Du, Z. Liang, M. Ma, Y. Guo, L. Xiong, Multilayer polymer nanocomposites based on interface engineering for high-performance capacitors, J Energy Storage 60 (2023). https://doi.org/10.1016/j.est.2023.106636.

[118] S. Mishra, R. Sahoo, L. Unnikrishnan, A. Ramadoss, S. Mohanty, S.K. Nayak, Investigation of the electroactive phase content and dielectric behaviour of mechanically stretched PVDF-GO and PVDF-rGO composites, Mater Res Bull 124 (2020). https://doi.org/10.1016/j.materresbull.2019.110732.

[119] S. Liu, S. Xue, W. Zhang, J. Zhai, Enhanced dielectric and energy storage density induced by surface-modified BaTiO3 nanofibers in poly(vinylidene fluoride) nanocomposites, Ceram Int 40 (2014) 15633–15640. https://doi.org/10.1016/j.ceramint.2014.07.083.

[120] Prateek, R. Bhunia, A. Garg, R.K. Gupta, Probing the Interface Activation in Designing Defect-Free Multilayered Polymer Nanocomposites for Dielectric Capacitor Applications, Journal of Physical Chemistry C 124 (2020) 22914–22924. https://doi.org/10.1021/acs.jpcc.0c05833.

[121] Z. Zichun, L. Haihui, Y. Zefeng, Y. Liangdong, X. Ruijie, X. Jiayi, L. Caihong, Z. Ting, Influence of melt stretching process on POK dielectric properties and relaxation behavior, Mater Lett 330 (2023) 133333. https://doi.org/10.1016/j.matlet.2022.133333.

[122] S. Debili, A. Gasmi, M. Bououdina, Synergistic effects of stretching/polarization temperature and electric field on phase transformation and piezoelectric properties of polyvinylidene fluoride nanofilms, Appl Phys A Mater Sci Process 126 (2020). https://doi.org/10.1007/s00339-020-03492-8.

[123] A. Mayeen, M.S. Kala, M.S. Jayalakshmy, S. Thomas, D. Rouxel, J. Philip, R.N. Bhowmik, N. Kalarikkal, Dopamine functionalization of BaTiO3: An effective strategy for the enhancement of electrical, magnetoelectric and thermal properties of BaTiO3-PVDF-TrFE nanocomposites, Dalton Transactions 47 (2018) 2039–2051. https://doi.org/10.1039/c7dt03389c.

[124] E. Stojchevska, R. Popeski-Dimovski, Ž. Kokolanski, C. Gualandi, A. Bužarovska, Effect of Particle Functionalization on Structural and Dielectric Properties of Flexible TPU/BaTiO 3 /MWCNTs Composite Films , Macromol Chem Phys (2023) 2200401. https://doi.org/10.1002/macp.202200401.

[125] Q.K. Feng, Q. Dong, D.L. Zhang, J.Y. Pei, Z.M. Dang, Enhancement of high-temperature dielectric energy storage performances of polyimide nanocomposites utilizing surface functionalized MAX nanosheets, Compos Sci Technol 218 (2022). https://doi.org/10.1016/j.compscitech.2021.109193.

[126] X. Chen, Q. Zhang, Z. Liu, Y. Sun, Q.M. Zhang, High dielectric response in dilute nanocomposites via hierarchical tailored polymer nanostructures, Appl Phys Lett 120 (2022) 162902. https://doi.org/10.1063/5.0087495.

[127] X. Ni, X. Wang, J. Lin, X. Liu, Z.K. Cui, P. Zuo, Q. Zhuang, Ultra-low dielectric loss and high thermal stability achieved by hierarchical microcapacitor structure in nanocomposites via surface topological modulation, Mater Today Energy 31 (2023). https://doi.org/10.1016/j.mtener.2022.101221.

[128] M.H. Zhang, J.L. Qi, Y.Q. Liu, S. Lan, Z.X. Luo, H. Pan, Y.H. Lin, High energy storage capability of perovskite relaxor ferroelectrics via hierarchical optimization, Rare Metals 41 (2022) 730–744. https://doi.org/10.1007/s12598-021-01869-z.

[129] X. Yang, X. Zhu, L. Ji, P. Hu, Z. Li, Largely enhanced energy storage performance in multilayered ferroelectric polymer nanocomposites with optimized spatial arrangement of ceramic nanofillers, Compos Part A Appl Sci Manuf 139 (2020). https://doi.org/10.1016/j.compositesa.2020.106111.

[130] N. Zhang, H. Zhao, C. Zhang, S. Gao, T. Zhu, J. Bai, Improved energy storage property in polyvinylidene fluoride-based multilayered composite regulated by oriented carbon nanotube@SiO2 nanowires, IET Nanodielectrics (2023). https://doi.org/10.1049/nde2.12045.

Chapter 2

Experimental techniques

2.1 Introduction

This chapter provides a comprehensive overview of the methodologies employed in the fabrication and analysis of ceramics and polymer nanocomposites, with a particular focus on polyvinylidene difluoride (PVDF) polymer and barium strontium titanate ($Ba_{0.8}Sr_{0.2}TiO_3$, BST) ceramic nanoparticles. The BST nanoparticles are prepared through the hydrothermal method and subsequently integrated into the PVDF matrix to form polymer-ceramic nanocomposites. The PVDF-BST nanocomposite films are fabricated using a tape-casting process. Various analytical tools are utilized to probe the structural, compositional and morphological aspects of both BST nanoparticles and PVDF-BST nanocomposite films. These tools include X-ray diffraction (XRD) for investigating the crystallographic structure, scanning electron microscopy (SEM) for assessing the surface morphology, and transmission electron microscopy (TEM) for determining the particle size of BST nanoparticles. Fourier transform infrared spectroscopy (FTIR) is employed to study the bonding and polymorphic forms within the PVDF-BST nanocomposite films. Dielectric measurements are conducted to gain insights into the capacitive and dielectric behavior of both BST pellets and PVDF-BST nanocomposite films. Electric displacement versus electric field measurements are carried out to ascertain the charging and discharging energy density and efficiency of the capacitors based on the synthesized PVDF-BST nanocomposite films. The electrical breakdown analysis is utterly important for the polymer-based nanocomposites employed for the high energy density capacitors. Danbridge Denmark 30 kV Non-destructive Insulation Tester with a ramp voltage of 1kV/sec is employed for measuring electrical breakdown strength.

This chapter briefly explains about the experimental techniques, processes and methods employed in the present thesis work.

2.2 Synthesis process

Barium strontium titanate ($Ba_{0.8}Sr_{0.2}TiO_3$, BST) nanoparticles have been synthesized by hydrothermal process. Tape casting technique have been employed for synthesizing the polyvinylidene fluoride (PVDF)-BST nanocomposite films, which is essential for the investigation of their dielectric and energy storage characteristics. The processes and methods used for synthesizing the BST nanoparticles and PVDF-BST nanocomposite films are explained in the subsequent sections.

2.2.1 Synthesis of barium strontium titanate ($Ba_{0.8}Sr_{0.2}TiO_3$) nanoparticles

The hydrothermal process is used for the synthesis of barium strontium titanate ($Ba_{0.8}Sr_{0.2}TiO_3$) nanoparticles. Here, barium chloride dihydrate ($BaCl_2 \cdot 2H_2O$), strontium chloride hexahydrate ($SrCl_2 \cdot 6H_2O$), and titanium trichloride ($TiCl_3$) (all from Sigma Aldrich) served as the precursor compounds. These compounds are precisely weighed to ensure a stoichiometric composition. $BaCl_2 \cdot 2H_2O$ and $SrCl_2 \cdot 6H_2O$ are dissolved in distilled water and stirred mechanically until a clear solution (designated as solution A) is achieved. Subsequently, $TiCl_3$ is added drop by drop to solution A, ensuring homogenization through magnetic stirring for 1 hour while maintaining a temperature of 50 °C (referred to as solution B). Following this, a NaOH solution is introduced into solution B under vigorous stirring, yielding a precipitate solution. This solution is then transferred to a Teflon-lined autoclave and placed inside an oven set to 180°C for 12 hours. The autoclave is then cooled to room temperature, and the resulting precipitates are subjected to six cycles of washing with distilled water. After washing, the precipitates are dried at 80 °C overnight and subsequently subjected to calcination at 800 °C for 2 hours to produce $(Ba,Sr)TiO_3$ nanoparticles.

2.2.2 Synthesis of polyvinylidene fluoride-$Ba_{0.8}Sr_{0.2}TiO_3$ nanocomposite films

PVDF-BST nanocomposites containing of different volume percentage loadings of BST nanoparticles are synthesized using the tape casting technique. Initially, commercially procured

polyvinylidene fluoride (PVDF) powder (Alfa Aesar) is dissolved in N,N-dimethylformamide (DMF) (Loba Chemie) and stirred using a magnetic stirrer at room temperature for 2 hours (solution I). Subsequently, different volume of the BST nanoparticles are introduced into solution I. After the addition of BST nanoparticles, the solution is subjected to ultrasonication for 30 minutes to ensure the proper dispersion of BST nanoparticles within the PVDF matrix. The sonicated solution is further stirred for 12 hours at 60 °C, ensuring the homogeneous distribution of BST nanoparticles in the PVDF matrix. This process results in the thickening of the solution, and the resultant solution is cast into thick films by using TMAX tape casting equipment preset at 70 °C for 2 hours. The complete evaporation of DMF is ensured by heating the nanocomposite films in a vacuum oven at 150 °C for 8 hours. Afterward, the nanocomposite films are allowed to cool in the air. A schematic diagram depicting the synthesis of PVDF-BST nanocomposite thick films is shown in Figure 2.1.

Fig. 2.1 Schematic representation of the tape casting process for making PVDF-BST nanocomposite thick films

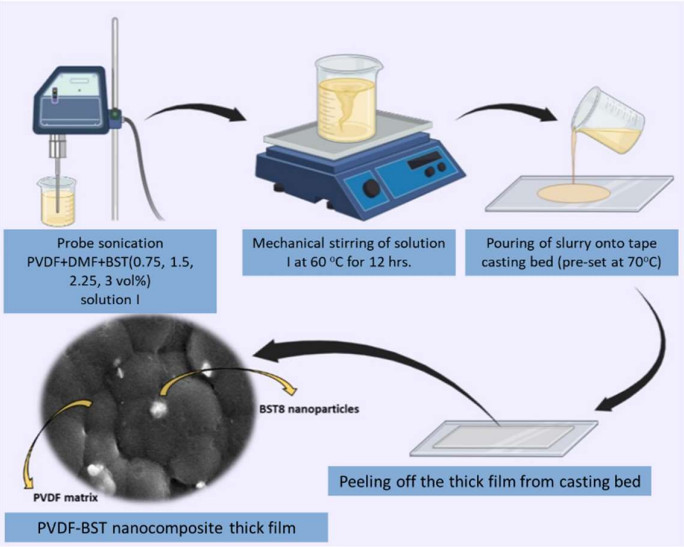

2.2.3 Functionalization of barium strontium titanate ($Ba_{0.8}Sr_{0.2}TiO_3$) nanoparticles

$(Ba,Sr)TiO_3$ (BST) nanoparticles synthesized by the hydrothermal method are subjected to functionalization with different functional groups, i.e. $-OH^{-1}$ and $-PO_4^{-3}$. The important chemicals for functionalizing with $-OH^{-1}$ and $-PO_4^{-3}$ are hydrogen peroxide (H_2O_2) and phosphoric acid (H_3PO_4), respectively. Initially, 3 grams of BST nanopowder is dispersed in 100 ml DI water and sonicated for 30 minutes. Subsequently, the solution is subjected to

magnetic stirring at 80 °C for 1 hour, followed by the addition of 100 ml of hydrogen peroxide (H_2O_2) and 100 ml of phosphoric acid (H_3PO_4) into the stirred solutions, respectively. The solutions are then continuously stirred until drying and afterwards, they are allowed to cool down to room temperature. The cooled solution is then centrifuged and washed with DI water at 10000 rpm for 10 minutes. The resulting centrifuged product is subsequently dried at 60°C for 12 hours, resulting in the functionalization of BST nanoparticles with $-OH^{-1}$ groups and -PO_4^{-3} groups, respectively. A schematic representation of the functionalization of BST nanoparticles using H_2O_2 is shown in Figure 2.2. Finally, the functionalized BST nanoparticles are incorporated into the PVDF polymer matrix at 3% volume loading, and the casting process for creating PVDF-BST nanocomposite films is carried out in the same manner as described in section 2.2.2 above.

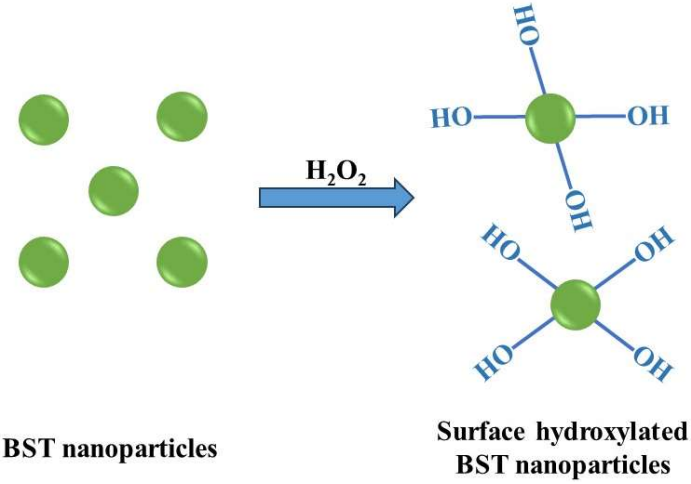

Fig. 2.2 Schematic representation of functionalization of BST nanoparticles using H_2O_2

2.3 Characterization techniques

The characterization techniques necessary for the detailed understanding about the dielectric and energy storage behavior of PVDF-BST nanocomposite films are broadly divided into two categories. The first one is the structural and morphological characterization, while the another one is the electrical characterization. These techniques are briefly described in the following subsections.

2.3.1 Structural characterizations

X-ray diffraction (XRD) and Fourier transform infrared (FTIR) are used for determining the presence of crystalline phase and molecular bonding pattern in the BST nanoparticles and PVDF-BST nanocomposites. These techniques are explained as follows:

2.3.1.1 X-ray diffraction

X-ray diffraction (XRD) is an indispensable analytical technique widely utilized in various fields of science and engineering, especially in materials research. It plays a pivotal role in characterizing the crystalline structure of materials by measuring the diffraction patterns resulting from X-ray beams interacting with the atomic arrangement within a sample. Through XRD analysis, we can identify crystallographic phases, determine lattice parameters and gain insights into the atomic positions within a crystalline material [1,2]. This information is invaluable in understanding the structural properties of materials, making XRD an essential tool for investigating the composition and stability of a wide range of substances, from minerals and metals to polymers and biomaterials. Incident X-rays give rise to constructive interference upon interaction with the sample, a phenomenon that satisfies the principles of Bragg's law, given as:

$$2d\ \mathrm{Sin}\theta = n\lambda \tag{2.1}$$

Here, the variable d represents the separation distance between diffracting planes in a crystal, θ signifies the incident angle, n is an integer and λ denotes the wavelength of the incident beam. X-rays are chosen as the preferred radiation source for generating diffraction patterns because their wavelength falls within a comparable range to the crystal plane spacing (typically 1-100 Å). The precise measurement of diffraction peak positions through XRD distinguishes it as the most effective method for characterizing both uniform and non-uniform strains within materials.

In this study, we have employed X-ray diffraction (XRD) utilizing a PANalytical instrument to distinguish and identify the crystallographic phases present in (Ba,Sr)TiO_3 (BST) nanoparticles and the PVDF-BST nanocomposite thick films.

2.3.1.2 Fourier transform infrared (FTIR) spectroscopy

Fourier transform infrared (FTIR) spectroscopy serves as a tool for elucidating information regarding the molecular structure and the vibrational or rotational characteristics of chemical bonds and identifying functional groups within a given compound or sample. The FTIR method operates in either absorption or transmission modes and when the sample is exposed to IR radiation, it selectively absorbs specific wavelengths, suggesting its unique characteristics. The infrared (IR) spectrum have a wavenumber range of 4000 cm^{-1} to 400 cm^{-1}. The infrared radiation from the source is directed to the interferometer, which splits the beam of radiation into two parts. Transmitted light falls onto two mirrors (one fixed and the other moving) and the reflected light coming from both mirrors at the beam splitter falls on the sample. These two rays reflected from the sample interfere and produce FTIR spectra, which are recorded by the detector. The remaining radiation is either transmitted or reflected, providing valuable information about the vibrational modes of atomic and molecular species, including changes in bond length (stretching) and bond angle (bending) [3,4].

In this investigation, FTIR spectra have been recorded using the Agilent Resolution Pro Cary 660 to examine the bonding patterns and various polymorphs within PVDF-BST nanocomposite thick films. Additionally, the confirmation of -OH group and -PO_4^{-3} group functionalization in BST nanoparticles and PVDF-BST nanocomposites has been established through FTIR measurements.

2.3.2 Morphological characterizations

The morphological characterization is essential for examining the surfaces and interfaces of the BST nanoparticles and PVDF-BST nanocomposites. The morphological character

determines the degree of compatibility of the BST nanofiller with the PVDF matrix, which influences their dielectric and energy storage behavior**.** Scanning electron microscopy (SEM) and high-resolution transmission electron microscopy (HRTEM) are used for these characterizations, which are discussed as follows:

2.3.2.1 Scanning electron microscopy (SEM)

Scanning electron microscopy (SEM) is a crucial imaging and analytical tool that plays an important role in scientific research and the characterization of materials. SEM allows us to explore the microscopic world with exceptional resolution, offering detailed insights into the surface morphology and structure of various materials, from biological specimens to engineered components. By employing a focused beam of electrons to interact with the sample's surface, SEM generates high-resolution images, enabling the visualization of features at the nanoscale [5]. Moreover, SEM is not limited to visual examination alone; it provides the capability for elemental analysis through energy-dispersive X-ray spectroscopy (EDS) attachments, making it a versatile tool for characterizing both the topography and composition of materials. SEM operates by directing a focused beam of high-energy electrons onto the surface of the sample. These electrons interact with the sample, causing the emission of secondary electrons and backscattered electrons. Detectors capture and analyze these emissions to create detailed images that reveal the surface morphology and composition of the material at high magnification.

During this investigation, the microstructure and surface morphology of BST nanoparticles and PVDF-BST nanocomposite thick films have been studied using the JEOL JSM-6610LV SEM instrument.

2.3.2.2 High-resolution transmission electron microscopy (HRTEM)

High-resolution transmission electron microscopy (HRTEM) stands out as a pivotal technique in material science for investigating the internal structure and analysis of features at the atomic

scale, typically within a range of a few nanometers. This method relies on the utilization of an electron beam to pass through the sample, generating a significantly magnified image of the specimen. A high voltage, typically in the kilovolt range, is applied to the cathode, thereby producing an electron beam that navigates through electromagnetic coils (lenses). To ensure optimal performance, the electron beam is accelerated through these lenses, possessing sufficient energy, typically in the range of 100 to 400 keV. This energy is crucial for generating an electron beam with a diameter of the order of tens of nanometers. This electron beam helps in generating a monochromatic image that reveals morphological, compositional, and crystallographic details of the sample. Notably, HRTEM has the capability to unveil the finest internal structures, reaching down to the scale of individual atoms [6].

In this study, JEOL 2100 F HRTEM is employed to examine the particle size and distribution of BST nanoparticles. The sample preparation for TEM has been done by adding a minute quantity of BST powder into ethanol and drop-casting this solution onto carbon-coated grids.

2.3.3 Electrical characterizations

The electrical characterization used in the present study includes the measurement of the electrical parameters at low voltage and high voltage. The low voltage (≤1V) is employed for studying the dielectric characteristics, i.e. dielectric constant and tangent loss. The measurement of the D-E loop and electrical breakdown strength involves high voltage (≥10kV), which are essential for ascertaining the energy storage behavior. These techniques are discussed briefly in the following subsections as follows:

2.3.3.1 Dielectric measurements

When a dielectric material is subjected to an electric field, it undergoes a phenomenon known as dielectric polarization. In contrast to electrical conductors, the electric charges within the dielectric do not flow; instead, they subtly shift from their average positions. This shift results in the displacement of positive charges in the direction of the applied field, while negative

charges move in the opposite direction. Consequently, an internal electric field is generated within the dielectric, mitigating the overall external electric field. The capacity of dielectric materials to store energy is ascribed to this polarization process, wherein electric charges undergo separation and alignment under the influence of the applied electric field. This phenomenon leads to an increase in capacitance. Various polarization mechanisms contribute to this effect, including electronic, ionic, molecular (dipole), and interfacial (space-charge) polarization. When an electric field is applied to each of these mechanisms in their normal state, charge displacement occurs, resulting in polarization aligned with the field direction. Describing the dielectric material as a capacitor, it stores electric charges ±Q (in coulombs) on its surfaces, between which a potential difference V (in volts) is applied. This relationship is governed by Q = CV. Here, C (in farads) denotes the capacitance of the system, representing the amount of electric charge that can be stored in the capacitor. The connection between C and the dielectric constant is given by C = $\frac{A\varepsilon_o\varepsilon_r}{d}$, where ε_o signifies the dielectric constant of free space (8.854 × 10^{-12} F/m), A (in meters) represents the area of the electrical conductor, d (in meters) denotes the thickness of the dielectric layer and ε_r is the dielectric constant of the dielectric material [7,8]. Commonly, the dielectric constant is assessed using instruments like LCR meters or impedance analyzers,

Fig.2.3. Schematic representation of the dielectric characteristic measurements setup

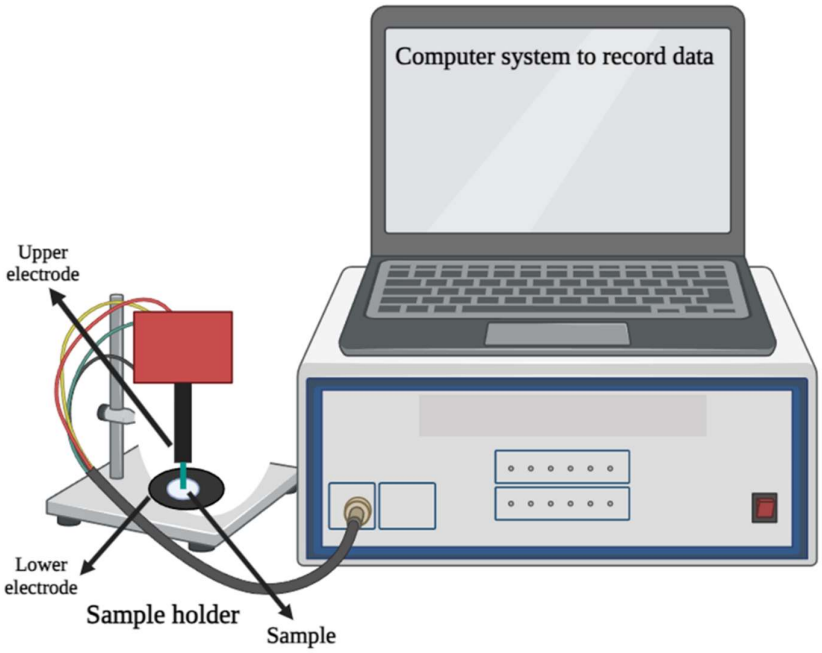

employing a parallel plate configuration with the sample subjected to a minimal voltage (e.g., 0.5 V-5 V). The formation of interfaces in polymer-ceramic nanocomposites markedly affects the dielectric behavior. The frequency-dependent dielectric constant offers insights into the relaxation phenomena taking place in various materials, whereas the temperature-dependent dielectric constant gives us information about the reliability of the material in harsh environments and its different applications.

On the other hand, the tangent loss (tan δ) is a measure of the energy lost as heat during each cycle of the electric field. Studying its variation with temperature can provide insights into the material's ability to dissipate heat and the presence of any temperature-dependent loss mechanisms. This information is crucial for applications where heat dissipation is a concern. It is dependent on the dielectric constant of a material as tan $\delta = \frac{\varepsilon''}{\varepsilon'}$ where ε' is the dielectric constant of the material and ε'' is known as the loss component. The dielectric properties of BST pellet and PVDF-BST nanocomposite thin films are measured under an applied voltage of ±1.0 V within the frequency range of 100 Hz-1 MHz and the temperature range of room temperature (RT)-150 ^{o}C using a Wayne Kerr 6500B impedance analyzer. This equipment is interfaced with the computer. To investigate these properties, silver electrodes are carefully applied to both sides of the pellet and nanocomposite films using silver paint. The schematic diagram for the dielectric constant and tangent loss measurements is shown in Fig. 2.3.

2.3.3.2 Displacement vs electric field (D-E loop) measurements

Upon the application of an external voltage, charges of equal magnitude but opposite signs accumulate at the electrodes, starting the charging process. This process establishes an internal electric field directed opposite to the external field and intensifies as the accumulated charges increase. In the course of the charging process, charges are mobilized by the external electric field, leading to the storage of electrostatic energy in the dielectric layer and the energy stored is represented by $W = \int_0^{Qmax} V.dQ$, where Q_{max} denotes the maximum charge attained at the

completion of the charging process, and dQ represents the incremental charge. For energy-storage electrostatic capacitors, the energy density U_{total} quantifies the performance capability of energy storage. It is expressed as the ratio of stored energy to the volume of the capacitor as $U_{total} = \frac{W}{A.d} = \frac{\int_0^{Qmax} V.dQ}{A.d} = \int_0^{Dmax} E.dD$, where D signifies the electrical displacement in the dielectric layer and E is the maximum electric field induced by the accumulated charges, equivalent to the external electric field. For dielectrics with high permittivity, D closely approximates the polarization (P) as per $D = \varepsilon_o E + P$ if $\varepsilon_o E >> P$ [9]. Consequently, $U_{total} = \int_0^{Pmax} E.dP = \int_0^{Emax} \varepsilon_o \varepsilon_r E.dE$, where ε_o is the vacuum permittivity, ε_r is the dielectric permittivity and E is the dielectric/breakdown strength [10]. The final energy efficiency (η) of the nanocomposites is calculated by using $\eta = \frac{Discharge\ energy\ density}{Charg\ \ energy\ density}$ x 100%. A schematic representation for the calculation of charging and discharging energy density using a unipolar D-E loop is shown in Fig. 1.1 of section 1.2 in Chapter 1.

Here, we have used a Radiant Precision Multiferroic II Ferroelectric Tester to measure the displacement loops (D-E) of the PVDF-BST nanocomposite thick films by applying a triangular wave of 10 Hz frequency.

2.3.2.4 Electrical breakdown strength measurements

For a capacitor, the electrostatic energy density is given as $(U_E) = \frac{1}{2}\varepsilon_r\varepsilon_0 E_b^2$, where ε_0, ε_r are the vacuum permittivity (8.854 x 10^{-12} F/m) & dielectric constant and E_b is the dielectric breakdown strength. So, the dielectric breakdown strength is related to the dielectric characteristics of the material. Electrical breakdown strength is a critical parameter that characterizes the ability of a material to withstand electrical stress without undergoing a sudden breakdown. The breakdown strength is typically measured as the maximum electric field that a material can endure before experiencing a breakdown, leading to the sudden and irreversible

conduction of electricity. The breakdown analysis is extremely essential for the nanocomposites to be employed for high-energy density capacitors.

In the present work, the breakdown strength of the PVDF-BST nanocomposites is measured by using the Danbridge Denmark 30 kV Non-destructive Insulation Tester with a ramp voltage of 1 kV/sec. A schematic diagram showing the process of breakdown measurement of the polymer-based nanocomposites is shown in Fig 2.4. A total of 10 specimens have been chosen for recording the breakdown strength. The electrical breakdown strength of any material is statistical in nature. Therefore, a two-parameter Weibull analysis is usually employed for the determination of actual breakdown strength. The Weibull equation is given as:

Fig 2.4: Schematic representation for the measurement of breakdown strength of the polymer based nanocomposites

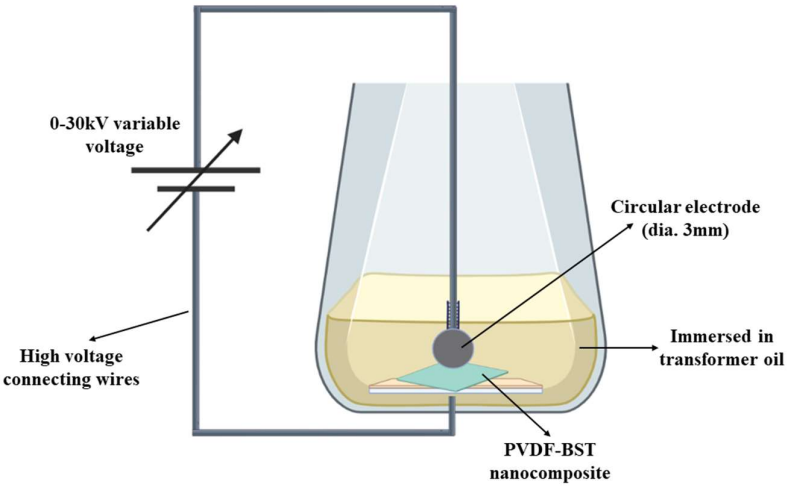

$$P_i = 1 - e^{[-\frac{E_i}{E_o}]m} \tag{2.2}$$

where P_i is the breakdown probability, m is the shape factor (Weibull modulus) for estimating data scattering, E_i is the average breakdown strength, and E_o is the field corresponding to 63.2% breakdown cumulative probability. The experimental plot is a straight line in the X-Y plane given by [11,12]:

$$X = ln(E_i) \text{ and } Y = ln(-\ln(1 - P_i)) \tag{2.3}$$

Now, to analyze the data using the Weibull distribution, the data is first sorted in ascending order of breakdown strength voltage and the respective Weibull probability is calculated for each data point using equation 2.2. Now, we plot the sorted data against their corresponding

Weibull probabilities. Afterward, a linear fit is done to the plotted data, and the slope of this fitted line gives us an estimate for the shape parameter (m), while the intercept of the fitted line gives the value of the breakdown strength of the material.

References:

[1] A. Khorsand Zak, W.H. Abd. Majid, M.E. Abrishami, R. Yousefi, X-ray analysis of ZnO nanoparticles by Williamson-Hall and size-strain plot methods, Solid State Sci 13 (2011) 251–256. https://doi.org/10.1016/j.solidstatesciences.2010.11.024.

[2] T. Ungár, J. Gubicza, P. Hanák, I. Alexandrov, Densities and character of dislocations and size-distribution of subgrains in deformed metals by X-ray diffraction profile analysis, Materials Science and Engineering A 319–321 (2001) 274–278. https://doi.org/10.1016/S0921-5093(01)01025-5.

[3] A.B.D. Nandiyanto, R. Oktiani, R. Ragadhita, How to read and interpret ftir spectroscope of organic material, Indonesian Journal of Science and Technology 4 (2019) 97–118. https://doi.org/10.17509/ijost.v4i1.15806.

[4] X. Cai, T. Lei, D. Sun, L. Lin, A critical analysis of the α, β and γ phases in poly(vinylidene fluoride) using FTIR, RSC Adv 7 (2017) 15382–15389. https://doi.org/10.1039/c7ra01267e.

[5] C.W. Oatley, The early history of the scanning electron microscope, J Appl Phys 53 (1982). https://doi.org/10.1063/1.331666.

[6] David B Williams, C Barry Carter, Transmission Electron Microscopy A Textbook for Materials Science, Second, Springer Science, New York, 2009.

[7] H.P. Palani Velayuda Shanmugasundram, E. Jayamani, K.H. Soon, A comprehensive review on dielectric composites: Classification of dielectric composites, Renewable and Sustainable Energy Reviews 157 (2022). https://doi.org/10.1016/j.rser.2022.112075.

[8] X. Hao, A review on the dielectric materials for high energy-storage application, J Adv Dielectr 03 (2013) 1330001. https://doi.org/10.1142/s2010135x13300016.

[9] H. Palneedi, M. Peddigari, G.T. Hwang, D.Y. Jeong, J. Ryu, High-Performance Dielectric Ceramic Films for Energy Storage Capacitors: Progress and Outlook, Adv Funct Mater 28 (2018). https://doi.org/10.1002/adfm.201803665.

[10] M.L. Müller, M.T. Becker, N. Strkalj, J.L. MacManus-Driscoll, Schottky-to-Ohmic switching in ferroelectric memristors based on semiconducting Hf0.93Y0.07O2 thin films, Appl Phys Lett 121 (2022) 093501. https://doi.org/10.1063/5.0095762.

[11] C. Chauvet, C. Laurent, Weibull statistics in short-term dielectric breakdown of thin polyethylene films, IEEE Transactions on Electrical Insulation 28 (1993) 18–29. https://doi.org/10.1109/14.192236.

[12] J. Wang, S. Liang, J. Xiong, B. Peng, L. He, Y. Xie, Z. Zhang, High Energy Density Nanocomposites with Layered Gradient Structure and Lysozyme-Modified Ba0.6Sr0.4TiO3 Nanoparticles, Compos Part A Appl Sci Manuf (2022) 107254. https://doi.org/10.1016/j.compositesa.2022.107254.

Chapter 3

Studies on the role of electric field-induced effects on the structural and dielectric behavior of polyvinylidene fluoride-barium strontium titanate flexible nanocomposites

3.1 Introduction

Polymer-based ceramic nanocomposites and their dielectric behavior have been in focus for the last decade due to their prospect of application in high-energy storage capacitors, embedded electronics, pulse power generation, etc. [1–3]. There are a large number of polymers that are utilized as a matrix for this purpose, e.g. bi-axially oriented polypropylene [4], polyamide [5], polyvinylidene fluoride (PVDF) [6,7], polyvinylidene fluoride-trifluoro ethylene **(**PVDF-TrFE) [8], polydimethylsiloxane **(**PDMS) [9] etc. All these polymers have a very low dielectric constant (< 12) [10,11]. The high dielectric constant ceramic particles are incorporated in the matrix of polymers, in order to make polymer-based nanocomposites, are consisting of lead zirconate titanate (PZT) (ε' ~600) [12], barium titanate ($BaTiO_3$) (ε' ~1700) [13], strontium titanate ($SrTiO_3$) (ε' ~1000) [14], calcium copper titanate (CCTO) (ε' ~60000) [13], titanium oxide (TiO_2) (ε' ~200) [15], etc. The composites based on high dielectric constant ceramic materials and low dielectric constant flexible polymers will have a moderate dielectric constant and low tangent loss. PVDF shows unique behavior among all dielectric polymers with its dielectric constant ~10, tangent loss ~0.05, and breakdown field ~500 MV/m [16]. Apart from this, its ease of processing, the existence of various crystalline phases (such as α, β, and γ crystalline phases), and associated electrical properties such as ferroelectric, piezoelectric, and pyroelectric [17] make it most suitable for making polymer-based ceramic nanocomposites. On the other hand, lead-free barium strontium titanate ($BaSrTiO_3$, BST) possesses very good dielectric behavior with a large dielectric constant over a wide temperature (-173 °C-120 °C) and frequency (100 Hz - 1 MHz) range [18,19]**.** Therefore, the dielectric, structural, and energy storage behavior of PVDF-BST nanocomposites has been widely investigated [7,20,21]. These days, polymer-ceramic nanocomposites with a low volume/weight percentage of ceramic loading, higher dielectric constant, and low loss are required

[22]. Several methods have been adopted to achieve high dielectric constant and low loss polymer-ceramic nanocomposites, such as a change in shape, size, and functionalization of the incorporated filler, stretching, poling the nanocomposites etc. [20,23–25]. Dopamine-modified $Ba_{0.6}Sr_{0.4}TiO_3$ (BST) nanofibers-PVDF nanocomposites are found to have much improved dielectric and energy storage behavior [18], which is attributed to surface modification by dopamine and large aspect ratio of BST nanofibers. The use of polyvinylpyrrolidone (PVP) linker layer as an adhesive in multilayered $BaTiO_3$ nanofibers/PVDF nanocomposites is found to improve the dielectric behavior and energy storage properties [26], which is caused by homogeneous surfaces due to the presence of the multilayer PVDF. The high discharge energy density in PVDF-based nanocomposites loaded with fine $Ba_{0.6}Sr_{0.4}TiO_3$ nanofibers along with a high dielectric constant (~22) has been achieved [27], which is assigned to the regulation of diameter of 1-D nanofiber and improvement of interfaces between ceramic filler and PVDF matrix. Dielectric constant and breakdown field are very important parameters for the material to be used for high-voltage capacitor applications. The higher volume/weight percentage loading of the ceramic particles in the polymer-based composites leads to a high dielectric constant, but the breakdown field decreases. Dielectric properties of polymer-based nanocomposites are improved by different methods of processing [28,29], interfacial modification [18,27], etc. The high value of the dielectric constant is usually obtained for higher loading of ceramic nanoparticles as well as poling at a very high voltage for a longer duration [23,30–32]. The processing techniques adopted for synthesizing nanocomposite thick films include tape-casting, solution casting, and spin casting [28,33–35]. The tape-casting method produces large area nanocomposite thick films of uniform thickness and ensures homogeneous dispersion of ceramic nanoparticles. The application of electric field is capable of rotating randomly aligned dipoles in the direction of the electric field

[36], which may change the crystalline phases of PVDF in PVDF-$Ba_{0.8}Sr_{0.2}TiO_3$ nanocomposite thick films. There, the motivation of the present work is based on the fact that the exposure of electric field on PVDF-$Ba_{0.8}Sr_{0.2}TiO_3$ nanocomposite thick films will finally affect the structural and dielectric properties at very small fractional loading of $Ba_{0.8}Sr_{0.2}TiO_3$ nanoparticle in PVDF matrix.

The present chapter reports the electric field-induced effect on the dielectric and structural behavior of tape-casted PVDF-$Ba_{0.8}Sr_{0.2}TiO_3$ nanocomposite thick films at very small loading of $Ba_{0.8}Sr_{0.2}TiO_3$ nanoparticles in PVDF matrix, which could be adopted as an efficient way for modification and tuning of dielectric behavior of nanocomposites.

3.2 Experimental

It includes the synthesis of PVDF-$Ba_{0.8}Sr_{0.2}TiO_3$ (BST) nanocomposite thick films along with their structural, morphological and dielectric studies, which are described in the following subsections.

3.2.1 Synthesis of PVDF-$Ba_{0.8}Sr_{0.2}TiO_3$ nanocomposite films

BST nanoparticles are synthesized using a hydrothermal method, as discussed in section 2.2.1 of experimental techniques (Chapter 2). A detailed flowchart for the synthesis of BST nanopowder is shown in Fig. 3.1. PVDF-BST nanocomposite film with 1.5 vol% loading of BST is prepared by tape-casting using the TMAX tape

Fig. 3.1: Detailed flowchart for the synthesis of BST nanopowder

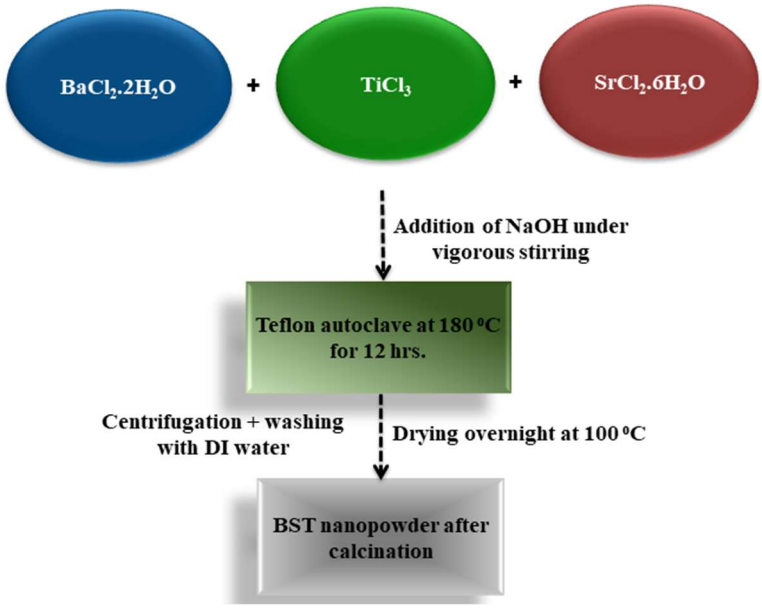

Fig. 3.2: Schematic diagram showing the application of electric field on the nanocomposites

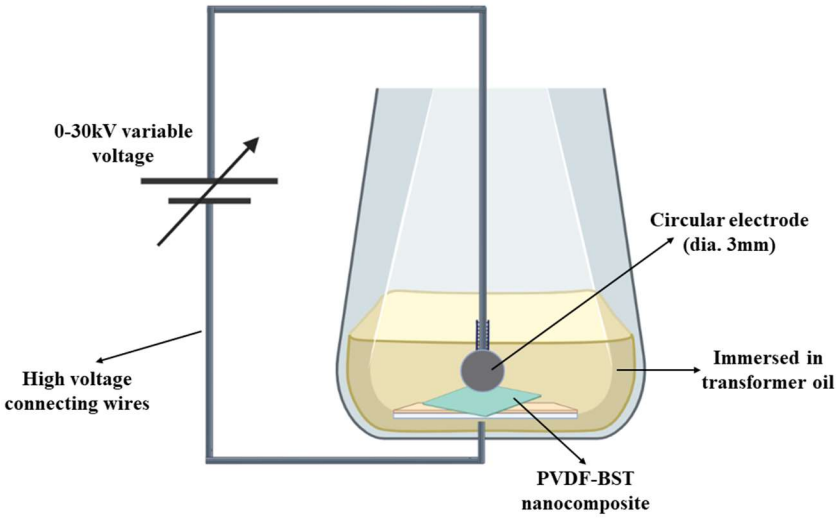

casting unit as discussed in section 2.2.2 of Chapter 2. The synthesized nanocomposite film is then cut into small pieces, which are subjected to an electric field of 22 kV/mm for 40 min, 50 min, and 60 min, respectively. The electric field is applied using Danbridge Denmark 30 kV Non-destructive Insulation Tester. A schematic diagram showing the electric field measurements is shown in Fig. 3.2. The samples have been named as 0 min, 40 min, 50 min and 60 min, respectively.

3.2.2 Structural studies of PVDF-$Ba_{0.8}Sr_{0.2}TiO_3$ nanocomposite films

X-ray diffraction (XRD), scanning electron microscopy (SEM) and transmission electron microscopy (TEM) have been employed to examine the phases and surface morphology of the PVDF-BST nanocomposite films, respectively. Fourier transform infrared spectroscopy (FTIR) has been utilized to analyze the bonding of different crystalline phases of PVDF matrix in PVDF-BST nanocomposite films, as detailed in section 2.3.1 of Chapter 2.

3.2.3 Dielectric studies of PVDF-$Ba_{0.8}Sr_{0.2}TiO_3$ nanocomposite films

The dielectric constant and tangent loss of the PVDF-BST nanocomposite thick films have been measured and analyzed at room temperature. The details of these techniques are already described in section 2.3.2 of Chapter 2.

3.3 Results and discussion

The results of structural, morphological and electrical studies are described in the subsequent sections.

3.3.1 Structural studies

The subsequent sections explain the results obtained from X-ray diffraction (XRD), Fourier transform infrared spectroscopy (FTIR) investigations, scanning electron microscopy (SEM), and transmission electron microscopy (TEM).

3.3.1.1 X-ray diffraction

PVDF-BST nanocomposite films are subjected to an external electric field of 22 kV/mm for different time duration. The presence of α and β crystalline phases for all films has been observed. The β phase with (110) plane at 20.4° and α phase with (020) plane of PVDF at 18.5° (JCPDS card no. 38-1638) are observed. The diffraction peaks at 22.5°, 31.8°, 39.30°, 45.6°, 51.3°, 56.8°, and 66.4° correspond to (100), (101), (111), (200), (210), (211), and (220) planes of BST with the tetragonal crystal structure (JCPDS card no. 44-0093) having lattice parameters a = b = 0.3977 nm, c = 0.3988 nm and average crystallite size of ~19 nm (as discussed in Table 3.1), which are observed for all the PVDF-BST nanocomposite films [20] [37]. The peak position, crystallite size, FWHM, and d-spacing of BST nanoparticles calculated from the XRD

Fig. 3.3: X-ray diffraction patterns of PVDF-BST nanocomposites exposed to the electric field for different time durations

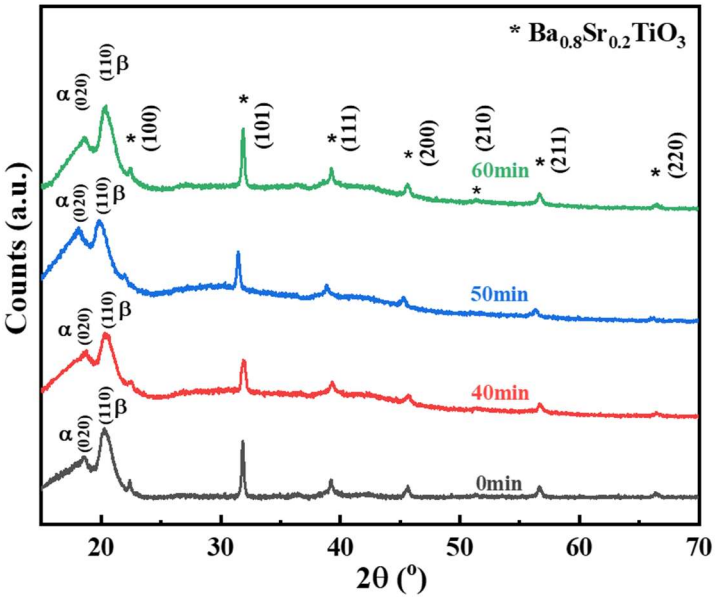

pattern using X'Pert Highscore Plus are shown in Table 3.1. The average crystallite size is ~19 nm, agreeing with the FESEM and TEM studies (discussed later in Sec. 3.3.1.3).

Table: 3.1 Peak position, crystallite size, d-spacing and FWHM of BST nanoparticles calculated from XRD pattern

S. No.	Peak pos. [° 2θ]	FWHM [° 2θ]	d-spacing [Å]	Crystallite size [nm]
1	22.5	0.247	3.984	~34
2	31.8	0.370	2.811	~23
3	39.3	0.442	2.290	~19
4	45.6	0.542	1.987	~16
5	56.8	0.680	1.619	~13
6	66.4	0.827	1.406	~11

So, the peaks of $Ba_{0.8}Sr_{0.2}TiO_3$ and PVDF are observed in all the nanocomposite films, confirming the incorporation of BST nanoparticles in the PVDF polymer matrix [38,39]. But, the duration of electric field application on PVDF-BST nanocomposite thick films affects the intensity of peaks corresponding to α and β phase of PVDF. With the increase in the time duration of application of the electric field, the intensity of the peak corresponding to the α phase at 18.5° decreases, whereas for the β phase at 20.4°, the intensity increases. The peak of β phase for the nanocomposite films having exposure to the electric field for 50 min and 60 min is more intense than the peak for the film having a lower duration of exposure to the electric field. The XRD studies confirm that the electric field induces the enhancement of the β phase in PVDF-BST nanocomposite thick films. Since X-ray diffraction only shows the probable evolution of the β phase induced by the electric field, Fourier transform infrared spectroscopy studies will further confirm these findings.

3.3.1.2 Fourier transform infrared spectroscopy

Fig. 3.4 shows the FTIR absorption spectra of PVDF-BST nanocomposite films in the range 1500-400 cm^{-1}. The formation of the β-phase of PVDF is observed at wavenumbers 429, 508, 835, 874, 1166, 1230, 1278, and 1401 cm^{-1} [40]. The characteristic peaks of the α and β phases of PVDF are summarized in Table 3.2. The absorption band at 606 cm^{-1} corresponding to the α phase is due to

the rocking vibration of the CF_2 group, whereas the band at 763 cm^{-1} is due to a mixture of CF_2 bending and GGG skeletal vibrations [41]. The peaks of α phase corresponding to the absorption band present at 763, 810, and 1112 cm^{-1} are absent in 50 min and 60 min samples, whereas the intensity of absorption bands corresponding to β phase at 874 and 1166 cm^{-1} increases. These studies confirm the formation of the β crystalline phase due to exposure to the electric field. The FTIR results are used to find the relative fraction of the β phase using absorption peaks of α and β phases, which is validated using the Beer-Lambert law. Accordingly, the relative fraction of the β phase is given by [42,43]:

Fig. 3.4: Fourier transform infrared absorption spectra of PVDF-BST nanocomposites exposed to the electric field for different time durations

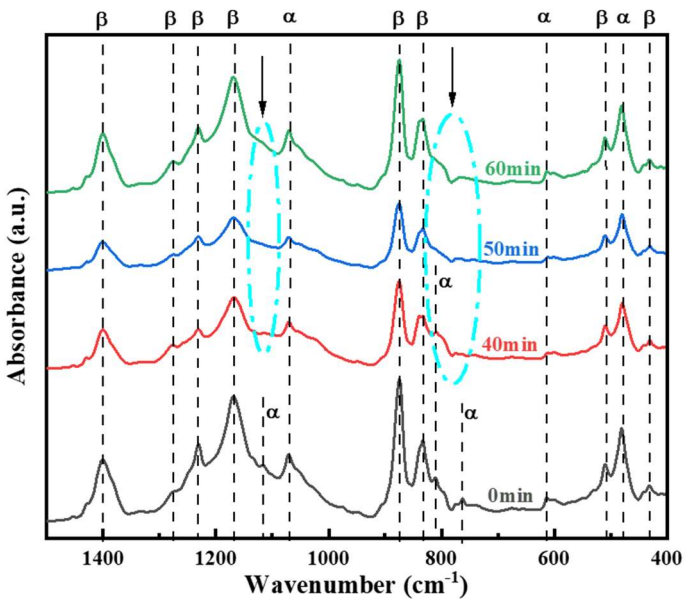

$$F(\beta) = \frac{X_\beta}{X_\alpha + X_\beta} = \frac{A_\beta}{(K_\beta/K_\alpha)A_\alpha + A_\beta} = \frac{A_\beta}{1.3A_\alpha + A_\beta} \quad (3.1)$$

where X_α and X_β in equation (1) represent the mass fraction of α and β phases, A_α and A_β represent the absorbance at 835 cm^{-1} and 763 cm^{-1}, respectively and the absorption coefficients are expressed by K_α (6.1×10^4 cm^2 mol^{-1}) and K_β (7.7×10^4 cm^2 mol^{-1}) at that particular wavenumber, respectively [42]. According to equation (1), it can be seen that the F(β) values of the 0 min, 40 min, 50 min, and 60 min samples are 33.32%, 4 7.50%, 50.19%, and 54.49%, respectively. The observed

Table: 3.2 FTIR characteristic diffraction peaks of α and β phase of PVDF

Crystalline phases	α	β
Wavenumber (cm^{-1})	478	429
	606	508
	763	835
	810	874
	1068	1166
	1112	1230
		1278
		1401

results further corroborate the evolution of β-phase in PVDF of PVDF-BST nanocomposites due to the increase in time duration of exposure to the electric field. The variation in the content of β-phase fraction with time duration to the electric field exposure for PVDF-BST nanocomposites is shown in Fig. 3.8.

3.3.1.3 Field emission scanning electron microscopy and transmission electron microscopy

Fig. 3.5: (a) FESEM of $Ba_{0.8}Sr_{0.2}TiO_3$ powder (inset: TEM image confirming the particle size), (b) Particle size distribution curve for $Ba_{0.8}Sr_{0.2}TiO_3$ particles (c) Lattice fringe pattern of $Ba_{0.8}Sr_{0.2}TiO_3$, (d) SAED pattern of $Ba_{0.8}Sr_{0.2}TiO_3$ powder, and (e) SEM micrograph of PVDF-BST nanocomposite

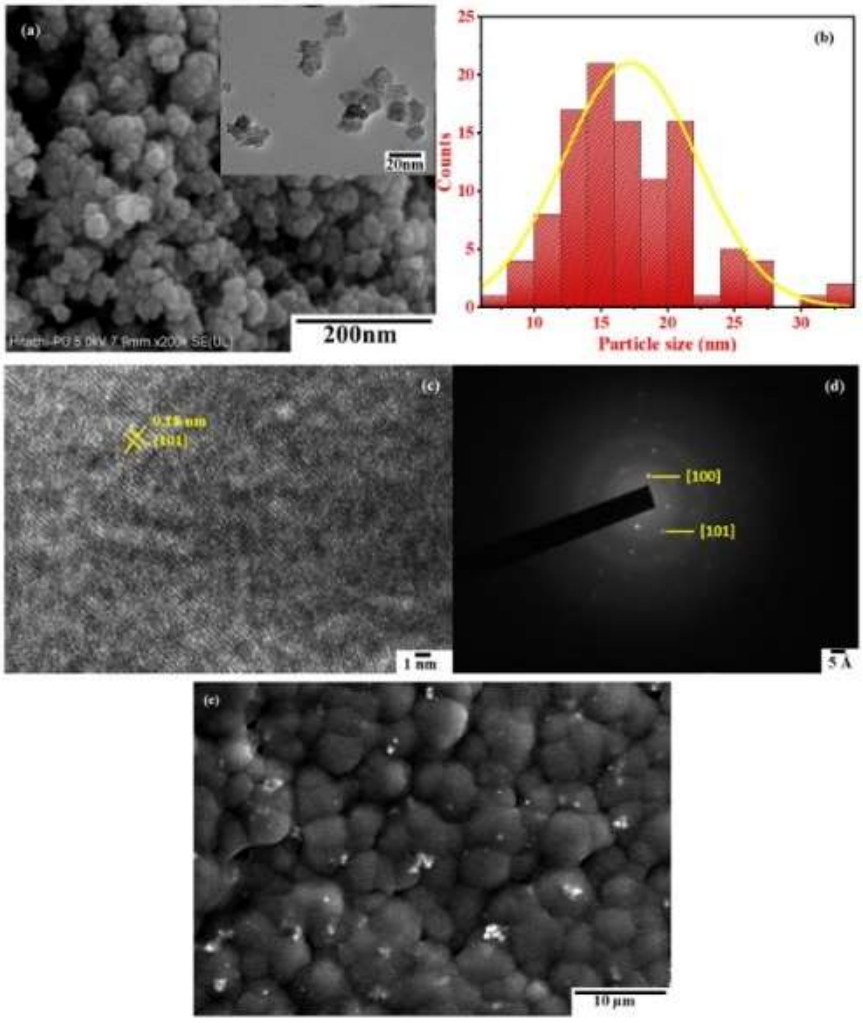

Fig. 3.5(a) shows the FESEM of the $Ba_{0.8}Sr_{0.2}TiO_3$ (BST) powder, which shows the agglomerates of the nanoparticles. The inset of Fig. 3.5(a) shows the transmission electron microscopy (TEM) image of (BST), which confirms the formation of nanoparticles in the range of 15-20 nm. The particle size distribution curve is shown in Fig. 3.5(b). Fig. 3.5(c) shows the fringe pattern of BST, which confirms the formation of

BST with the separation between lattice planes of 0.18 nm corresponding to the [101] plane. The selected area diffraction (SAED) pattern of the synthesized BST powder clearly shows [100] and [101] planes in Fig. 3.5(d) [37], which matches with the XRD of BST powder. Fig. 3.5(e) shows the surface scanning electron micrograph (SEM), revealing the homogeneous distribution of BST nanoparticles in the PVDF polymer matrix. This uniform distribution of ceramic particles in the polymer matrix ensures a good quality PVDF-BST nanocomposite thick film with a uniform dielectric constant.

3.3.2 Electrical studies

The electrical studies in the subsequent sections include dielectric constant and tangent loss of the PVDF-BST nanocomposite thick films, which are used in the Cole-Cole analysis.

3.3.2.1 Dielectric studies

The electric field-induced effect on the dielectric properties of PVDF-BST nanocomposites is very important in its application for various purposes. The BST nanoparticle will experience a much lower field as compared to the polymer PVDF by virtue of its high dielectric constant [44,45]. The XRD and IR studies have already confirmed the electric field-induced evolution of the β phase in PVDF-BST nanocomposites. The variation of dielectric constant (ε') with frequency for the PVDF-BST nanocomposite films exposed to the electric field of 22 kV/mm for different time durations is shown in Fig. 3.6(a). The dielectric constant is found to increase with the increase in the duration of the applied electric field. But the frequency from where the dielectric constant starts decreasing is shifting towards lower values with an increase in the time duration of the applied electric field. A decrease in frequency is associated with the increase of dipolar relaxation time, which might be due to the decrease of mobility of the dipoles/charge carriers in the polymeric chain or polymeric chain as a whole. Though the value of dielectric constant for the PVDF-BST nanocomposite

Fig. 3.6: Frequency dependent (a) real, (b) imaginary dielectric constant and (c) tangent loss for PVDF-BST nanocomposites

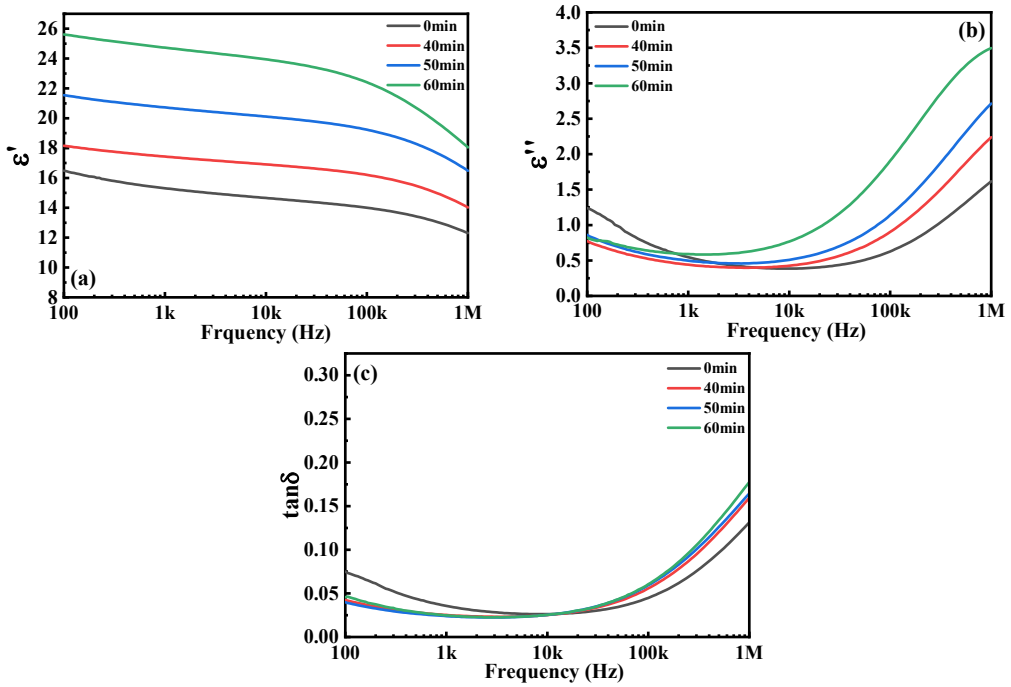

exposed to the electric field of 22 kV/mm for 60 min is highest, i.e., ~25 at 1 kHz, but the trend of variation is found to be different.

All PVDF-BST nanocomposites are showing nearly constant dielectric constant in the frequency range 100 Hz-100 kHz. The high values of ε' in this frequency range can be ascribed to interfacial polarization present due to the difference in dielectric constant values of the filler (i.e., BST) and the polymer matrix (i.e., PVDF) [46]. The decrease in ε' with increasing frequency (>100 kHz) is due to a lag in the frequency of the applied field and the dipolar orientation in PVDF-BST nanocomposites [47]. A comparative table of observed dielectric constant and tangent loss is shown in Table 3.3. The observed high value of dielectric constant with an increase of exposure time of applied electric field is ascribed to:

i. The evolution of the β phase of PVDF in PVDF-BST nanocomposites and decrease of mobility of polymeric chain.
ii. Enhancement of the β phase leads to an increase in the dipolar density.

iii. The application of the electric field promotes the accumulation of space charges in the polymer near the interface, which increases the internal field in the ceramics phase and removes the discontinuity of the electric displacement at the interface, leading to an increase in the dielectric constant.

Significant enhancement in the dielectric properties resulting from the interfaces between the BST/PVDF and CH_2-CF_2 in PVDF. These interfaces might be forming the parallel capacitance network, which enhances the dielectric constant[48]. The tangent loss, imaginary component of dielectric constant, and Cole-Cole analysis have also been carried out in order to get more insight into the physical phenomena taking place due to the application of the electric field. The tangent loss (Fig. 3.6(c)) decreases in the range of 100 Hz to 10 kHz due to molecular motions in the crystalline regions of PVDF (α relaxation) [50], whereas increased tangent loss for the frequencies greater than 100 kHz could be caused by β-relaxation effects in the copolymer, which arise from the micro-Brownian motion of non-crystalline chain segments [44,45,47,50]. The values of the dielectric constant and tangent loss at 1 kHz are summarized in Table 3.4.

Table: 3.3 Comparative data for dielectric constant and tangent loss of PVDF-BST nanocomposites

S. No.	Year	Material	Dielectric (1kHz)	Loss (1kHz)	References
1.	2012	PVDF-BST	~12.5 (at 4.4% loading)	~0.04	[18]
2.	2015	PVDF-ST	~12.5 (at 5% loading)	~0.04	[51]
3.	2016	PVDF-BST	~16 (at 5% loading)	~0.04	[19]
4.	2017	PVDF-BT	~13 (at 5% loading)	~0.05	[29]
5.	2018	PVDF-BST	~ 21 (at 5% loading)	~0.04	[20]
6.	2020	PVDF-BT	~13 (at 5% loading)	~0.05	[52]
7.	Present work	PVDF-BST	~25 (at 5% loading)	~0.02	Present work

The variation of the imaginary part of the dielectric constant (ε") with frequency is shown in Fig. 3.6(b). It indicates almost similar behavior as that of tangent loss. Initially, the decrease of ε" up to the frequency of 10 kHz is observed, which is caused by molecular motion in the crystalline region of PVDF [49]. But for frequencies greater than 10 kHz, ε" increases, and it attains a peak at different frequencies for the PVDF-BST nanocomposite films exposed to the electric field for different time durations. This peak shifts towards the lower frequency with an increase in the time duration of electric field exposure, showing a complete correlation with frequency from where the dielectric constant starts decreasing. The peak in ε" might be originating from the micro-Brownian motion of the amorphous chain segment [46,47], which controls the charge carrier transport. The relaxation of dipoles becomes slower with the increased exposure time of the applied electric field; that's why the peak at the higher frequency is shifting towards a lower frequency. The Cole-Cole analysis has been widely used for understanding dielectric relaxation. The Cole-Cole shows the plot between the real and imaginary parts of the dielectric constant. According to Debye relaxation theory (equation (2)), the real part and imaginary part of the dielectric constant are related as:

Table: 3.4 Dielectric constant and tangent loss at 1 kHz for PVDF-BST nanocomposites

Sample	0min	40min	50min	60min
ε' (1kHz)	~15	~17	~21	~25
Tanδ (1kHz)	~0.04	~0.03	~0.02	~0.02

$$(\varepsilon' - \varepsilon_\infty)^2 + (\varepsilon'')^2 = (\varepsilon_0 - \varepsilon_\infty)^2 \quad (3.2)$$

where ε_∞, ε_0 are dielectric constant at infinite frequency and static dielectric constant, respectively. The difference of ε_s and ε_∞ i.e., Δε measures the dielectric strength. Fig. 3.7 shows the Cole-Cole plot of PVDF-BST nanocomposites exposed to the electric field for different durations. The absence of complete semicircles indicates that Debye-type relaxation is not exactly taking place in PVDF-BST nanocomposites. Therefore, approximated Debye-type relaxation is used to

understand the relaxation process in PVDF-BST nanocomposites. Also, the relaxation time (i.e., $\tau = \frac{1}{2\pi f_{max}}$) is found to increase with the increase of time duration of exposure of the electric field, which might be arising due to an increase in the motion of the charge carrier at the amorphous crystalline interface of PVDF in PVDF-BST nanocomposites. The dielectric strength $\Delta\varepsilon$ (ε_0 - ε_∞) estimated from Cole-Cole plots for different time durations of the applied electric field are given in Table 3.5. The number density of dipoles (N) contributing to the dipolar relaxation process can be estimated using the following equation:

Fig. 3.7: Cole-Cole plots for PVDF-BST nanocomposites exposed to the electric field for different time durations

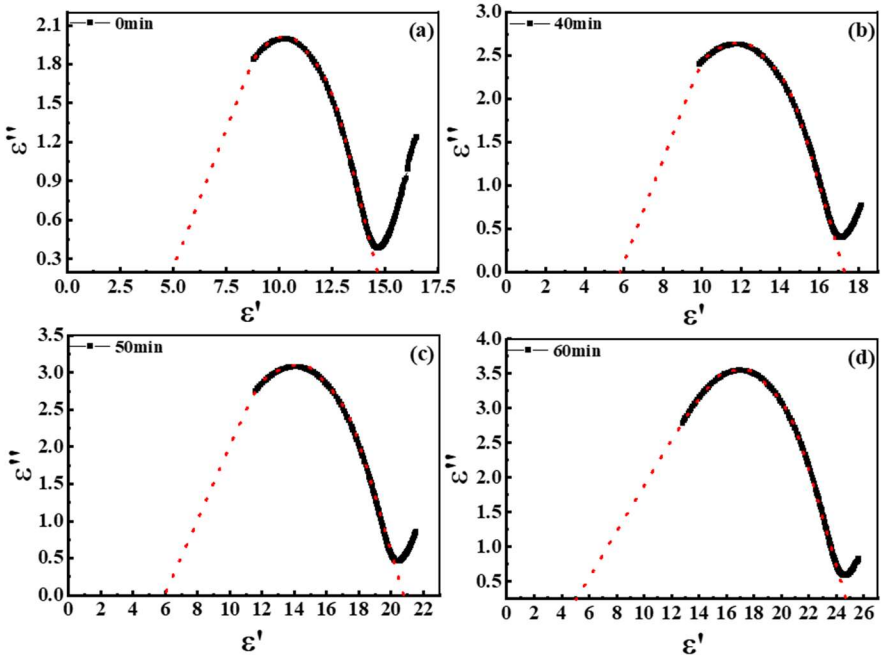

$$\Delta\varepsilon = \frac{N\mu^2 sin^2\frac{\alpha}{2}}{3\varepsilon_0 kT} \tag{3.3}$$

where $\Delta\varepsilon$, N, μ, α, k, ε_o and T are dielectric strength, the number density of dipoles, dipole moment, the angle between dipole moments in two possible directions, Boltzmann's constant, absolute dielectric constant and the absolute temperature, respectively. Modifying this equation for PVDF-BST nanocomposites, equation (3) gets modified as:

$$\Delta\varepsilon = \frac{N}{3\varepsilon_0 kT}\left(\mu_1{}^2 sin^2\frac{\alpha_1}{2} + \mu_2{}^2 sin^2\frac{\alpha_2}{2}\right) \tag{3.4}$$

where μ_1 and μ_2 represent the dipole moment of prominent dipoles present in the ceramic and polymeric phases of PVDF-BST nanocomposites. For the polar -CF_2- groups in PVDF, μ_1=1.66 Debye and α_1=105.3° while, for the polar tetragonal phase for BST, μ_2 = 2.30 Debye and α_2=180° [53]. The obtained number density of dipoles (N) for all the samples is listed in Table 3.5. The number density of dipoles for the pristine sample is 1.34 x 10^{28} cm^{-3}, which increased up to 2.83 x 10^{28} cm^{-3} for the nanocomposite exposed to the electric field for 60 min. The variation of dipolar density along with the β phase of PVDF for the PVDF-BST nanocomposites exposed to the electric field for different time durations are shown in Fig. 3.8. The density of dipoles in PVDF-BST nanocomposites thick films exposed to the electric field for 60 min has become more than double as compared to pristine film, which is attributed to the evolution of the β phase of PVDF in PVDF-BST nanocomposite.

Fig. 3.8: Variation of β fraction and number density of dipoles for PVDF-BST nanocomposites exposed to the electric field for different time durations

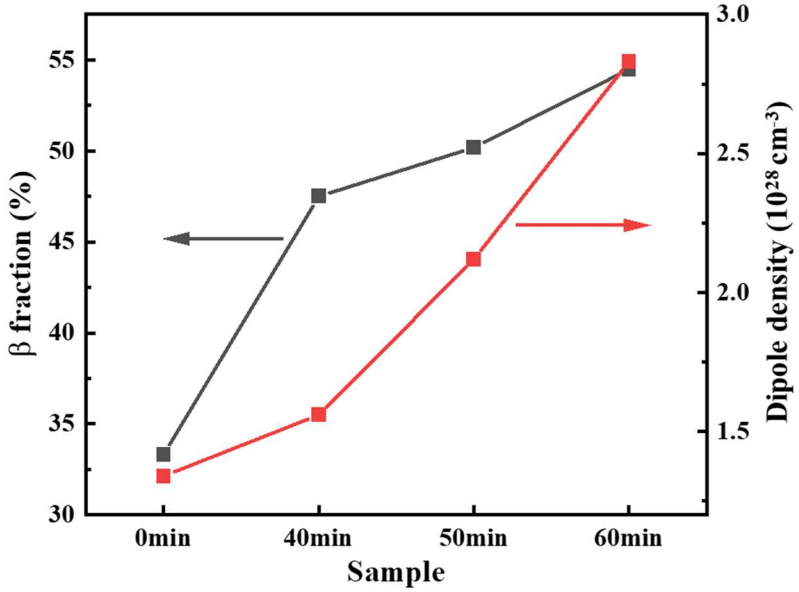

Table: 3.5 Dielectric strength, β fraction, the number density of dipoles, and relaxation time for PVDF-BST nanocomposites

Sample	Dielectric strength (Δε)	β fraction (%)	Number density of dipoles (N, in cm^{-3})	Relaxation time (τ, in sec)
0min	9.5	33.32	1.34 x 10^{28}	4.08 x 10^{-8}
40min	11	47.5	1.56 x 10^{28}	4.54 x 10^{-8}
50min	15	50.19	2.12 x 10^{28}	4.82 x 10^{-8}
60min	20	54.49	2.83 x 10^{28}	1.13 x 10^{-7}

3.4 Conclusion

The flexible polyvinylidene fluoride (PVDF)-$Ba_{0.8}Sr_{0.2}TiO_3$ (BST) nanocomposite thick films of thickness ~100 μm have been synthesized by tape-casting technique. A detailed study of the electric field-induced effect on dielectric and structural properties of PVDF-BST nanocomposite thick films has been carried out. The XRD and IR studies reveal the evolution of the β phase of PVDF for the PVDF-BST nanocomposites. The dielectric constant at 1 kHz for the films exposed to the electric field for 60 min duration is increased up to ~25 as compared to ~15 for unexposed films, whereas the tangent loss does not exhibit significant change. The significant enhancement in the dielectric constant is attributed to the evolution of the β phase in PVDF and enhancement in dipolar density due to modification in the structural and interfacial behavior as well as molecular motion of the dipoles in the polymeric chain. Electric field-induced modification of dielectric properties (i.e., high dielectric constant and low tangent loss) could be adopted as an effective strategy for the development of flexible nanocomposite films with very low loading of ceramic filler for different electronic applications, including high energy density capacitors.

References

[1] H. Hu, F. Zhang, S. Luo, W. Chang, J. Yue, C.-H. Wang, Recent advances in rational design of polymer nanocomposite dielectrics for energy storage, Nano Energy 74 (2020) 104844. https://doi.org/10.1016/j.nanoen.2020.104844.

[2] V. Jella, S. Ippili, J.H. Eom, S.V.N. Pammi, J.S. Jung, V.D. Tran, V.H. Nguyen, A. Kirakosyan, S. Yun, D. Kim, M.R. Sihn, J. Choi, Y.J. Kim, H.J. Kim, S.G. Yoon, A comprehensive review of flexible piezoelectric generators based on organic-inorganic metal halide perovskites, Nano Energy 57 (2019) 74–93. https://doi.org/10.1016/j.nanoen.2018.12.038.

[3] M. Safaei, H.A. Sodano, S.R. Anton, A review of energy harvesting using piezoelectric materials: State-of-the-art a decade later (2008-2018), Smart Mater Struct (2019). https://doi.org/10.1088/1361-665X/ab36e4.

[4] M.-S. Zheng, Y.-T. Zheng, J.-W. Zha, Y. Yang, P. Han, Y.-Q. Wen, Z.-M. Dang, Improved dielectric, tensile and energy storage properties of surface rubberized BaTiO 3 /polypropylene nanocomposites, Nano Energy 48 (2018) 144–151. https://doi.org/10.1016/j.nanoen.2018.03.049.

[5] I. Hammami, H. Hammami, J. Soulestin, M. Arous, A. Kallel, Thermal and dielectric behavior of polyamide-6/clay nanocomposites, Mater Chem Phys 232 (2019) 99–108. https://doi.org/10.1016/j.matchemphys.2019.04.048.

[6] L. Li, B. Zhou, J. Ye, W. Wu, F. Wen, Y. Xie, P. Bass, Z. Xu, L. Wang, G. Wang, Z. Zhang, Enhanced dielectric and energy-storage performance of nanocomposites using interface-modified anti-ferroelectric fillers, J Alloys Compd 831 (2020) 154770. https://doi.org/10.1016/j.jallcom.2020.154770.

[7] X. Hu, Y. Zhou, J. Liu, B. Chu, Improved flexoelectricity in PVDF/barium strontium titanate (BST) nanocomposites, J Appl Phys 123 (2018). https://doi.org/10.1063/1.5022650.

[8] N. Meng, X. Zhu, R. Mao, M.J. Reece, E. Bilotti, Nanoscale interfacial electroactivity in PVDF/PVDF-TrFE blended films with enhanced dielectric and ferroelectric properties, J Mater Chem C Mater 5 (2017) 3296–3305. https://doi.org/10.1039/C7TC00162B.

[9] G. Rajitha, R.K. Dash, Optically transparent and high dielectric constant reduced graphene oxide (RGO)-PDMS based flexible composite for wearable and flexible sensors, Sens Actuators A Phys 277 (2018) 26–34. https://doi.org/10.1016/j.sna.2018.04.040.

[10] M. Guo, J. Jiang, Z. Shen, Y. Lin, C.-W. Nan, Y. Shen, High-Energy-Density Ferroelectric Polymer Nanocomposites for Capacitive Energy Storage: Enhanced Breakdown Strength and Improved Discharge Efficiency, Materials Today 29 (2019) 49–67. https://doi.org/10.1016/j.mattod.2019.04.015.

[11] J. Jiang, Z. Shen, J. Qian, Z. Dan, M. Guo, Y. Lin, C.W. Nan, L. Chen, Y. Shen, Ultrahigh discharge efficiency in multilayered polymer nanocomposites of high energy density, Energy Storage Mater 18 (2019) 213–221. https://doi.org/10.1016/j.ensm.2018.09.013.

[12] M. Kumar, R. Rai, N. Kumar, G. Sharma, A.K. Singh, S. Kumar, Crystal structure correlation of ferroelectric and dielectric properties of Nb doped PZT95/5, Journal of Materials Science: Materials in Electronics 30 (2019) 5014–5020. https://doi.org/10.1007/s10854-019-00798-z.

[13] C. Manière, G. Riquet, S. Marinel, Dielectric properties of flash spark plasma sintered BaTiO3 and CaCu3Ti4O12, Scr Mater 173 (2019) 41–45. https://doi.org/10.1016/j.scriptamat.2019.07.048.

[14] W. Pan, M. Cao, H. Hao, Z. Yao, Z. Yu, H. Liu, Defect engineering toward the structures and dielectric behaviors of (Nb, Zn) co-doped SrTiO3 ceramics, J Eur Ceram Soc 40 (2020) 49–55. https://doi.org/10.1016/j.jeurceramsoc.2019.09.027.

[15] A.K. Abdul Gafoor, M.M. Musthafa, P.P. Pradyumnan, AC conductivity and diffuse reflectance studies of Ag-TiO 2 nanoparticles, J Electron Mater 41 (2012) 2387–2392. https://doi.org/10.1007/s11664-012-2174-7.

[16] W. Xia, Z. Zhang, PVDF-based dielectric polymers and their applications in electronic materials, IET Nanodielectrics 1 (2018) 17–31. https://doi.org/10.1049/iet-nde.2018.0001.

[17] A. Ahmed, I.A. Goldthorpe, A.K. Khandani, Electrically tunable materials for microwave applications Improved designs of tunable ferroelectric capacities for microwave applications APPLIED PHYSICS REVIEWS Electrically tunable materials for microwave applications, Citation: Applied Physics Reviews J. Appl. Phys. Appl. Phys. Lett 2 (2015) 11302–2150. https://doi.org/10.1063/1.1505669.

[18] Y. Song, Y. Shen, P. Hu, Y. Lin, M. Li, C.W. Nan, Significant enhancement in energy density of polymer composites induced by dopamine-modified Ba 0.6 Sr 0.4 TiO 3 nanofibers, Appl Phys Lett 101 (2012) 152904. https://doi.org/10.1063/1.4760228.

[19] Z.B. Pan, L.M. Yao, J.W. Zhai, S.H. Liu, K. Yang, H.T. Wang, J.H. Liu, Fast discharge and high energy density of nanocomposite capacitors using Ba0.6Sr0.4TiO3 nanofibers, Ceram Int 42 (2016) 14667–14674. https://doi.org/10.1016/j.ceramint.2016.06.090.

[20] Y. Xie, W. Jiang, T. Fu, J. Liu, Z. Zhang, S. Wang, Achieving High Energy Density and Low Loss in PVDF/BST Nanodielectrics with Enhanced Structural Homogeneity, ACS Appl Mater Interfaces 10 (2018) 29038–29047. https://doi.org/10.1021/acsami.8b10354.

[21] M. Feng, Q. Chi, Y. Feng, Y. Zhang, T. Zhang, C. Zhang, Q. Chen, Q. Lei, High energy storage density and efficiency in aligned nanofiber filled nanocomposites with multilayer structure, Compos B Eng 198 (2020) 108206. https://doi.org/10.1016/j.compositesb.2020.108206.

[22] S. Liu, J. Zhai, A small loading of surface-modified Ba0.6Sr0.4TiO3 nanofiber-filled nanocomposites with enhanced dielectric constant and energy density, RSC Adv. 4 (2014) 40973–40979. https://doi.org/10.1039/C4RA04369C.

[23] I.O. Pariy, A.A. Ivanova, V.V. Shvartsman, D.C. Lupascu, G.B. Sukhorukov, M.A. Surmeneva, R.A. Surmenev, Poling and annealing of piezoelectric Poly(Vinylidene fluoride) micropillar arrays, Mater Chem Phys 239 (2020) 122035. https://doi.org/10.1016/j.matchemphys.2019.122035.

[24] P. Sapkota, S. Ueno, I. Fujii, G.P. Khanal, S. Kim, S. Wada, Influence of grain size effect and Ba/Ti ratios on dielectric, ferroelectric, and piezoelectric properties of BaTiO 3 ceramics, Jpn J Appl Phys 58 (2019) SLLC05. https://doi.org/10.7567/1347-4065/ab3b1c.

[25] M. Feng, C. Zhang, G. Zhou, T. Zhang, Y. Feng, Q. Chi, Q. Lei, Enhanced Energy Storage Characteristics in PVDF-Based Nanodielectrics with Core-Shell Structured and Optimized Shape Fillers, IEEE Access 8 (2020) 81542–81550. https://doi.org/10.1109/ACCESS.2020.2991058.

[26] Prateek, S. Siddiqui, R. Bhunia, N. Singh, A. Garg, R.K. Gupta, Interface modulation in multi-layered BaTiO 3 nanofibers/PVDF using the PVP linker layer as an adhesive for high energy density capacitor applications, Mater Adv 1 (2020) 680–688. https://doi.org/10.1039/D0MA00240B.

[27] X. Xiong, D. Shen, Q. Zhang, H. Yang, J. Wen, Z. Zhou, Achieving high discharged energy density in PVDF-based nanocomposites loaded with fine Ba0.6Sr0.4TiO3 nanofibers, Composites Communications 25 (2021) 100682. https://doi.org/10.1016/j.coco.2021.100682.

[28] Z. Wang, T. Wang, C. Wang, Y. Xiao, P. Jing, Y. Cui, Y. Pu, Poly(vinylidene fluoride) Flexible Nanocomposite Films with Dopamine-Coated Giant Dielectric Ceramic Nanopowders, Ba(Fe0.5Ta0.5)O3, for High Energy-Storage Density at Low Electric Field, ACS Appl Mater Interfaces 9 (2017) 29130–29139. https://doi.org/10.1021/acsami.7b08664.

[29] Y. Wang, Y. Hou, Y. Deng, Effects of interfaces between adjacent layers on breakdown strength and energy density in sandwich-structured polymer composites, Compos Sci Technol 145 (2017) 71–77. https://doi.org/10.1016/j.compscitech.2017.04.003.

[30] R. Bhunia, D. Ghosh, B. Ghosh, S. Hussain, R. Bhar, A.K. Pal, Some aspects of microstructural and dielectric properties of nanocrystalline CdS/poly(vinylidene fluoride) composite thin films, Polym Int 64 (2015) 924–934. https://doi.org/10.1002/pi.4866.

[31] R. Senthil Kumar, T. Sarathi, K.K. Venkataraman, A. Bhattacharyya, Enhanced piezoelectric properties of polyvinylidene fluoride nanofibers using carbon nanofiber and electrical poling, Mater Lett (2019) 126515. https://doi.org/10.1016/j.matlet.2019.126515.

[32] S. Liu, S. Xue, W. Zhang, J. Zhai, Enhanced dielectric and energy storage density induced by surface-modified BaTiO3 nanofibers in poly(vinylidene fluoride) nanocomposites, Ceram Int 40 (2014) 15633–15640. https://doi.org/10.1016/j.ceramint.2014.07.083.

[33] V. Vinothini, P. Singh, M. Balasubramanian, Optimization of barium titanate nanopowder slip for tape casting, J Mater Sci 41 (2006) 7082–7087. https://doi.org/10.1007/s10853-006-0940-8.

[34] Z.P. Zheng, S.P. Gong, S.F. Cheng, D.X. Zhou, Y.X. Hu, H. Liu, Fabrication of BaTiO3-Based Semiconducting Ceramic Thick Films by Aqueous Tape Casting, Key Eng Mater 368–372 (2008) 469–471. https://doi.org/10.4028/www.scientific.net/KEM.368-372.469.

[35] L. Wang, F. Gao, J. Xu, K. Zhang, J. Kong, M. Reece, H. Yan, Enhanced dielectric tunability and energy storage properties of plate-like Ba0.6Sr0.4TiO3/poly(vinylidene fluoride) composites through texture arrangement, Compos Sci Technol 158 (2018) 112–120. https://doi.org/10.1016/j.compscitech.2018.02.015.

[36] Introduction-to-Electrodynamics-Griffiths-Solutions, (n.d.).

[37] P. Gupta, A. Kumar, M. Tomar, V. Gupta, D.P. Singh, Enhanced dielectric properties and suppressed leakage current density of PVDF composites flexible film through small loading of

submicron Ba0.7Sr0.3TiO3crystallites, Journal of Materials Science: Materials in Electronics 28 (2017) 11806–11812. https://doi.org/10.1007/s10854-017-6987-2.

[38] B.A. Newman, C.H. Yoon, K.D. Pae, J.I. Scheinbeim, Piezoelectric activity and field-induced crystal structure transitions in poled poly(vinylidene fluoride) films, J Appl Phys 50 (1979) 6095–6100. https://doi.org/10.1063/1.325778.

[39] S. Chen, K. Yao, F.E.H. Tay, C.L. Liow, Ferroelectric poly(vinylidene fluoride) thin films on Si substrate with the B phase promoted by hydrated magnesium nitrate, J Appl Phys 102 (2007). https://doi.org/10.1063/1.2812702.

[40] X. Cai, T. Lei, D. Sun, L. Lin, A critical analysis of the α, β and γ phases in poly(vinylidene fluoride) using FTIR, RSC Adv 7 (2017) 15382–15389. https://doi.org/10.1039/c7ra01267e.

[41] S. Kaur, D.P. Singh, On the structural, dielectric and energy storage behaviour of PVDF-CaCu3Ti4O12 nanocomposite films, Mater Chem Phys 239 (2020) 122301. https://doi.org/10.1016/j.matchemphys.2019.122301.

[42] Y. Ren, Y. Wang, W. Zhang, X. Yan, B. Huang, Improved battery performance contributed by the optimized phase ratio of β and α of PVDF, RSC Adv 9 (2019) 29760–29764. https://doi.org/10.1039/c9ra04724g.

[43] L. Ruan, X. Yao, Y. Chang, L. Zhou, G. Qin, X. Zhang, Properties and applications of the β phase poly(vinylidene fluoride), Polymers (Basel) 10 (2018) 1–27. https://doi.org/10.3390/polym10030228.

[44] R.I. Mahdi, W.H. Abd Majid, Piezoelectric and pyroelectric properties of BNT-base ternary lead-free ceramic-polymer nanocomposites under different poling conditions, RSC Adv 6 (2016) 81296–81309. https://doi.org/10.1039/c6ra12033d.

[45] R.I. Mahdi, W.C. Gan, N.A. Halim, T.S. Velayutham, W.H.A. Majid, Ferroelectric and pyroelectric properties of novel lead-free polyvinylidenefluoride-trifluoroethylene-Bi0.5Na0.5TiO3 nanocomposite thin films for sensing applications, Ceram Int 41 (2015) 13836–13843. https://doi.org/10.1016/j.ceramint.2015.08.069.

[46] C. V. Chanmal, J.P. Jog, Study of dielectric behavior in PVDF/clay nanocomposites, E-Polymers (2009) 1–8. https://doi.org/10.1515/epoly.2009.9.1.1333.

[47] R.K. Goyal, A.B. Kulkarni, Electrical properties of novel three-phase polymer nanocomposites with a high dielectric constant, J Phys D Appl Phys 45 (2012). https://doi.org/10.1088/0022-3727/45/46/465302.

[48] S. Kaur, A.L. Sharma, A. Kumar, D.P. Singh, Enhanced dielectric properties of the poly(vinylidene fluoride)-CaCu3Ti4O12 nanocomposite thick films by quenching in ice water, Mater Chem Phys 254 (2020). https://doi.org/10.1016/j.matchemphys.2020.123530.

[49] C. V. Chanmal, J.P. Jog, Dielectric relaxations in PVDF/BaTiO3 nanocomposites, Express Polym Lett 2 (2008) 294–301. https://doi.org/10.3144/expresspolymlett.2008.35.

[50] S. Nayak, D. Khastgir, Polydimethylsiloxane-PbZr 0.52 Ti 0.48 O 3 nanocomposites with high permittivity: Effect of poling and temperature on dielectric properties, J Appl Polym Sci 136 (2019) 47307. https://doi.org/10.1002/app.47307.

[51] S. Liu, J. Zhai, Improving the dielectric constant and energy density of poly(vinylidene fluoride) composites induced by surface-modified SrTiO3 nanofibers by polyvinylpyrrolidone, J Mater Chem A Mater 3 (2015) 1511–1517. https://doi.org/10.1039/c4ta04455j.

[52] H. Zhang, M.A. Marwat, B. Xie, M. Ashtar, K. Liu, Y. Zhu, L. Zhang, P. Fan, C. Samart, Z.G. Ye, Polymer Matrix Nanocomposites with 1D Ceramic Nanofillers for Energy Storage Capacitor Applications, ACS Appl Mater Interfaces 12 (2020) 1–37. https://doi.org/10.1021/acsami.9b15005.

[53] M. Sharma, A. Gaur, J.K. Quamara, Temperature-dependent dielectric response of (1-x)PVDF/(x)BaTiO 3 nanocomposite films, Physica B Condens Matter 563 (2019) 23–29. https://doi.org/10.1016/j.physb.2019.03.027.

Chapter 4

Studies on the effect of interfacial layers on the temperature-dependent dielectric and impedance behavior of flexible polyvinylidene fluoride-barium strontium titanate nanocomposites

4.1 Introduction

Polymer-ceramic nanocomposites have attracted considerable attention because of their prospects for application in advanced electronics and electrical power systems, such as aerospace, power systems, electric vehicles, and pulsed power applications [1–3]. These polymer nanocomposites are expected to operate efficiently in the higher-temperature range (room temperature to 100 °C), which is possible only when their electric properties, such as dielectric constant, tangent loss, and dielectric breakdown strength, remain stable in that operating temperature range [4–6]. A variety of polymer-ceramic nanocomposites have been explored for this purpose and include polymers such as poly(vinylidene difluoride) (PVDF), poly(vinylidene difluoride–trifluoroethylene), biaxially oriented polypropylene, and polyimide [6–11] and nanoceramic fillers such as $BaTiO_3$, $Ba_xSr_{1-x}TiO_3$, $PbZr_xTi_{1-x}O_3$, HfO_2, boron nitride, and Al_2O_3 [12–16]. Despite there being many choices, some electrical parameters are always compromised by another electrical parameter; for example, adding conducting fillers such as graphene [17], carbon nanotubes [14], and aluminum fibers [18] to the polymer matrix provides a nanocomposite with an increased dielectric constant along with increased tangent loss and electrical conductivity [19]. The size of the ceramic fillers also affects the performance of the nanocomposites. Composites with smaller filler sizes will be more beneficial since they have a more uniform morphology. These days, polymer-ceramic nanocomposites with a low weight/volume percentage of ceramic loading, high dielectric constant, and low tangent loss are required [3,8,9,20,21], as these nanocomposites having low tangent loss do not compromise with breakdown strength. Thus, the choice of polymer, ceramic filler, and filler size plays a very important role in the designing of polymer-ceramic nanocomposites with a high dielectric constant and a low tangent loss over a wide temperature range [22,23].

Several research groups have investigated the dielectric behavior of polymers/polymer-ceramic nanocomposites over a broad temperature range [4,24–28]. Recently, Wang et al. [4] studied

the dielectric and energy storage properties of layered polymer-ceramic nanocomposites over a broad temperature range (room temperature to 150 °C). The layered nanocomposites are synthesized with alternate layers of boron nitride nanosheet/polyetherimide and TiO_2 nanorod array/polyetherimide. For a 7 vol% ceramic–loaded layered composite, the activation energy is approximately 0.77 eV, while the dielectric constant and tangent loss at 1 kHz and room temperature are 7.12 and 0.013, respectively, and decreased to 6.9 and 0.01, respectively, at 120 °C. The decrease in the conduction process due to the increased activation energy is assigned as the main cause of the decreased tangent loss with increasing temperature. Polyimide and Al_2O_3, HfO_2, and TiO_2 nanocomposites are investigated in another study for high-temperature capacitive energy storage [6]. A considerably stable dielectric constant and a considerably stable tangent loss over a wide temperature range are found, but the dielectric constant is very small (less than 5). A possible reason for the thermal stability of the dielectric behavior is not suggested. The microstructure and temperature-dependent dielectric properties of PVDF–submicron hollow-sphere $Ba_{0.6}Sr_{0.4}TiO_3$ composites have also been studied [25]. At very high loading (i.e., 40 vol% loading of submicron hollow-sphere $Ba_{0.6}Sr_{0.4}TiO_3$), the observed dielectric constant and tangent loss are 15 and 0.03, respectively. The increase of the dielectric constant and tangent loss with increasing temperature is ascribed to mitigated interfacial bonding between the polymer and $Ba_{0.6}Sr_{0.4}TiO_3$. Studies of the dielectric constant and thermal stability of flexible composite films of PVDF-polyacrylonitrile revealed a dielectric constant and tangent loss at 1 kHz and room temperature of approximately 38 and approximately 0.05, respectively [26]; however, the loading of $BaTiO_3$ nanoparticles is very high, i.e., 64.7 vol%. Although the dielectric constant and tangent loss increased slightly to 41.5 and 0.08, respectively, at 120 °C, a reason for these observations is not given. Core-shell-structured Al-PVDF nanocomposites showed an increase in the dielectric constant and tangent loss with increasing temperature due to the gradually increased mobility of molecular chain

segments of PVDF [27]. Barium strontium titanate-based PVDF-poly(methyl methacrylate) trilayer nanocomposites exhibited a dielectric constant and tangent loss of 7 and 0.04, respectively. The low tangent loss at elevated temperatures is caused by the limitation of the migration of ions by the poly(methyl methacrylate) layer [24]. Most of the investigations based on the temperature-dependent breakdown strength and discharge energy density have been performed on low dielectric constant–based polymer-ceramic nanocomposites [4,6,24,25]. On the other hand, many studies have already reported on PVDF, poly(vinylidene difluoride–trifluoroethylene), and ceramic nanocomposites exhibiting a relatively very high dielectric constant and high discharge energy density [6–9,29], but they lack investigations of temperature dependency. Earlier studies confirmed that the thermal stability of the dielectric behavior (dielectric constant and tangent loss) is very important for the designing of polymer-ceramic nanocomposites for high energy density capacitors to be used at high temperatures and in harsh conditions. An understanding of the physical phenomena for the observed behavior would be very useful since it will help in the development of nanocomposite thick films with tailored dielectric behavior.

In the present chapter, the temperature-dependent dielectric behavior, AC conductivity, and impedance of PVDF-$Ba_{0.8}Sr_{0.2}TiO_3$ (BST) nanocomposite thick films are studied. A phenomenological model based on the Lewis model [30,31] is proposed to understand the role of various interfaces and the translational motion of the polymeric chain of PVDF for the observed experimental behavior.

4.2 Experimental

This chapter involves the fabrication of nanocomposite films comprising PVDF-$Ba_{0.8}Sr_{0.2}TiO_3$ and the consequent examination of their structural and temperature-dependent dielectric characteristics. The experimental studies are discussed in the following subsections.

4.2.1 Synthesis of PVDF-$Ba_{0.8}Sr_{0.2}TiO_3$ nanocomposite films

Fig. 4.1. Synthesis of PVDF-BST nanocomposite thick films

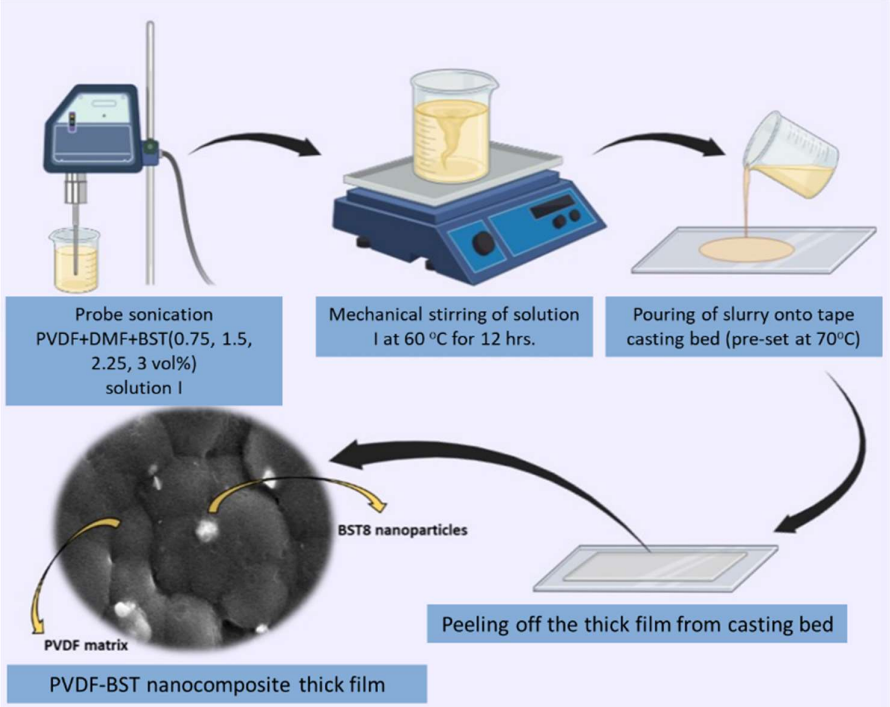

The synthesis of $Ba_{0.8}Sr_{0.2}TiO_3$ (BST) nanoparticles involves a hydrothermal method, followed by calcination at 800°C for a duration of 2 hours. Utilizing a tape casting technique outlined in section 2.2.3 (Chapter 2), nanocomposite films of PVDF-BST are fabricated with varying vol% loadings of BST nanoparticles. Specifically, films are produced at four different vol% concentrations 0.75%, 1.5%, 2.25%, and 3 vol% designated as PVDF-0.75BST, PVDF-1.5BST, PVDF-2.25BST, and PVDF-3BST, respectively. Fig. 4.1 shows a schematic for the synthesis of the PVDF-BST nanocomposite thick films.

4.2.2 Structural studies of PVDF-$Ba_{0.8}Sr_{0.2}TiO_3$ nanocomposite films

X-ray diffraction (XRD) patterns of the BST powder and the PVDF-BST nanocomposite films, along with Fourier transform infrared (FTIR) spectra of the nanocomposites have been recorded to investigate their phases and crystallinity. Microstructural and morphological characteristics of the BST powder are studied with a transmission electron microscope (TEM), while the surfaces of the PVDF-BST nanocomposites are studied with a scanning electron microscope (SEM).

4.2.3 Dielectric studies of PVDF-$Ba_{0.8}Sr_{0.2}TiO_3$ nanocomposite films

Dielectric properties (i.e., dielectric constant and tangent loss) of the nanocomposite films have been measured in the frequency range from 100 Hz to 1 MHz from room temperature to 150 °C. These dielectric parameters are used to calculate the temperature-dependent AC conductivity, activation energy and impedance of the PVDF-BST nanocomposite films.

4.3 Results and discussion

The results of structural and electrical studies are described in the subsequent sections.

4.3.1 Structural studies

The structural studies include X-ray diffraction (XRD) and Fourier transform infrared spectroscopy (FTIR) investigations. Whereas the scanning electron microscopy (SEM) and transmission electron microscopy (TEM) are used for morphological studies. The results of these studies are included in the following subsections.

4.3.1.1 X-ray diffraction

Fig. 4.2 shows the XRD patterns of BST nanopowder and PVDF-BST nanocomposite films. The peak at 2θ corresponding to 18.5° (020) is designated to the α phase of PVDF, and the higher-intensity peak at 20.4° (110) confirms the presence of the β phase of PVDF [32]. The peak at 31.8° represents the (101) plane of BST powder, and the BST powder showed a tetragonal

Fig. 4.2. X-ray diffraction patterns of BST powder and PVDF-BST nanocomposite thick films

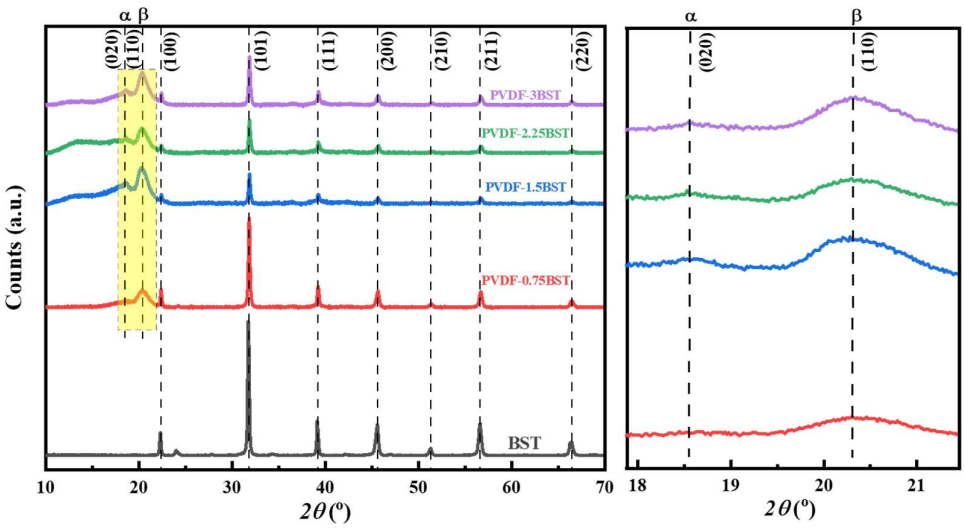

geometry with a = b = 0.39771 nm and c = 0.39883 nm, corresponding to ICDD card number 00-044-0093. The modified Scherer's formula is used to calculate the crystallite size of BST, which is approximately 19 nm. The crystallite size obtained is confirmed by transmission electron microscopy. The interplanar spacing (d spacing) for the intense peak at 31.8° for the BST powder is 0.281 nm. The diffractogram shows that as the volume percentage of nanoparticles increases in the PVDF matrix, the relative peak intensity of the β phase at 20.4° increases.

4.3.1.2 Fourier transform infrared spectroscopy

Fig. 4.3 shows the Fourier transform infrared spectra of PVDF nanocomposite thick films with different loading volume percentages of BST nanoparticles from 1600 cm^{-1} to 400 cm^{-1}. It is found that each nanocomposite film exhibits the characteristic bands of the α and β phases of PVDF. The absorption bands at 486 cm^{-1} (CF_2 wagging), 612 cm^{-1} and 763 cm^{-1} (CF_2 bending and skeletal bending) correspond to the α phase of PVDF. The bands at 510 cm^{-1} (CF_2 stretching), 835 cm^{-1} and 872 cm^{-1} (CH_2 rocking, CF_2 stretching, and skeletal C–C stretching) are attributed to the β phase of PVDF. The peaks at 1168 cm^{-1} and 1230 cm^{-1} are associated with CH_2 wagging

Fig. 4.3. Fourier transform infrared absorption spectra of PVDF-BST nanocomposite thick films

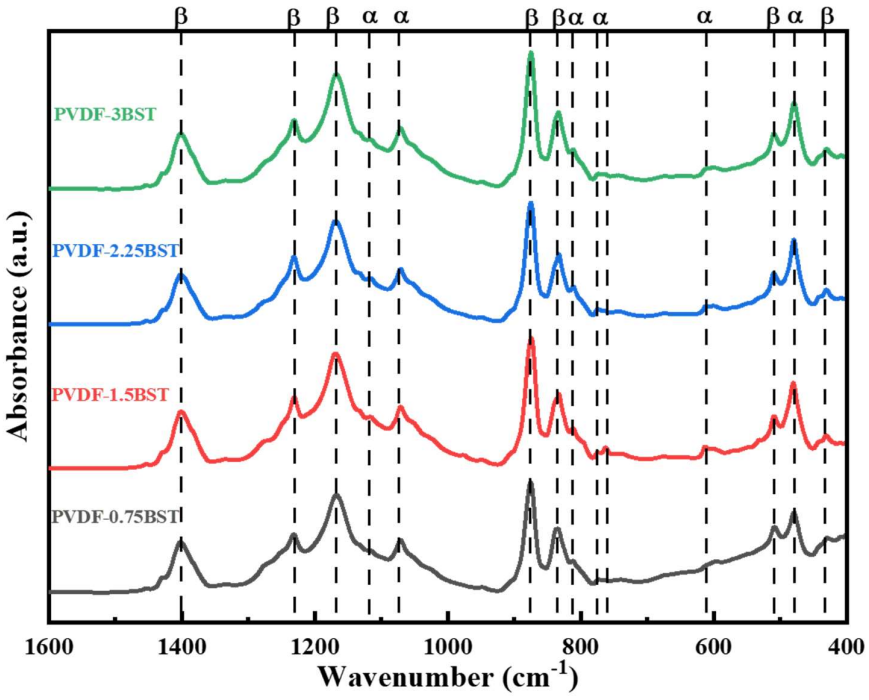

and rocking [33]. The peaks at 1234 cm^{-1} and 1402 cm^{-1} correspond to the β phase of PVDF. Also, the band at 1070 cm^{-1} gives the impression of bending of the C–C–C group [33,34].

It is well known that the β crystalline phase is polar in nature, whereas the α phase is nonpolar. The variation in the fractional content of the β phase of PVDF in the PVDF-BST nanocomposite thick films with different loading volume percentages of BST nanoparticles is also determined. The β-phase content has been determined by using the Beer-Lambert law as [35]:

$$F(\beta) = \frac{X_\beta}{X_\alpha + X_\beta} = \frac{A_\beta}{(K_\beta/K_\alpha)A_\alpha + A_\beta} = \frac{A_\beta}{1.3A_\alpha + A_\beta} \quad (4.1)$$

where X_α and X_β in equation (1) represent the mass fraction of α and β phases, A_α and A_β represent the absorbance at 763 cm^{-1} and 835 cm^{-1}, respectively. The absorption coefficients are expressed by K_α (6.1×10^4 cm^2 mol^{-1}) and K_β (7.7×10^4 cm^2 mol^{-1}) at that particular wavenumber, respectively [35]. The values of A_α and A_β are taken from the IR absorption spectra shown in section 3 of the manuscript. The variation of β-phase content with increasing vol% loading of BST in the PVDF-BST nanocomposite thick films is shown in Fig. 4.4. The content of the β phase of PVDF in the PVDF-BST nanocomposite thick films is found to increase with an increase in the loading of BST nanoparticles.

Fig.: 4.4 Variation of β-phase content with increasing vol% loading of BST in the PVDF-BST nanocomposite thick films

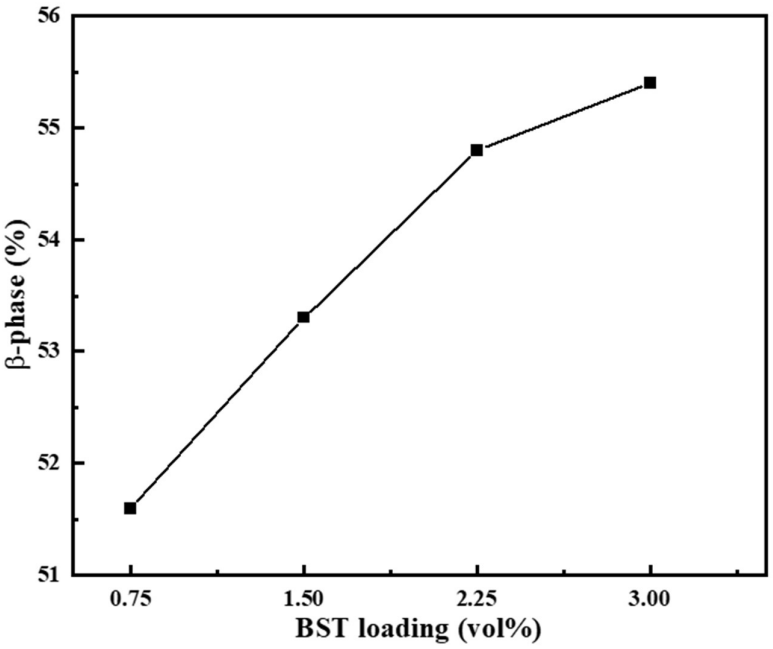

4.3.1.3 Scanning electron microscopy

Fig. 4.5. (a) SEM and (b) particle size distribution of the synthesized BST nanoparticles, and (c)–(f) SEM micrographs of PVDF-BST nanocomposite thick films

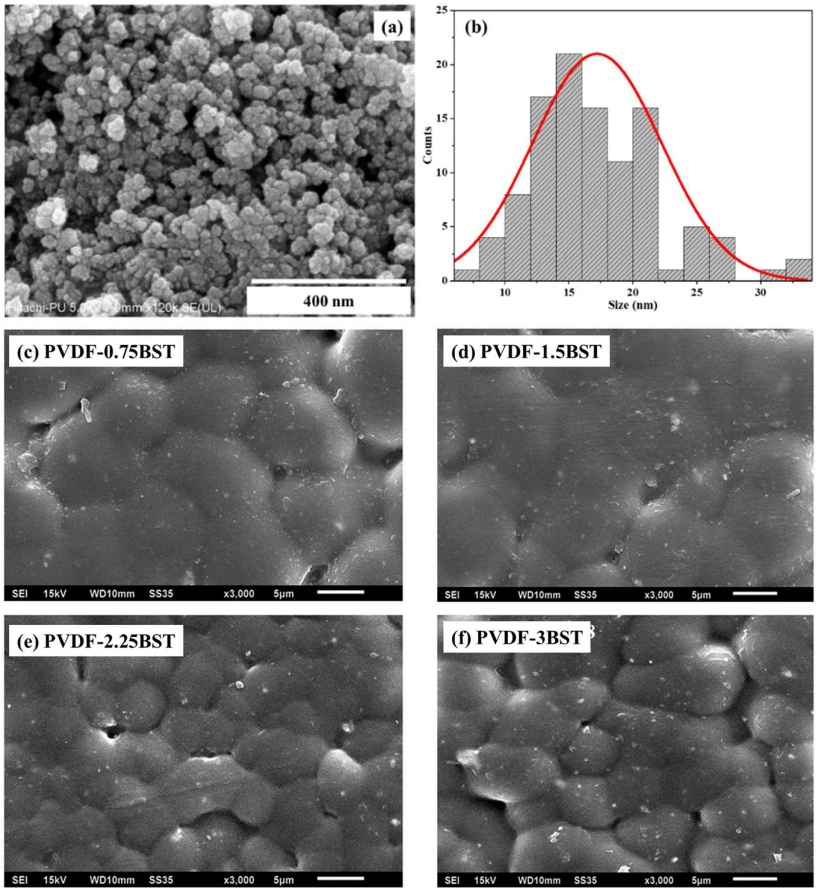

Fig.4. 5(a) shows a scanning electron micrograph of BST nanoparticles, and Fig. 4.5(b) shows the particle size distribution of these nanoparticles. The average size of the BST nanoparticles is approximately 17 nm, which is consistent with the crystallite size calculated from XRD and the particle size observed by transmission electron microscopy. Fig. 4.5(c)-4.5(f) shows scanning electron micrographs of the PVDF-BST nanocomposite films. The presence of spherulite-like particles of PVDF, along with embedded BST nanoparticles, can be clearly seen in Fig. 4.5(c). At a low loading volume percentage of BST, the boundaries among the PVDF spherulite-like particles are not very distinct and clear, whereas, with an increase in loading volume percentage (more than 1.5%), the boundaries among the PVDF spherulite-like particles become clearer along with a decrease in the size of the PVDF particles [36]. The incorporation of BST nanoparticles above a certain volume percentage (more than 1.5 vol%) might change the local charge

distribution, changing the interfacial force at PVDF/BST or PVDF/PVDF interfaces. These interfacial forces might decrease the size of PVDF spherulite-like particles.

4.3.1.4 Transmission electron microscopy

Fig. 4.6. (a) HRTEM image and (b) the fringe pattern (the inset shows the selected-area electron diffraction pattern) of the BST nanoparticles

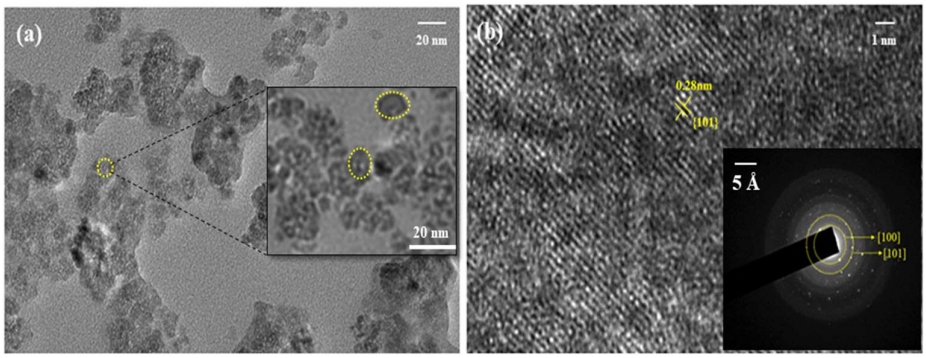

Fig. 4.6 shows the particle size of the BST nanoparticles and the lattice fringe pattern. Agglomeration of the BST nanoparticles can be seen in Fig. 4.6(a). The particle size is found to be approximately 17 nm. Fig. 4.6(b) shows an interplanar spacing of 0.28 nm for the (101) lattice plane. These observations are in agreement with the XRD results for BST nanoparticles. The inset in Fig. 4.6(b) shows the selected area electron diffraction pattern along with marked lattice planes of the BST nanoparticles.

4.3.2 Electrical studies

The electrical studies include the results of temperature-dependent dielectric constant and tangent loss of the PVDF-BST nanocomposite thick films. These parameters are used to calculate the AC conductivity and impedance of the nanocomposite films.

4.3.2.1 Dielectric studies

Fig. 4.7 shows the variation of the dielectric constant (ε′) and tangent loss (tan δ) of the PVDF-BST nanocomposite films with frequency at room temperature. An increase in the dielectric constant with an increase in the loading volume percentage of BST is observed in all the films. Moreover, the trend of the variation of the dielectric constant with frequency is also similar for

Fig. 4.7. Variation of dielectric constant and loss tangent with frequency at room temperature for PVDF-BST nanocomposite thick films

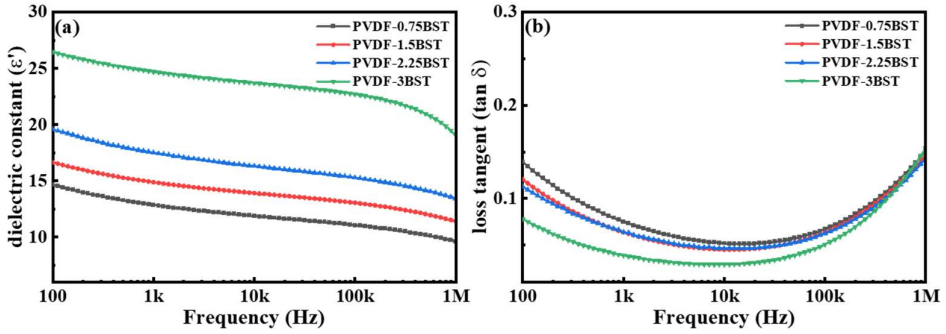

all the nanocomposite films. The increase of the dielectric constant with the increase of the loading of BST nanoparticles is ascribed to the increase of the local electric field in the PVDF-BST nanocomposite films [37]. The dielectric constant is found to decrease from 100 Hz to 1 kHz, which is associated with the decrease of surface or space charge polarization at the interfaces between PVDF and BST [38]. The dielectric constant remains almost the same in the frequency range from 1 kHz to 100 kHz, which is attributed to the dielectric behavior of BST [39]. The decrease in the dielectric constant for frequencies greater than 100 kHz is due to the characteristic α-phase relaxation of PVDF [40].

Fig.: 4.8 Variation of dielectric constant with temperature for the as-prepared $Ba_{0.8}Sr_{0.2}TiO_3$ nanoparticles at 1 kHz frequency

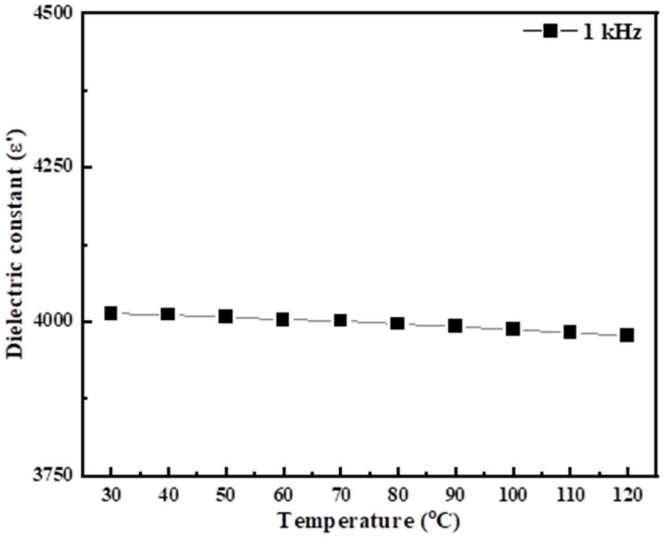

The tangent loss in a dielectric material arises mainly due to (i) surface/interface polarization, which is associated with space charge migration, (ii) the response of dipoles with the frequency of the applied field and (iii) DC conductivity.

The trend of the variation of the tangent loss for all the PVDF-BST nanocomposite thick films is similar and follows the same trend as for the dielectric constant. The tangent loss decreases with increasing frequency in the frequency range from 100 Hz to 1 kHz, whereas for frequencies in the range from 1 kHz to 100 kHz, it is nearly constant. For frequencies greater than 100 kHz, the tangent loss increases. These are the general features observed for all the nanocomposite films. Table 4.1 shows the dielectric constant, tangent loss, AC conductivity, and activation energy for different PVDF-BST nanocomposites at 1 kHz and room temperature. The importance of the dielectric stability of PVDF-BST nanocomposites at elevated temperatures is a deciding parameter for their application in high energy density capacitors [4]. Therefore, an understanding of the dielectric behavior and relaxation mechanism at high temperatures is needed. The dielectric constant of an as-prepared BST pellet is also measured; the variation of the dielectric constant shows nearly temperature-independent behavior until 120 °C. The data is shown in Fig. 4.8.

Table: 4.1 Dielectric constant, loss tangent, AC conductivity, and activation energy of PVDF-BST nanocomposite thick films at room temperature

Sample	ε′ at 1 kHz	tan δ at 1 kHz	σ_{AC} (S/m) at 1 kHz	E_a (eV)
PVDF-0.75BST	~13	~0.06	~7×10^{-8}	~0.25
PVDF-1.5BST	~15	~0.04	~5×10^{-8}	~0.23
PVDF-2.25BST	~18	~0.06	~6×10^{-8}	~0.16
PVDF-3BST	~25	~0.03	~8×10^{-6}	~0.15

Here, the temperature-dependent dielectric constant and tangent loss of PVDF-BST nanocomposite films are investigated. The glass transition temperature of amorphous polymers is a very important parameter for determining their applicability in polymer-ceramic nanocomposites [41]. On the other hand, the melting temperature is significant for nanocomposites based on crystalline polymers such as PVDF [41]. The melting temperature of PVDF is approximately 169 °C [41]; therefore, the temperature-dependent dielectric behavior is investigated up to 150 °C. Fig. 4.9 shows the temperature-dependent dielectric constant and

tangent loss of PVDF-BST nanocomposites at 1 kHz. The trend of the variation of the dielectric constant is nearly the same as the trend of the variation of the tangent loss. The dielectric constant of all the PVDF-BST nanocomposite films is nearly constant up to 70 °C because, in this temperature range the dielectric constant is determined mainly by the BST content. The CH_2–CF_2 dipole-related polar groups of PVDF are frozen and orientational polarization is not established [42]. Moreover, the role of PVDF/BST interfaces may also not be significant up to 70 °C. BST shows nearly temperature-independent behavior by virtue of its paraelectric nature above room temperature [25]. For temperatures greater than 70 °C, the dipoles of PVDF gain mobility and the time required for the establishment of the polarization is decreased.

Fig. 4.9. Variation of dielectric constant and loss tangent with temperature for PVDF-BST nanocomposite thick films at 1 kHz

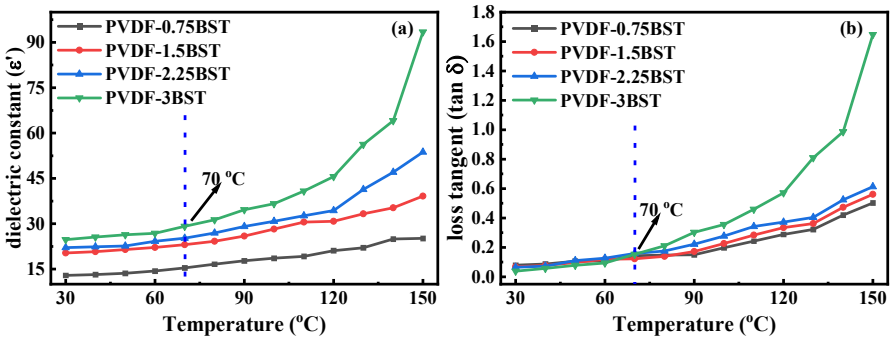

At higher temperatures, the evolution of orientational polarization caused by the translational motion of the PVDF molecular chain is the main cause of the increase in the dielectric constant [25,43,44]. The presence of ions and space charge at the PVDF/BST interface could also be the cause of the increase in polarization. At temperatures greater than 120 °C, the nanocomposites with BST loading greater than 1.5 vol% exhibit a sharp increase in the dielectric constant. The softening of PVDF at relatively lower temperatures and, hence increased movement among the polar molecules might be the associated cause of this sharp increase of the dielectric constant and tangent loss.

4.3.2.2 AC conductivity studies

Fig. 4.10(a) shows the variation of AC conductivity of the PVDF-BST nanocomposite with 3 vol% loading of BST (PVDF-3BST) with frequency at different temperatures. Fig. 4.10(b) shows the variation of AC conductivity with temperature for different PVDF-BST nanocomposites at 1 kHz. It can be seen from the plots that the AC conductivity of the PVDF-BST nanocomposite films is influenced by frequency and temperature. The following observations have been made:

(a) AC conductivity at constant temperature increases with frequency.

(b) AC conductivity increases with temperature at all frequencies.

The electrical conductivity of a material is determined by the type and mobility of the charge carriers. The relationship between the motion of charge carriers (including electrons, ions, defects, and dipoles) and the frequency can be described by Jonscher's power law as [10]

$$\sigma_{AC} = \sigma_{DC} + A\omega^{n} \qquad (0 < n < 1), \tag{4.1}$$

where A is the strength of polarization, n represents the degree of interaction between mobile ions and the surrounding lattice, and ω is the probing frequency. The whole conduction phenomenon is analyzed within the framework of Jonscher's power law [45,46] and thermally activated transport [4,46,47]. The value of n and its variation with temperature gives the physical phenomenon responsible for conduction. If $n \leq 1$, hopping motion involves a translational motion with sudden hopping; if $n > 1$, then localized hopping is present in the motion [47]. The values of A and n are very important for understanding the inherent physics. The values of these parameters are calculated for all the PVDF-BST nanocomposite thick films at different temperatures. The values of parameters' A' and 'n' for PVDF-BST nanocomposite thick films in different temperature ranges are given in Table 4.2.

In our case, for all the nanocomposites in the temperature range from 30 °C to 150 °C, n is found to be less than 1. Therefore, the most dominant conduction mechanism to explain the

transport properties in the present case is possibly the correlated barrier hopping model [10,46]. According to this model, because of thermal activation, charge carriers hop between two sites, increasing the AC conductivity of the PVDF-BST nanocomposite films.

Fig. 4.10. Variation of (a) AC conductivity with frequency for PVDF-3BST nanocomposite and (b) AC conductivity with temperature for different PVDF-BST nanocomposite thick films at 1 kHz

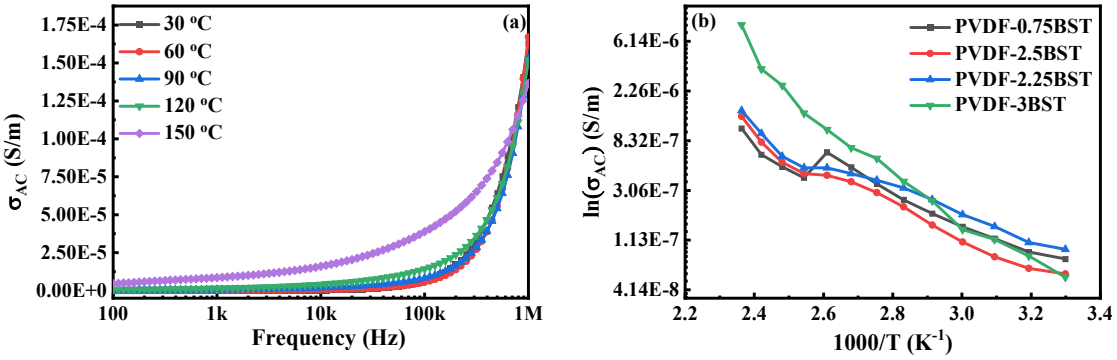

Table: 4.2 Parameters obtained from Jonscher's plot for the PVDF-BST nanocomposite thick films at 30 °C, 60 °C, 90 °C, 120 °C and 150 °C

Sample	Temperature	- ln(A)	A	n
PVDF-0.75BST	30 °C	26.128	4.49×10^{-12}	0.939
	60 °C	24.640	1.99×10^{-11}	0.948
	90 °C	22.304	2.05×10^{-10}	0.773
	120 °C	24.324	2.73×10^{-11}	0.995
	150 °C	21.842	3.26×10^{-10}	0.809
PVDF-1.5BST	30 °C	26.429	3.32×10^{-12}	0.943
	60 °C	24.762	1.76×10^{-11}	0.928
	90 °C	21.966	2.88×10^{-10}	0.717
	120 °C	21.049	7.21×10^{-10}	0.646
	150 °C	20.432	1.33×10^{-9}	0.637
PVDF-2.25BST	30 °C	25.897	5.66×10^{-12}	0.958
	60 °C	24.182	3.14×10^{-11}	0.905
	90 °C	22.535	1.63×10^{-10}	0.773
	120 °C	21.801	3.40×10^{-10}	0.692
	150 °C	20.833	8.96×10^{-10}	0.659
PVDF-3BST	30 °C	22.534	1.63×10^{-10}	0.834
	60 °C	21.002	7.56×10^{-9}	0.716
	90 °C	20.093	1.87×10^{-9}	0.638
	120 °C	20.044	1.97×10^{-9}	0.609
	150 °C	19.497	3.40×10^{-9}	0.592

Fig. 4.11 shows very interesting results. The value of n is nearly constant (approximately 0.9) in the temperature range from 30 °C to 60 °C for PVDF-BST nanocomposites with BST loading of 2.25 vol% or less, whereas a sharp decrease in n occurs for the PVDF-3BST nanocomposite.

Fig. 4.11. Variation of (a) *n* with temperature for different PVDF-BST nanocomposites at 1 kHz (the inset shows the variation of *A* with temperature) and (b) *n* with BST loading volume percentage for different PVDF-BST nanocomposite films at 1 kHz

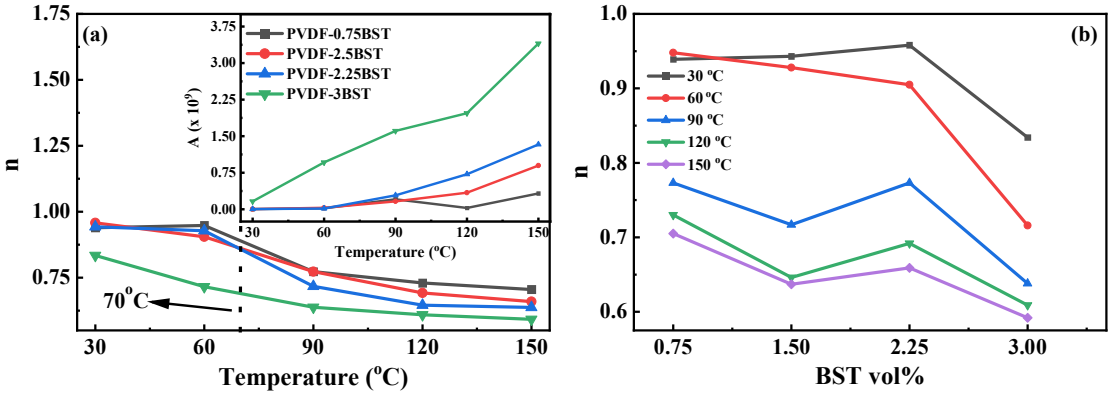

The value of n shows a decreasing trend in the temperature range from 60 °C to 120 °C for all the PVDF-BST nanocomposites. The constant value of n (approximately 0.9) with BST loading up to 2.25 vol% for the PVDF-BST nanocomposites indicates that the number of hopping sites is nearly constant in the temperature range from 30 °C to 60 °C, whereas the number of thermally induced hopping sites (defects, ions, and space charge) might be increasing in the PVDF-BST nanocomposites. The thermally induced abrupt increase in the number of hopping sites occurs in the temperature range from 60 °C to 120 °C; beyond 120 °C, the evolution of hopping sites saturates.

The parameter A in Jonscher's law gives the strength of polarization. The variation of A with temperature for all the PVDF-BST nanocomposites is shown in the inset in Fig. 4.11(a). The increase of A with temperature might be related to the enhanced molecular motion of PVDF in the PVDF-BST nanocomposites [25], which in turn increases the polarizability. A similar trend is found for the variation of the dielectric constant with temperature. Fig. 4.11(b) shows the variation of n with the loading volume percentage of BST nanoparticles for the PVDF-BST

nanocomposite thick films at different temperatures. It is seen that n is almost constant for the nanocomposite with BST loading of up to 2.25 vol%. A sudden decrease in n is seen for the PVDF-3BST nanocomposite thick film owing to an increase in the number of hopping sites. This analysis reveals the evolution of hopping sites with temperature for the conduction of charge carriers. Hence, it is pertinent to investigate thermally activated transport by the Arrhenius equation, which is given as

$$\sigma_{AC} = \sigma_o \exp\left(\frac{-E_a}{kT}\right), \quad (4.2)$$

Fig.: 4.12 Variation of fitting of σ_{ac} as a function of inverse temperature (K^{-1}) for the PVDF-BST nanocomposite thick films

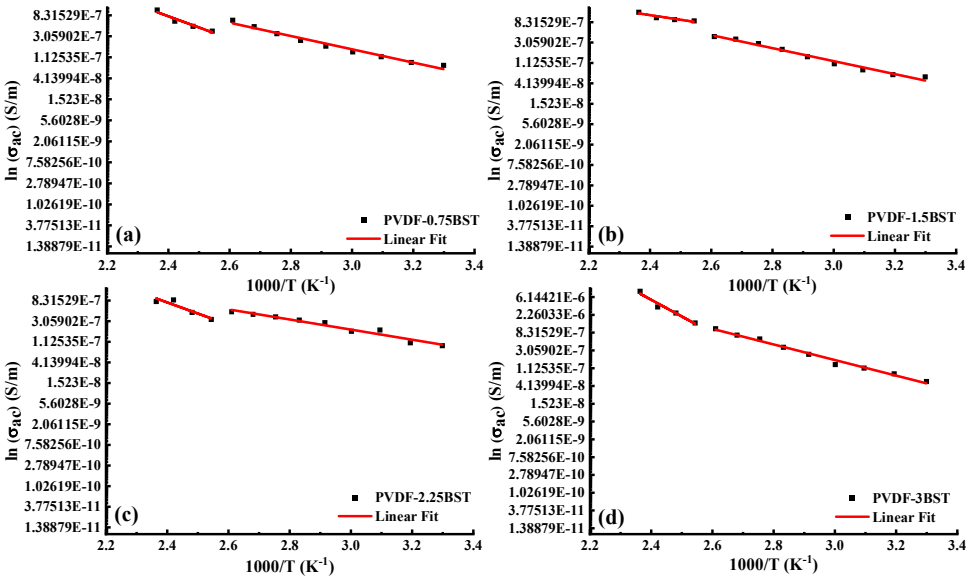

where σ_o is a constant, E_a is the activation energy (the minimum energy required for conduction from one site to another), k is Boltzmann's constant, and T is the temperature at which the study is being done. It is clear from Fig. 4.10 (a) that the AC conductivity of the nanocomposite thick films increases with increasing temperature. Also, the AC conductivity data shown in Fig. 4.12 has been fitted in two ranges, (i) RT-110 ^oC and (ii) 120 ^oC-150 ^oC, with activation energies E_{a1} and E_{a2} (summarized in Table 4.3). The resultant activation energy has been taken as the average of these two values. The observation of a decrease in the activation energy with an increase in the loading of BST nanoparticles in the PVDF matrix

implies that the barrier height facilitating the hopping of the charge carriers decreases with the increase in the loading of BST [10].

The AC conductivity is maximum for the PVDF-3BST nanocomposite, which has the lowest activation energy of approximately 0.15 eV. The conductivity at lower temperatures is predominantly due to long-distance hopping of charge carriers, while at higher temperatures, it may also be attributed to an increase in the thermally induced hopping sites (defects, ions, space charge), which leads to an increase in the activation energy of the nanocomposite thick films [46,48].

Table: 4.3 Values of activation energy for the PVDF-BST nanocomposite thick films in different temperature ranges

Sample	PVDF-0.75BST	PVDF-1.5BST	PVDF-2.25BST	PVDF-3BST
E_{a1} (eV)	0.19	0.14	0.19	0.11
E_{a2} (eV)	0.32	0.32	0.13	0.19
E_a (average) (eV)	0.25	0.23	0.16	0.15

4.3.2.3 Impedance studies

Fig. 4.13. Variation of real and imaginary parts of the impedance with temperature for (a) PVDF-0.75BST, (b) PVDF-1.5BST, (c) PVDF-2.25BST, and (d) PVDF-3BST nanocomposite thick films and (e) equivalent electrical circuit

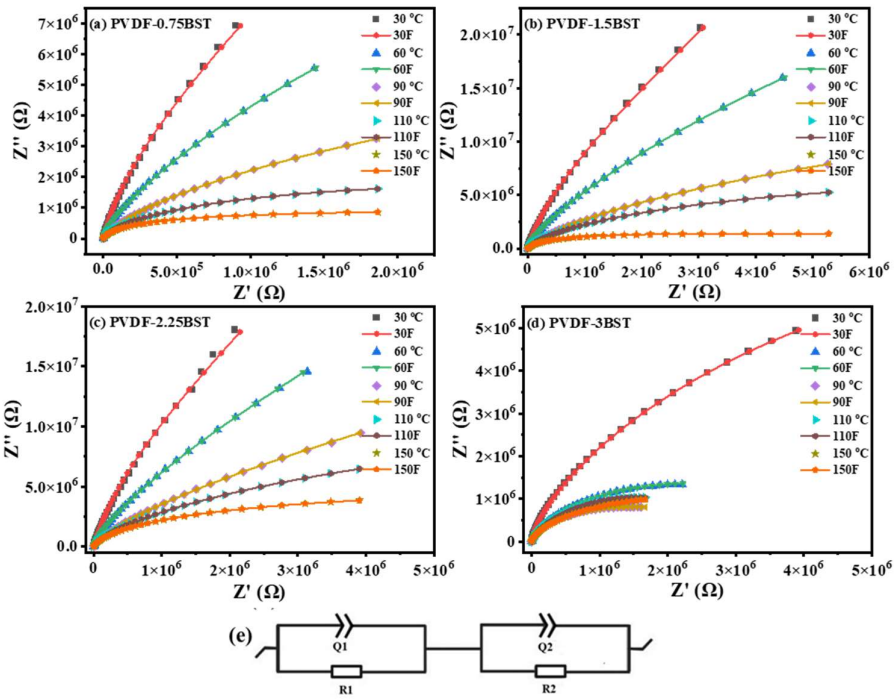

To develop more understanding of the effect of temperature and BST loading in the PVDF-BST nanocomposites on the thermally induced relaxation process, complex

impedance analysis is performed. Fig. 4.13(a)-4.13(d) shows Nyquist plots for the PVDF-BST nanocomposites at different temperatures. The absence of complete semicircles can be seen here for all the nanocomposites, which confirms non-Debye-type relaxation behavior. Also, it is clear from these plots that as the temperature increases, the Nyquist plot tends more and more toward the real axis of the impedance for all the PVDF-BST nanocomposite samples. These observations are related to the decrease in resistance of PVDF-BST nanocomposite grains, which decreases with increasing temperature [10]. The Nyquist plots are fitted with an equivalent electrical circuit, as shown in Fig. 4.13(e). The fitted data is denoted using an F in front of the temperature (such as 30F, 60F, etc.).

The series combination of these two parallel circuits shows the best fit of the experimental data. Here, R1 and Q1 and R2 and Q2 represent the resistance and constant phase element of the grains and the grain boundaries, respectively. PVDF-BST particulates (as seen by scanning electron microscopy) represent the grains, and the interfacial space between any two PVDF-BST particulates represents the grain boundary. The temperature-dependent conductivity revealed that some kind of leakage might be happening in all the PVDF-BST nanocomposites. The leakage is responsible for the nonideal capacitive behavior of the PVDF-BST nanocomposites. Hence, a constant phase element is added in the equivalent circuit; the constant phase element is determined by [49]

$$Q = \frac{1}{(i\omega)^{\alpha}C} \tag{4.3}$$

where α is 0 for an ideal resistor and 1 for an ideal capacitor. The fitting parameters are summarized in Table 4.4. R1 and R2 decrease with increasing temperature for all the nanocomposite films, as shown in Table 4.4. The resistance R2 associated with grain boundary in the PVDF-3BST nanocomposite thick film decreases from 18.8 MΩ to approximately 4.5 MΩ, which is caused by thermally induced hopping of the charge carriers in the grain boundaries [10,46]. So, it can be said that the resistance due to grains and grain boundaries

decreases because of thermal agitation and the existence of thermally activated conduction mechanisms in the grains and grain boundaries of the nanocomposite thick films.

Table: 4.4 Fitting parameters from the Nyquist plots for PVDF-BST nanocomposite thick films at different temperatures

Sample	Parameter	30 °C	60 °C	90 °C	110 °C	150 °C
PVDF-0.75BST	R1 (MΩ)	70.34	6.61	0.72	0.37	0.10
	Q1 (F $s^{(a-1)}$)	0.27×10^{-9}	0.27×10^{-9}	0.28×10^{-9}	0.33×10^{-9}	0.31×10^{-9}
	a1	0.965	0.970	0.971	0.961	0.962
	R2 (MΩ)	470	60.16	20.08	5.90	3.56
	Q2 (F $s^{(a-1)}$)	89.93×10^{-12}	0.56×10^{-9}	3.47×10^{-9}	6.69×10^{-9}	16.58×10^{-9}
	a2	0.934	0.691	0.562	0.556	0.496
PVDF-1.5BST	R1 (MΩ)	140	13.01	1.14	0.60	0.15
	Q1 (F $s^{(a-1)}$)	91.76×10^{-12}	93.09×10^{-12}	95.36×10^{-12}	91.8×10^{-12}	94.23×10^{-12}
	a1	0.963	0.967	0.969	0.971	0.975
	R2 (MΩ)	210	201	47.5	22.68	5.19
	Q2 (F $s^{(a-1)}$)	15.47×10^{-12}	0.29×10^{-9}	1.62×10^{-9}	2.30×10^{-9}	6.09×10^{-9}
	a2	1	0.638	0.553	0.550	0.512
PVDF-2.25BST	R1 (MΩ)	190	12.65	0.71	0.51	0.26
	Q1 (F $s^{(a-1)}$)	0.1052×10^{-9}	0.10×10^{-9}	0.11×10^{-9}	0.10×10^{-9}	0.10×10^{-9}
	a1	0.966	0.969	0.971	0.971	0.974
	R2 (MΩ)	430	150.2	50.22	39.24	17.19
	Q2 (F $s^{(a-1)}$)	14.81×10^{-12}	0.49×10^{-9}	2.03×10^{-9}	1.91×10^{-9}	3.55×10^{-9}
	a2	1	0.551	0.491	0.558	0.529
PVDF-3BST	R1 (MΩ)	2.36	0.32	0.14	0.14	0.66
	Q1 (F $s^{(a-1)}$)	0.17×10^{-9}	0.16×10^{-9}	0.10×10^{-9}	0.12×10^{-9}	0.11×10^{-9}
	a1	0.946	0.955	0.982	0.969	0.971
	R2 (MΩ)	18.58	4.64	3.36	4.02	4.52
	Q2 (F $s^{(a-1)}$)	1.95×10^{-9}	7.15×10^{-9}	11.47×10^{-9}	9.67×10^{-9}	14.89×10^{-9}
	a2	0.593	0.519	0.483	0.494	0.469

Note: For Q1 and Q2, the units are F $s^{(a-1)}$, where F represents Farads, s denotes the complex frequency variable, and a is the dimensionless constant that characterizes the behavior of the constant phase element.

4.3.3 Mechanism: effect of polymer-ceramic nanoparticle interfacial layers

The incorporation of nanoparticles in polymeric material makes the surface of the nanoparticles positively charged [50]. Therefore, the interface between the polymer matrix and the

nanoparticles affects the charge distribution, the polarization, and hence the dielectric behavior. The effect of the interface on these properties has already been explored by two important models proposed by Lewis [30,31] and Tanaka [50]. The experimental observation in the present work can be described by the Lewis model. The surface of BST nanoparticles incorporated in the PVDF matrix becomes positively charged (Fig. 4.14). The charged interface in PVDF-BST nanocomposites comprises three charged layers that determine the dielectric properties. The formation of an electrical double layer at the PVDF and BST interface occurs as a result of the charge redistribution in the PVDF matrix via coulombic attraction caused by charged BST nanoparticles. These double layers are termed the Stern layer and the Gouy-Chapman diffused layer [30,31,51]. The Stern layer exists around the surface of the BST nanoparticles and consists of small molecules, adsorbed ions, etc., which cannot move freely, whereas the diffused layer is formed around the Stern layer by the distribution of charges (positive and negative). This layer may be treated as a space charge zone. When the temperature of the PVDF-BST nanocomposites is increased from 30 °C to 70 °C, frozen ions of the Stern layer and space charge of the diffused layer do not have sufficient thermal energy to increase the interfacial polarization.

Fig. 4.14. Mechanism responsible for the observed experimental behavior

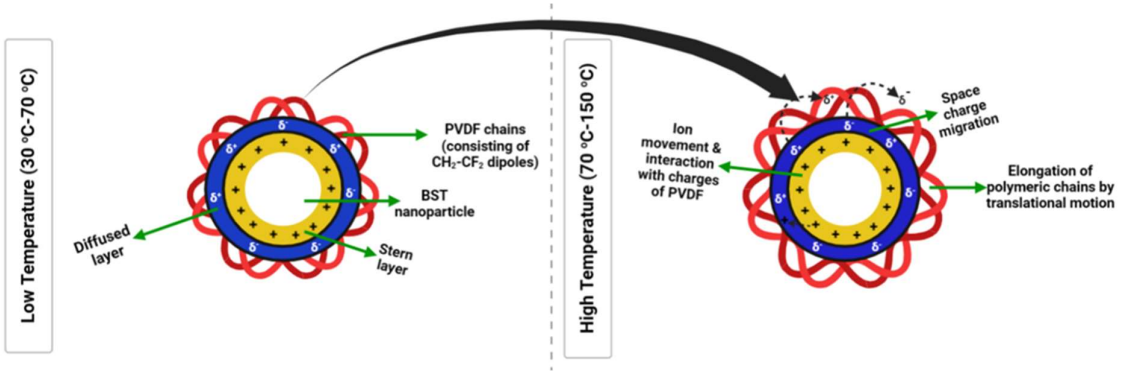

Moreover, translational motion in the polymeric chains also does not occur. When the temperature becomes greater than 70 °C, thermal migration of frozen ions and space charge occurs, which causes the interfacial polarization. The thermally induced motion in the

polymeric chain also causes an increase in the dipole moment. The increase in the interfacial polarization and the thermally induced dipole moment is ascribed to the increase in the dielectric constant. On the other hand, the migration of space charge of the inner layer and ions of the outer layer causes the tangent loss to increase with increasing temperature. The conduction of ions/space charge leaves sites called hopping sites. The increase in the number of hopping sites with temperature is attributed to an increase in conductivity and a decrease in impedance. Hence, interfacial polarization in the double layer between PVDF-BST nanocomposites and translational motion in polymeric chains of PVDF is attributed to the observed dielectric, AC conductivity, and impedance behavior.

4.4 Conclusion

Flexible PVDF-BST nanocomposite thick films (approximately 80 μm) with different loading volume percentages of BST nanoparticles are synthesized by the tape casting method. The dielectric constant and tangent loss of all the PVDF-BST nanocomposites remain nearly constant until 70 °C, and with further increase of the temperature (> 70 °C), the dielectric constant and tangent loss increase. An increase in the AC conductivity and a decrease in the impedance are observed with an increase in temperature for the PVDF-BST nanocomposites. Impedance analysis confirmed non-Debye-type relaxation behavior for all the nanocomposite thick films, and the dipolar contribution to the polarization increased with increasing temperature. A possible mechanism for the increase of the dielectric constant, tangent loss, and AC conductivity and the decrease of impedance with increasing temperature for the PVDF-BST nanocomposite thick films is proposed, which relies on the Lewis model and the interfacial double-layer model. Thermally-induced translational motion of polymeric chains of PVDF, the motion of ions, and the migration of space charge in the interfacial layer of the PVDF matrix and BST nanoparticles might be attributed to the observed dielectric behavior. These investigations and analyses are important as the suitable interfacial modification of the

polymer-ceramic interface in the nanocomposites could passivate the migration of space charge and the motion of ions in the interfacial layers, which might prevent the increase in the tangent loss of the nanocomposites with temperature.

References

[1] Prateek, R. Bhunia, S. Gupta, A. Garg, R.K. Gupta, In-situ fabrication of barium titanate@polyvinyl pyrrolidone in polyvinylidene fluoride polymer nanocomposites for dielectric capacitor applications, Journal of Polymer Science 60 (2022) 961–967. https://doi.org/10.1002/pol.20210628.

[2] Y. Guo, S. Liu, S. Wu, J. Xu, E. Pawlikowska, W. Bulejak, M. Szafran, A. Rydosz, F. Gao, Enhanced tunable dielectric properties of Ba0.6Sr0.4TiO3/PVDF composites through dual-gradient structural engineering, J Alloys Compd (2022) 166034. https://doi.org/10.1016/j.jallcom.2022.166034.

[3] S. Kaur, D.P. Singh, Significantly improved dielectric and energy storage behavior of the surface functionalized CaCu3Ti4O12 nanoparticles in PVDF-CaCu3Ti4O12 nanocomposites, J Alloys Compd 918 (2022) 165500. https://doi.org/10.1016/J.JALLCOM.2022.165500.

[4] P. Wang, L. Yao, Z. Pan, S. Shi, J. Yu, Y. Zhou, Y. Liu, J. Liu, Q. Chi, J. Zhai, Q. Wang, Ultrahigh Energy Storage Performance of Layered Polymer Nanocomposites over a Broad Temperature Range, Advanced Materials 33 (2021). https://doi.org/10.1002/adma.202103338.

[5] Z. Jiang, Y. Yuan, H. Yang, E. Li, S. Zhang, Excellent thermal stability and energy storage properties of lead-free Bi0.5Na0.5TiO3-based ceramic, Journal of the American Ceramic Society 105 (2022) 4027–4038. https://doi.org/10.1111/jace.18332.

[6] D. Ai, H. Li, Y. Zhou, L. Ren, Z. Han, B. Yao, W. Zhou, L. Zhao, J. Xu, Q. Wang, Tuning Nanofillers in In Situ Prepared Polyimide Nanocomposites for High-Temperature Capacitive Energy Storage, Adv Energy Mater 10 (2020). https://doi.org/10.1002/aenm.201903881.

[7] Z.M. Dang, J.K. Yuan, J.W. Zha, T. Zhou, S.T. Li, G.H. Hu, Fundamentals, processes and applications of high-permittivity polymer–matrix composites, Prog Mater Sci 57 (2012) 660–723. https://doi.org/10.1016/J.PMATSCI.2011.08.001.

[8] H. Chen, Y.F. Hou, Z.J. Wu, P. Du, L.H. Luo, W.P. Li, Simultaneous enhancement of discharge energy density and efficiency in the PMMA and PVDF blend films via introducing the Ni(OH)2 nanosheets, J Alloys Compd 862 (2021). https://doi.org/10.1016/j.jallcom.2021.158688.

[9] S. Koner, P. Deshmukh, A. Ahlawat, A.K. Karnal, S. Satapathy, Studies on structural, dielectric, impedance spectroscopy and magneto-dielectric properties of La0.7Ba0.3MnO3/P(VDF-TrFE) multiferroic (0–3) nanocomposite films, J Alloys Compd 868 (2021). https://doi.org/10.1016/j.jallcom.2021.159104.

[10] H.H. Singh, H.B. Sharma, Impedance spectroscopy and transport properties of polymer-based flexible nanocomposites, Solid State Commun 319 (2020). https://doi.org/10.1016/j.ssc.2020.114012.

[11] S. Sharma, S.S. Mishra, R. Kumar, R.M. Yadav, Recent progress on polyvinylidene difluoride-based nanocomposites: applications in energy harvesting and sensing, New Journal of Chemistry 46 (2022) 18613–18646. https://doi.org/10.1039/d2nj00002d.

[12] A.I. Ali, M.M. Hassan, G. Goda Mohammed, H.Y. Abdel El-Hamid, H. Awad, Preparation, structural and dielectric properties of nanocomposite Al2O3/BaTiO3 for multilayer

ceramic capacitors applications, Journal of Materials Research and Technology 18 (2022) 2083–2092. https://doi.org/10.1016/j.jmrt.2022.03.041.

[13] H. Hammami, M. Arous, M. Lagache, A. Kallel, Study of the interfacial MWS relaxation by dielectric spectroscopy in unidirectional PZT fibres/epoxy resin composites, J Alloys Compd 430 (2007) 1–8. https://doi.org/10.1016/j.jallcom.2006.04.048.

[14] U. Yaqoob, G.S. Chung, Effect of surface treated MWCNTs and BaTiO3nanoparticles on the dielectric properties of a P(VDF-TrFE) matrix, J Alloys Compd 695 (2017) 1231–1236. https://doi.org/10.1016/j.jallcom.2016.10.250.

[15] Y. Shang, Y. Feng, C. Li, C. Zhang, T. Zhang, Y. Zhang, Y. Zhang, C. Song, Q. Chi, Energy storage properties of P(VDF-TrFE-CTFE)-based composite dielectrics with uniform and gradient-doped boron nitride nanosheets, IET Nanodielectrics 5 (2022) 50–61. https://doi.org/10.1049/nde2.12024.

[16] H. Zhang, X. Yao, L. Zhang, Microstructure and dielectric properties of barium strontium titanate thick films and ceramics with a concrete-like structure, Journal of the American Ceramic Society 90 (2007) 2333–2339. https://doi.org/10.1111/j.1551-2916.2007.01742.x.

[17] H. Luo, Z. Wu, X. Zhou, Z. Yan, K. Zhou, D. Zhang, Enhanced performance of P(VDF-HFP) composites using two-dimensional BaTiO3 platelets and graphene hybrids, Compos Sci Technol 160 (2018) 237–244. https://doi.org/10.1016/j.compscitech.2018.03.034.

[18] Y. Zhou, Y. Bai, K. Yu, Excellent thermal conductivity and dielectricproperties of polyimide composites filledwith silica coated self-passivated aluminumfibers and nanoparticles, Appl. Phys. Lett 102 (2013) 252903. https://doi.org/10.1063/1.4812653.

[19] S.H. Xie, B.K. Zhu, X.Z. Wei, Z.K. Xu, Y.Y. Xu, Polyimide/BaTiO3composites with controllable dielectric properties, Compos Part A Appl Sci Manuf 36 (2005) 1152–1157. https://doi.org/10.1016/j.compositesa.2004.12.010.

[20] L. Han, H. Wang, Q. Tang, X. Lang, X. Wang, Y. Zong, C. Zong, Preparation of graphene/polypropylene composites with high dielectric constant and low dielectric loss *via* constructing a segregated graphene network, RSC Adv 11 (2021) 38264–38272. https://doi.org/10.1039/D1RA06138K.

[21] H. Zhang, Y. Zhu, Z. Li, P. Fan, W. Ma, B. Xie, High discharged energy density of polymer nanocomposites containing paraelectric SrTiO 3 nanowires for flexible energy storage device, J Alloys Compd 744 (2018) 116–123. https://doi.org/10.1016/j.jallcom.2018.02.052.

[22] D.Q. Tan, Review of Polymer-Based Nanodielectric Exploration and Film Scale-Up for Advanced Capacitors, Adv Funct Mater 30 (2020). https://doi.org/10.1002/adfm.201808567.

[23] Y. Zhou, Q. Li, B. Dang, Y. Yang, T. Shao, H. Li, J. Hu, R. Zeng, J. He, Q. Wang, A Scalable, High-Throughput, and Environmentally Benign Approach to Polymer Dielectrics Exhibiting Significantly Improved Capacitive Performance at High Temperatures, Advanced Materials 30 (2018). https://doi.org/10.1002/adma.201805672.

[24] R.P. Nie, Y. Li, L.C. Jia, J. Lei, H.D. Huang, Z.M. Li, PVDF/PMMA dielectric films with notably decreased dielectric loss and enhanced high-temperature tolerance, J Polym Sci B Polym Phys 57 (2019) 1043–1052. https://doi.org/10.1002/polb.24858.

[25] Y. Guo, K. Zhang, N. Meng, W. Wu, Y. Wang, J. Xu, E. Pawlikowska, M. Szafran, F. Gao, Microstructure and dielectric properties of sub-micron hollow sphere

(Ba0.6Sr0.4)TiO3/PVDF composites, IET Nanodielectrics 2 (2019) 135–141. https://doi.org/10.1049/iet-nde.2019.0013.

[26] B. Wang, Y. Ma, B. Na, R. Lv, H. Liu, W. Li, H. Zhou, Enhanced dielectric thermal stability and permittivity of flexible composite films based on BaTiO3 nanoparticles highly filled PVDF/PAN blend nanofibrous membranes, Polym Compos 39 (2018) E1841–E1848. https://doi.org/10.1002/pc.24829.

[27] Y. Gong, W. Zhou, X. Sui, Y. Kou, L. Xu, Y. Duan, F. Chen, Y. Li, X. Liu, H. Cai, Q. Chen, Z.M. Dang, Core-shell structured Al/PVDF nanocomposites with high dielectric permittivity but low loss and enhanced thermal conductivity, Polym Eng Sci 59 (2019) 103–111. https://doi.org/10.1002/pen.24872.

[28] R. Sahoo, S. Mishra, A. Ramadoss, S. Mohanty, S. Mahapatra, S.K. Nayak, Temperature-dependent dielectric properties of metal-doped ZnO nanofiller reinforced PVDF nanocomposites, Mater Res Bull 132 (2020). https://doi.org/10.1016/j.materresbull.2020.111005.

[29] D. Lai, Z. Yao, W. You, B. Gao, Q. Guo, P. Lu, A. Ullah, H. Hao, M. Cao, H. Liu, Regulating energy storage performances of 0.85NaNbO3-0.15Bi(Zn2/3Nb1/3)O3 ceramics using BaTiO3, Journal of Materiomics 8 (2022) 166–173. https://doi.org/10.1016/j.jmat.2021.04.001.

[30] T.J. Lewis, Interfaces are the dominant feature of dielectrics at the nanometric level, in: IEEE Transactions on Dielectrics and Electrical Insulation, 2004: pp. 739–753. https://doi.org/10.1109/TDEI.2004.1349779.

[31] T.J. Lewis, Nanometric Dielectrics, IEEE Transactions on Dielectrics and Electrical Insulation 1 (1994) 812–825. https://doi.org/10.1109/94.326653.

[32] P. Gupta, A. Kumar, M. Tomar, V. Gupta, D.P. Singh, Enhanced dielectric properties and suppressed leakage current density of PVDF composites flexible film through small loading of submicron Ba0.7Sr0.3TiO3crystallites, Journal of Materials Science: Materials in Electronics 28 (2017) 11806–11812. https://doi.org/10.1007/s10854-017-6987-2.

[33] S. Roy, P. Thakur, N.A. Hoque, B. Bagchi, N. Sepay, F. Khatun, A. Kool, S. Das, Electroactive and High Dielectric Folic Acid/PVDF Composite Film Rooted Simplistic Organic Photovoltaic Self-Charging Energy Storage Cell with Superior Energy Density and Storage Capability, ACS Appl Mater Interfaces 9 (2017) 24198–24209. https://doi.org/10.1021/acsami.7b05540.

[34] M. Arjun Hari, K. Rakesh, R.S. Divya, L. Rajan, C.K. Subash, S. Varghese, Influence of Nanosilica in PVDF Thin Films for Sensing Applications, in: 2021 IEEE International Symposium on Smart Electronic Systems (ISES) (Formerly INiS), IEEE, 2021: pp. 70–73. https://doi.org/10.1109/iSES52644.2021.00027.

[35] B. Lin, Z.-T. Li, Y. Yang, Y. Li, J.-C. Lin, X.-M. Zheng, F.-A. He, K.-H. Lam, Enhanced dielectric permittivity in surface-modified graphene/PVDF composites prepared by an electrospinning-hot pressing method, Compos Sci Technol (2019). https://doi.org/10.1016/j.compscitech.2019.01.003.

[36] W. Ma, J. Zhang, S. Chen, X. Wang, β-Phase of poly(vinylidene fluoride) formation in poly(vinylidene fluoride)/poly(methyl methacrylate) blend from solutions, Appl Surf Sci 254 (2008) 5635–5642. https://doi.org/10.1016/j.apsusc.2008.03.012.

[37] Kittle Charles, Introduction to solid state physics, Eighth edition, John Wiley & Sons Inc., New York, USA, 1971.

[38] A. Mayeen, M.S. Kala, M.S. Jayalakshmy, S. Thomas, D. Rouxel, J. Philip, R.N. Bhowmik, N. Kalarikkal, Dopamine functionalization of BaTiO3: An effective strategy for the enhancement of electrical, magnetoelectric and thermal properties of BaTiO3-PVDF-TrFE nanocomposites, Dalton Transactions 47 (2018) 2039–2051. https://doi.org/10.1039/c7dt03389c.

[39] Z. Song, S. Zhang, H. Liu, H. Hao, M. Cao, Q. Li, Q. Wang, Z. Yao, Z. Wang, M.T. Lanagan, Improved Energy Storage Properties Accompanied by Enhanced Interface Polarization in Annealed Microwave-Sintered BST, Journal of the American Ceramic Society 98 (2015) 3212–3222. https://doi.org/10.1111/jace.13741.

[40] C. V. Chanmal, J.P. Jog, Dielectric relaxations in PVDF/BaTiO3 nanocomposites, Express Polym Lett 2 (2008) 294–301. https://doi.org/10.3144/expresspolymlett.2008.35.

[41] W.N. dos Santos, J.A. de Sousa, R. Gregorio, Thermal conductivity behaviour of polymers around glass transition and crystalline melting temperatures, Polym Test 32 (2013) 987–994. https://doi.org/10.1016/j.polymertesting.2013.05.007.

[42] L. Wang, F. Gao, K. Zhang, M. Wang, M. Qin, J. Kong, Effect of hot pressing temperature on dielectric and energy storage properties of Ba0.6Sr0.4TiO3/ poly(vinylidene fluoride) composites, IEEE Transactions on Dielectrics and Electrical Insulation 24 (2017) 704–711. https://doi.org/10.1109/TDEI.2017.006191.

[43] S. Chen, K. Yao, F.E.H. Tay, C.L. Liow, Ferroelectric poly(vinylidene fluoride) thin films on Si substrate with the B phase promoted by hydrated magnesium nitrate, J Appl Phys 102 (2007). https://doi.org/10.1063/1.2812702.

[44] F.C. Sun, A.M. Dongare, A.D. Asandei, S. Pamir Alpay, S. Nakhmanson, Temperature dependent structural, elastic, and polar properties of ferroelectric polyvinylidene fluoride (PVDF) and trifluoroethylene (TrFE) copolymers, J Mater Chem C Mater 3 (2015) 8389–8396. https://doi.org/10.1039/C5TC01224D.

[45] A. Chawla, S. Verma, I. Pushkarna, P.S. Malhi, A. Singh, P.D. Babu, M. Singh, Phase evolution and magnetoelectric coupling studies in multiferroic Fe doped BST solid solutions, Appl Phys A Mater Sci Process 127 (2021). https://doi.org/10.1007/s00339-021-04740-1.

[46] M. Jebli, J. Dhahri, M.A. Albedah, M. ben Henda, H. Belmabrouk, M.L. Bouazizi, A. Hamdi, An investigation of the temperature- and frequency- dependent conductivity behavior and electrical properties of Ba0.97La0.02Ti0.9Nb0.08O3 compound using impedance spectroscopy, J Mol Struct 1254 (2022). https://doi.org/10.1016/j.molstruc.2021.132238.

[47] A. Bendahhou, K. Chourti, M. Loutou, S. el Barkany, M. Abou-Salama, Impact of rare earth (RE3+ = La3+, Sm3+) substitution in the A site perovskite on the structural, and electrical properties of Ba(Zr0.9Ti0.1)O3 ceramics, RSC Adv 12 (2022) 10895–10910. https://doi.org/10.1039/d2ra01483a.

[48] H.H. Singh, H.B. Sharma, Impedance spectroscopy and transport properties of polymer-based flexible nanocomposites, Solid State Commun 319 (2020). https://doi.org/10.1016/j.ssc.2020.114012.

[49] J.B. Jorcin, M.E. Orazem, N. Pébère, B. Tribollet, CPE analysis by local electrochemical impedance spectroscopy, in: Electrochim Acta, 2006: pp. 1473–1479. https://doi.org/10.1016/j.electacta.2005.02.128.

[50] Z. Pan, L. Yao, J. Zhai, X. Yao, H. Chen, Interfacial Coupling Effect in Organic/Inorganic Nanocomposites with High Energy Density, Advanced Materials 30 (2018). https://doi.org/10.1002/adma.201705662.

[51] T. Tanaka, Dielectric nanocomposites with insulating properties, in: IEEE Transactions on Dielectrics and Electrical Insulation, 2005: pp. 914–928. https://doi.org/10.1109/TDEI.2005.1522186.

Chapter 5

Studies on the dielectric and energy storage behavior of the specially architectured trilayered polyvinylidene fluoride-$Ba_{0.8}Sr_{0.2}TiO_3$ nanocomposites at low loading of nanofiller

5.1 Introduction

Polymer-ceramics nanocomposites have received huge demand due to their capacitative energy storage performance and its application in pulsed power systems such as military, aerospace and hybrid electric vehicles, etc. [1,2]. Pulsed power application requires a capacitor which can deliver a large amount of current in a very short span of time, which requires a capacitor bank with capacitors of very high discharge energy density. The performance of these capacitors is primarily determined by two physical parameters, i.e., (i) dielectric constant related with the ability to store the charge and (ii) breakdown strength. The structured thin film that could be deposited over a large volume will miniaturize the electronic and serve the purpose in a better way. Fundamentally, the electrostatic energy density of a linear dielectric material is given as [3]:

$$\text{energy density } (U_E) = \frac{1}{2}\varepsilon_r\varepsilon_0 E_b^2 \tag{5.1}$$

where ε_0, ε_r are the vacuum permittivity (8.854 x 10^{-12} F/m) & dielectric constant and E_b is the dielectric strength. The ceramics (such as $BaTiO_3$ (BT), $BaSrTiO_3$ (BST), $PbZrTiO_3$ (PZT), HfO_2, etc.) based capacitors possess high dielectric constant(~4,000), but have very low breakdown strength (~150 MV/m) [4–6]. On the other hand, ceramic materials structured in the form of thin films have very high energy density (~43 J/cc), but they could not be deposited over large volumes [7]. Therefore, ceramic materials are not suitable to meet the growing demand for pulsed power applications. On the other hand, polymer ceramic nanocomposites would be the most suitable choice for high energy density capacitors due to their ease of processability, moderate dielectric constant(~16-40) and high breakdown strength (~500MV/m) [8,9]. These nanocomposites consist of high dielectric ceramic nanoparticles embedded in a dielectric polymer (such as poly(methyl methacrylate) (PMMA), epoxy resin, polyvinylidene difluoride (PVDF), polypropylene (PP), etc.) [10–14]. Plethora of research investigations have been done to synthesize polymer ceramic nanocomposites with high

discharge energy density (U_D) and high breakdown strength (BDS) [15–17]. But, the polymer-ceramic nanocomposites having high efficiency (η) and discharge energy density are pertinently important for efficient pulsed power applications. Usually, high discharge energy densities have been achieved in polymer ceramic nanocomposites at higher vol% loading of ceramic nanoparticles [18,19]. The high loading of ceramic nanoparticles always compromises with the BDS, which is not favorable for the energy storage behavior. Several approaches have been adopted to achieve high energy density, breakdown strength and efficiency by improving the connectivity between polymer matrix and ceramic nanoparticles [18,20].

Table 5.1: Comparison of dielectric constant(ε'), tangent loss (tanδ), discharge energy density (U_D), breakdown strength (BDS) and efficiency (η) in different polymer-ceramic nanocomposites

Material	Loading	ε'	Tanδ	U_D	BDS	% η	Ref.
PVDF/BST	7.5 vol%	22	0.05	6.95 Jcm^{-3} at 350 MV/m	325 MV/m	50	[21]
PVDF/BT	20 vol%	25	0.05	4.4 Jcm^{-3} at 120 MV/m	-	78	[22]
PVDF/BT	15 vol%	16	0.04	3.2 Jcm^{-3} at 2800 kV/cm	2883 kV/cm	30	[23]
PVDF/BT	10 wt%	19.4	0.07	4.12 Jcm^{-3} at 400 MV/m	389 MV/m	-	[16]
PVDF/BT	20 vol%	23	0.04	4.08 Jcm^{-3} at 150 MV/m	193 MV/m	69	[24]
PVDF/BF	5 wt%	15	0.04	1.15 Jcm^{-3} at 800 kV/cm	1000 kV/cm	73	[25]
PVDF/BT	60 wt%	14	0.06	1.56 Jcm^{-3} at 120 MV/m	120 MV/m	71	[26]
PVDF/BT-CF	7 wt%	13	0.03	5.6 Jcm^{-3} at 263 kV/mm	263 kV/mm	57	[27]
PVDF/BST	3 vol%	25	0.03	7.8 Jcm^{-3} at 1400 kV/cm	282 MV/m	92.9	This work

The incorporation of a large volume percentage (~20%) of tetradecyl phosphonic acid-modified $BaTiO_3$ in the PVDF matrix has shown the discharge energy density and efficiency of ~ 4.4 Jcm^{-3} and ~ 78%, respectively, which is ascribed to the improved compatibility between polymeric matrix and surface modified $BaTiO_3$ nanoparticles [22]. Homogeneous interfaces with $BaTiO_3$ nanoparticles (BTNPs)/poly(vinylidene fluoride) (PVDF) multilayered

nanocomposites have been synthesized by using the spin coating technique, where PVP is employed as a linker to connect the top and bottom layers [23]. For 15 vol% loaded BT nanoparticles, trilayered nanocomposites demonstrate the U_D of ~2 Jcm^{-3} and dielectric BDS of 224.9 MV/m, which is caused by the interfacial homogeneity due to the presence of PVP layers. In a research report, where enhanced discharge energy density (~1.56 Jcm^{-3}) and efficiency (~71%) at low field (120 MV/m) is achieved in the heterojunction structure where high ion polarized $BaTiO_3$ films are sandwiched between PVDF layers [26]. The observed properties are supported by inhibition in the formation of conducting paths due to the spacer layer of $BaTiO_3$ films. A comparative table consisting of the dielectric permittivity, tangent loss, discharge energy density, breakdown strength and efficiency is given in table 5.1. The current research trend elucidates about the quest for the low-loaded polymer-ceramic nanocomposites with superior efficiency, discharge energy density and excellent dielectric properties.

Therefore, the present chapter is aimed at the synthesis of trilayered PVDF-BST nanocomposites with very small vol% loading of BST nanoparticles (i.e., 0.75%, 1.50%, 2.25% and 3.00%) for achieving the excellent dielectric properties, efficiency and discharge energy density.

5.2 Experimental

This chapter involves the fabrication of specially architectured trilayered nanocomposite films comprising PVDF-$Ba_{0.8}Sr_{0.2}TiO_3$. The structural, dielectric, displacement versus electric field and electrical breakdown strength studies of these films have been carried out, which are discussed as follows.

5.2.1 Synthesis of PVDF-$Ba_{0.8}Sr_{0.2}TiO_3$ nanocomposite films

The $Ba_{0.8}Sr_{0.2}TiO_3$ (BST) nanoparticles are produced with the hydrothermal method [28]. The poly(vinylidene)fluoride-$Ba_{0.8}Sr_{0.2}TiO_3$ (PVDF-BST) nanocomposites are prepared using the

Fig.:5.1 Schematic representation of the synthesis of specially architecture nanocomposite films

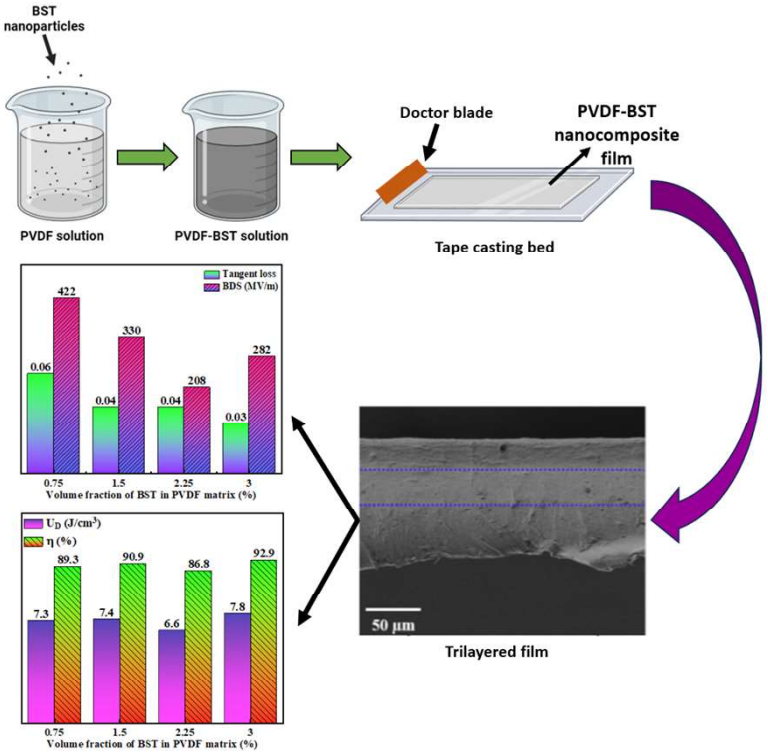

tape casting technique with 0.75, 1.50, 2.25 and 3.00 vol % BST nanoparticles into the PVDF polymer matrix. The trilayered PVDF-BST nanocomposites are made by casting the top and bottom layers in the same direction, whereas the middle layer is casted in the opposite direction. The schematic of specially architecture nanocomposite films is shown in Fig. 5.1. The individual nanocomposite thick films stacked over one another in this way are subjected to a hot press with 250 kN pressure for 5 minutes at 150 ^oC to get the trilayered nanocomposite films. The samples have been named as 0.75% BST, 1.50% BST, 2.25% BST and 3.00% BST, respectively.

5.2.2 Structural studies of PVDF-$Ba_{0.8}Sr_{0.2}TiO_3$ nanocomposite films

Transmission electron microscope (TEM) is used to study the microstructural characteristics of the BST nanoparticles, while the surface and cross-section of the trilayer PVDF-BST nanocomposites films along with the morphology of single-layer PVDF-BST nanocomposites are analyzed with a field emission scanning electron microscope (FESEM). The crystallinity of the BST powder and the nanocomposites is identified using X-ray diffraction (XRD) along with the Fourier-transform infrared (FTIR) spectra of the trilayered PVDF-BST nanocomposites.

5.2.3 Electrical studies of PVDF-$Ba_{0.8}Sr_{0.2}TiO_3$ nanocomposite films

An impedance analyzer has been used to measure the room temperature dielectric properties of these nanocomposites in the frequency range of 100 Hz to 1 MHz with an oscillating voltage of ± 1V across the samples. The breakdown strength (BDS) of PVDF-BST nanocomposites is measured by using Danbridge 30 kV Non-Destructive Insulation Tester (Denmark), whereas dielectric displacement vs. electric field (D-E) loops are measured by employing a 10 Hz triangular wave.

5.3 Results and discussion

The results of structural, morphological and electrical studies are described in subsequent subsections.

5.3.1 Structural studies

The results of the X-ray diffraction (XRD), Fourier transform infrared spectroscopy (FTIR), field emission scanning electron microscopy (FESEM) and transmission electron microscopy (TEM) are explained in subsequent subsections.

5.3.1.1 X-ray diffraction

Fig. 5.2 presents the X-ray diffraction (XRD) patterns of both BST nanoparticles and trilayered PVDF-BST nanocomposites with different vol% loading of BST nanoparticles. The (101) plane of BST is denoted by the intense peak at 31.8° with tetragonal geometry (ICDD card no. 00-044-0093). The crystallite size of these nanoparticles is calculated using a modified Scherer's formula, which came out to be ~19 nm & confirmed with TEM (discussed later). Thermal strain due to the calcination of BST nanopowder and

Fig.:5.2 XRD pattern of $Ba_{0.8}Sr_{0.2}TiO_3$ nanoparticles and different trilayered PVDF-BST nanocomposites

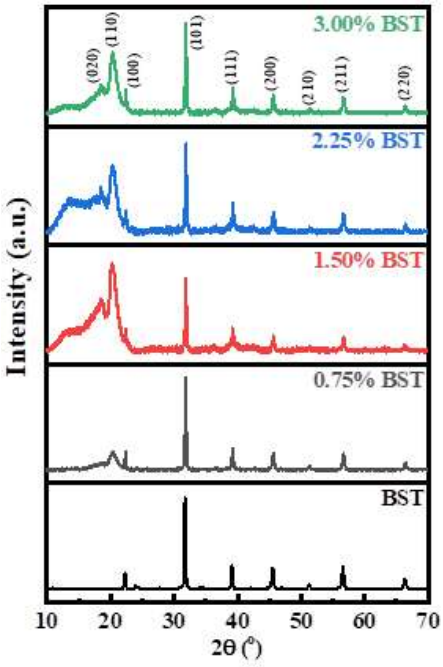

instrument broadening could also be the cause of the broadening of diffraction peaks in the XRD pattern. Therefore, the particle size has also been calculated with the Williamson-Hall method [29]. The peak broadening of the material due to lattice strain can be calculated using the following relationship [29]:

$$\beta_{hkl}\cos\theta = \frac{K\lambda}{D} + 4\eta\sin\theta \qquad (5.1)$$

where λ is the wavelength of the X-rays used (1.54Å), θ is the Bragg angle, D is the average crystalline size measured in the direction perpendicular to the surface of the specimen, K is a constant (K=0.94) and η is the strain in the material. Equation (5.1) is called the Williamson-Hall (W-H) equation and the plot of $\beta_{hkl}\cos\theta$ (y-axis) vs. $4\sin\theta$ (x-axis) is known as the W-H plot. The estimated value of the strain is calculated from the slope of the linear fit of the data, which comes out to be 1.2856 x 10^{-4}. The intercept of the linear fit gives the value of the crystallite size, which is ~19 nm for the synthesized BST nanopowder. From Fig. 5.3, it is conventional to say that the estimated value of lattice strain is appropriate as the data points are less scattered from the linear fit. The better fit of the experimental data points confirms the uniformity of the lattice strain in the synthesized BST powder. The 2θ peak at 18.5° (020) designates the α-phase of PVDF, which is nonpolar, whereas the presence of β phase of PVDF (which is polar) is confirmed by the higher intensity peak at 20.4° (110) [30].

Fig.:5.3 W-H plot for $Ba_{0.8}Sr_{0.2}TiO_3$ powder

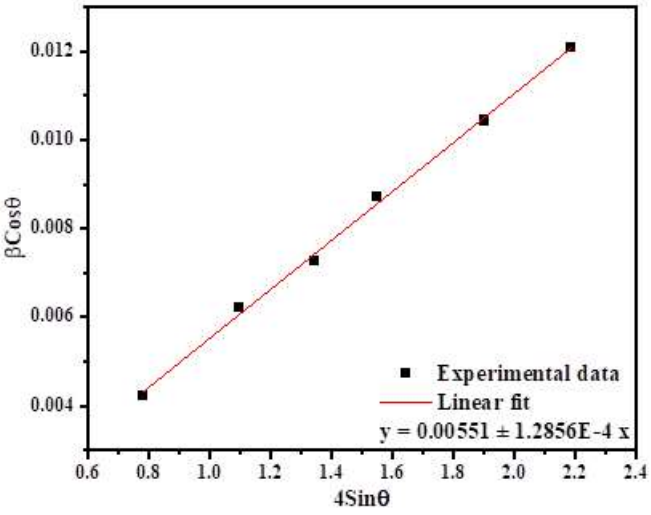

5.3.1.2 Fourier transform infrared spectroscopy

Fig. 5.4 displays the FTIR spectra from 1600 cm^{-1} to 400 cm^{-1} for different trilayered PVDF-BST nanocomposites. For all the trilayered PVDF-BST nanocomposites, transmittance peaks

of two crystalline PVDF phases (i.e., the α-phase and the β-phase) are observed. The transmission bands at 486 cm^{-1}, 612 cm^{-1} and 763 cm^{-1}, respectively, belong to wagging, bending and skeletal bending of CF_2 in the PVDF, which resembles the α-phase. The bands at 510 cm^{-1} and 1168 cm^{-1} are associated with CF_2 stretching,

Fig.:5.4 The FTIR transmittance spectrum of different trilayered PVDF-BST nanocomposites

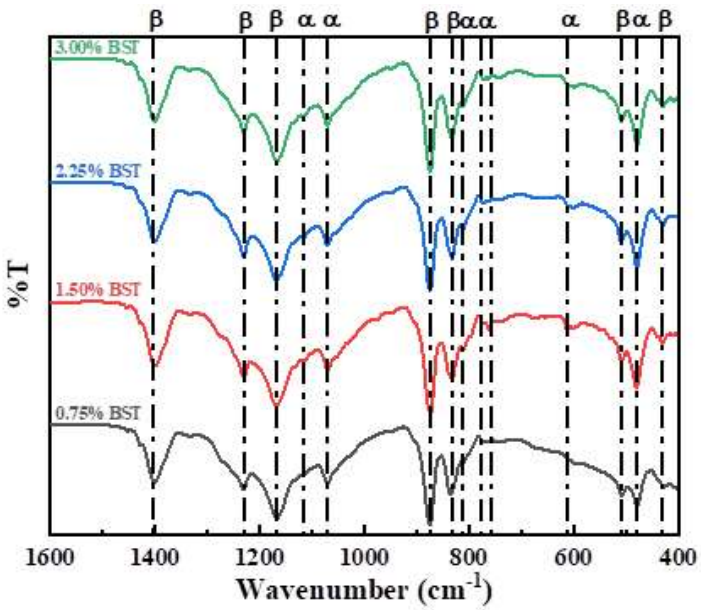

whereas the bands at 835 cm^{-1} and 872 cm^{-1} represent the rocking and wagging of CH_2, respectively. The band at 1230 cm^{-1} associates itself with the skeletal C-C stretching. All these bands, along with the bands at 1234 cm^{-1} and 1402 cm^{-1}, represent the β phase of PVDF [31,32]. The bending of the C-C-C group is confirmed by the 1070 cm^{-1} peak [31,32]. The variation of β fraction with different vol% loading of BST nanoparticles in PVDF has also been calculated using the Beer-Lambert law as [33,34]:

Fig.:5.5 Variation of β fraction with different volume fraction loading of BST nanoparticles in the PVDF matrix

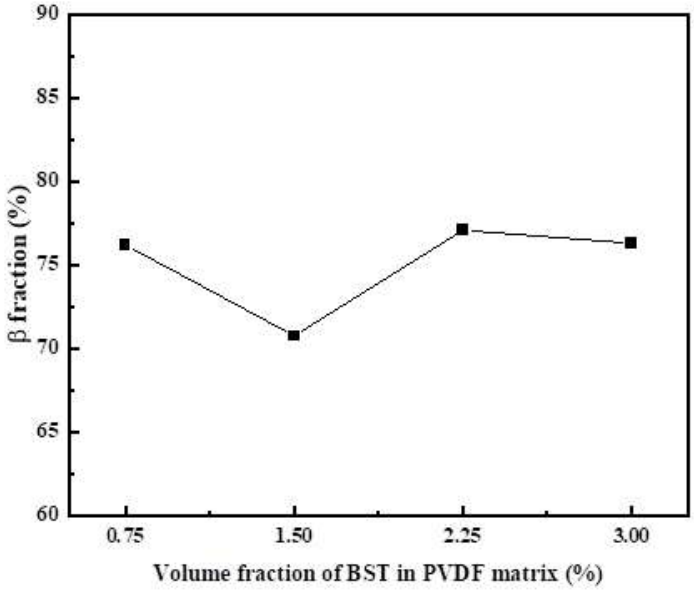

$$F(\beta) = \frac{X_\beta}{X_\alpha + X_\beta} = \frac{A_\beta}{(K_\beta/K_\alpha)A_\alpha + A_\beta} = \frac{A_\beta}{1.3A_\alpha + A_\beta} \quad (5.2)$$

where X_α and X_β in equation (B) represent the mass fraction of α and

β phases, A_α and A_β represent the absorbance at 763 cm^{-1} and 835 cm^{-1}, respectively. The absorption coefficients are expressed by K_α ($6.1x10^4$ cm^2 mol^{-1}) and K_β ($7.7x10^4$ cm^2 mol^{-1}) at that particular wavenumber, respectively [33]. The variation of β-phase content with increasing wt% loading of BST in the trilayered PVDF-BST nanocomposite thick films is shown in Fig. 5.5.

5.3.1.3 Field emission scanning electron microscopy

Fig. 5.6 is showing the surface scanning electron microscope (SEM) images of poly(vinylidene)fluoride-$Ba_{0.8}Sr_{0.2}TiO_3$ (PVDF-BST) single-layer nanocomposites with (a) 0.75, (b) 1.50, (c) 2.25 and (d) 3.00 vol% loading of BST nanoparticles. No agglomeration of BST nanoparticles is visible in the synthesized single-layer PVDF-BST nanocomposite.

Fig.:5.6 SEM images of PVDF-BST single-layer nanocomposites with (a) 0.75, (b) 1.50, (c) 2.25 and (d) 3.00 vol% loading of BST nanoparticles

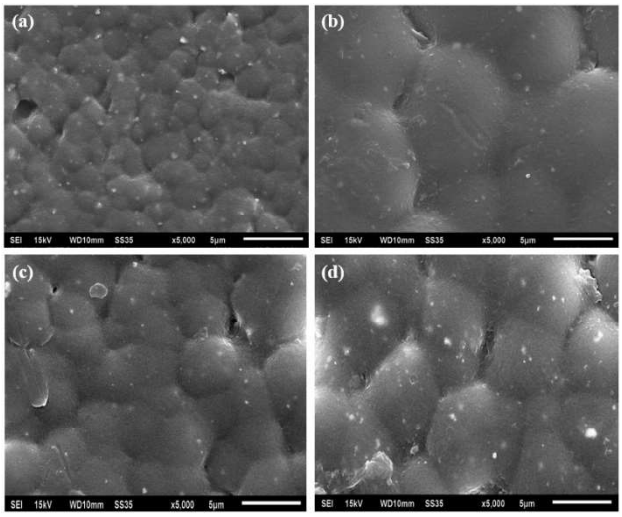

Fig. 5.7 (a) displays the surface of the FESEM image of PVDF-BST trilayered nanocomposite with 3 vol% concentration of BST nanoparticles after hot-pressing. Fig. 5.7 (b) shows the embedded BST nanoparticles in the PVDF polymer matrix. Upon inspecting the surface of the trilayered nanocomposite films after hot pressing, the absence of agglomeration of BST nanoparticles in the PVDF matrix is observed. Further analysis of FESEM micrographs also indicates that the BST nanoparticles

Fig.:5.7 (a), (b) Surface field emission scanning electron microscope (FESEM) image and (c) cross-sectional FESEM image of PVDF-BST trilayered nanocomposite with 3 vol% loading

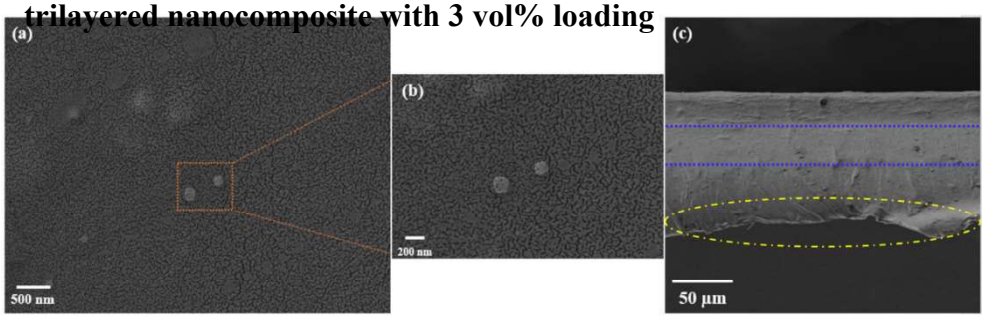

are properly embedded in each layer of the trilayered nanocomposites. The cross-sectional FESEM of PVDF-BST nanocomposites have been carried out for the conspicuous inspection of the formation of trilayered nanocomposites. The thickness of this hot-pressed trilayered thick film comes out to be ~70 μm (single layer thickness ~25 μm). It can be observed here that the layers have diffused into each other due to the hot-pressing process. The bending of the film (marked in yellow color) around the edge is observed due to the high power of the electron beam of the FESEM apparatus. The three-layer structure can be distinguished by the difference in the color contrast presented in the cross-sectional FESEM image of the PVDF-BST nanocomposite. This color contrast is occurring due to the variation in the distribution of the BST nanoparticles in each layer. The top and bottom layers, which are casted in the same direction, are dark in color as compared to the middle layer, which is casted in the opposite direction and is lighter in color.

5.3.1.4 Transmission electron microscopy

Fig.:5.8 (a) FESEM image and (b) High-resolution transmission electron microscope (HRTEM) fringe pattern (inset: SAED pattern) of the BST nanoparticles

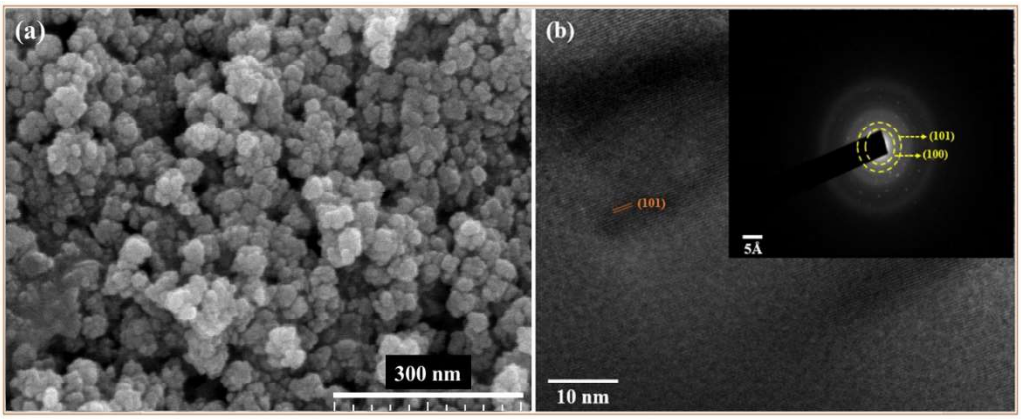

Fig. 5.8 (a) displays the field emission scanning electron micrograph (FESEM) of $Ba_{0.8}Sr_{0.2}TiO_3$ nanoparticles at a 300 nm scale. For these nanoparticles, the average size comes out to be ~17 nm, which is in agreement with the particle size observed in transmission electron microscopy (TEM) analysis and with the XRD results. For the (101) lattice plane of BST nanoparticles, an interplanar spacing of 0.28 nm is observed in Fig. 5.8 (b). The inset of

Fig. 5.8 (b) is showing the selected area electron diffraction (SAED) pattern, where the lattice planes of the BST nanoparticles are clearly visible, which are marked for reference.

5.3.2 Electrical studies

The electrical studies include dielectric behavior and electrical displacement vs electric field (D-E) studies. The discharging energy density, as well as energy efficiency of all the PVDF/BST trilayered nanocomposite thick films, have been calculated from electrical displacement vs electric field data. The results of these studies are discussed in the following subsections.

5.3.2.1 Dielectric studies

The frequency dependence of the dielectric constant and tangent loss for the pure PVDF nanocomposite is shown in Fig 5.9 (a). It can be observed here that with higher values at lower frequencies than at higher frequencies. At 1 kHz, the dielectric constant is ~10, with a tangent loss value of ~0.03. Within the range of 1 kHz-100 kHz, the dielectric constant remains relatively stable. Beyond the 100 kHz threshold, a decrease in the dielectric constant is observed, which is attributed to the α_c relaxation of

Fig.:5.9 Variation of the dielectric constant and tangent loss (a) for pure PVDF nanocomposite, (b) and (c) for the PVDF-BST trilayered nanocomposites at room temperature

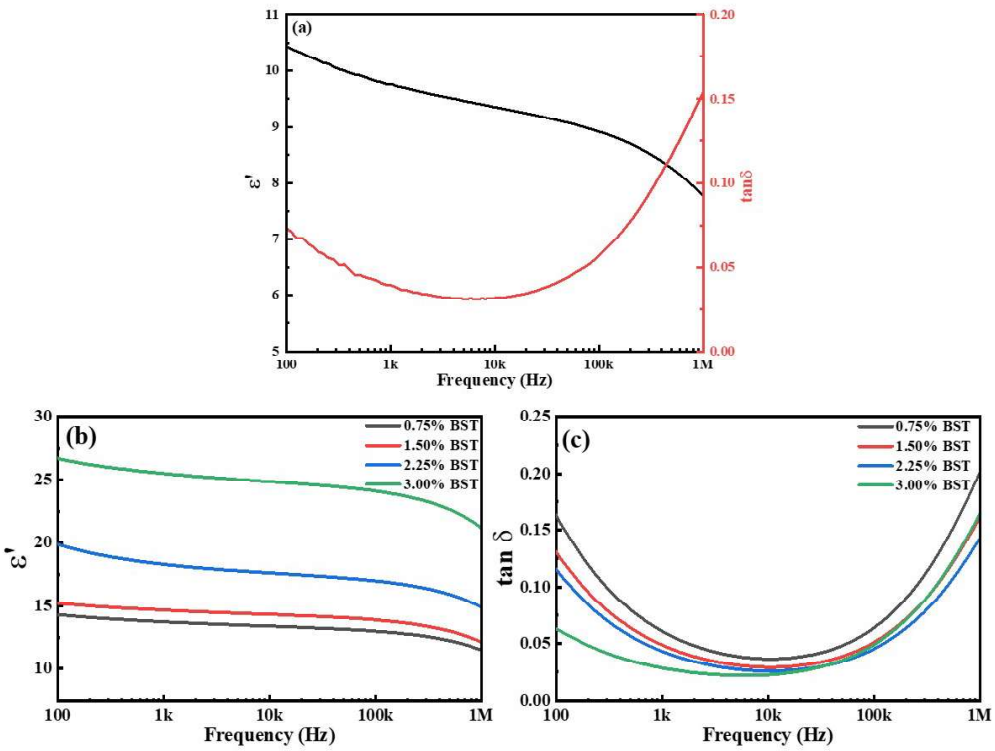

the PVDF polymer. The tangent loss remains relatively stable within the frequency range of 1 kHz-100 kHz and exhibits an increase leading to a peak value for frequencies beyond 100 kHz, a characteristic behavior associated with the α_c relaxation of PVDF. The influence of conduction electrons and interfacial polarization mechanisms is predominant at lower frequencies (up to 100 kHz), while losses arising from dipolar relaxation involving the CH_2 and CF_2 dipoles of PVDF become dominant at higher frequencies [35].

Fig. 5.9 (b) and (c) illustrate the room temperature behavior of dielectric constant(ε') and tangent loss (tan δ) of the trilayered PVDF-BST nanocomposites with frequency. It is observed that the variational trend of ε' and tan δ is similar for all the trilayered nanocomposites with frequency. With increased vol% loading of BST nanoparticles, the ε' of the nanocomposites increases (i.e. ~12 for 0.75 vol% loading and ~25 for 3.00 vol% loading at 1 kHz), which can be ascribed to the stronger local field caused by the ceramic nanoparticles than the polymer matrix and Maxwell-Wagner-Sillar interfacial polarization [36,37]. From 100 Hz to 1 kHz, the permittivity decreases, which is ascribed to the reduction of interfacial polarization due to the space charge generated at the PVDF/BST interface [38], whereas from 1 kHz to 100 kHz, it almost remains constant, which can be associated to the BST's dielectric behavior [39]. When the applied electric field has a frequency >100 kHz, the decrease in ε' is noticed in all the trilayered nanocomposites, which is caused by α-dipolar relaxation evolving due to the micro-Brownian motion of the polymeric chain [35]. The single-layer polymer-ceramic nanocomposites have more dielectric constant by virtue of the increased loading of ceramic nanoparticles. In contrast, the observation of a high dielectric constant in the trilayered PVDF-BST nanocomposites can be understood by taking the polarization phenomenon at the interlayer (layer/layer) interface [40] and the polymer-ceramic interface in the individual layer of the trilayered nanocomposites. Polymer chain mobility, chain conformation, coulombic potential, crystallinity, etc., also affect the dielectric constant in the single-layer PVDF-BST

nanocomposites [41,42]. But in the present case, redistribution of interfacial local electric field between the layers of PVDF-BST nanocomposites leads to induced polarization [43,44]. The interaction between two layers also creates interfacial dipoles [45,46]. The induced polarization between the layers and the creation of interfacial dipoles are responsible for the increased dielectric permittivity. The PVDF-BST nanocomposite shows the notable enhancement in the dielectric constant merely at 3.00 vol% loading of the BST nanoparticles due to the following reasons:

1. The distribution of BST nanoparticles at the interface in the trilayered nanocomposites creates an additional local electric field.
2. The surface of BST nanoparticles becomes positively charged [47], which interacts with the CF_2 dipoles of PVDF and increases the dielectric constant of the nanocomposite.

Table 5.2: Value of dielectric constant, tangent loss, discharge energy density, ΔP, breakdown strength, distortion parameter m and the efficiency of different PVDF-BST trilayered nanocomposite films

Sample	Dielectric constant (at 1kHz)	Tangent loss (at 1kHz)	Discharge energy density (J/cc)	ΔP (P_{max} - P_r) (μC/cm^2)	BDS (MV/m)	Efficiency (%)
0.75% BST	~13	~0.06	7.3	1.113	~422	89.3
1.50% BST	~15	~0.04	7.4	1.116	~330	90.9
2.25% BST	~18	~0.04	6.6	1.004	~208	86.8
3.00% BST	~25	~0.03	7.8	1.202	~282	92.9

The variation of tangent loss with frequency is of peculiar interest since it is an important factor influencing the energy efficiency and the electrical breakdown strength (BDS) of the trilayered nanocomposites. The trilayer PVDF-BST nanocomposites with 0.75%-2.25% v/v loading of BST show a similar variational trend of tangent loss. The tangent loss of all trilayered PVDF-BST nanocomposites is higher at 100 Hz, which decreases with an increase in frequency (100

Hz-10 kHz). The high value of the tangent loss at 100 Hz is caused by the molecular motion of polymeric chains and the internal rotation of the crystal. A similar kind of observation is reported elsewhere [48,49]. The value of tanδ for these nanocomposites decreases in the 100 Hz-10 kHz frequency range and increases for the frequencies >10 kHz. Initial decrease of tangent loss is associated with surface/interface polarization [40] at various interfaces such as electrode-sample interface, PVDF/BST interface and the interface among the layers of trilayered nanocomposites.

The increase of tangent loss for frequencies >10 kHz is related with the segmental relaxation of polymeric chains i.e., α-relaxation and dipolar relaxation among the interfacial layers due to the developed local electric field [35]. Though, the trend of variation of the tangent loss behavior has also been found to be similar for PVDF-BST nanocomposite loaded with 3 vol% of BST. But, the rate of decrease of tangent loss between 100 Hz-10 kHz range is lower as compared to other PVDF-BST trilayer nanocomposites. The lower rate is ascribed to the decreased surface/interfacial polarization due to better connectivity between PVDF/BST of PVDF with BST and among the layers of trilayered nanocomposites. It also has the lowest value of tangent loss (~0.03) at 1 kHz. For better understanding, a comparative table consisting of the dielectric permittivity, tangent loss, discharge energy density, breakdown strength and efficiency for different polymer-ceramic nanocomposites is given in table 5.2.

5.3.2.2 Breakdown strength studies

Fig. 5.10 shows the breakdown strength of each trilayered PVDF-BST nanocomposite using 10 data points for the Weibull distribution analysis. Two-parameter Weibull analysis is conveniently used for breakdown analysis of this kind of nanocomposites; accordingly:

$$P_i = 1 - e^{[-\frac{E_i}{E_o}]m} \tag{5.3}$$

where P_i is the breakdown probability, m is the shape factor (Weibull modulus) for estimating data scattering, E_i is the average breakdown strength, and E_o is the field corresponding to 63.2%

breakdown cumulative probability. The experimental plot is a straight line in the X-Y plane given by [50,51]:

$$X = ln(E_i) \text{ and } Y = ln(-\ln(1-P_i)) \qquad (5.4)$$

Fig.:5.10 Weibull distribution of different PVDF-BST trilayered nanocomposite films

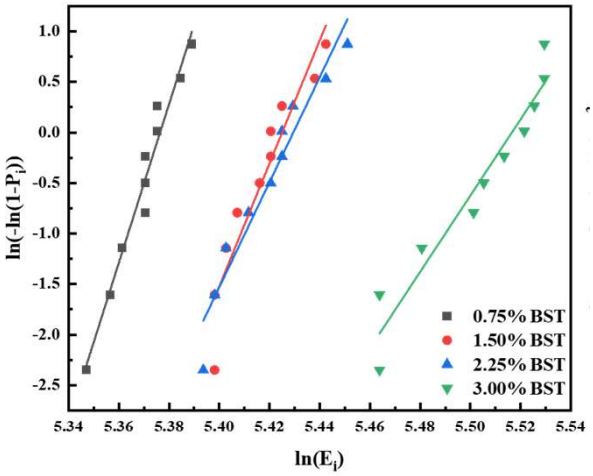

A total of 10 measurements are done for each PVDF-BST trilayered nanocomposite to obtain these Weibull distribution curves. The value of scattering parameter m of the trilayered PVDF-BST nanocomposites with 0.75, 1.50, 2.25 and 3.00 vol% BST loading is 78.4, 60.8, 51.9 and 37.7, along with r^2 values of 0.96, 0.90, 0.94 and 0.94, respectively. The high "m" values have also been reported earlier [52,53]. The loading of BST nanoparticles decreases the breakdown strength (E_b). The value of E_b for PVDF-BST trilayered nanocomposites determined from Weibull distribution is found to be ~422, ~330, ~208 and ~282 MV/m for 0.75%, 1.50%, 2.25% and 3.00% volume percent loading of BST nanoparticles, respectively. The increase in ceramic nanoparticle loading decreases the breakdown strength because the percolation threshold of ceramic fillers is reached and sometimes it is due to the worsened dispersion of nanoparticles in the polymer matrix due to

Fig.:5.11 Bar diagram showing the tangent loss and breakdown strength with the volume fraction of BST in the PVDF matrix

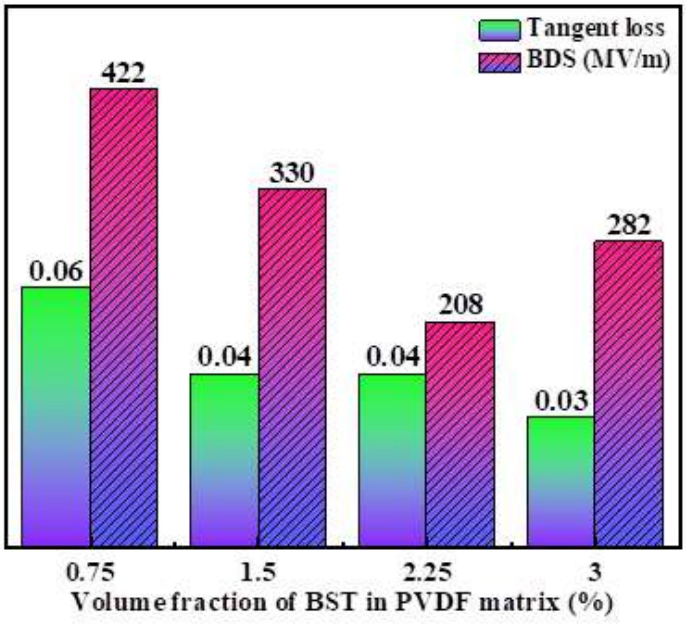

aggregation of nanoparticles; it is also observed in other reports [44,54]. Since the tangent loss, leakage current and breakdown strength are related with electric field-induced conduction in the PVDF-BST trilayered nanocomposites. Therefore, the bar diagram showing the values of breakdown strength, along with the tangent loss, is shown in Fig. 5.11. Though the increase in loading decreases the electric breakdown strength (BDS), but when the loading of BST nanoparticles is changed from 2.25 vol% to 3.00 vol%, the BDS is found to increase from ~208 MV/m to ~282 MV/m, which is attributed to the blocking of charges evoluted at the interface by electric field [44]. The studies on breakdown strength clearly demonstrate the increased BDS (~282 MV/m) for 3.00 vol% loaded PVDF-BST trilayered nanocomposite. The trilayered nanocomposites exhibit spatial variation in the local electric field at the interfaces of PVDF-BST nanocomposites, which might be preventing the conduction of the charge carriers. The restriction of movement of charge carriers is ascribed to the increased BDS for 3.00 vol% PVDF-BST trilayered nanocomposite films.

5.3.2.3 Dielectric displacement and energy storage behavior studies

In Fig. 5.12, the charging energy density (U_C), as shown in the grey area, is calculated using $\int_0^{Pmax} E.dP$, whereas discharge energy density (U_D), as shown in the shaded area, is calculated using $\int_{Pr}^{Pmax} E.dP$ and the final energy efficiency (η) is calculated by using the following formula:

$$\% \eta = \frac{Discharge\ energy\ density\ (U_D)}{Charge\ energy\ density\ (U_C)} \text{ x } 100\% \quad (5.4)$$

The discharge energy density and the efficiency of the PVDF-BST trilayered nanocomposites are discussed in detail in the main manuscript, whereas Fig. 5.13 shows the charging energy density of the trilayered PVDF-BST nanocomposites with varying electric field. The lower values of polarization with high charging and discharging energy densities have been reported earlier by various research groups [22,55–58].

Fig.:5.12 Schematic representation of charging energy density (U_C) in grey area and discharging energy density (U_D) in shaded area with the electric field (E)

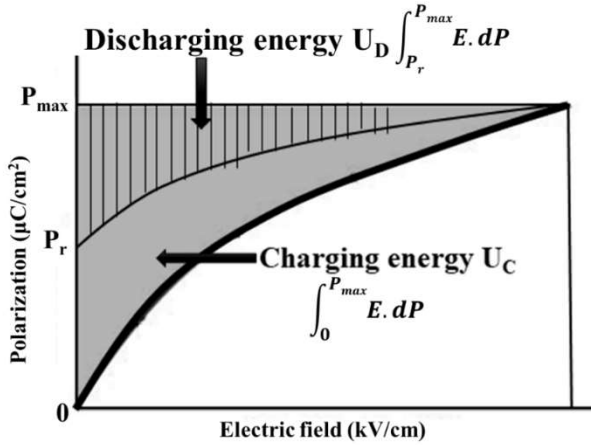

Fig. 5.14 (a) to 5.14 (d) sequentially displays the D-E hysteresis loops, discharging energy densities, the efficiency and the variation of P_{max}-P_r with increased concentration of the BST in the PVDF matrix of different PVDF-BST trilayered nanocomposites at a frequency of 10 Hz. All the nanocomposites show a slim loop, which is typical for relaxor ferroelectrics [50], having negligible residual polarization. This unipolar D-E loop is used to calculate the charging energy density, discharging energy density (U_D) and efficiency (η) [3]. 3 vol% loaded PVDF-BST trilayered nanocomposite has the highest maximum polarization (P_{max}) ~1.30 μC/cm^2. The similar polarization values have been reported elsewhere [60]. The observed maximum polarization is attributed to the formation of additional dipoles at polymer/polymer, polymer/ceramic and surface at the interlayer of PVDF-BST trilayered nanocomposites [61]. The value of P_{max}-P_r should be maximum for high discharging energy density. The plot of P_{max}-P_r of different trilayered PVDF-BST nanocomposite thick films is given in Fig. 5.14 (d). P_{max}-P_r has been found to be maximum (1.202 μC/cm^2) for the 3 vol% BST nanoparticles loaded trilayered nanocomposite. The same composition of trilayered nanocomposite has a U_D of ~7.8 J/cc and a maximum %η

Fig.:5.13 Charging energy density of different PVDF-BST trilayered nanocomposite films

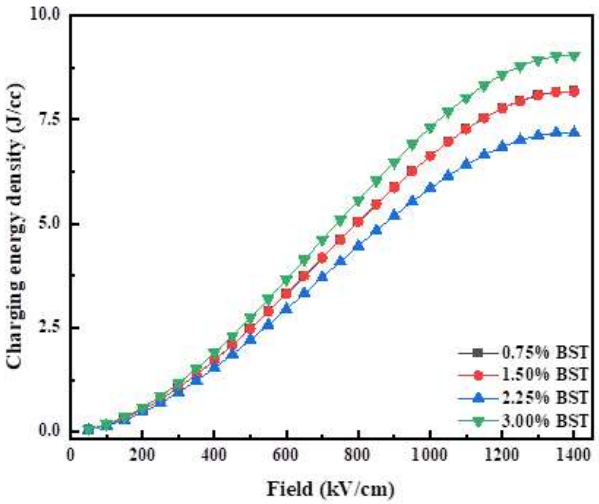

Fig.:5.14 (a) D-E hysteresis loop, (b) discharging energy density, (c) efficiency and (d) the variation of P_{max}-P_r with volume fraction of BST in the PVDF matrix of different PVDF-BST trilayered nanocomposite thick films

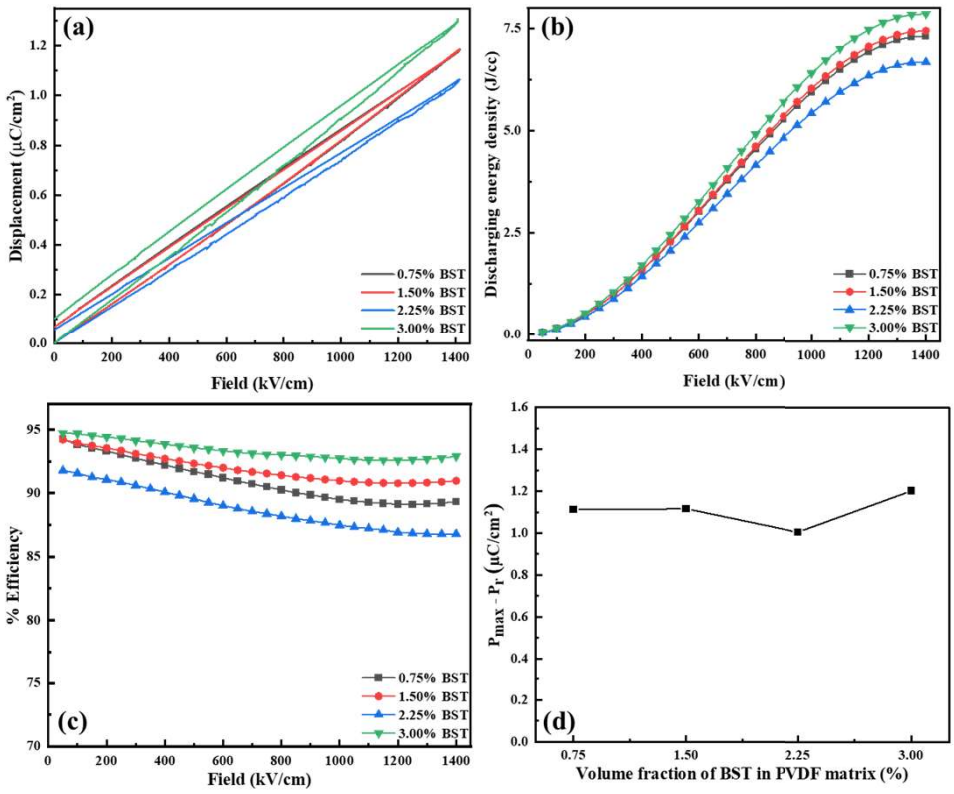

of ~93%. Therefore, high discharge energy density along with high efficiency has been achieved. The combined dielectric, breakdown strength, leakage current density and energy storage behavior of the PVDF-BST trilayered nanocomposites highlights the superiority of the 3 vol% loaded trilayered nanocomposite, which are as follows:

(i) It exhibits a high ε' (~25) and low tanδ (~0.03) at 1 kHz.

(ii) It has moderately high BDS (~282 MV/m) as well as low leakage current density.

(iii) It also possesses ultrahigh efficiency (~93%) and enhanced U_D (~7.8 J/cc at 1400 kV/cm).

These spectacular and encouraging results of PVDF-BST trilayered nanocomposites could be understood by a mechanism which relies on the nature of various interfaces and distribution of the local electric field. The mechanism is discussed in the following section.

5.3.3 Mechanism

The schematic of the mechanism responsible for ultrahigh efficiency and enhanced discharge energy density exhibited by the PVDF-BST trilayer nanocomposite is shown in Fig. 5.15. The upper & lower layers are taken along the casting direction, whereas the middle layer is opposite to the casting direction. All these layers are stacked together by hot pressing. This arrangement leads to spatial distribution in dielectric permittivity, which creates spatial variation in the local electric field. This local electric field opposes the external electric field-induced injection of the charge carriers, restricting the movement of the space charges and, hence increasing the breakdown strength by preventing the formation of electrical treeing [62]. It is also the reason for the decreased tangent loss. The decreased tangent loss leads to the slim D-E loops, which leads to the ultrahigh efficiency. Interfacial polarization among the layers and within the layers creates additional dipoles [63,64], which is associated to the enhanced dielectric constant and polarization. Therefore, trilayered PVDF-BST nanocomposites with ultrahigh efficiency and enhanced discharging energy density are making them suitable for high-energy-density capacitors.

Fig.:5.15 Mechanism showing the presence of interfacial layers and locally induced electric field in the trilayered PVDF-BST nanocomposite films

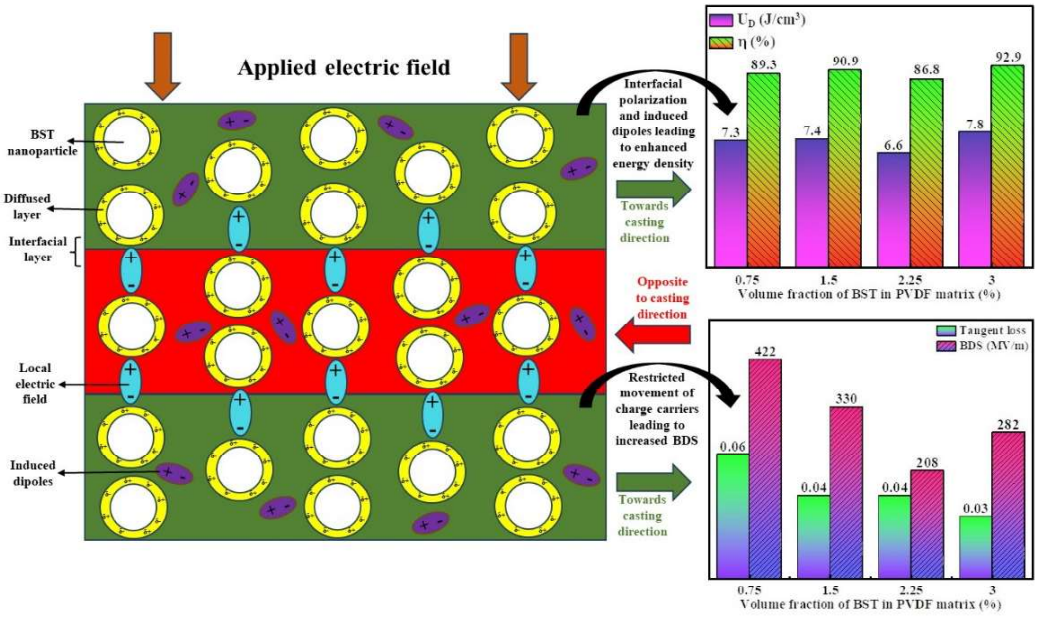

5.4 Conclusion

The PVDF-BST trilayered nanocomposites (with different vol% loading of BST nanoparticles, i.e. 0.75%, 1.50%, 2.25% and 3.00%) have been processed by the tape casting method. The structural and morphological studies have confirmed the formation of PVDF-BST trilayered nanocomposites. PVDF-BST trilayered nanocomposite consisting of 3.00 vol% of BST nanoparticles exhibited high dielectric constant(~25), low tangent loss (~0.03), and anomalously high BDS (~282 MV/m). Moreover, PVDF-BST trilayered nanocomposite with 3.00 vol% BST loading has the ultrahigh efficiency (~93%) and U_D (~7.8 J/cc at 1400 kV/cm). A mechanism for the excellent energy storage behavior and dielectric properties have been proposed. Where, low tangent loss and high BDS are associated with the spatial variation of the local electric field at interlayer interfaces of PVDF-BST trilayered nanocomposites. This local electric field restricts the external electric field-induced movement of charge carriers and space charges in the nanocomposites. The enhanced discharge energy density is associated with the formation of additional interfacial dipoles at various interfaces such as interlayer, intralayer (PVDF/PVDF), and PVDF/BST interfaces, whereas ultra-high efficiency is assigned to the decreased hysteretic polarization caused by the prevention of the external electric field induced movement of the charge carriers. These investigations would be adopted as a futuristic strategy for developing excellently efficient polymer-ceramic nanocomposites for the high energy density capacitors used in pulsed power applications.

References

[1] C. Wang, X. Zhao, L. Ren, L. Yu, Y. Jin, W. Tan, W. Zheng, H. Li, L. Yang, R. Liao, Enhanced dielectric and energy storage properties of P(VDF-HFP) through elevating β -phase formation under unipolar nanosecond electric pulses, Appl Phys Lett 122 (2023). https://doi.org/10.1063/5.0128998.

[2] A. Jain, Y.G. Wang, L.N. Shi, Recent developments in BaTiO3 based lead-free materials for energy storage applications, J Alloys Compd 928 (2022). https://doi.org/10.1016/j.jallcom.2022.167066.

[3] S. Kaur, A. Kumar, A.L. Sharma, D.P. Singh, Dielectric and energy storage behavior of CaCu 3 Ti 4 O 12 nanoparticles for capacitor application, Ceram Int 45 (2019) 7743–7747. https://doi.org/10.1016/j.ceramint.2019.01.077.

[4] F. Ali, D. Zhou, M. Ali, H.W. Ali, M. Daaim, S. Khan, M.M. Hussain, N. Sun, Recent Progress on Energy-Related Applications of HfO2-Based Ferroelectric and Antiferroelectric Materials, ACS Appl Electron Mater 2 (2020) 2301–2317. https://doi.org/10.1021/acsaelm.0c00304.

[5] Y. Su, B. Zhao, Y. Wang, W. Li, P. Yuan, R. Xue, H. Wang, F. Zhang, W. Zhang, W. Zhao, R. Ma, D. Hu, Enhanced energy density for 3D BaTiO3/MF/PVDF nanocomposites in low electric strength, Surfaces and Interfaces 37 (2023). https://doi.org/10.1016/j.surfin.2023.102729.

[6] F. Liu, Q. Li, Z. Li, L. Dong, C. Xiong, Q. Wang, Ternary PVDF-based terpolymer nanocomposites with enhanced energy density and high power density, Compos Part A Appl Sci Manuf 109 (2018) 597–603. https://doi.org/10.1016/j.compositesa.2018.03.019.

[7] S. Yu, C. Zhang, M. Wu, H. Dong, L. Li, Ultra-high energy density thin-film capacitors with high power density using BaSn0.15Ti0.85O3/Ba0.6Sr0.4TiO3 heterostructure thin films, J Power Sources 412 (2019) 648–654. https://doi.org/10.1016/j.jpowsour.2018.12.012.

[8] Y. Wang, J. Zhang, H. Gao, Y. Yao, C. Pu, J. Wang, L. Ren, Q. Zong, The interface effects on the breakdown strength of multilayer PVDF-based capacitors, Polymer (Guildf) 270 (2023). https://doi.org/10.1016/j.polymer.2023.125803.

[9] Y. Dong, Z. Wang, S. Huo, J. Lin, S. He, Improved Dielectric Breakdown Strength of Polyimide by Incorporating Polydopamine-Coated Graphitic Carbon Nitride, Polymers (Basel) 14 (2022). https://doi.org/10.3390/polym14030385.

[10] Z. Xie, D. Liu, Y. Xiao, K. Wang, Q. Zhang, K. Wu, Q. Fu, The effect of filler permittivity on the dielectric properties of polymer-based composites, Compos Sci Technol (2022) 109342. https://doi.org/10.1016/j.compscitech.2022.109342.

[11] A. Mukherjee, B. Dasgupta Ghosh, Synthesis of functionalized ZnO nanoflake loaded polyvinylidene fluoride composites with enhanced energy storage properties, Polym Compos 44 (2023) 2488–2499. https://doi.org/10.1002/pc.27258.

[12] M. Chang, Y. Liu, K. Li, M. Che, K. Guo, Impact dynamics and polarization mechanism of BaxSr1−xTiO3 particles reinforced polydimethylsiloxane composites, Polym Compos (2023). https://doi.org/10.1002/pc.27621.

[13] Y. Tang, H. Liu, X. Wang, S. Cheng, Q. Gao, J. Liu, S. Guan, S. Zhao, Enhanced dielectric performance of polydimethylsiloxane-based ternary composites films via tailored

hydrogen bonds between carbon nanotube and barium titanate as modified fillers, Journal of Vinyl and Additive Technology 28 (2022) 184–195. https://doi.org/10.1002/vnl.21879.

[14] B. Wang, Y. Ma, B. Na, R. Lv, H. Liu, W. Li, H. Zhou, Enhanced dielectric thermal stability and permittivity of flexible composite films based on BaTiO3 nanoparticles highly filled PVDF/PAN blend nanofibrous membranes, Polym Compos 39 (2018) E1841–E1848. https://doi.org/10.1002/pc.24829.

[15] J. Zhong, H. Ju, C. Fu, X. Ran, W. Nie, Tuning ferroelectric response of electroactive materials by controlling multilayered structures to achieve excellent energy storage performance, Adv Eng Mater (2022). https://doi.org/10.1002/adem.202101770.

[16] Y. sheng Zhang, M. Wang, C. Yang, Y. wen Shao, X. dong Qi, J. hui Yang, Y. Wang, Heterogeneous BaTiO3@Ag core-shell fibers as fillers for polymer dielectric composites with simultaneously improved dielectric constant and breakdown strength, Composites Communications 27 (2021). https://doi.org/10.1016/j.coco.2021.100874.

[17] L. Gao, J. Zhang, Z. Chen, X. Wang, Enhancing energy storage property of polymer nanocomposites by rationally regulating shell thickness of core–shell structured nanoparticles, Polym Compos 44 (2023) 3567–3579. https://doi.org/10.1002/pc.27345.

[18] S. Peng, X. Du, Z. Liang, M. Ma, Y. Guo, L. Xiong, Multilayer polymer nanocomposites based on interface engineering for high-performance capacitors, J Energy Storage 60 (2023). https://doi.org/10.1016/j.est.2023.106636.

[19] X. Lu, L. Zhang, Y. Tong, Z.Y. Cheng, BST-P(VDF-CTFE) nanocomposite films with high dielectric constant, low dielectric loss, and high energy-storage density, Compos B Eng 168 (2019) 34–43. https://doi.org/10.1016/j.compositesb.2018.12.059.

[20] J. Zhou, D. Hou, S. Cheng, J. Zhang, W. Chen, L. Zhou, P. Zhang, Recent advances in dispersion and alignment of fillers in PVDF-based composites for high-performance dielectric energy storage, Mater Today Energy 31 (2023) 101208. https://doi.org/10.1016/j.mtener.2022.101208.

[21] Z.B. Pan, L.M. Yao, J.W. Zhai, S.H. Liu, K. Yang, H.T. Wang, J.H. Liu, Fast discharge and high energy density of nanocomposite capacitors using Ba0.6Sr0.4TiO3 nanofibers, Ceram Int 42 (2016) 14667–14674. https://doi.org/10.1016/j.ceramint.2016.06.090.

[22] H. Ye, H. Chen, X. Zhang, Y. Chen, W. Shao, L. Xu, Electron structure in modified BaTiO3/ poly(vinylidene fluoride) nanocomposite with high dielectric property and energy density, IET Nanodielectrics 2 (2019) 70–77. https://doi.org/10.1049/iet-nde.2018.0029.

[23] Prateek, R. Bhunia, A. Garg, R.K. Gupta, Probing the Interface Activation in Designing Defect-Free Multilayered Polymer Nanocomposites for Dielectric Capacitor Applications, Journal of Physical Chemistry C 124 (2020) 22914–22924. https://doi.org/10.1021/acs.jpcc.0c05833.

[24] X. Sang, X. Li, D. Zhang, X. Zhang, H. Wang, S. Li, Improved Dielectric Properties and Energy Storage Densities of BaTiO3 Doped PVDF Composites by Heat Treatment and Surface Modification of BaTiO3, J Phys D Appl Phys (2022). https://doi.org/10.1088/1361-6463/ac4942.

[25] A. Sasmal, P. Maiti, S. Maity, S. Sen, A. Arockiarajan, Air-plasma discharged PVDF based binary magnetoelectric composite for simultaneously enhanced energy storage and conversion efficiency, Appl Phys Lett 122 (2023). https://doi.org/10.1063/5.0137968.

[26] T. Wang, R.C. Peng, G. Dong, Y. Du, S. Zhao, Y. Zhao, C. Zhou, S. Yang, K. Shi, Z. Zhou, M. Liu, J. Pan, Enhanced Energy Density at a Low Electric Field in PVDF-Based Heterojunctions Sandwiched with High Ion-Polarized BTO Films, ACS Appl Mater Interfaces 14 (2022) 17849–17857. https://doi.org/10.1021/acsami.2c02327.

[27] Q. Wang, J. Zhang, Z. Zhang, Y. Hao, K. Bi, Enhanced dielectric properties and energy storage density of PVDF nanocomposites by co-loading of BaTiO3 and CoFe2O4 nanoparticles, Adv Compos Hybrid Mater 3 (2020) 58–65. https://doi.org/10.1007/s42114-020-00138-4.

[28] C. Baek, J.E. Wang, D.S. Kim, D.K. Kim, Hydrothermal Synthesis and Dielectric Properties of Ba1−xSrxTiO3 Nanoparticles with Enhanced Uniformity, J Nanosci Nanotechnol 16 (2016) 11652–11657. https://doi.org/10.1166/jnn.2016.13568.

[29] V. Mote, Y. Purushotham, B. Dole, Williamson-Hall analysis in estimation of lattice strain in nanometer-sized ZnO particles, Journal of Theoretical and Applied Physics 6 (2012) 6. https://doi.org/10.1186/2251-7235-6-6.

[30] E. Gutiérrez-Fernández, J. Sena-Fernández, E. Rebollar, T.A. Ezquerra, F.J. Hermoso-Pinilla, M. Sanz, O. Gálvez, A. Nogales, Development of polar phases in ferroelectric poly(vinylidene fluoride) (PVDF) nanoparticles, Polymer (Guildf) (2022) 125540. https://doi.org/10.1016/j.polymer.2022.125540.

[31] M. Arjun Hari, K. Rakesh, R.S. Divya, L. Rajan, C.K. Subash, S. Varghese, Influence of Nanosilica in PVDF Thin Films for Sensing Applications, in: 2021 IEEE International Symposium on Smart Electronic Systems (ISES) (Formerly INiS), IEEE, 2021: pp. 70–73. https://doi.org/10.1109/iSES52644.2021.00027.

[32] S. Roy, P. Thakur, N.A. Hoque, B. Bagchi, N. Sepay, F. Khatun, A. Kool, S. Das, Electroactive and High Dielectric Folic Acid/PVDF Composite Film Rooted Simplistic Organic Photovoltaic Self-Charging Energy Storage Cell with Superior Energy Density and Storage Capability, ACS Appl Mater Interfaces 9 (2017) 24198–24209. https://doi.org/10.1021/acsami.7b05540.

[33] B. Lin, Z.-T. Li, Y. Yang, Y. Li, J.-C. Lin, X.-M. Zheng, F.-A. He, K.-H. Lam, Enhanced dielectric permittivity in surface-modified graphene/PVDF composites prepared by an electrospinning-hot pressing method, Compos Sci Technol (2019). https://doi.org/10.1016/j.compscitech.2019.01.003.

[34] S. Jaidka, A. Aggarwal, S. Chopra, D.P. Singh, Significantly Enhanced Dielectric Behavior of Polyvinylidene Fluoride-Barium Strontium Titanate Flexible Nanocomposite Thick Films: Role of Electric Field-Induced Effects, J Electron Mater 51 (2022) 5429–5439. https://doi.org/10.1007/s11664-022-09784-4.

[35] C. V. Chanmal, J.P. Jog, Dielectric relaxations in PVDF/BaTiO3 nanocomposites, Express Polym Lett 2 (2008) 294–301. https://doi.org/10.3144/expresspolymlett.2008.35.

[36] Kittle Charles, Introduction to solid state physics, Eighth edition, John Wiley & Sons Inc., New York, USA, 1971.

[37] M. Feng, Q. Chi, Y. Feng, Y. Zhang, T. Zhang, C. Zhang, Q. Chen, Q. Lei, High energy storage density and efficiency in aligned nanofiber filled nanocomposites with multilayer structure, Compos B Eng 198 (2020). https://doi.org/10.1016/j.compositesb.2020.108206.

[38] A. Mayeen, M.S. Kala, M.S. Jayalakshmy, S. Thomas, D. Rouxel, J. Philip, R.N. Bhowmik, N. Kalarikkal, Dopamine functionalization of BaTiO3: An effective strategy for the enhancement of electrical, magnetoelectric and thermal properties of BaTiO3-PVDF-TrFE

nanocomposites, Dalton Transactions 47 (2018) 2039–2051. https://doi.org/10.1039/c7dt03389c.

[39] Z. Song, S. Zhang, H. Liu, H. Hao, M. Cao, Q. Li, Q. Wang, Z. Yao, Z. Wang, M.T. Lanagan, Improved Energy Storage Properties Accompanied by Enhanced Interface Polarization in Annealed Microwave-Sintered BST, Journal of the American Ceramic Society 98 (2015) 3212–3222. https://doi.org/10.1111/jace.13741.

[40] N. Meng, X. Ren, J. Wu, E. Bilotti, M.J. Reece, H. Yan, Low-cost Free-standing ferroelectric polymer films with high polarization produced via pressing-and-folding, Journal of Materiomics 8 (2022) 640–648. https://doi.org/10.1016/j.jmat.2021.11.009.

[41] T. Tanaka, Dielectric nanocomposites with insulating properties, in: IEEE Transactions on Dielectrics and Electrical Insulation, 2005: pp. 914–928. https://doi.org/10.1109/TDEI.2005.1522186.

[42] N.W. Ashcroft, N.D. Mermin, Solid State Physics, 1975.

[43] A. Ahmad, G. Liu, S. Cao, X. Liu, J. Luo, L. Han, H. Tong, J. Xu, Significantly Improved Dielectric Performance of All-Organic Parylene/Polyimide/Parylene Composite Films with Sandwich Structure, Macromol Rapid Commun (2022). https://doi.org/10.1002/marc.202200568.

[44] C. Zhang, Z. Shi, F. Mao, C. Yang, J. Yang, X. Zhu, H. Zuo, Polymer composites with balanced dielectric constant and loss via constructing trilayer architecture, J Mater Sci 53 (2018) 13230–13242. https://doi.org/10.1007/s10853-018-2545-4.

[45] S. Kaur, D.P. Singh, On the structural, dielectric and energy storage behaviour of PVDF- CaCu3Ti4O12 nanocomposite films, Mater Chem Phys 239 (2020) 122301. https://doi.org/10.1016/j.matchemphys.2019.122301.

[46] E.S. Kadir, R.N. Gayen, R. Paul, S. Biswas, Interfacial effects on ferroelectric and dielectric properties of GO reinforced free-standing and flexible PVDF/ZnO composite membranes: Bias dependent impedance spectroscopy, J Alloys Compd 843 (2020). https://doi.org/10.1016/j.jallcom.2020.155974.

[47] S. Jaidka, S. Chopra, A. Aggarwal, D.P. Singh, Effect of interfacial layers on the temperature-dependent dielectric and impedance behavior of flexible PVDF-BST nanocomposite thick films, Journal of Physics and Chemistry of Solids 184 (2024) 111667. https://doi.org/10.1016/j.jpcs.2023.111667.

[48] K. Nakagawa, Y. Ishida, Dielectric Relaxations and Molecular Motions in Poly(vinylidene Fluoride) with Crystal Form II, Journal of Polymer Science 11 (1973) 1503–1533.

[49] Y. Miyamoto, H. Miyaji, K. Asai, Anisotropy of Dielectric Relaxation in Crystal Form II of Poly(viny1idene Fluoride), Journal of Polymer Science 18 (1980) 597–606.

[50] C. Chauvet, C. Laurent, Weibull statistics in short-term dielectric breakdown of thin polyethylene films, IEEE Transactions on Electrical Insulation 28 (1993) 18–29. https://doi.org/10.1109/14.192236.

[51] J. Wang, S. Liang, J. Xiong, B. Peng, L. He, Y. Xie, Z. Zhang, High Energy Density Nanocomposites with Layered Gradient Structure and Lysozyme-Modified Ba0.6Sr0.4TiO3 Nanoparticles, Compos Part A Appl Sci Manuf (2022) 107254. https://doi.org/10.1016/j.compositesa.2022.107254.

[52] H. Silau, N.B. Stabell, F.R. Petersen, M. Pham, L. Yu, A.L. Skov, Weibull Analysis of Electrical Breakdown Strength as an Effective Means of Evaluating Elastomer Thin Film Quality, Adv Eng Mater 20 (2018). https://doi.org/10.1002/adem.201800241.

[53] B. Luo, X. Wang, Y. Wang, L. Li, Fabrication, characterization, properties and theoretical analysis of ceramic/PVDF composite flexible films with high dielectric constant and low dielectric loss, J Mater Chem A Mater 2 (2014) 510–519. https://doi.org/10.1039/c3ta14107a.

[54] P. Kim, N.M. Doss, J.P. Tillotson, P.J. Hotchkiss, M.J. Pan, S.R. Marder, J. Li, J.P. Calame, J.W. Perry, High energy density nanocomposites based on surface-modified BaTiO3 and a ferroelectric polymer, ACS Nano 3 (2009) 2581–2592. https://doi.org/10.1021/nn9006412.

[55] S. Kaur, D.P. Singh, Significantly improved dielectric and energy storage behavior of the surface functionalized CaCu3Ti4O12 nanoparticles in PVDF-CaCu3Ti4O12 nanocomposites, J Alloys Compd 918 (2022). https://doi.org/10.1016/j.jallcom.2022.165500.

[56] Y. Fan, X. Huang, G. Wang, P. Jiang, Core-Shell Structured Biopolymer@BaTiO3 Nanoparticles for Biopolymer Nanocomposites with Significantly Enhanced Dielectric Properties and Energy Storage Capability, Journal of Physical Chemistry C 119 (2015) 27330–27339. https://doi.org/10.1021/acs.jpcc.5b09619.

[57] S. Chen, S. Chen, R. Qiao, H. Xu, Z. Liu, H. Luo, D. Zhang, Enhanced dielectric constant of PVDF-based nanocomposites with one-dimensional core-shell polypyrrole/sepiolite nanofibers, Compos Part A Appl Sci Manuf 145 (2021). https://doi.org/10.1016/j.compositesa.2021.106384.

[58] G. Meng, J. She, C. Wang, W. Wang, C. Pan, Y. Cheng, Sandwich-Structured h-BN/PVDF/h-BN Film With High Dielectric Strength and Energy Storage Density, Front Chem 10 (2022). https://doi.org/10.3389/fchem.2022.910305.

[59] W. Huang, Y. Chen, X. Li, G. Wang, N. Liu, S. Li, M. Zhou, X. Dong, Ultrahigh recoverable energy storage density and efficiency in barium strontium titanate-based lead-free relaxor ferroelectric ceramics, Appl Phys Lett 113 (2018). https://doi.org/10.1063/1.5054000.

[60] M. Feng, Q. Chi, Y. Feng, Y. Zhang, T. Zhang, C. Zhang, Q. Chen, Q. Lei, High energy storage density and efficiency in aligned nanofiber filled nanocomposites with multilayer structure, Compos B Eng 198 (2020). https://doi.org/10.1016/j.compositesb.2020.108206.

[61] P. Hu, Y. Shen, Y. Guan, X. Zhang, Y. Lin, Q. Zhang, C.W. Nan, Topological-structure modulated polymer nanocomposites exhibiting highly enhanced dielectric strength and energy density, Adv Funct Mater 24 (2014) 3172–3178. https://doi.org/10.1002/adfm.201303684.

[62] P. Hu, Y. Shen, Y. Guan, X. Zhang, Y. Lin, Q. Zhang, C.W. Nan, Topological-structure modulated polymer nanocomposites exhibiting highly enhanced dielectric strength and energy density, Adv Funct Mater 24 (2014) 3172–3178. https://doi.org/10.1002/adfm.201303684.

[63] E. Baer, L. Zhu, Dielectric Phenomena in Polymers and Multilayered Dielectric Films, Macromolecules 50 (2017) 2239–2256. https://doi.org/10.1021/acs.macromol.6b02669.

[64] J. Zhu, J. Shen, S. Guo, H.J. Sue, Confined distribution of conductive particles in polyvinylidene fluoride-based multilayered dielectrics: Toward high permittivity and breakdown strength, Carbon N Y 84 (2015) 355–364. https://doi.org/10.1016/j.carbon.2014.12.031.

Chapter 6

Studies on the effect of the surface-modified $Ba_{0.8}Sr_{0.2}TiO_3$ nanoparticles on the dielectric and energy storage performance of the trilayered PVDF/$Ba_{0.8}Sr_{0.2}TiO_3$ nanocomposites films

6.1 Introduction

Polymer-based dielectric nanocomposites have drawn considerable attention due to their high energy storage properties, which are useful in various technological and strategic applications such as pulsed power systems, smart grids, etc. [1,2]. There are numerous polymers which fall under the category of dielectric polymers, such as poly(methyl methacrylate) (PMMA), polydimethylsiloxane (PDMS), polyvinylidene difluoride (PVDF), polyethylene terephthalate (PET), polyvinyl alcohol (PVA), etc. [3]. Among them, PVDF and its copolymers are at the edge due to the existence of α, β, γ, and δ crystalline phases. The alignment of dipoles in crystalline phases offers a relatively high dielectric constant (~11) and low tangent loss (~0.02) [4]. The stored energy density in a dielectric material is given by $U = \frac{1}{2}\varepsilon_r\varepsilon_0 E_b^2$, where ε_0, ε_r and E_b are the vacuum permittivity, dielectric constant and breakdown strength, respectively[1]. On the other hand, ceramic materials such as $BaTiO_3$ (BT, ε'~1000) [5], (Ba, Sr)TiO_3 (BST, ε'~3000) [6], $CaCu_3Ti_4O_{12}$ (CCTO, ε'~5000) [5], $PbZrTiO_3$ (PZT, ε'~1300) [7], etc. provides high dielectric constant, whereas polymers are adored with connatural high breakdown strength. Among the galaxy of available dielectric ceramics, BST exhibits an exceptionally high dielectric constant (2500-3000) at room temperature and possesses a stable dielectric constant over wide temperature (room temperature - 120°C) and frequency range (100 Hz - 1 MHz) [8,9]. Therefore, PVDF-BST nanocomposites consisting of ceramic nanoparticles would be an excellent material for energy storage applications. The large difference in the physical and dielectric properties of polymer and ceramic nanoparticles creates charged interfaces, interfacial ion migration and distribution of local electric field, which combinely lead towards decreased breakdown strength (E_b) [10,11]. The decreased breakdown strength, increased loss and hysteretic behavior in electric field-dependent displacement in polymer-ceramic nanocomposites deteriorate the capacitive energy storage performance.

The effort to improve these parameters for developing polymer ceramic nanocomposites for energy storage applications have been undertaken in the investigations by different research groups [12–14]. The investigations carried out have adopted several approaches based on the engineered processing, such as the use of nanowires, nanotubes etc., [13,15], functionalization [16,17], poling [18], incorporation of wide band gap nanoparticles [19,20] and engineered multilayer structure [21,22] in the dielectric polymer ceramic nanocomposites. The incorporation of $Ba_{0.6}Sr_{0.4}TiO_3$ nanotubes with a large aspect ratio and large surface area leads to enhanced dielectric properties of the PVDF-based nanocomposites. The value of the dielectric constant and tangent loss at 1 kHz is observed to be 50 and 0.07, respectively, for 10 vol% loading of the nanotubes. The study does not have any mention about the breakdown strength and energy storage properties [15].

The incorporation of surface-modified ceramic nanoparticles has a positive influence on the dielectric and energy storage behavior [14,16,23–26], where the surface of ceramic nanoparticles has been modified with different functional groups such as $-NH_2$ [14], -OH [23], dopamine [24] etc. The ceramic-polymer nanocomposites consisting of -OH modified $Ba_{0.6}Sr_{0.4}TiO_3$ nanofibers exhibit enhanced dielectric constant (~24), reduced loss (~0.02), discharge energy density (~6.4 J/cc), energy efficiency (~70 %) and improved breakdown electric field strength (~398 MV/m) at a 10% volume fraction [23]. Significantly improved results have been assigned to the combined effect of the large aspect ratio and the surface modification-induced improvement in the crystallinity of the PVDF. The surface modification of the ceramic filler by PO_4^{-3} group [treating with phosphoric acid (H_3PO_4)] has been found to significantly affect the mechanical strength, i.e. flexural strength and elastic modulus in various composites [27,28]. The modification in the mechanical behavior is assigned to increased surface roughness and surface chemical activity. But, the effect of the incorporation of surface-modified ceramic nanoparticles by PO_4^{-3} group in the polymeric matrix on the dielectric and

energy storage behavior have not been investigated. These investigations are utterly important as the increased surface chemical activity at the interfaces of ceramic nanoparticles and polymeric matrix may have a positive influence on the dielectric, breakdown strength and energy storage behavior. Further, for improving the dielectric properties, breakdown strength and energy storage performance, the concept of specially architectured nanocomposite films have also been employed, such as opposite lamellar-structured fillers [26], gradient structure [29], layered structure [10,30], multilayered structure [21,22] etc. The BFO/MgO-PVDF/PMMA composite-based lemmelar structured film with 0.9 wt% loading has shown an energy density of 9.93 J/cc at 409.6 MV/m. But the energy efficiency is only 66% which is due to increased hysteretic loss. Also, the dielectric constant and tangent loss are observed to be 10 and 0.04 at 1 kHz. The interfacial polarization and local field at heterojunction are assigned for the observed behavior [26]. On the other hand, Wang *et al.* [31] synthesized multilayer all polymer PVDF/P(VDF-HFP)/PVDF composite films using the spin-coating technique, which showed an improved breakdown strength of 449.2 MV/m and a discharged energy density of 6.24 J/cc. This increase in the breakdown strength and energy storage performance is ascribed to the enhanced interfacial polarization effect and reduced leakage current in the multilayer films. The dielectric constant and tangent loss for the multilayer composite film came out to be 8 and 0.02, respectively, at 1 kHz.

Table 6.1 provides a comparative overview of the work undertaken by various research groups consisting of functionalized ceramic nanoparticles in different polymer matrices. The considered parameters for the comparison include the volume/weight percentage of functionalized ceramic nanoparticles with different functional groups in the polymeric matrix and its influence on the dielectric properties (dielectric constant and tangent loss, discharge energy density, energy efficiency and breakdown strength).

Table 6.1: Comparison of dielectric constant (ε'), tangent loss (tanδ), discharge energy density (U_D), breakdown strength (BDS) and efficiency (η) in different polymer-ceramic nanocomposites

Material	Loading	ε'	Tanδ	U_D	% η	BDS	Ref.
PVDF/CCTO-NH_2	8 vol%	19	0.03	1.2 J/cc at 500 kV/cm	65	-	[14]
PVDF/BT-H_2O_2	30 wt%	50	0.30	0.15 J/cc at 100 kV/cm	84	10 MV/m	[16]
PVDF/BT-KH550	20 vol%	26	0.12	4.2 J/cc at 150 MV/m	70	230 MV/m	[17]
PVDF/BT@Ag	10 wt%	20	0.03	4.12 J/cc at 389 MV/m	-	389 MV/m	[25]
PVDF-HFP/BT-PVP	5 vol%	19	0.06	6 J/cc at 250 MV/m	70	275 MV/m	[32]
PVDF/BT-TDPA	20 vol%	25	0.05	4.4 J/cc at 120 MV/m	78	120 MV/m	[33]
PVDF/BST-P	3 vol%	30	0.04	7.97 J/cc at 1800 kV/cm	98	381 MV/m	This work

The existing work highlights that the combination of the incorporated surface-modified nanoparticles and the specially architectured polymer ceramic nanocomposite thick films might lead to improved dielectric properties, breakdown strength and energy storage performance. The present chapter consists of a detailed investigation of the dielectric properties, breakdown strength and energy storage performance (discharge energy density and energy efficiency) of trilayered PVDF-BST films consisting of very low-loaded surface modified BST nanoparticles.

6.2 Experimental

The studies mentioned in this chapter are focused around the synthesis of $Ba_{0.8}Sr_{0.2}TiO_3$ nanoparticles functionalized using H_2O_2 and H_3PO_4 with their respective abbreviated nomination as BST-H and BST-P and their incorporation into the PVDF polymer matrix. The following sections explain the synthesis of functionalized $Ba_{0.8}Sr_{0.2}TiO_3$ nanoparticles incorporated into the PVDF matrix for fabricating the specially architectured trilayered films. These films are subjected to a comprehensive investigation of structural, morphological as well as dielectric, electrical breakdown strength and energy storage behavior.

6.2.1 Synthesis of functionalized $Ba_{0.8}Sr_{0.2}TiO_3$ nanoparticles

The BST nanoparticles have been synthesized using the hydrothermal method [34], as discussed in section 2.2.1 of Chapter 2 and the functionalization of the BST nanoparticles is done using H_2O_2 and H_3PO_4, as detailed in section 2.2.3 of Chapter 2.

6.2.2 Synthesis of PVDF-functionalized $Ba_{0.8}Sr_{0.2}TiO_3$ nanocomposite trilayered films

Initially, PVDF powder (Alfa Aesar) is dissolved in DMF solvent and sonicated for 30 minutes. 3 volume percent of the H_2O_2 and H_3PO_4 functionalized $Ba_{0.8}Sr_{0.2}TiO_3$ nanoparticles viz. BST-H and BST-P are added to the sonicated PVDF solution. The mixtures are stirred at 60°C for 12 hours using a mechanical stirrer. The homogenized solutions are then cast onto the bed of a TMAX tape casting unit set at 70°C and dried for 2 hours in the air. The dried nanocomposite films of PVDF, PBST-H and PBST-P are peeled off and placed in a vacuum oven for 8 hrs, which is pre-heated at 150°C. Subsequently, the nanocomposite thick films are cooled down to ambient temperature. The hot-pressing process involved the stacking of three layers of individual nanocomposite films placed over one another. Hot-pressing is done at a pressure of 250 kN for 5 minutes at a temperature of 150°C.

6.2.3 Structural studies of PVDF-functionalized $Ba_{0.8}Sr_{0.2}TiO_3$ nanocomposite trilayered films

The crystallinity of both the functionalized BST powder and the PVDF-functionalized BST nanocomposites is characterized using X-ray diffraction (XRD), along with the Fourier-transform infrared (FTIR) spectra analysis of the functionalized BST nanoparticles and the trilayered PVDF-functionalized BST nanocomposites. The functionalization of the BST nanoparticles is further confirmed by using energy dispersive spectroscopy (EDS) mapping of H_3PO_4-treated BST nanoparticles. Additionally, the surface and cross-section of the trilayered PVDF-functionalized BST nanocomposites have been studied by using a field emission scanning electron microscope (FESEM).

6.2.4 Electrical studies of PVDF-functionalized $Ba_{0.8}Sr_{0.2}TiO_3$ trilayered nanocomposite films

An impedance analyzer has been used to measure the room temperature dielectric properties of the functionalized nanocomposites in the frequency range of 100 Hz to 1 MHz with an oscillating voltage of ± 1V across the samples. The breakdown strength (BDS) of PVDF-functionalized BST nanocomposites is measured by using a Danbridge 30 kV Non-Destructive Insulation Tester (Denmark), whereas dielectric displacement vs. electric field (D-E) loops are measured by employing a 10 Hz triangular wave.

6.3 Results and discussion

The results of structural and electrical studies are discussed in the subsequent subsections.

6.3.1 Structural studies

The subsequent sections explore the findings obtained from X-ray diffraction (XRD), Fourier transform infrared spectroscopy (FTIR), field emission scanning electron microscopy (FESEM) and electron dispersion spectroscopy (EDS).

6.3.1.1 X-ray diffraction

Fig. 6.1 shows the X-ray diffraction (XRD) patterns of pure PVDF, PBST-H and PBST-P nanocomposite thick films. The XRD peaks observed at 2θ values of 18.5° and 26.5° confirm the presence of the α-crystalline phase of PVDF, whereas the prominent peak at 20.2° corresponds to the β-crystalline phase [35]. These crystalline phases are showing their presence in pure PVDF, PBST-H and PBST-P thick films.

Fig.6.1: XRD spectra of pure PVDF film, PBST-H and PBST-P trilayered nanocomposite films

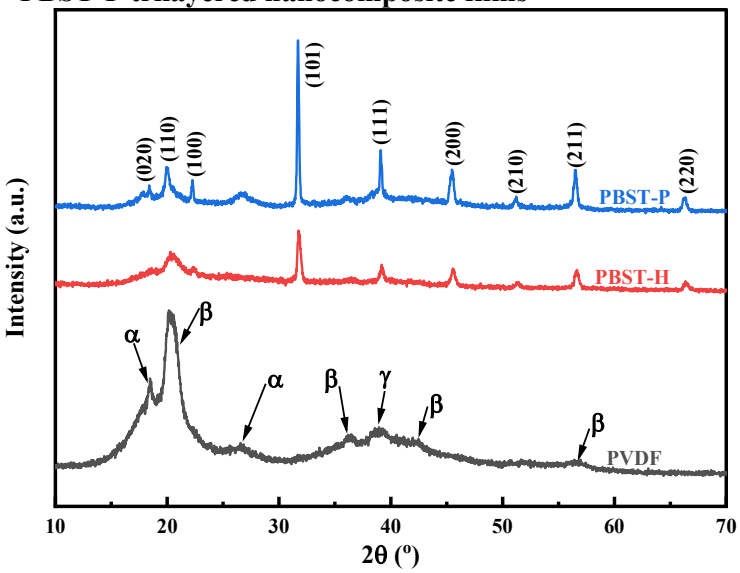

Additionally, the XRD peaks at 36.2°, 42.5°, and 56.8° correspond to the β-phase of the PVDF [35]. A low-intensity XRD peak observed at 39.1° has been observed in all nanocomposite films, which corresponds to the γ-phase of PVDF [36]. However, this peak gets merged with the (111) crystal plane of BST in PBST-H and PBST-P thick films. The high-intensity peak observed at 31.8° for PBST-H and PBST-P corresponds to the (101) crystal plane of the functionalized BST nanoparticles (ICDD card number 00-044-0093). The XRD pattern have also indicated that the surface functionalization of BST nanoparticles did not change its crystal structure in the nanocomposites, as well as the proper inclusion of functionalized nanoparticles in the PVDF matrix.

6.3.1.2 Fourier transform infrared spectroscopy

Fig. 6.2 shows the FTIR spectra of $Ba_{0.8}Sr_{0.2}TiO_3$ nanoparticles functionalized with H_2O_2 (BST-H) and H_3PO_4 (BST-P), along with pure BST nanoparticles. The IR spectra of BST-P show the bands at wavenumbers 1145 cm^{-1}, 1063 cm^{-1}, 1018 cm^{-1}, 957 cm^{-1}, and 890 cm^{-1}, which correspond to the stretching vibrations of the phosphate (PO_4^{-3}) group, while the bands at 599 cm^{-1}, 569 cm^{-1}, and 549 cm^{-1} indicate the bending vibrations of the phosphate group. The BST-H nanoparticles exhibit bands at 1635 cm^{-1} and 1574 cm^{-1}, which corresponds to the -OH group-related vibrations [37,38]. The IR spectra have given a confirmatory signature of surface modification of BST nanoparticles with $-OH^-$ and PO_4^{-3}

Fig.6.2: FTIR spectrum of BST nanoparticles functionalized with different surface modifiers

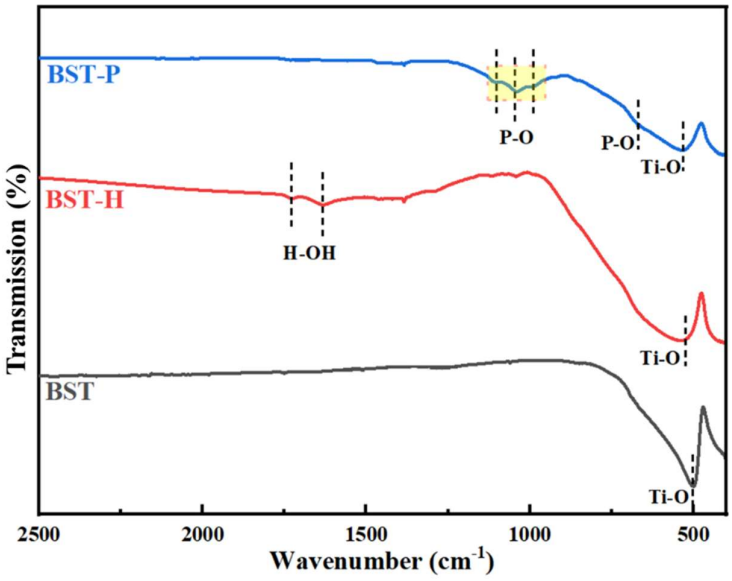

functional groups. These functional groups will have a bridging role with CH_2-CF_2 dipoles of the PVDF polymer with the functionalized BST nanoparticles [39].

Fig. 6.3 shows the IR spectra of the PBST-P, PBST-H and pure PVDF nanocomposite films. The characteristic IR bands of the α crystalline phase of the PVDF are observed at wavenumbers 530 cm^{-1}, 614 cm^{-1}, 763/766 cm^{-1}, 795 cm^{-1}, 854 cm^{-1}, 1149 cm^{-1}, 1330 cm^{-1} and 1382 cm^{-1}, common in all the nanocomposite films [40]. The IR bands of the β crystalline phase of the PVDF are observed at 600 cm^{-1}, 840 cm^{-1}, 878 cm^{-1}, and 948 cm^{-1} [40]. The bands at 510 cm^{-1} correspond to both α/β phases of PVDF, whereas the bands at 1070 cm^{-1} and 1454 cm^{-1} indicate the presence of β/γ phases [40]. The band observed at 840 cm^{-1} corresponds to β-phase, while the bands at 430 cm^{-1} and 490 cm^{-1} correspond to β/γ phases of PVDF. These bands are more distinct and clear for PBST-P films as compared to PBST-H and pure PVDF films. The band at 510 cm^{-1} corresponding to either α or β phase has only been observed in PBST-P film, whereas it is absent in PBST-H and pure PVDF films. It is clearly marked in the IR spectra shown in Fig. 6.3. The IR studies confirm that the incorporation of the functionalized BST nanoparticles in the PVDF polymer matrix (i.e., PBST-P and PBST-H films) leads to the evolution of β and γ crystalline phases, which are polar in nature and possess very good dielectric and energy storage properties [40,41]. Another

Fig.6.3: FTIR spectrum of functionalized PVDF, PBST-H and PBST-P trilayered nanocomposite films with different surface modifiers

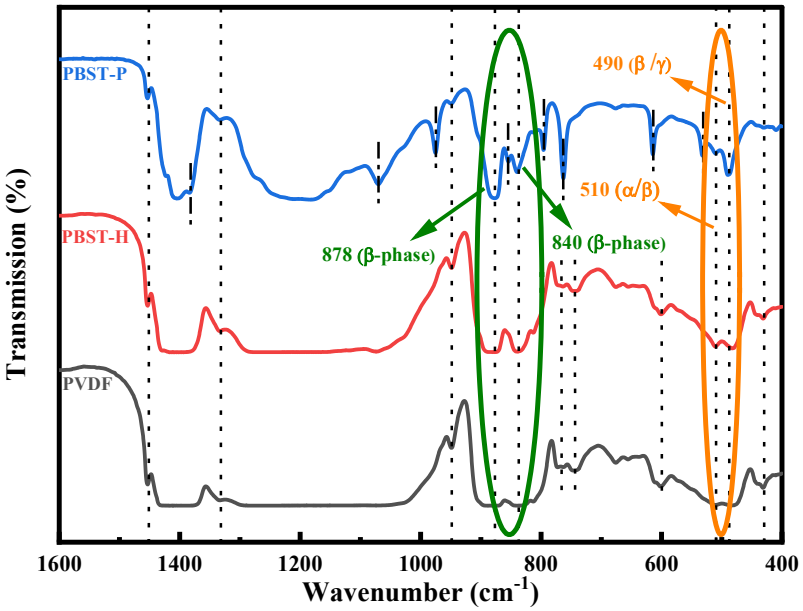

important observation indicates that the emergence of β and γ crystalline phases in PBST-P films are more prominent as compared to PBST-H films.

6.3.1.3 Field emission scanning electron microscopy

The modification of the surface of ceramic nanoparticles in the polymer matrix has also been found to change the surface morphology due to enhanced compatibilities as well as modification in the interfacial forces between ceramic nanoparticles and polymers. The field emission scanning electron microscopy (FESEM) studies have also been carried out for all the nanocomposite films. Fig. 6.4 shows the FESEM micrographs of H_3PO_4 functionalized BST nanoparticles, the surface of PBST-P nanocomposite film and the

Fig.6.4: FESEM images of (a) H_3PO_4 functionalized BST nanoparticles, (b) surface of PBST-P nanocomposite and (c) cross-section of the PBST-P trilayered nanocomposite film

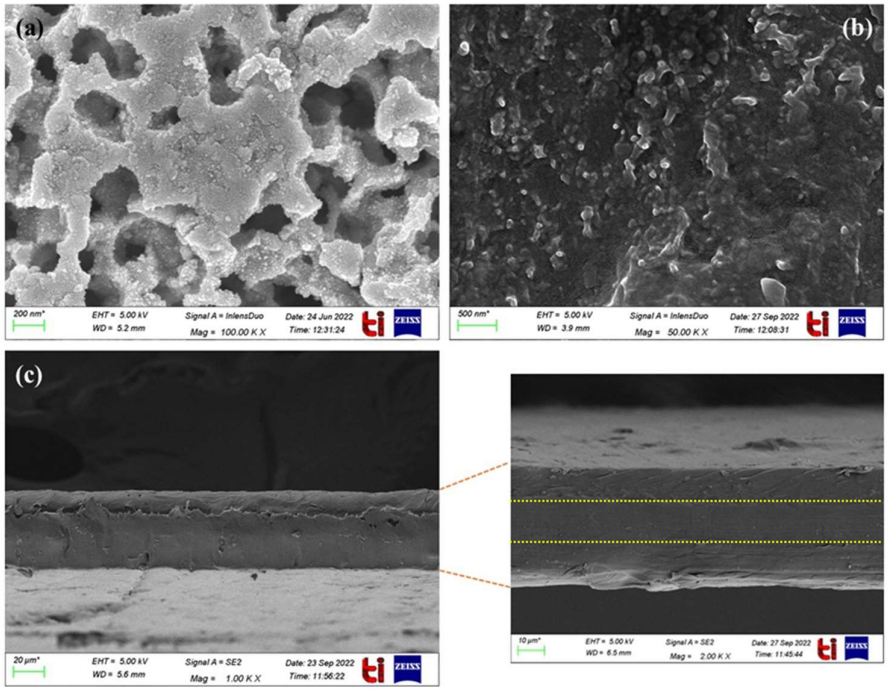

Fig.6.5: FESEM images of (a) unfunctionalized BST nanoparticles and (b) H_2O_2 functionalized BST nanoparticles

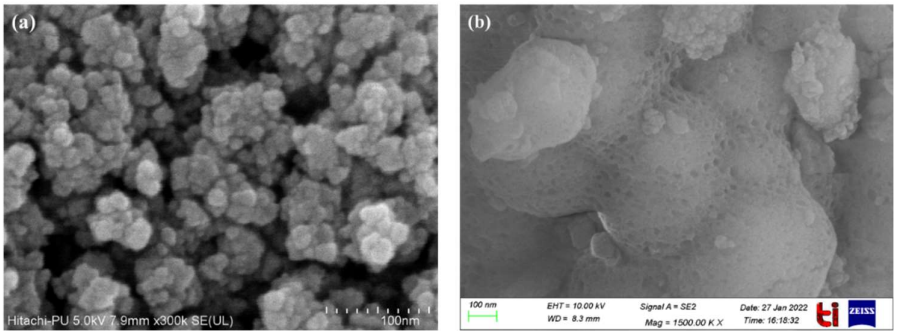

cross-section of PBST-P film. The FESEM images of unfunctionalized and -OH functionalized BST nanoparticles, PBST and PBST-H films are given in Fig. 6.5.

It can be seen that the surface of H_3PO_4 functionalized BST nanoparticles is porous and rough, which is in agreement with earlier reports [27,42]. The incorporation of these nanoparticles in the PVDF polymer matrix results into the homogeneous distribution of H_3PO_4 functionalized BST nanoparticles. The porous structure of BST-P particles and increased chemical activity at the BST-P/PVDF interface lead towards a completely covered surface of the BST-P nanoparticles with PVDF. The observed surface morphology of PBST-P nanocomposites could be due to the following reasons:

a) *The increase in surface roughness could further help increase the adhesion at interfaces between BST-P nanoparticles and the PVDF polymer matrix.*

b) *The surface roughness and porous structure of H_3PO_4 functionalized BST nanoparticles, which allow PVDF to seep in through the BST nanoparticles. This will increase the compatibility between the interfaces of BST nanoparticles and the PVDF matrix.*

Fig.6.6: FESEM images of (a) the surface of PBST film, (b) the surface of PBST-H nanocomposite and (c) the cross-section of the PBST-H nanocomposite film

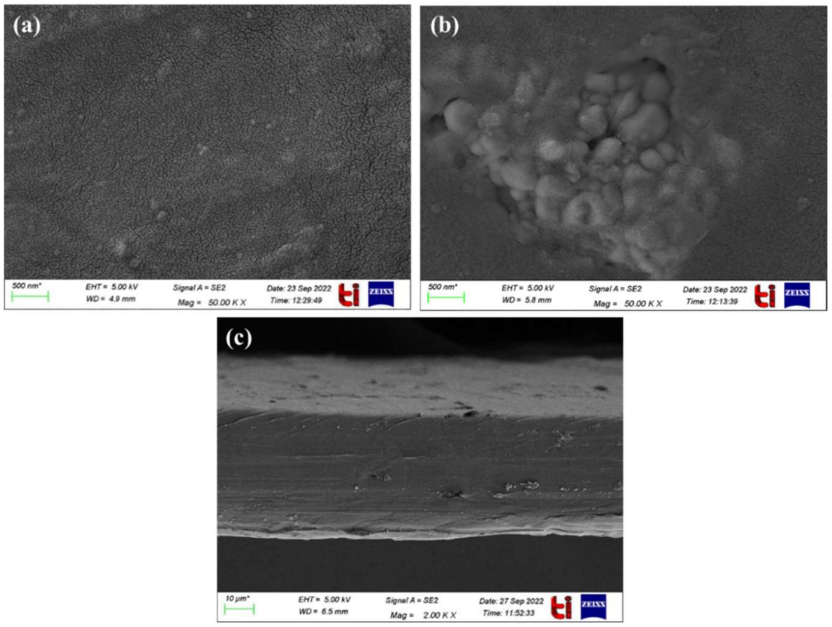

c) *PO_4^{-3} group attached with BST nanoparticles creates a better bridging network with $-F^{-2}$ of CF_2 dipoles of PVDF due to the variation in the coordination numbers* [43].

On the other hand, H_2O_2 surface-functionalized and unfunctionalized BST nanoparticles do not show that degree of compatibility with the PVDF matrix, as seen in Fig. 6.6. The functionalization of the BST nanoparticles is further confirmed by using energy dispersive spectroscopy (EDS) mapping of H_3PO_4-treated BST nanoparticles, as shown in Fig. 6.7. It is seen here that all the elements (i.e., Ba, Sr, Ti, O and P) are present on the clustered surface of the treated BST nanoparticles. Carbon is present in the mapping because the sample is prepared on carbon tape for testing.

Fig.6.7: EDS mapping of BST nanoparticles functionalized with H_3PO_4

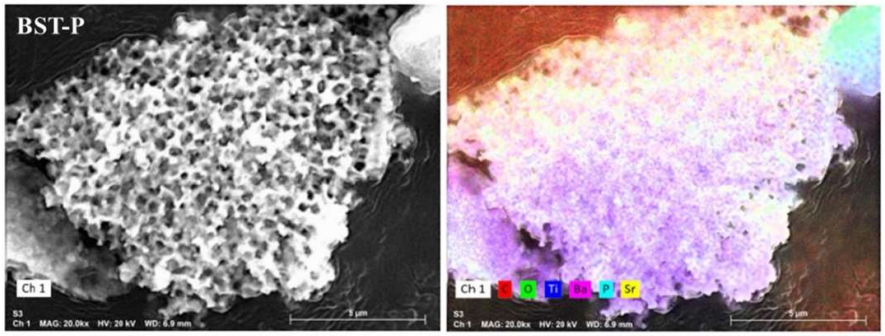

6.3.2 Electrical studies

The electrical studies include dielectric behavior and electrical displacement vs electric field (D-E) studies. The discharging energy density, as well as energy efficiency of all the PVDF/functionalized BST trilayered nanocomposite thick films, have been calculated from electrical displacement vs. electric field data. The results of these studies are discussed in the following subsections.

6.3.2.1 Dielectric studies

Fig. 6.8 (a) and (b) show the variation of dielectric constant and tangent loss of the trilayered pure PVDF film, PBST-H and PBST-P nanocomposite films. The dielectric constant of PVDF, PBST-H and PBST-P films has been found to be ~11, ~24, & ~32 and ~10, ~22, & ~30, respectively, at the frequencies 100 Hz and 1 kHz. The dielectric constant of PBST-H and PBST-P films has been found to be higher as compared to that of the pure PVDF film. The high value of the dielectric constant in the nanocomposite films consisting of functionalized

BST nanoparticles is caused by the high permittivity of BST itself, increased interfacial polarization due to the Maxwell-Wagner-Sillars polarization effects [44] and the increased bridging effect mediated by oxygen between PVDF/BST interface [10]. The dielectric constant shows a decrease for frequencies greater than 100 kHz, which is associated with the α-relaxations caused by the motion of polymeric chains of the PVDF polymer matrix [45]. The onset frequency of the decrease in the dielectric constant is the lowest (~385 kHz) for PBST-P nanocomposite film, which means that the incorporation of phosphate-functionalized BST nanoparticles slows down the micro-Brownian motion in the polymeric chains. On the other hand, for PBST-H, this onset frequency is 690 kHz, whereas for pure PVDF, it may be beyond 1 MHz. The variation of dielectric constant and tangent loss with frequency for PVDF-BST (PBST) nanocomposite film is given in Fig. 6.9. The dielectric constant of PBST-P nanocomposite thick film is remarkably higher, which is ascribed to the enhanced linkages between the PVDF matrix and $-PO_4^{-3}$ functionalized BST nanoparticles, as well as the

Fig.6.8: Variation of (a) dielectric constant and (b) tangent loss with frequency for pure PVDF film, PBST-H and PBST-P trilayered nanocomposite films

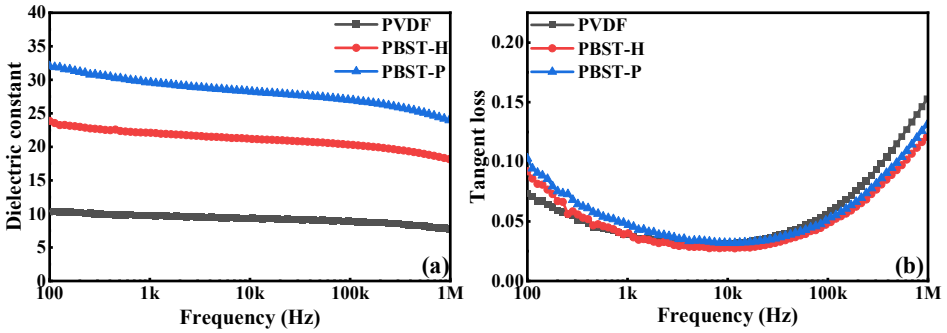

Fig.6.9: Variation of dielectric constant and tangent loss with frequency for PBST nanocomposite

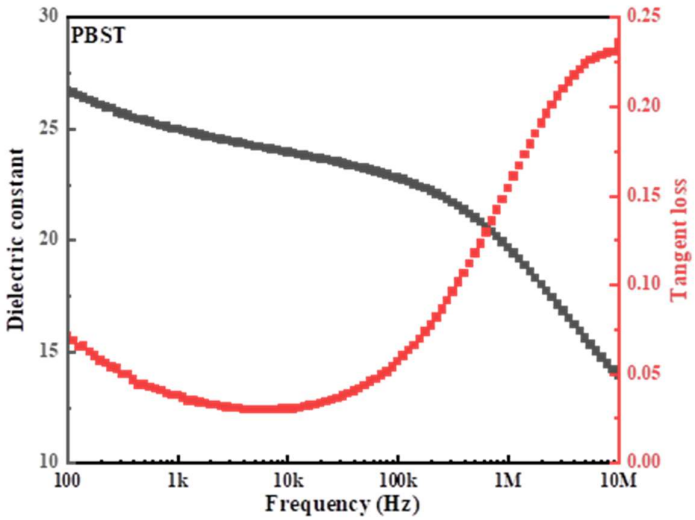

increased interfacial polarization due to the better interconnect between the $-PO_4^{-3}$ group of BST nanoparticles and $-F^-$ group of PVDF [43]. The tangent loss of all the films shows a decrease in the frequency range of 100 Hz-10 kHz. This decrease of loss is caused by the surface/surface polarization due to various interfaces such as the sample/electrode interface, the interface among the layers of the films, as well as PVDF/functionalized BST interfaces [10,14]. The tangent loss is found to increase for frequencies greater than 10 kHz, which is ascribed to the α-relaxations, dipolar relaxation within the PVDF, as well as at the interfaces [9,45]. The local electric field arising due to the interaction between interfacial charges and the dipolar field of the functionalized BST nanoparticles, as well as PVDF also contributes in increasing the tangent loss. The dielectric constant and tangent loss at 1 kHz for pure PVDF film, PBST-H and PBST-P nanocomposite trilayered films is shown in Fig. 6.10 in the form of a bar graph.

Fig.6.10: The dielectric constant and tangent loss at 1kHz for pure PVDF film, PBST-H and PBST-P trilayered nanocomposite films

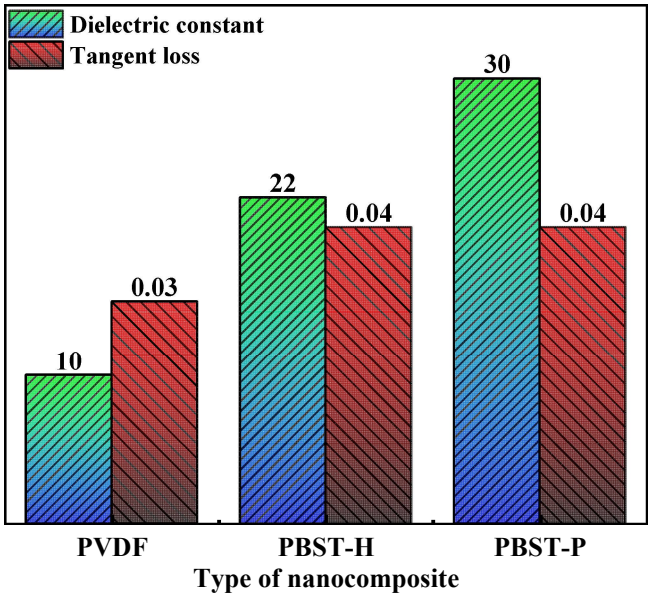

6.3.2.2 Breakdown strength studies

The dielectric breakdown strength of polymer-based nanocomposites to be employed for energy storage purposes plays a significant role as it affects the energy storage behavior in an exponential fashion. Two-parameter Weibull statistical analysis is normally used to determine the electrical breakdown strength (BDS). The Weibull equation is given as:

$$P_i = 1 - \exp\left(\frac{E_i}{E_o}\right)^{\gamma} \quad (6.1)$$

where P_i is the breakdown probability, E_i is the average breakdown strength, E_o is the field corresponding to 63.2% breakdown cumulative probability and γ is the shape factor (Weibull modulus) for estimating data scattering and its value is related with the uniformity of the breakdown strength throughout the polymer nanocomposite films, i.e., microscopic inhomogeneity. The experimental plot is a straight line given by [46]:

$$X = ln(E_i) \text{ and } Y = ln(-\ln(1 - P_i)) \quad (6.2)$$

High breakdown strength ensures the sustainability of the electric displacement/polarization at high fields. Fig. 6.11 shows the Weibull distribution curve depicting the breakdown strength (BDS) for PVDF film, PBST-H and PBST-P nanocomposite film. Ten data points are taken for calculating the breakdown strength of the nanocomposites. The experimental values of the BDS are ~578 MV/m, ~318 MV/m and ~381 MV/m for PVDF, PBST-H and PBST-P nanocomposite films, respectively. A noticeable decrease in the breakdown strength of the nanocomposites as compared to the pure PVDF is observed when functionalized BST nanoparticles are added to the polymer matrix. The decrease in the breakdown strength in the nanocomposite films consisting of nanoparticles is ascribed to the electronic and morphological defects, which gives the percolative conducting path at the ceramic nanoparticle/polymer interface [47].

Fig.6.11: Weibull distribution curve of PVDF film, PBST-H and PBST-P trilayered nanocomposite films

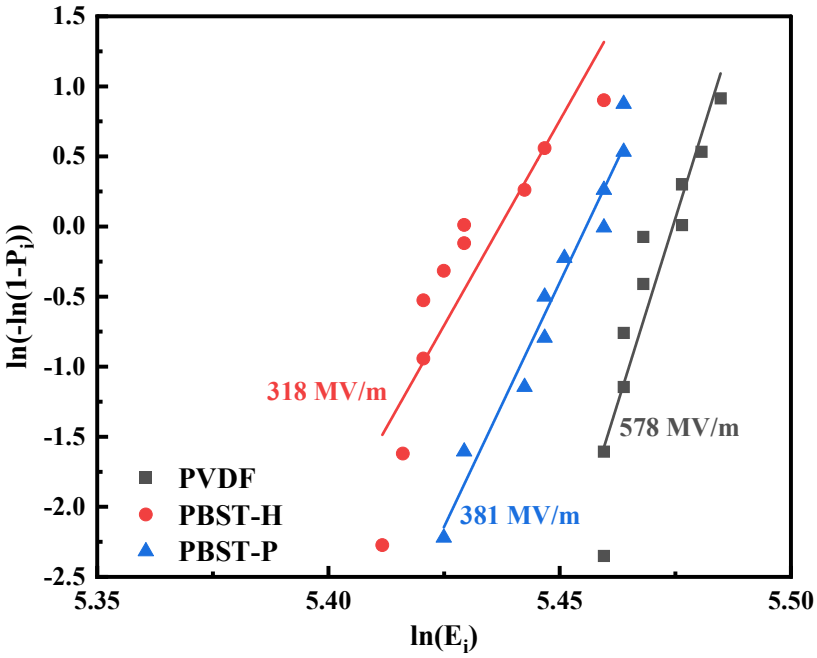

The interfacial morphological defects create the space charge, which are excited at a lower electric field as compared to the bound charges in the nanocomposite films. The observed breakdown behavior is very interesting since the incorporation of H_3PO_4-modified BST nanoparticles in the PVDF matrix possesses high breakdown strength as compared to H_2O_2-modified BST nanoparticles incorporated in the PVDF matrix. The interaction of the -OH group with the F^- ion of the PVDF matrix forms the hydrogen bond, which is widely reported in the literature [15,23,33,48]. This interaction has also been found to improve the dielectric and energy storage behavior. The $-PO_4^{-3}$ group-modified BST nanoparticles incorporated in the PVDF matrix serve as a better network modifier between PVDF and BST-P by breaking the linkages joined by O_2^- of $-PO_4^{-3}$ and F_2^- of PVDF. The local environment and PVDF/BST-P interface is expanded to high coordination numbers [43]. The increased networking leads to modification in the crystalline structure of PVDF and improved surface morphology, as evidenced in IR and FESEM studies. The interface of PVDF/BST have modified charge density, which causes the increased breakdown strength.

6.3.2.3 Dielectric displacement and energy storage behavior studies

Undoubtedly, the increase in breakdown strength is essential in order to have very good energy storage properties. The discharge energy density and efficiency are also the key parameters for energy storage devices. Therefore, unipolar displacement vs. electric field (D-E) loop studies have been carried out. Fig. 6.12 (a), (b) and (c) shows the displacement-electric field loop (D-E loop), discharge energy density and efficiency of the PVDF film, PBST-H and PBST-P nanocomposite films varying with the applied electric field, respectively. The value of saturation polarization for PBST-H and PBST-P is ~1.43 and ~1.41μC/cm^2, which is much higher than pure PVDF film (~1.11 μC/cm^2). Also, the remanent polarization is very low in PBST-P nanocomposite films, which leads to the increased discharge energy density and higher energy efficiency. The value of discharge energy density at 1800 kV/cm is calculated using U_D

= ∫E.dD, which comes out to be 6.09, 6.71 and 7.97 J/cc for PVDF, PBST-H and PBST-P, respectively.

Moreover, the energy efficiency of the nanocomposites is observed to be ~80%, ~78% and ~98% for PVDF, PBST-H and PBST-P nanocomposites, respectively, at 1800 kV/cm. The energy efficiency of these nanocomposites has been calculated as the ratio of the discharging energy density to the charging energy density. For a given material, charging energy density (U_C) is calculated using $\int_0^{Pmax} E.dP$, whereas discharge energy density (U_D) is calculated using $\int_{Pr}^{Pmax} E.dP$ and the final energy efficiency (η) is calculated by using the following formula [10]:

Fig.6.12: Variation of (a) displacement, (b) discharge energy density and (c) efficiency with the electric field of the PVDF, PBST-H and PBST-P trilayered nanocomposite films

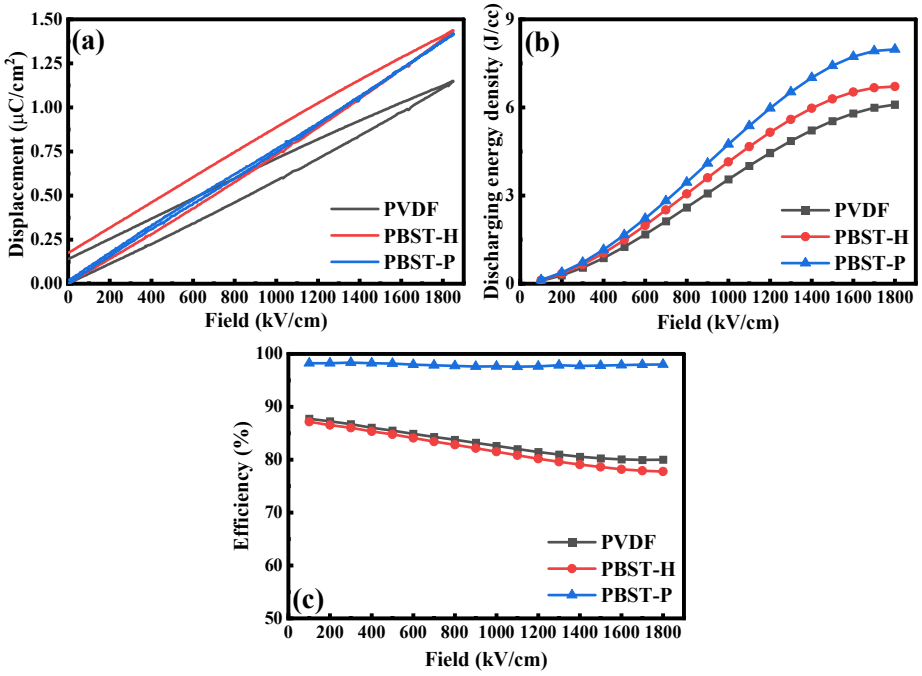

$$\% \eta = \frac{Discharge\ energy\ density\ (U_D)}{Charge\ energy\ density\ (U_C)} \times 100\% \quad (6.3)$$

The D-E loop, discharge energy density and efficiency of PBST trilayered nanocomposite film are shown in Fig. 6.13. The discharge energy density, breakdown strength and efficiency of the pure PVDF, PBST-H and PBST-P nanocomposite multilayer films are shown in Fig. 6.14 in the form of a bar chart. The low value of remanent displacement and less hysteresis losses are momentous for high discharge energy density and energy efficiency, respectively [49,50]. The

PBST-P nanocomposite film possesses a higher discharge energy density (7.97 J/cc at 1800 kV/cm) and ultrahigh efficiency (~98%). The PBST-P nanocomposite multilayer thick films exhibit superior dielectric properties, breakdown strength, discharge energy density and ultra-high energy efficiency as compared to PBST-H films.

Fig.6.13: Variation of (a) displacement and (b) discharge energy density & efficiency of PBST nanocomposite film with the electric field

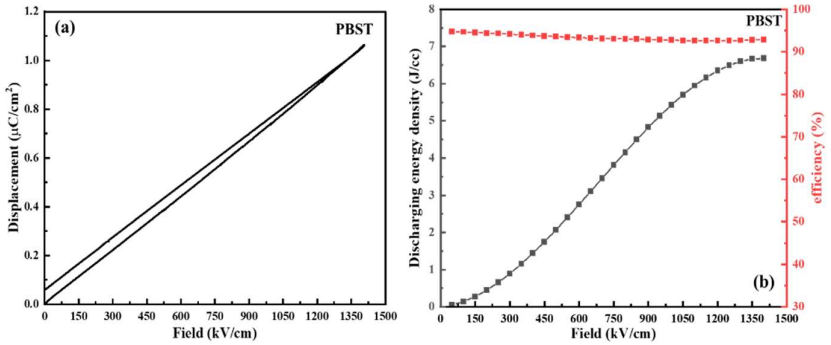

The following section explains the mechanism responsible for the observed superior dielectric properties, electrical breakdown strength and energy storage properties of PBST-P trilayered nanocomposite films.

Fig.6.14: The discharge energy density, breakdown strength and efficiency for pure PVDF film, PBST-H and PBST-P trilayered nanocomposite films

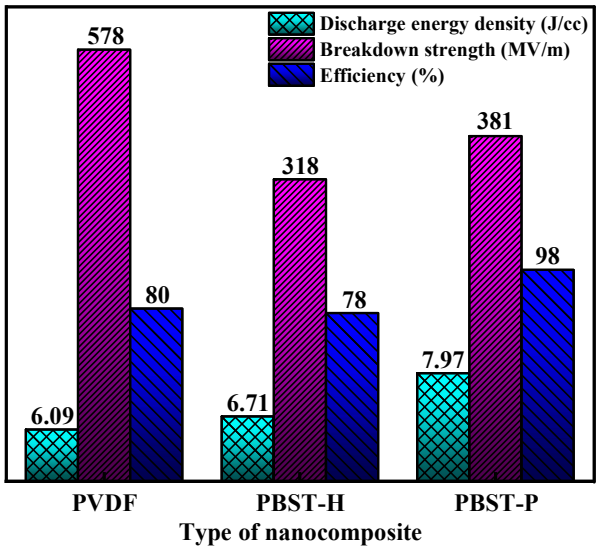

6.3.3 Mechanism

The schematic representation of the mechanism is shown in Fig. 6.15; the incorporation of $-PO_4^{-3}$ surface-modified BST into the PVDF matrix (i.e., PBST-P nanocomposite trilayered films) provides the flexibility of change of coordination states of phosphorous with respect to fluoride ions of PVDF [43], which can act as a better bridging network at the interfaces. The resulting interfacial forces rotate the CH_2 and CF_2 dipole of the PVDF matrix polymer matrix, which leads to the evolution of β and γ crystalline phases as

evidenced by IR studies. The linkage between BST nanoparticle with PVDF matrix via the $-PO_4^{-3}$ group creates a strong bridging network as compared to that via $-OH^-$ ions (shown in Fig. 6.15). Interfacial network modification at the PVDF/BST-P interface and interfaces among the different layers creates additional dipoles, which enhances the polarization as well as the dielectric constant.

Fig. :6.15 Mechanism showing the interaction of $-OH^-$ and $-PO_4^{-3}$ ions with the BST nanoparticles and PVDF polymer matrix for PBST-H and PBST-P trilayered nanocomposite films

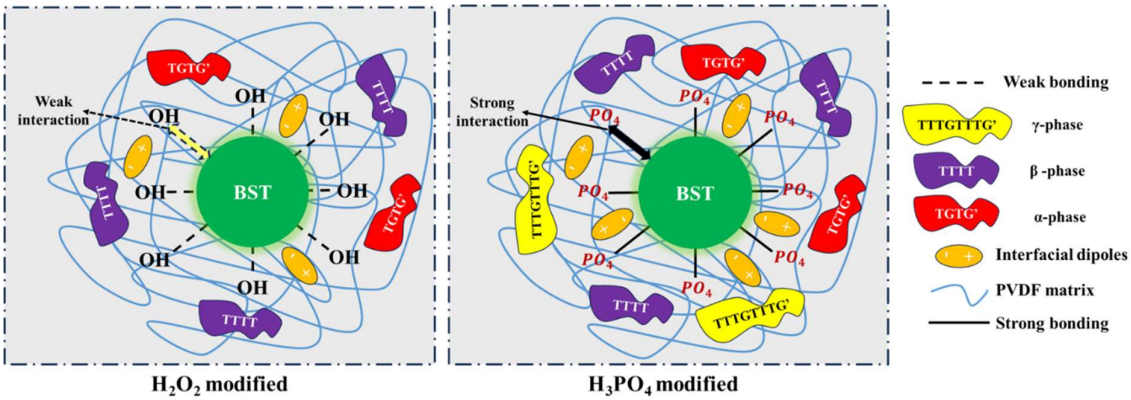

The formation of the local electric field at the interface of PBST-P multilayer films is much stronger as compared to the PBS-H multilayer films. This local field at the interfaces resists the externally applied electric field and prevents the PBST-P multilayer film to have electrical breakdown at a low field. The prompt switching of dipoles [51] with the reversal of the electric field is caused by γ-phase as well as smaller crystallites in PBST-P multilayer nanocomposite films. This prompt switching of the dipoles decreases the hysteretic behavior in the D-E loops, which in turn leads to ultrahigh-energy efficiency.

6.4 Conclusion

The trilayered PVDF-BST nanocomposite films have been synthesized by tape casting. The surface of BST nanoparticles is modified with PO_4^{-3} and $-OH^-$ functional groups, the respective films consisting of these nanoparticles are named as PBST-P and PBST-H films. The inclusion of surface-modified nanoparticles strongly affects the structural and morphological features of the trilayered films. The PBST-P film exhibits the evolution of β and

γ crystalline phases of PVDF along with improved surface morphology. The PBST-P trilayered films are found to exhibit superior dielectric properties, breakdown strength, discharge energy density and energy efficiency with their respective values of ~30 at 1 kHz, 381 MV/m, 7.97 J/cc at 1800 kV/cm and 98%. The improved structural and morphological properties, as well as superior dielectric properties and energy storage performance is attributed to the better bridging network created between $-F^{-2}$ of CF_2 dipoles of PVDF with PO_4^{-3} group of BST-P nanoparticles. These interactions lead to enhancement in the PVDF/BST-P interface and interlayer interfaces, introducing extra dipoles and establishing a strong local electric field at the interfaces for an improved interfacial network. The qualitative explanation of the involved mechanism is also discussed. The study may lead towards the novel ways of developing polymer-ceramic nanocomposites for high-energy density capacitors, where the incorporation of functionalized nanoparticles in the polymer matrix is accompanied by the architectured structure.

References

[1] Z. Yao, Z. Song, H. Hao, Z. Yu, M. Cao, S. Zhang, M.T. Lanagan, H. Liu, Homogeneous/Inhomogeneous-Structured Dielectrics and their Energy-Storage Performances, Advanced Materials 29 (2017). https://doi.org/10.1002/adma.201601727.

[2] P. Zhao, Z. Cai, L. Chen, L. Wu, Y. Huan, L. Guo, L. Li, H. Wang, X. Wang, Ultra-high energy storage performance in lead-free multilayer ceramic capacitors: Via a multiscale optimization strategy, Energy Environ Sci 13 (2020) 4882–4890. https://doi.org/10.1039/d0ee03094e.

[3] L. Li, L. Han, H. Hu, R. Zhang, A review on polymers and their composites for flexible electronics, Mater Adv (2023). https://doi.org/10.1039/D2MA00940D.

[4] J. Li, Q. Meng, W. Li, Z. Zhang, Influence of crystalline properties on the dielectric and energy storage properties of poly(vinylidene fluoride), J Appl Polym Sci 122 (2011) 1659–1668. https://doi.org/10.1002/app.34020.

[5] L. Singh, U.S. Rai, K.D. Mandal, B.C. Sin, H. Il Lee, H. Chung, Y. Lee, Comparative dielectric studies of nanostructured BaTiO3, CaCu3Ti4O12 and 0.5BaTiO3· 0.5CaCu3Ti4O12 nano-composites synthesized by modified sol-gel and solid state methods, Mater Charact 96 (2014) 54–62. https://doi.org/10.1016/j.matchar.2014.07.019.

[6] X. Wei, X. Yao, Nonlinear dielectric properties of barium strontium titanate ceramics, Materials Science and Engineering B 99 (2003) 74–78. https://doi.org/10.1016/S0921-5107(02)00423-3.

[7] X. Dong, B. Lee, A. Ghulam, J. Akedo, H.K. Yu, J.Y. Choi, J.H. Park, Dielectric properties of lead zirconate titanate/Au composite film prepared by aerosol deposition, Mater Chem Phys 284 (2022). https://doi.org/10.1016/j.matchemphys.2022.126078.

[8] X. Lu, L. Zhang, Y. Tong, Z.Y. Cheng, BST-P(VDF-CTFE) nanocomposite films with high dielectric constant, low dielectric loss, and high energy-storage density, Compos B Eng 168 (2019) 34–43. https://doi.org/10.1016/j.compositesb.2018.12.059.

[9] S. Jaidka, S. Chopra, A. Aggarwal, D.P. Singh, Effect of interfacial layers on the temperature-dependent dielectric and impedance behavior of flexible PVDF-BST nanocomposite thick films, Journal of Physics and Chemistry of Solids 184 (2024) 111667. https://doi.org/10.1016/j.jpcs.2023.111667.

[10] S. Jaidka, D.P. Singh, Ultrahigh efficiency and enhanced discharge energy density at low loading of nanofiller in trilayered polyvinylidene fluoride-Ba0.8Sr0.2TiO3 nanocomposites, Polym Compos (2023). https://doi.org/10.1002/pc.28081.

[11] H. Li, M. Du, X. Yang, X. Liu, Enhancing high-temperature breakdown strength of polyetherimide dielectric nanocomposites with MgO nanosheets by inhibiting charge migration, J Appl Polym Sci (2023). https://doi.org/10.1002/app.54389.

[12] L. Yao, Z. Pan, J. Zhai, G. Zhang, Z. Liu, Y. Liu, High-energy-density with polymer nanocomposites containing of SrTiO3 nanofibers for capacitor application, Compos Part A Appl Sci Manuf 109 (2018) 48–54. https://doi.org/10.1016/j.compositesa.2018.02.040.

[13] S. Cheng, M. Yang, J. Fu, R. Wang, J. He, Q. Li, Surface-coated polymer nanocomposites containing z-aligned high-k nanowires as high-performance dielectrics at elevated temperatures, IET Nanodielectrics (2023). https://doi.org/10.1049/nde2.12060.

[14] S. Kaur, D.P. Singh, Significantly improved dielectric and energy storage behavior of the surface functionalized CaCu3Ti4O12 nanoparticles in PVDF-CaCu3Ti4O12 nanocomposites, J Alloys Compd 918 (2022). https://doi.org/10.1016/j.jallcom.2022.165500.

[15] S. Liu, S. Xue, W. Zhang, J. Zhai, G. Chen, Significantly enhanced dielectric property in PVDF nanocomposites flexible films through a small loading of surface-hydroxylated Ba0.6Sr0.4TiO3 nanotubes, J Mater Chem A Mater 2 (2014) 18040–18046. https://doi.org/10.1039/c4ta04051a.

[16] G.H. Tabhane, S.M. Giripunje, S.B. Kondawar, Intensifying energy density, dielectric and mechanical properties of electroactive β-PVDF/f-BTO nanocomposites, Physica B Condens Matter 571 (2019) 149–161. https://doi.org/10.1016/j.physb.2019.06.064.

[17] X. Sang, X. Li, D. Zhang, X. Zhang, H. Wang, S. Li, Improved Dielectric Properties and Energy Storage Densities of BaTiO3 Doped PVDF Composites by Heat Treatment and Surface Modification of BaTiO3, J Phys D Appl Phys (2022). https://doi.org/10.1088/1361-6463/ac4942.

[18] S. Nayak, D. Khastgir, Polydimethylsiloxane-PbZr 0.52 Ti 0.48 O 3 nanocomposites with high permittivity: Effect of poling and temperature on dielectric properties, J Appl Polym Sci 136 (2019) 47307. https://doi.org/10.1002/app.47307.

[19] L. Jin, J. Liu, L. Zhu, J. Ding, Y. Zhang, Z. Jiang, Crosslinked poly (aryl ether ketone)/boron nitride nanocomposites containing a stable chemical bonding structure as high temperature dielectrics, Compos Sci Technol 213 (2021). https://doi.org/10.1016/j.compscitech.2021.108949.

[20] L. Ren, L. Yang, S. Zhang, H. Li, Y. Zhou, D. Ai, Z. Xie, X. Zhao, Z. Peng, R. Liao, Q. Wang, Largely enhanced dielectric properties of polymer composites with HfO2 nanoparticles for high-temperature film capacitors, Compos Sci Technol 201 (2021). https://doi.org/10.1016/j.compscitech.2020.108528.

[21] Z. Lu, G. Wang, W. Bao, J. Li, L. Li, A. Mostaed, H. Yang, H. Ji, D. Li, A. Feteira, F. Xu, D.C. Sinclair, D. Wang, S.Y. Liu, I.M. Reaney, Superior energy density through tailored dopant strategies in multilayer ceramic capacitors, Energy Environ Sci 13 (2020) 2938–2948. https://doi.org/10.1039/d0ee02104k.

[22] N. Zhang, H. Zhao, C. Zhang, S. Gao, T. Zhu, J. Bai, Improved energy storage property in polyvinylidene fluoride-based multilayered composite regulated by oriented carbon nanotube@SiO2 nanowires, IET Nanodielectrics (2023). https://doi.org/10.1049/nde2.12045.

[23] L. Shaohui, Z. Jiwei, W. Jinwen, X. Shuangxi, Z. Wenqin, Enhanced energy storage density in poly(vinylidene fluoride) nanocomposites by a small loading of suface-hydroxylated Ba0.6Sr 0.4TiO3 nanofibers, ACS Appl Mater Interfaces 6 (2014) 1533–1540. https://doi.org/10.1021/am4042096.

[24] A. Mayeen, M.S. Kala, M.S. Jayalakshmy, S. Thomas, D. Rouxel, J. Philip, R.N. Bhowmik, N. Kalarikkal, Dopamine functionalization of BaTiO3: An effective strategy for the enhancement of electrical, magnetoelectric and thermal properties of BaTiO3-PVDF-TrFE nanocomposites, Dalton Transactions 47 (2018) 2039–2051. https://doi.org/10.1039/c7dt03389c.

[25] Y. sheng Zhang, M. Wang, C. Yang, Y. wen Shao, X. dong Qi, J. hui Yang, Y. Wang, Heterogeneous BaTiO3@Ag core-shell fibers as fillers for polymer dielectric composites with

simultaneously improved dielectric constant and breakdown strength, Composites Communications 27 (2021). https://doi.org/10.1016/j.coco.2021.100874.

[26] L. Jing, W. Li, C. Gao, M. Li, W. Fei, Excellent energy storage properties achieved in PVDF-based composites by designing the lamellar-structured fillers, Compos Sci Technol 227 (2022). https://doi.org/10.1016/j.compscitech.2022.109568.

[27] D. Shelly, T. Nanda, R. Mehta, Novel epoxy-based glass fiber reinforced composites containing compatibilized para-aramid fibers and silanized nanoclay for improved impact strength, Polym Compos 43 (2022) 1357–1370. https://doi.org/10.1002/pc.26453.

[28] S.J. Park, M.K. Seo, T.J. Ma, D.R. Lee, Effect of chemical treatment of Kevlar fibers on mechanical interfacial properties of composites, J Colloid Interface Sci 252 (2002) 249–255. https://doi.org/10.1006/jcis.2002.8479.

[29] H. Bai, G. Ge, F. Yan, K. Zhu, J. Lin, C. Shi, J. Qian, Z. Wang, B. Shen, J. Zhai, Interfacial polarization regulation of ultrathin 2D nanosheets inducing high energy storage density of polymer-based nanocomposite with opposite gradient architecture, Energy Storage Mater 46 (2022) 503–511. https://doi.org/10.1016/j.ensm.2022.01.026.

[30] Y. Wang, Y. Hou, Y. Deng, Effects of interfaces between adjacent layers on breakdown strength and energy density in sandwich-structured polymer composites, Compos Sci Technol 145 (2017) 71–77. https://doi.org/10.1016/j.compscitech.2017.04.003.

[31] Y. Wang, J. Zhang, H. Gao, Y. Yao, C. Pu, J. Wang, L. Ren, Q. Zong, The interface effects on the breakdown strength of multilayer PVDF-based capacitors, Polymer (Guildf) 270 (2023). https://doi.org/10.1016/j.polymer.2023.125803.

[32] Z. Li, F. Liu, G. Yang, H. Li, L. Dong, C. Xiong, Q. Wang, Enhanced energy storage performance of ferroelectric polymer nanocomposites at relatively low electric fields induced by surface modified BaTiO3 nanofibers, Compos Sci Technol 164 (2018) 214–221. https://doi.org/10.1016/j.compscitech.2018.05.052.

[33] H. Ye, H. Chen, X. Zhang, Y. Chen, W. Shao, L. Xu, Electron structure in modified BaTiO3/ poly(vinylidene fluoride) nanocomposite with high dielectric property and energy density, IET Nanodielectrics 2 (2019) 70–77. https://doi.org/10.1049/iet-nde.2018.0029.

[34] S. Jaidka, A. Aggarwal, S. Chopra, D.P. Singh, Significantly Enhanced Dielectric Behavior of Polyvinylidene Fluoride-Barium Strontium Titanate Flexible Nanocomposite Thick Films: Role of Electric Field-Induced Effects, J Electron Mater 51 (2022) 5429–5439. https://doi.org/10.1007/s11664-022-09784-4.

[35] P. Singh, H. Borkar, B.P. Singh, V.N. Singh, A. Kumar, Ferroelectric polymer-ceramic composite thick films for energy storage applications, AIP Adv 4 (2014). https://doi.org/10.1063/1.4892961.

[36] S.A. Salman, F.T.M. Noori, A.K. Mohammed, Preparation and Characterizations of Poly (vinylidene fluoride) (PVDF)/Ba0.6Sr0.4TiO3 (BST) Nanocomposites, 2018. http://www.ripublication.com5008.

[37] B. Röska, S.H. Park, D. Behal, K.U. Hess, A. Günther, G. Benka, C. Pfleiderer, M. Hoelzel, T. Kimura, Determination of the hydrogen-bond network and the ferrimagnetic structure of a rockbridgeite-Type compound, Fe2+Fe3+3.2(Mn2+Zn)0.8(PO4)3(OH)4.2(HOH)0.8, Journal of Physics Condensed Matter 30 (2018). https://doi.org/10.1088/1361-648X/aac0cd.

[38] A.B.D. Nandiyanto, R. Oktiani, R. Ragadhita, How to read and interpret ftir spectroscope of organic material, Indonesian Journal of Science and Technology 4 (2019) 97–118. https://doi.org/10.17509/ijost.v4i1.15806.

[39] K.G. Kelele, H.C.A. Murthy, R. Balachandran, A. Tadesse, Y. Nikodimos, L.T. Tufa, J. Lee, Synthesis and characterization of Mo-doped barium strontium titanate nanopowder via slow injection sol–gel processing, Chemical Papers 77 (2023) 129–139. https://doi.org/10.1007/s11696-022-02458-9.

[40] X. Cai, T. Lei, D. Sun, L. Lin, A critical analysis of the α, β and γ phases in poly(vinylidene fluoride) using FTIR, RSC Adv 7 (2017) 15382–15389. https://doi.org/10.1039/c7ra01267e.

[41] S. Kaur, A.L. Sharma, A. Kumar, D.P. Singh, Enhanced dielectric properties of the poly(vinylidene fluoride)-CaCu3Ti4O12 nanocomposite thick films by quenching in ice water, Mater Chem Phys 254 (2020). https://doi.org/10.1016/j.matchemphys.2020.123530.

[42] Z. Lu, Y. Zhao, Z. Su, M. Zhang, B. Yang, The Effect of Phosphoric Acid Functionalization of Para-aramid Fiber on the Mechanical Property of Para-aramid Sheet, J Eng Fiber Fabr 14 (2018). http://www.jeffjournal.org.

[43] D. Möncke, H. Eckert, Review on the structural analysis of fluoride-phosphate and fluoro-phosphate glasses, Journal of Non-Crystalline Solids: X 3 (2019). https://doi.org/10.1016/j.nocx.2019.100026.

[44] W. Wu, W. Zhao, Q. Sun, B. Yu, X. Yin, X. Cao, Y. Feng, R.K.Y. Li, J. Qu, Surface treatment of two dimensional MXene for poly(vinylidene fluoride) nanocomposites with tunable dielectric permittivity, Composites Communications 23 (2021). https://doi.org/10.1016/j.coco.2020.100562.

[45] C. V. Chanmal, J.P. Jog, Dielectric relaxations in PVDF/BaTiO3 nanocomposites, Express Polym Lett 2 (2008) 294–301. https://doi.org/10.3144/expresspolymlett.2008.35.

[46] J. Wang, S. Liang, J. Xiong, B. Peng, L. He, Y. Xie, Z. Zhang, High Energy Density Nanocomposites with Layered Gradient Structure and Lysozyme-Modified Ba0.6Sr0.4TiO3 Nanoparticles, Compos Part A Appl Sci Manuf (2022) 107254. https://doi.org/10.1016/j.compositesa.2022.107254.

[47] Y. Feng, F. Zhou, Y. Dai, Z. Xu, Q. Deng, C. Peng, High dielectric and breakdown performances achieved in PVDF/graphene@MXene nanocomposites based on quantum confinement strategy, Ceram Int 46 (2020) 17992–18001. https://doi.org/10.1016/j.ceramint.2020.04.114.

[48] B. Lin, Z.-T. Li, Y. Yang, Y. Li, J.-C. Lin, X.-M. Zheng, F.-A. He, K.-H. Lam, Enhanced dielectric permittivity in surface-modified graphene/PVDF composites prepared by an electrospinning-hot pressing method, Compos Sci Technol (2019). https://doi.org/10.1016/j.compscitech.2019.01.003.

[49] J. Zhou, D. Hou, S. Cheng, J. Zhang, W. Chen, L. Zhou, P. Zhang, Recent advances in dispersion and alignment of fillers in PVDF-based composites for high-performance dielectric energy storage, Mater Today Energy 31 (2023) 101208. https://doi.org/10.1016/j.mtener.2022.101208.

[50] S. Peng, X. Du, Z. Liang, M. Ma, Y. Guo, L. Xiong, Multilayer polymer nanocomposites based on interface engineering for high-performance capacitors, J Energy Storage 60 (2023). https://doi.org/10.1016/j.est.2023.106636.

[51] J. Li, J. Claude, L.E. Norena-Franco, S. Il Seok, Q. Wang, Electrical energy storage in ferroelectric polymer nanocomposites containing surface-functionalized BaTiO3 nanoparticles, Chemistry of Materials 20 (2008) 6304–6306. https://doi.org/10.1021/cm8021648.

Chapter 7

Conclusions and future scope

7.1 Introduction

The polymer ceramic nanocomposite dielectric materials have become of special interest in the global research and development due to its prospect of application in the high-energy density capacitors for pulsed power applications, electrical vehicles, inverters etc. The performance of a high energy density capacitor relies on the various parameters such as high dielectric constant, high dielectric breakdown strength and low tangent loss. The polymers have a low dielectric constant and high dielectric breakdown strength, whereas the ceramics have a high dielectric constant and low breakdown strength. This complimentary feature is utilized for developing the polymer-ceramic nanocomposites with moderate dielectric constant, low tangent loss and high dielectric breakdown strength, which are useful characteristics of a material for high-energy density capacitors. Among the galaxy of polymer dielectric materials, polyvinylidene difluoride (PVDF) is one such polymer that is used as the polymer matrix in such nanocomposites because it has various crystalline phases (i.e., α, β, γ and δ) with different dielectric and polarization properties, high breakdown strength (~500 MV/m), dielectric constant (~10-15) and tangent loss (~0.03). Apart from these properties, it is easy to process and dielectric properties can be tuned by modifying the processing conditions. The barium strontium titanate (BST) stands out as a suitable ceramic nanofiller in the polymer matrix due to its remarkable combination of high dielectric constant (~3000) and minimal tangent loss (~0.02) over a wide frequency range (100 Hz-1 MHz). Though the choice of the polymer dielectric and the ceramic nanofiller for developing the polymer ceramic nanocomposites is the primary requirement, but the dielectric properties and energy storage behavior can be modified by the various other methods such as shape and size of the nanofiller (such as the use of nanowires (NW), nanotubes (NT), nanofibers (NF), etc.,), its functionalization, poling, incorporation of wide band gap nanofillers and engineered multilayer structure. An enhancement in the dielectric constant, breakdown strength and energy storage performance of

the polymer-ceramic nanocomposites is observed through the integration of surface-modified ceramic nanofillers, which enhances the compatibility between the polymer matrix and the surface functionalized nanofiller via the use of various functional groups, such as -OH, -NH_2, etc.

The nanocomposites of PVDF as a matrix with BST as a nanofiller could be of great importance so as to understand the underlying physics behind the interactions at the interfacial sites of the nanocomposite as well as their potential application in pulsed power systems and high energy density capacitors. Therefore, in the present study entitled "*Effect of functionalization of (Ba,Sr)TiO_3 on dielectric and energy storage behavior of PVDF-(Ba,Sr)TiO_3 nanocomposites*" the structural, dielectric, breakdown strength and energy storage properties of polyvinylidene difluoride-barium strontium titanate (PVDF-$Ba_{0.8}Sr_{0.2}TiO_3$) nanocomposites have been investigated.

7.2 Component of study

The exploration of the dielectric and energy storage characteristics of nanocomposites comprising polyvinylidene fluoride and barium strontium titanate (PVDF-$Ba_{0.8}Sr_{0.2}TiO_3$) has been conducted. The various elements analyzed in these investigations are discussed in the following sections.

7.3 Results and conclusion

The results of structural, dielectric, breakdown strength and energy storage properties of $Ba_{0.8}Sr_{0.2}TiO_3$ as well as PVDF-$Ba_{0.8}Sr_{0.2}TiO_3$ nanocomposite and the significant conclusions derived from the present work have been briefly summarized in the subsequent sections.

7.3.1 Polyvinylidene fluoride-$Ba_{0.8}Sr_{0.2}TiO_3$ flexible nanocomposite films

Polyvinylidene fluoride (PVDF)-$Ba_{0.8}Sr_{0.2}TiO_3$ (BST) nanocomposite thick film with 1.5 volume percent loading and thickness ~100 μm has been synthesized by tape-casting technique. The thick film is cut into small pieces and subjected to an external electric field of 22 kV/mm

for different time durations of 40 min, 50 min and 60 min. The XRD and IR studies reveal the evolution of the β phase of PVDF for the PVDF-$Ba_{0.8}Sr_{0.2}TiO_3$ nanocomposites. The dielectric constant at 1 kHz for the films exposed to the electric field for 60 min duration is increased up to ~25 as compared to ~15 for unexposed films, whereas the tangent loss does not exhibit significant change. The significant enhancement in the dielectric constant is attributed to the evolution of the β phase in PVDF and enhancement in dipolar density due to modification in the structural and interfacial behavior as well as molecular motion of the dipoles in the polymeric chain.

7.3.2 Temperature-dependent dielectric and impedance behavior of flexible Polyvinylidene fluoride-$Ba_{0.8}Sr_{0.2}TiO_3$ flexible nanocomposite films

Flexible PVDF-$Ba_{0.8}Sr_{0.2}TiO_3$ nanocomposite thick films of thickness ~80 μm with 0.75, 1.5, 2.25 and 3 volume percentage loading of $Ba_{0.8}Sr_{0.2}TiO_3$ nanoparticles are synthesized by the tape casting method. The dielectric constant and loss tangent of all the PVDF-$Ba_{0.8}Sr_{0.2}TiO_3$ nanocomposites remains nearly constant until 70 °C, and with further increase of the temperature (> 70 °C), the dielectric constant and loss tangent increase. An increase in the AC conductivity and a decrease in the impedance are observed with an increase in temperature for the PVDF-$Ba_{0.8}Sr_{0.2}TiO_3$ nanocomposites. Impedance analysis confirmed non-Debye-type relaxation behavior for all the nanocomposite thick films. A possible mechanism for the increase of the dielectric constant, loss tangent, and AC conductivity and the decrease of impedance with increasing temperature for the PVDF-$Ba_{0.8}Sr_{0.2}TiO_3$ nanocomposite thick films is proposed, which relies on the Lewis model and the interfacial double-layer model. Thermally-induced translational motion of polymeric chains of PVDF, the motion of ions, and the migration of space charge in the interfacial layer of the PVDF matrix and $Ba_{0.8}Sr_{0.2}TiO_3$ nanoparticles might be attributed to the observed dielectric behavior.

7.3.3 The specially architectured trilayered polyvinylidene fluoride-$Ba_{0.8}Sr_{0.2}TiO_3$ nanocomposite films

The PVDF-$Ba_{0.8}Sr_{0.2}TiO_3$ trilayered nanocomposites with different volume percent loading of $Ba_{0.8}Sr_{0.2}TiO_3$ nanoparticles, i.e., 0.75%, 1.50%, 2.25% and 3.00%, have been processed by the tape casting method. PVDF-$Ba_{0.8}Sr_{0.2}TiO_3$ trilayered nanocomposite consisting of 3.00 vol% of $Ba_{0.8}Sr_{0.2}TiO_3$ nanoparticles exhibited high dielectric permittivity (~25), low tangent loss (~0.03), and anomalously high BDS (~282 MV/m). Moreover, PVDF-$Ba_{0.8}Sr_{0.2}TiO_3$ trilayered nanocomposite with 3.00 vol% BST loading has the ultrahigh efficiency (~93%) and U_D (~7.8 J/cc at 1400 kV/cm). A mechanism for the excellent energy storage behavior and dielectric properties has been proposed. Where low tangent loss and high BDS are associated with the spatial variation of the local electric field at interlayer interfaces of PVDF-$Ba_{0.8}Sr_{0.2}TiO_3$ trilayered nanocomposites. The enhanced discharge energy density is associated with the formation of additional interfacial dipoles at various interfaces such as interlayer, intralayer (PVDF/PVDF), and PVDF/$Ba_{0.8}Sr_{0.2}TiO_3$ interfaces, whereas ultra-high efficiency is assigned to the decreased hysteretic polarization caused by the prevention of the external electric field induced movement of the charge carriers.

7.3.4 The specially architectured trilayered polyvinylidene fluoride-$Ba_{0.8}Sr_{0.2}TiO_3$ nanocomposite films incorporated with functionalized BST nanoparticles

Tape-casted multilayer PVDF-$Ba_{0.8}Sr_{0.2}TiO_3$ nanocomposite films have been synthesized, incorporating surface-modified $Ba_{0.8}Sr_{0.2}TiO_3$ nanoparticles with PO_4^{-3} and $-OH^-$ groups, resulting in PBST-P and PBST-H films, respectively. The inclusion of these modified nanoparticles strongly influenced the structural and morphological features of the films. PBST-P exhibited improved surface morphology and the evolution of β and γ crystalline phases in PVDF. The PBST-P films demonstrated superior dielectric properties, breakdown strength (381 MV/m), discharge energy density (7.97 J/cc at 1800 kV/cm), and energy efficiency (98%). The enhanced properties have been attributed to a better bridging network formed between the CF_2 dipoles of PVDF and the PO_4^{-3} groups of BST-P nanoparticles, leading to improved interfaces

and introducing extra dipoles. The study suggests novel approaches for developing high-energy density capacitors using functionalized nanoparticles in a polymer matrix with an architectured structure.

7.4 Future scope of the thesis

Apart from studies carried out in this thesis, there are still some investigations of futuristic technological and academic importance. These studies may further improve the dielectric behavior, breakdown strength and energy storage performance of PVDF-(Ba,Sr)TiO_3 nanocomposites. They are as follows:

1. The graded PVDF-(Ba,Sr)TiO_3 multilayer nanocomposite films (where the concentration of (Ba,Sr)TiO_3 in each layer will be varied). This kind of structure may have a positive impact on the dielectric behavior and energy storage performance.
2. The encapsulation of (Ba,Sr)TiO_3 nanoparticles with low dielectric materials such as SiO_2, etc., before incorporating them into the PVDF matrix, will passivate the PVDF/(Ba,Sr)TiO_3 interface. This process may produce PVDF-(Ba,Sr)TiO_3 nanocomposite thick films with improved dielectric and energy storage behavior at higher temperatures (RT-100 ^oC).
3. The heterogeneous PVDF-(Ba,Sr)TiO_3 nanocomposite thick films (where the sandwiched structure PVDF film and (Ba,Sr)TiO_3 nanoparticle will be formed) could also lead to improved energy storage performance.

Journal of Electronic Materials (2022) 51:5429–5439
https://doi.org/10.1007/s11664-022-09784-4

ORIGINAL RESEARCH ARTICLE

Significantly Enhanced Dielectric Behavior of Polyvinylidene Fluoride-Barium Strontium Titanate Flexible Nanocomposite Thick Films: Role of Electric Field-Induced Effects

Sachin Jaidka[1] · Arun Aggarwal[2] · Sandeep Chopra[2] · Dwijendra P. Singh[1]

Received: 2 March 2022 / Accepted: 17 June 2022 / Published online: 9 July 2022

Abstract

The polyvinylidene fluoride (PVDF)-0.05$Ba_{0.8}Sr_{0.2}TiO_3$ (BST) nanocomposite (0.05 is the fractional weight of BST) facile thick films of thickness ~100 µm have been synthesized by tape-casting. The synthesized films are exposed to an electric field of 22 kV/mm (for different time durations, 0 min, 40 min, 50 min, and 60 min) to investigate the electric field-induced effects on dielectric and structural properties of nanocomposite thick films. Structural studies have shown that the electric field increases the β phase of PVDF in PVDF-BST nanocomposites. The most prominent effect of the applied electric field is observed in the dielectric behavior of the nanocomposite thick films. The film exposed to the electric field for 60 min has the highest dielectric constant (~25) and very low tangent loss (~0.02) at 1 kHz, whereas the unexposed film of nanocomposite has a dielectric constant of ~15 and tangent loss (~0.03). The approximated Debye relaxation theory has been used to understand the correlation between dielectric and structural observations. Analysis confirms the duration of exposure to the electric field enhances the β-phase, which causes the increase in the density of dipoles. The enhanced dielectric performance is attributed to the increased dipolar density due to modification in the structural and interfacial behavior as well as molecular motion of the dipoles in the polymeric chain.

Keywords BST · PVDF · polymer-ceramic nanocomposites · dielectric constant · impedance analysis

Introduction

Polymer-based ceramic nanocomposites and their dielectric behavior have been the focus of research for the last decade due to their prospect of application in high-energy storage capacitors, embedded electronics, pulse power generation, etc.[1–3] There are a large number of polymers that are utilized as a matrix for this purpose, e.g. biaxially oriented polypropylene,[4] polyamide,[5] polyvinylidene fluoride (PVDF),[6,7] polyvinylidene fluoride-trifluoroethylene (PVDF-TrFE),[8] polydimethylsiloxane (PDMS)[9], etc. All these polymers have a very low dielectric constant (< 12).[10,11] Ceramic particles with a high dielectric constant are incorporated into the matrix of polymers in order to make polymer-based nanocomposites that consist of lead zirconate titanate (PZT) (ε' ~600),[12] barium titanate ($BaTiO_3$) (ε' ~1700) ,[13] strontium titanate ($SrTiO_3$) (ε' ~1000),[14] calcium copper titanate (CCTO) (ε' ~60000),[13] titanium oxide (TiO_2) (ε' ~200),[15] etc. The composites based on high dielectric constant ceramic materials and low dielectric constant flexible polymers have a moderate dielectric constant and low tangent loss. PVDF shows unique behavior among all dielectric polymers with its dielectric constant ~10, tangent loss ~0.05, and breakdown field ~500 MV/m.[16] Apart from this, its ease of processing, the existence of various crystalline phases (such as α, β, and γ crystalline phases), and associated electrical properties such as ferroelectric, piezoelectric, and pyroelectric[17] make it most suitable for making polymer-based ceramic nanocomposites. On the other hand, lead-free barium strontium titanate ($BaSrTiO_3$, BST) possesses very good dielectric behavior with a large dielectric constant over a wide temperature (−173°C to 120°C) and

✉ Dwijendra P. Singh
dpsingh@thapar.edu

[1] Energy Materials Lab, School of Physics and Materials Science, Thapar Institute of Engineering and Technology, Patiala, Punjab, India

[2] Terminal Ballistics Research Laboratory (TBRL), DRDO, Chandigarh, India

Journal of Physics and Chemistry of Solids 184 (2024) 111667

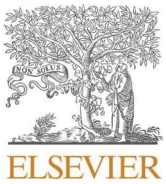

Contents lists available at ScienceDirect

Journal of Physics and Chemistry of Solids

journal homepage: www.elsevier.com/locate/jpcs

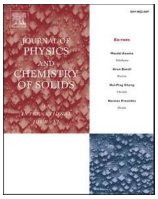

Effect of interfacial layers on the temperature-dependent dielectric and impedance behavior of flexible PVDF-BST nanocomposite thick films

Sachin Jaidka [a], Sandeep Chopra [b], Arun Aggarwal [b], Dwijendra P. Singh [a,*]

[a] Energy Materials Lab, School of Physics and Materials Science, Thapar Institute of Engineering and Technology, Patiala, Punjab, India
[b] Terminal Ballistics Research Laboratory, Defence Research and Development Organisation, Chandigarh, India

ARTICLE INFO

Keywords:
Poly(vinylidene difluoride)-$Ba_{0.8}Sr_{0.2}TiO_3$ nanocomposites
Dielectric properties
Impedance spectroscopy
AC conductivity
Interfacial effects

ABSTRACT

High energy storage performance of polymer-ceramic nanocomposites at elevated temperatures (room temperature to 100 °C) becomes unstable because of thermally unstable dielectric behavior (permittivity and loss tangent). Therefore, the present work describes the experimental and analytical investigation of the temperature-dependent dielectric behavior, AC conductivity, and impedance of flexible poly(vinylidene difluoride) (PVDF)-$Ba_{0.8}Sr_{0.2}TiO_3$ (BST) nanocomposite thick films. An increase in the dielectric constant and a decrease in the loss tangent is found with an increase in the loading of BST nanoparticles in the nanocomposite thick films. The highest dielectric constant, approximately 25, and the lowest loss tangent, approximately 0.03, are observed for 10 wt% BST–loaded PVDF-BST nanocomposite at 1 kHz; the dielectric constant and the loss tangent increase to approximately 93 and approximately 1.64, respectively, at 150 °C. The dielectric constant and the loss tangent of all the PVDF-BST nanocomposites are thermally stable up to 70 °C, and then increase with further increase of the temperature. A phenomenological model is proposed to explain the experimentally observed behavior, which might be attributed to the thermally induced translational motion in the polymeric chains of PVDF, the motion of ions, and the migration of space charge in the interfacial layer of the PVDF matrix and BST nanoparticles.

1. Introduction

Polymer-ceramic nanocomposites have attracted considerable attention because of their prospects for application in advanced electronics and electrical power systems, such as aerospace, power system, electric vehicle, and pulsed power applications [1–3]. These polymer nanocomposites are expected to operate efficiently in the higher-temperature range (room temperature to 100 °C), which is possible only when their electric properties, such as dielectric constant, loss tangent, and dielectric breakdown strength, remain stable in that operating temperature range [4–6]. A variety of polymer-ceramic nanocomposites have been explored for this purpose, and include polymers such as poly(vinylidene difluoride) (PVDF), poly(vinylidene difluoride–trifluoroethylene), biaxially oriented polypropylene, and polyimide [6–11] and nanoceramic fillers such as $BaTiO_3$, $Ba_xSr_{1-x}TiO_3$, $PbZr_xTi_{1-x}O_3$, HfO_2, boron nitride, and Al_2O_3 [12–16]. Despite there being much choice, some electrical parameters are always compromised by another electrical parameter; for example, adding conducting fillers such as graphene [17], carbon nanotubes [14], and aluminum fibers [18] to the polymer matrix provides a nanocomposite with an increased dielectric constant along with increased dielectric loss and electrical conductivity [19]. The size of the ceramic fillers also affects the performance of the nanocomposites. Composites with smaller filler sizes will be more beneficial since they have a more uniform morphology. These days, polymer-ceramic nanocomposites with a low vol/wt percentage of ceramic loading, high dielectric constant, and low loss tangent are required [3,8,9,20,21], as these nanocomposites having low loss tangent do not compromise with breakdown strength. Thus, the choice of polymer, ceramic filler, and filler size plays a very important role in the designing of polymer-ceramic nanocomposites with a high dielectric constant and a low loss tangent over a wide temperature range [22,23].

Several research groups have investigated the dielectric behavior of polymers/polymer-ceramic nanocomposites over a broad temperature range [4,24–28]. Recently, Wang et al. [4] studied the dielectric and energy storage properties of layered polymer-ceramic nanocomposites over a broad temperature range (room temperature to 150 °C). The layered nanocomposites were synthesized with alternate layers of boron nitride nanosheet/polyetherimide and TiO_2 nanorod array/polyetherimide. For a 7 vol% ceramic–loaded layered composite, the activation

* Corresponding author.
E-mail address: dpsingh@thapar.edu (D.P. Singh).

https://doi.org/10.1016/j.jpcs.2023.111667
Received 13 May 2023; Received in revised form 16 September 2023; Accepted 18 September 2023
Available online 27 September 2023

Received: 5 October 2023 | Revised: 15 December 2023 | Accepted: 15 December 2023

DOI: 10.1002/pc.28081

RESEARCH ARTICLE

Polymer COMPOSITES WILEY

Ultrahigh efficiency and enhanced discharge energy density at low loading of nanofiller in trilayered polyvinylidene fluoride-$Ba_{0.8}Sr_{0.2}TiO_3$ nanocomposites

Sachin Jaidka | **Dwijendra P. Singh**

Energy Materials Lab, Department of Physics and Materials Science, Thapar Institute of Engineering and Technology, Patiala, Punjab, India

Correspondence
Dwijendra P. Singh, Energy Materials Lab, Department of Physics and Materials Science, Thapar Institute of Engineering and Technology, Patiala, Punjab, India.
Email: dpsingh@thapar.edu

Abstract

Poly(vinylidene)fluoride-$Ba_{0.8}Sr_{0.2}TiO_3$ (PVDF-BST) trilayered nanocomposites (with different vol% loading of BST nanoparticles, i.e. 0.75%, 1.50%, 2.25% and 3.00%) has been processed by the tape casting technique. The upper and lower layers of the nanocomposites are casted in the same direction, whereas the middle layer is casted in the opposite direction. The trilayered PVDF-BST nanocomposite consisting of 3.00 vol% of BST nanoparticles exhibited high dielectric permittivity (~25), low tangent loss (~0.03) and moderately high breakdown strength (BDS ~282 MV/m). Moreover, it also possesses a high discharge energy density (~7.8 J/cc at 1400 kV/cm) and efficiency (~93%). A mechanism for the excellent energy storage behavior and dielectric properties has been proposed. Where, moderately high BDS and low tangent loss are associated with the spatial distribution of the local electric field at interlayer interfaces of PVDF-BST trilayered nanocomposites, which restricts the conduction of charge carriers at high electric field. The ultrahigh efficiency and enhanced discharge energy density is attributed to the formation of interfacial dipoles at various interfaces such as interlayer, intralayer (PVDF/PVDF), and PVDF/BST interfaces. These investigations would be adopted as a futuristic strategy for developing excellently efficient polymer-ceramic nanocomposites for the high energy density capacitors used in pulsed power applications.

Highlights

- PVDF-BST trilayered nanocomposites exhibit high ε' ~25 and low tanδ ~0.03.
- Nanocomposite shows ultra-high energy efficiency ~93% and enhanced U_D ~ 7.8 J/cc.
- Mechanism for the excellent energy storage and dielectric properties
- Relies on the interfacial dipoles and distribution of the local electric field.

KEYWORDS

breakdown strength; charge–discharge efficiency, dielectric properties; discharge energy density; PVDF nanocomposites

Sachin PhD thesis

ORIGINALITY REPORT

10%	3%	7%	1%
SIMILARITY INDEX	INTERNET SOURCES	PUBLICATIONS	STUDENT PAPERS

PRIMARY SOURCES

1	Zhifeng Yu, Shuanglin Wu, Chenhao Ji, Feng Tang, Leibing Zhang, Fenglin Huang. "Enhancing the β Phase of Poly(vinylidene fluoride) Nanofibrous Membranes for Thermostable Separators in Lithium-Ion Batteries", ACS Applied Nano Materials, 2023 Publication	2%
2	vdoc.pub Internet Source	2%
3	Submitted to Thapar University, Patiala Student Paper	1%
4	Jibo Huang, Manwen Yao, Xi Yao. "High Breakdown Strength, Energy Density, and Fast Discharge Times in PLZST Films Achieved by Designed Double-Blocking Structures", ACS Applied Energy Materials, 2021 Publication	1%
5	Ziming Cai, Chaoqiong Zhu, Limin Guo, Longtu Li, Xiaohui Wang. "Ceramic dielectrics for MLCCs", Institution of Engineering and Technology (IET), 2020	1%